Deciphering Osmolyte-Protein Interaction through Associated Water Stabilization Mechanism

A Thesis
Submitted in Partial Fulfillment of the Requirements
for the Degree of

DOCTOR OF PHILOSOPHY

by

KULDEEP SINGH NEGI

Roll No. 19107279

to the

Department of Chemistry
Indian Institute of Technology Kanpur
Kanpur, India

August, 2025

This page left blank intentionally

CERTIFICATE

It is certified that the work reported in the thesis entitled "**Deciphering Osmolyte-Protein Interaction through Associated Water Stabilization Mechanism**" has been carried out by **Mr. Kuldeep Singh Negi** under my supervision and has not been submitted elsewhere for a degree.

August, 2025

(*Prof. Pratik Sen*)

IIT Kanpur

Thesis Supervisor

Department of Chemistry

Indian Institute of Technology Kanpur

Kanpur, U.P. India- 208016

This page left blank intentionally

DECLARATION

This is to certify that the thesis titled "**Deciphering Osmolyte-Protein Interaction through Associated Water Stabilization Mechanism**" has been authored by me. It presents the research conducted by me under the supervision of **Prof. Pratik Sen**.

To the best of my knowledge, it is an original work, both in terms of research content and narrative, and has not been submitted elsewhere, in part or in full, for a degree. Further, due credit has been attributed to the relevant state-of-the-art and collaborations (if any) with appropriate citations and acknowledgements, in line with established norms and practices.

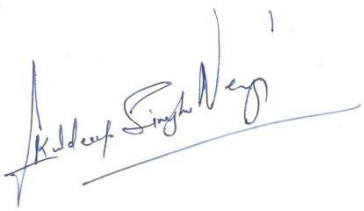

Signature
Name: Kuldeep Singh Negi
Roll No. 19107279
Programme: PhD
Department: Chemistry
Indian Institute of Technology Kanpur
Kanpur 208016

This page left blank intentionally

Department of Chemistry
Indian Institute of Technology Kanpur

Certificate of course work

This is to certify that **Mr. Kuldeep Singh Negi** has satisfactorily completed all the courses required for the Ph.D degree. The courses include:

CHM 629A Principles of Physical Chemistry

CHM 685A Molecule Radiation Interaction

CHM 664A Modern Physical Methods in Chemistry

CHM 600A Mathematics for Chemistry

CHM 799 Research

CHM 800A General Seminar

CHM 801A Graduate Seminar

Mr. Kuldeep Singh Negi was admitted to the candidacy of the Ph.D degree in July 2019 after he successfully completed the written and oral qualifying examinations.

Head
Department of Chemistry
Indian Institute of Technology Kanpur
Kanpur – 208016, India

Convenor, DPGC
Department of Chemistry
Indian Institute of Technology Kanpur
Kanpur – 208016, India

This page left blank intentionally

Dedicated to

My Family

This page left blank intentionally

Acknowledgements

As I reach the final stage of my PhD journey, I realize that one of the most challenging and perhaps the most meaningful tasks is to express my gratitude. The path to this point has been made possible by the steadfast support of many individuals, without whom this journey would not have been conceivable.

I am and will always remain deeply grateful to ***Prof. Pratik Sen*** *for giving me the opportunity to join his lab as a Ph.D. scholar. At the beginning of my journey, I found it difficult to approach him due to my introverted nature, but he quickly created an environment where I felt comfortable communicating with him. It is no surprise that people often say he is a genuinely kind and approachable person.*

Throughout my research journey, he has been the one I turned to the most for discussions, guidance, and clarity. His ability to sense a student's level of understanding and adjust his explanations accordingly is a testament to his intelligence and empathy as a mentor. There were many moments of uncertainty and self-doubt during my Ph.D., and it was his support, encouragement, and confidence in me that helped me navigate those phases and continue moving forward.

Prof. Sen's mentorship goes far beyond academic guidance, his patience, trust, and consistent support, even when I faced personal challenges, have played a crucial role in my progress. He has always stood by me, guiding me not only as a researcher but also as a person trying to find my place in this field. These qualities make him not just a mentor, but a true teacher in every sense.

My journey began in 2019, when I stepped into the unfamiliar world of research. I was filled with questions, Now what? and How? as I tried to navigate this new culture of lab life, something I had never experienced before. In the beginning, adapting to this environment was challenging. My introverted nature, along with language barriers, often made communication difficult within the lab. As a result, I initially faced several misunderstandings, particularly with ***Dr. Nilimesh Das****.*

However, with time, those difficulties gave way to understanding and support. Dr. Nilimesh Das, along with other seniors in the lab, played a crucial role in helping me grow both academically and personally. He was one of the first alongside my supervisor to introduce me to the research topic that eventually became the foundation of this thesis. I am sincerely thankful to him and to all my seniors for their guidance and encouragement throughout this journey.

In the beginning, we were five of us, ***Dr. Arghya, Mr. Tanmoy, Mr. Sandeep, Mr. Abhijit****, and me who joined the lab together in 2019. The group was later joined by*

more members, Mr. Suman Bhowmik and Mr. Subhendu, Mr. Arnab. From the very start, I never felt alone among them. They were always there to help me, no matter what the situation. Over the course of our journey, I learned a great deal from each of them not just about research, but also about life. Our frequent discussions, both academic and otherwise, as well as the late-night movies and shared meals, created memories I will always cherish. These moments and their companionship will be deeply missed in the days to come.

*I would like to thank my lab juniors—**Mr. Bhupinder, Ms. Patralekha, Mr. Dipankar Mondal, Mr. Akash Rana, Mr. Harshit Karnwal, Mr. Himanshu**, and **Mr. Subhajit Rana**—for always bringing positivity and warmth to the lab environment. Their cheerful presence, enthusiasm, and supportive nature created a lively and welcoming atmosphere, even during the most stressful times. I truly feel fortunate to have had such wonderful juniors around me during my Ph.D. journey.*

*I feel privileged to have crossed paths with some truly wonderful individuals outside the lab during my time at IIT Kanpur. **Dr. Bharat Singh** and **Dr. Manish Vashisht** stood by me during difficult times and offered guidance when I needed it most. My batchmates, **Dr. Ashwini, Dr. Nikhil**, and **Mr. Suraj**, were always there to help and support me in every possible way. I also enjoyed their company while playing the badminton.*

*A special mention goes to **Dr. Geetanjali Negi**, the only woman in my close friend circle, whose strength, support, and thoughtful guidance have meant a lot to me. I am also grateful to have met **Mr. Sidhartha** and **Mr. Rudra**, juniors whose exceptional understanding and intellect have continuously inspired me. Though I met them later in my journey, their presence left a lasting impact.*

*I would also like to take this opportunity to express my sincere gratitude to the anonymous reviewers of my research papers. Their thoughtful critiques and insightful questions pushed me to deepen my understanding and view my work from new perspectives. I am equally thankful to the many great scientists whose work has been a constant source of inspiration throughout my journey, especially late **Prof. Ahmed Zewail, Prof. Biman Bagchi,** and late **Prof. Kankan Bhattacharyya**. Their pioneering contributions have profoundly influenced the way I think about science and research.*

*Lastly, I bow my head in gratitude to the **Almighty**, who has blessed me with a family whose unwavering love and support made this journey possible. I feel truly fortunate to have parents like **Mr. Swarup Singh Negi** and **Mrs. Munni Devi**, who have stood by me throughout my life and always gave me the freedom to pursue my dreams*

*without hesitation. I would also like to thank my **grandmother (nani ji)**, whose strength and resilience have always been a source of deep inspiration for me. I have often drawn motivation from the hardships she endured with grace and determination.*

*I am equally thankful to my **brother, Mr. Pradeep Singh Negi**, and my **sister, Mrs. Seema Rawat**, whose constant encouragement and belief in me gave me the strength to never give up, even during the toughest moments. Their presence in my life has been a pillar of strength. I remain forever grateful to the Almighty for everything.*

Jai Badri-Kedar

Kuldeep Singh Negi

This page left blank intentionally

SYNOPSIS

Name of Student:	Kuldeep Singh Negi
Roll No.	19107279
Degree for which submitted:	Ph.D.
Department:	Chemistry
Thesis Title:	**Deciphering Osmolyte-Protein Interaction through Associated Water Stabilization Mechanism**
Name of Thesis Supervisor:	Prof. Pratik Sen
Month and year of thesis submission:	August 2025

Proteins are the molecular workhorses of life, orchestrating the intricate symphony of biological functions that sustain all living systems. From facilitating movement and metabolism to enabling signal transduction and immune defence, proteins lie at the core of cellular machinery. Structurally, proteins are composed of amino acid residues linked via peptide bonds, and under physiological conditions they fold into specific three-dimensional (3D) structures. This structural specificity underlies their functional diversity and arises from the distinct number, sequence, and arrangement of amino acids within each protein.

Proteins are, however, only marginally stable under physiological conditions. Minor changes in environmental parameters such as pH, salt concentration, ionic strength, temperature, or the presence of solutes can perturb their conformation and compromise their function. Nature, in response to such fluctuations, has evolved a remarkable defence strategy. Cells accumulate small organic molecules under stress, not only to regulate cell volume by maintaining the osmotic balance and but also to preserve the functional integrity of biomacromolecules. These molecules, known as osmolytes, include sugars, polyols, amino acids, methylamines, etc.

Osmolytes are recognized not only for their role in maintaining cellular homeostasis but also for their ability to stabilize macromolecules like proteins under stress. This protective role has been harnessed in biotechnology and pharmaceutical industries, where osmolytes help maintain protein stability during storage and transport. Therefore, a comprehensive understanding of protein–osmolyte interactions is vital, given their biological relevance and industrial utility.

Over the years, considerable efforts have been devoted in elucidating the mechanisms of protein–osmolyte interactions. Two dominant theories have emerged, namely the **preferential interaction theory** and the **water structure modulation theory**. The preferential interaction theory considers protein–osmolyte–water interactions and suggests that osmolytes excluded from the protein surface tend to stabilize the protein, while those that preferentially accumulate at the surface promote destabilization. This concept mimics the phenomenon of surface tension; however, direct measurement of surface tension at the protein–solvent interface remains technically challenging, limiting its broader application. On the other hand, the water structure modulation theory posits that osmolytes that enhance water structure contribute to protein stabilization, whereas those that disrupt water structure led to destabilization. While conceptually useful, this theory only accounts for osmolyte–water interactions and lacks the complexity needed to explain protein-specific effects, such as differential stabilization of various proteins by the same osmolyte, concentration-dependent reversal of stabilization, and so on.

To address these limitations and to better explain protein-dependent responses to osmolytes, in this thesis, I have proposed a new hypothesis, the **Associated Water Stabilization Mechanism (AWSM)**. This hypothesis integrates the roles of protein–osmolyte–water interactions and focuses particularly on the behaviour of water molecules forming the hydration layer, also referred to as biological water or associated water, that directly interacts with the protein surface. This interfacial water behaves differently from bulk water and plays a crucial role in maintaining protein structure and dynamics. This thesis investigates how osmolytes influence

both bulk and associated water dynamics, and how modulation of the associated water layer alters protein's interior interactions, ultimately impacting the protein's thermal stability. Furthermore, this framework has been employed to account for protein-specific effects that existing theories fail to fully explain, offering a more unified understanding of protein–osmolyte interactions at the molecular level.

1. Osmolyte induced protein stabilization: modulation of associated water dynamics might be a key factor

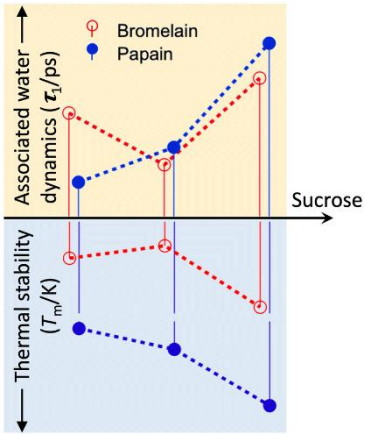

Kuldeep Singh Negi *et al. Phys. Chem. Chem. Phys.*, **2023**, *25*, 32602-32612

The mechanism of protein stabilization by osmolytes remains one of the most important and long-standing puzzles. The traditional explanation of osmolyte-induced stability through the preferential exclusion of osmolytes from the protein surface has been seriously challenged by observations such as the concentration-dependent reversal of osmolyte-induced stabilization/destabilization. The more modern explanation of protein stabilization/destabilization by osmolytes considers an indirect effect due to osmolyte-induced distortion of the water structure. It provides a general mechanism, but there are numerous examples of protein-specific effects, *i.e.*, a particular osmolyte might stabilize one protein, but destabilize the other, which cannot be rationalized through such an explanation. Herein, we hypothesized that osmolyte-induced modulation of associated water might be a

critical factor in controlling protein stability in such a medium. Taking different osmolytes and papain as a protein, we proved that our proposal could explain protein stability in osmolyte media. Stabilizing osmolytes rigidify associated water structures around the protein, whereas destabilizing osmolytes make them flexible. The strong correlation between the stability and the associated water dynamics, and the fact that such dynamics are very much protein-specific, establishes the importance of considering the modulation of associated water structures in explaining the osmolyte-induced stabilization/destabilization of proteins. More interestingly, we took another protein, bromelain, for which a traditionally stabilizing osmolyte, sucrose, acts as a stabilizer at higher concentrations but as a destabilizer at lower concentrations. Our proposal successfully explains such protein-specific observations, which are probably inexplicable by any known mechanisms. We believe this report will trigger much research in this area.

2. Interplay between Protein Fluctuation and Associated Water Dynamics on the Osmolyte induced Protein Stabilization

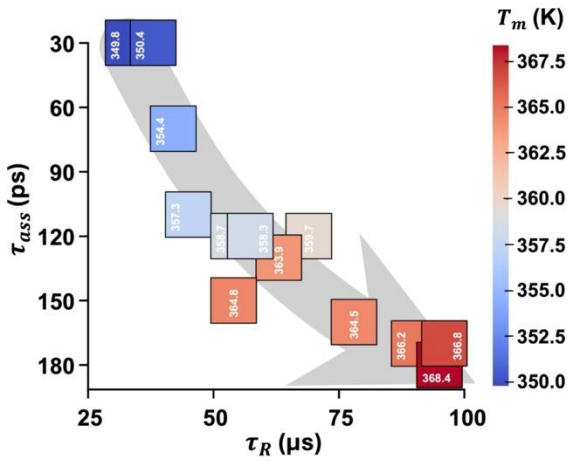

Kuldeep Singh Negi *et al. Biophys. J.*, **2025**, *124*, 2082 – 2091

The mechanism behind osmolyte-induced protein stabilization remains elusive despite extensive research. Amongst various hypotheses, the associated water

modulation hypothesis has proven to be the most effective in explaining osmolyte-induced stabilization effects. In my previous work, it has been demonstrated that osmolytes that slow down associated water dynamics enhance protein thermal stability, whereas those that accelerate it promote destabilization. However, the molecular basis of this correlation remains unclear. Using fluorescence correlation spectroscopy, we observe that osmolyte-induced changes in the associated water dynamics directly affect the internal flexibility of the protein, which is assessed through conformational fluctuation dynamics, serving as a tool to measure the protein's internal flexibility. The osmolytes that induce retardation in the associated water dynamics make the interior of the protein more rigid, as reflected by the slowed conformational fluctuation dynamics of the protein, leading to enhanced thermal stabilization. The destabilizers induce effects that are exactly opposite to stabilizers. These findings provide new insights into the interplay of associated water dynamics, protein flexibility, and stability, contributing to a deeper understanding of osmolyte induced protein stabilization.

3. Mechanistic insights deciphering the distinct response of proteins towards osmolyte: An AWSM perspective

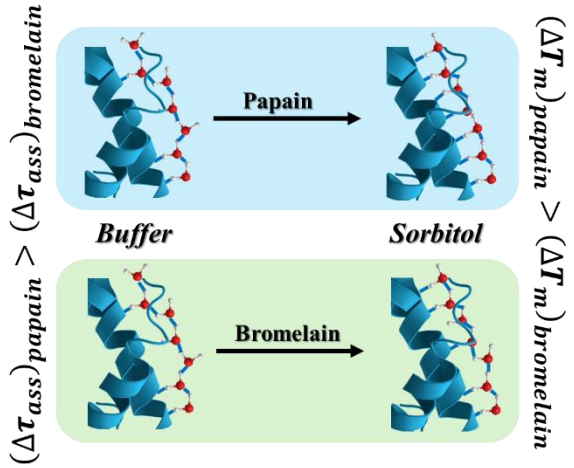

Kuldeep Singh Negi *et al. Manuscript under preparation*

While earlier studies established the critical role of associated water dynamics in protein stabilization and proposed a mechanistic link through internal conformational rigidity, they did not account for the varying degrees of stabilization observed across different proteins under identical osmolyte conditions. This chapter addresses that gap. In this study, we examine how sorbitol modulates the thermal stability of two model proteins, bromelain and papain, through changes in hydration dynamics and internal flexibility. We propose the Associated Water Stabilization Mechanism (AWSM) to describe how osmolyte-enhanced water–water and water–residue interactions near the protein surface promote stabilization of the protein's interior by dampening conformational mobility. While both proteins conform to this model, papain exhibits greater stabilization than bromelain. This enhanced effect can be understood within the AWSM framework by analysing changes relative to buffer conditions rather than comparing absolute parameters. The greater retardation of associated water dynamics in papain leads to stronger internal stabilization and superior thermal resilience. These results reinforce the importance of hydration-layer dynamics in protein stabilization and establish AWSM as a useful framework for interpreting protein-specific responses to osmolytes.

4. Dropping the Guard: How Denaturants Undermine Osmolyte-Mediated Protection

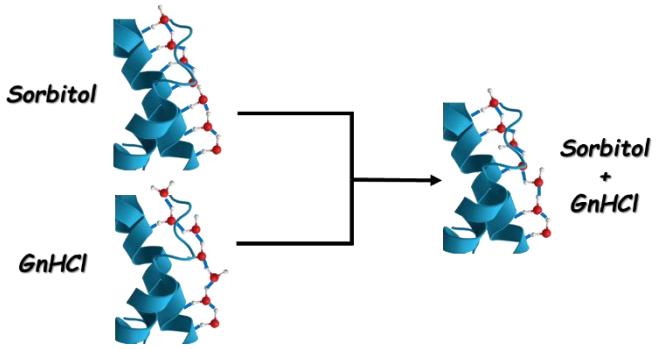

Kuldeep Singh Negi *et al. Manuscript under preparation*

Deciphering how stabilizing osmolytes and destabilizing agents modulate protein stability is essential for understanding protein folding and function under cellular stress. In this study, we explore the mechanism by which a chemical denaturant counteracts the stabilizing effect of an osmolyte on the protease papain. Under the lens of our proposed Associated Water Stabilization Mechanism (AWSM), we demonstrate that sorbitol enhances protein thermal stability by strengthening water–water and water–protein surface interactions, which in turn promote cohesive bonding among core amino acid residues. Conversely, guanidinium hydrochloride (GnHCl) disrupts these hydration networks and weakens residue-residue interactions, leading to destabilization. When both osmolyte (sorbitol) and denaturant (GnHCl) are present together, GnHCl diminishes the efficacy of sorbitol by reducing its ability to enhance the local water structure, thereby attenuating the strengthening of the protein's interior and counteracting the stabilizing effect of sorbitol on the thermal stability of papain. Our findings indicate that the counteracting influence of GnHCl on sorbitol-induced stabilization can be understood within the AWSM framework. Apart from a weak direct interaction between sorbitol and GnHCl, their opposing impacts on hydration dynamics also contribute to the counteraction effect. This study highlights AWSM as a promising conceptual tool for understanding protein-osmolyte interactions and offers molecular-level insight into how chemical

This page left blank intentionally

Table of Content

This page left blank intentionally

Chapter 1

Introduction

A Short Summary

Of

Protein, Osmolyte and their Interaction

1.1 Proteins in Focus: A Concise Overview

Origin of life on planet is a mystery and is not understood completely yet. Still a significant progress has been made to understand the involvement of molecular machineries in processing and regulating the molecular events to sustain life. As per the current understanding cell is considered, that basic biological entity wherein different compartments with or without defined boundaries provides space for specific functions and reactions [1]. One such compartment is the nucleus where the chromosomes carrying the genetic information are processed to produce small molecular machines commonly known as protein in the cytoplasm [2]. These protein molecules are popular in biological sciences for their importance in the proper functioning of the body to sustain life. These molecules are known to perform different roles inside a body as enzymes, hormones, antibodies, as energy source, in balancing fluid and electrolyte, involved in acid-base balance, in transport, in wound healing, tissues regeneration and nerve function [3,4]. These important functions of protein throughout the body in different cells makes them the subject of utmost importance in life science.

1.1.1 Protein: Function and Conformation

Protein is an array of 20 natural amino acids joined by peptide bonds [5] where the information on the sequence/arrangement of amino acids within the array is hidden in the deoxyribonucleic acid (DNA) which are carried by chromosomes [6]. Different segments in this single chain of amino acid residues transforms into different three-dimensional (3D) structures namely alpha-helix, beta-sheet, beta-turn, random-coil which are known by secondary structures of protein [7,8]. These secondary structures of protein when combined is known as the three-dimensional structure of protein and in general, this 3D structure of the protein is considered as the functional form of protein [9]. In some cases, the multimeric forms are the only functional form and are known by the name quaternary structure [10,11]. Proteins with different number and arrangement of amino acid residues in the sequence adopts different conformation and perform different function [12–15] as is illustrated in Scheme 1. The protein drew

its functional specificity from its 3D structure which varies from protein to protein [9].

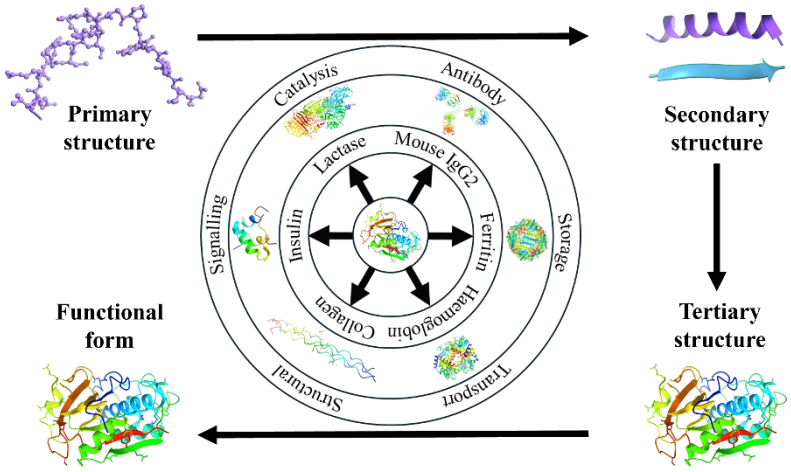

Scheme 1: Schematic representation of the hierarchy in the structure of protein and different types of function that proteins perform.

1.1.2 Thermodynamics of Protein

The stability of the protein is generally described by the equilibrium shown in scheme 2.

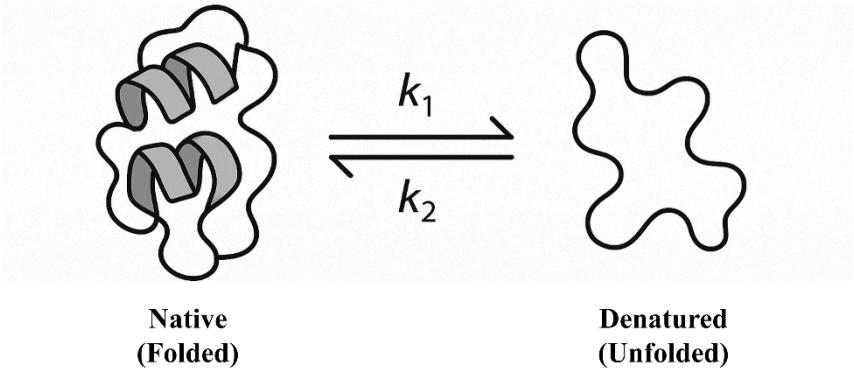

Scheme 2: Schematic representation of the protein unfolding equilibrium.

Where the native state is considered as the functionally active form and the denatured state is considered as the functionally inactive form [16–18]. The free energy change ($\Delta G_{unfolding}$) of denaturation associated with this equilibrium is just ~ 5-20 kcal/mol [17,19–22] and thus the folded states are considered stable than the unfolded states. To understand how much stable this equilibrium is we took a hydrogen bond

among water molecules as a reference. The free energy change (ΔG_{H-bond}) associated with this hydrogen bond is typically ~ 5 kcal/mol which is considered very weak interaction as hydrogen bond is a physical bond [23]. On comparing the $\Delta G_{unfolding}$ for protein stability associated to the equilibrium with that of the ΔG_{H-bond} associated with the hydrogen bond formation among the water molecules it can be deduced that the protein equilibrium is only one to four times stronger than that of the water-water hydrogen bond [24]. This is the reason the protein equilibrium is always considered weakly stable, and the folded state is thus said to be marginally stable than that of unfolded state [25].

1.1.3 Protein under Environmental Stress

As we have seen in the last section that the protein equilibrium is marginally stable. Thus, any perturbation in the environmental conditions like variation in the conditions of temperature, pressure, pH, salt concentration etc. might disturb the equilibrium by favouring the unfolded conformation along with other non-native conformations of the protein and thus make the protein functionally inactive or inefficient [26]. This inactive form may have corresponding repercussions on the functioning of the cell and the body. Generally, the energy landscape associated with the folding of the protein is given by protein funnel diagram [27]. In the energy landscape of protein folding, a polypeptide chain explores many conformational states at higher free energy levels. As folding progresses and free energy decreases, the number of accessible conformations narrows, guiding the protein toward its thermodynamically stable native state. However, under certain cellular or environmental stresses, proteins can become kinetically trapped in intermediate states that lose native interactions. These misfolded conformations may adopt alternative folding pathways, sometimes leading to aggregated states that provide thermodynamic stabilization. Such non-native aggregates are often associated with cytotoxicity and are implicated in protein misfolding diseases, including Alzheimer's, Parkinson's, and prion-related disorders [28]. The Scheme 3 represents some of the proteins and the disease associated with their misfolding.

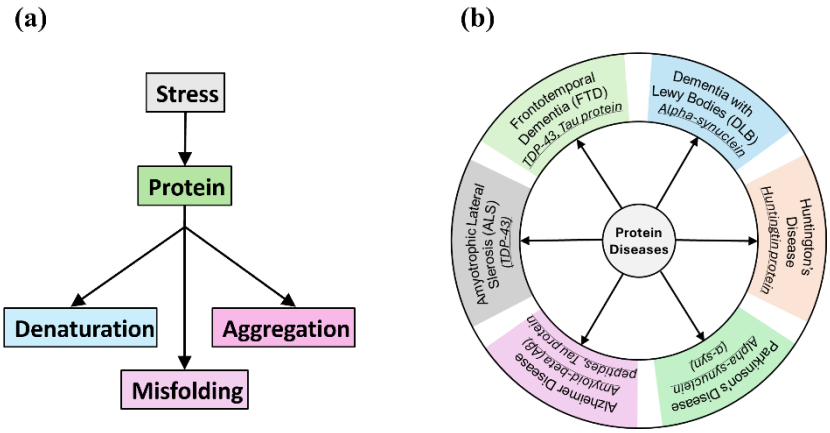

Scheme 3: Schematic representation of (a) possible outcomes of stress on protein, (b) diseases associated with protein misfolding and aggregation.

1.2 Osmolyte: Natural Remedy against Environmental Stress

Nature is conscious and quite smart as it by itself searches for the optimum solution to treat the problem, whatever the environmental conditions are, and evolution that we use to read and talk about is one of the outcomes of several smart and ideal adjustments of nature over time within various forms of life on earth. The cellular membrane act as a semipermeable membrane which allows the movement of water molecules in and out of the cell [29,30]. Cell volume changes continuously whenever the extracellular or the intracellular environment encounter perturbation in terms of temperature, pH, ion concentration etc [31]. The cell function depends on its volume and thus to function properly against such perturbed environment it regulates its volume by employing the phenomenon of osmosis. Here, in this process the cell uses the ions and small organic solutes for volume regulation by allowing the movement of water molecules in and out of the cell through osmosis [32]. It has been observed in some type of organism that even in the situation of high variations in the osmotic pressure the concentration of potassium ions [K^+] inside the cell changes a little [32,33]. It has also been observed that initially to balance the osmotic pressure variation the ions come into action later the small organic solutes take the charge to counteract the osmotic pressure imbalance in a long run. That's the reason these small organic

solutes are selectively termed as osmolyte [32,34,35]. The cell employed the osmolyte either by synthesising itself inside the cell or by incorporating through proper channel across the cell membrane [34]. Intracellular space is occupied by the biomacromolecules which includes protein as well and it has been observed that these osmolyte molecules apart from regulating the cell volume also interact with these protein molecules to provide stabilization against the natural environmental stresses [34,35]. These osmolyte molecules are the small organic solutes from different classes of compounds which includes sugars, polyols, amino acids, methyl amines and their derivatives [34,36,37] (Scheme 4). As these osmolyte molecules interact favourably with the protein, these also find their application in the biopharmaceutical industries and thus makes it important to understand the mechanism of interaction among the two.

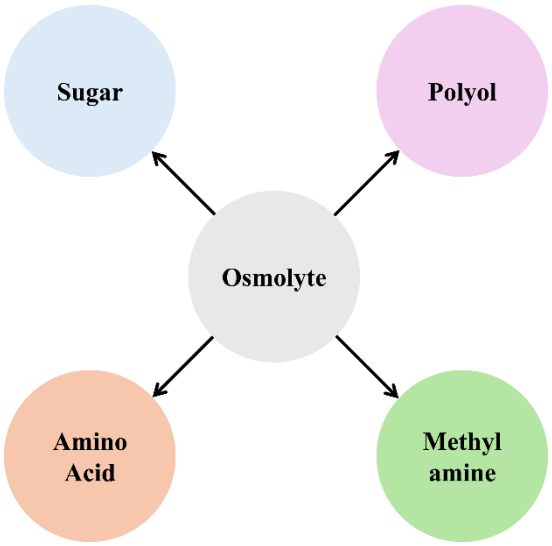

Scheme 4: Schematic representation of the types of osmolytes present in nature.

1.3 Protein-Osmolyte Interaction: Current Understanding

Lot of efforts has been made in the past to understand the mechanism of interaction of osmolyte with protein to impart extra stabilization against the changed environmental conditions. Still the mechanism of interaction is not fully understood so far, although a significant progress has been achieved in this direction and we can say, we are not blind in explaining these interactions.

As per the present understanding these interactions are defined by employing two different theories, first is the "*Preferential Interaction Mechanism*" which is also known as "direct mechanism" and the other is "*Water Structure Modulation Mechanism*" and this also termed as "indirect mechanism".

1.3.1 Preferential interaction Mechanism

Preferential interaction mechanism was first proposed by Timasheff's group where the emphasis is given on the interaction among protein-water-osmolyte molecules [38]. This theory is purely based on the surface tension phenomenon. It has been shown experimentally that on the addition of the solute to the protein-water system, the added solute distributes at the surface of the protein (near to the protein) differently than that at the bulk [39,40] (away from protein). The concentration of the added solute could be more at the surface of the protein with respect to the bulk and vice-versa, depending on the nature of the solute[38,41,42]. The type of distribution describes the effect of the added osmolyte on the stability of the protein. This theory uses a parameter by the name "*preferential interaction coefficient*" designated by "$\Gamma_{2,3}$" which describes the concentration of added solute at the surface of the protein relative to the bulk where the subscript 1,2,3 represent water, protein, added solute respectively [39] as shown in Scheme 5.

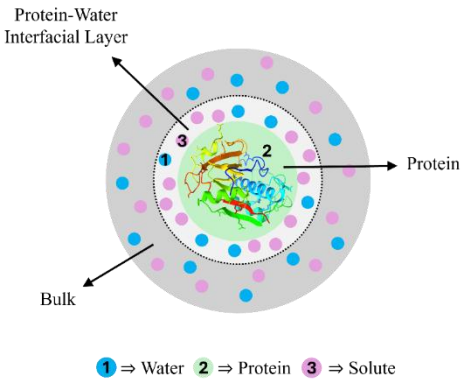

Scheme 5: Schematic representation of the types of water (associated water and bulk water) around protein molecule.

Before going into the conclusion of the theory it is requisite to understand the background of the theory. Here the researcher experimentally [40] evaluated the excess free energy at the surface of the protein on the addition of unit amount of the solute $\left(\frac{\partial \mu_2}{\partial m_3}\right)_{T,P,m_2}$. $\left(\frac{\partial \mu_2}{\partial m_3}\right)_{T,P,m_2}$ and $\Gamma_{2,3}$ are related by the relation,

$$\left(\frac{\partial \mu_2}{\partial m_3}\right)_{T,P,m_2} \propto -\Gamma_{2,3} \qquad (1.3.1)$$

Where μ, m represents the chemical potential at the surface of the protein and mass of the solute respectively. It has been observed that the osmolyte molecules for which, the parameter $\left(\frac{\partial \mu_2}{\partial m_3}\right)_{T,P,m_2}$ gives positive values the preferential interaction coefficient ($\Gamma_{2,3}$) took negative values which means the osmolyte that increases the surface energy of protein will be concentrated less on the surface of the protein relative to the bulk and vice-versa as pictorially represented in scheme 6. Proteins are experimentally found to be thermally stabilized where preferential interaction coefficient took negative values.

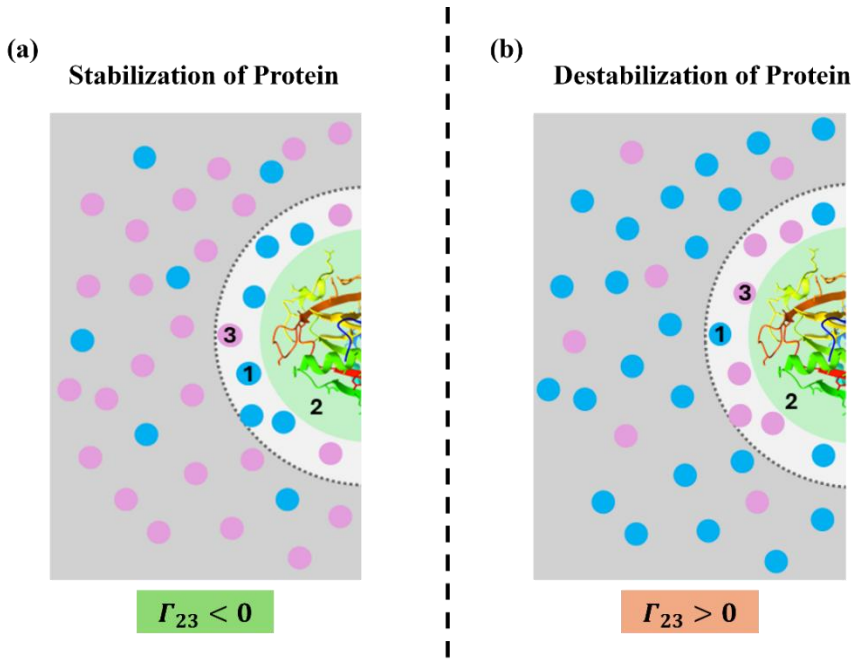

Scheme 6: Schematic representation of the distribution of (a) stabilizing and (b) destabilizing osmolytes around the protein described by preferential interaction mechanism.

The explanation for the correlation between negative values of preferential interaction coefficient and stabilization of protein was provided. For a protein the transformation from folded to the unfolded state could be represented [43] as shown in Scheme 7. For an osmolyte, the addition of which increases the free energy of the protein (folded state) is assumed to increase the free energy of the protein further on extension (unfolding) of the protein. Thus, the total free energy for the process of denaturation of protein as shown in Scheme 7 will be positive.

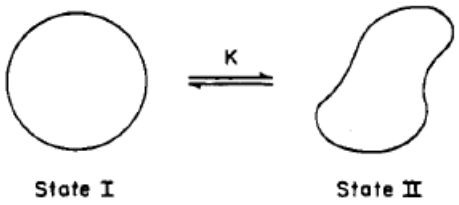

Scheme 7: Schematic representation of the unfolding equilibrium of protein (taken from reference [43]).

The overall situation of protein denaturation in aqueous osmolyte solution could be observed thermodynamically as given in the Scheme 8 for better understanding [43]. Through this scheme the direct transfer of protein from water to the aqueous osmolyte solution could be seen through two different processes obeying the Hess's law of constant heat summation which states the overall energy associated with the process depends on the initial and final state of the system irrespective of the path followed in going from the initial state to achieve the final state. The compact (circular) state represents the native state of the protein, and the extended (distorted) state represents the unfolded state of the protein. ΔG_1 and ΔG_4 represents the free energy change involved in the process of denaturation (unfolding) of protein within the water and aqueous osmolyte solution respectively. ΔG_3 and ΔG_2 represents the free energy change associated with the transfer of native and denatured state from

water to the aqueous solution of osmolyte respectively. So, for the whole process represented in scheme 8 the overall free energy change will be 0 i.e.,

$$\Delta G_1 + \Delta G_2 - \Delta G_3 - \Delta G_4 = 0 \quad (1.3.2)$$

Thus,

$$\Delta G_1 + \Delta G_2 = \Delta G_3 + \Delta G_4 \quad (1.3.3)$$

As protein denaturation is an unfavourable process, $\Delta G_1 > 0$ and for an osmolyte that increases the free energy of the protein in folded state ($\Delta G_3 > 0$), the free energy change for the protein in transferring the unfolded state from water to the aqueous osmolyte solution will be more unfavourable ($\Delta G_2 >> 0$) and thus,

$$\Delta G_2 > \Delta G_3 \quad (1.3.4)$$

And the equations 1.3.3 and 1.3.4 combinedly says that,

$$\Delta G_4 > \Delta G_1 \quad (1.3.5)$$

which establishes that the osmolyte that increases the chemical potential at the surface of the protein and thus distributes itself around the protein in a fashion where the concentration of the added osmolyte is less at the surface of the protein relative to the bulk defined by the negative value of the preferential interaction coefficient stabilizes the protein and vice-versa. The justification for this stabilization is given by saying that the added osmolyte which increases the chemical potential at the surface of the protein increases the surface tension at the protein-water interface and thus the protein tries to keep itself in a state or conformation which shares less surface area with the water i.e., the folded state. Thus, the protein in the presence of such osmolyte gets stabilized. The added osmolyte which decreases the chemical

potential at the surface of the protein reduces the surface tension at the protein-water interface and protein tries to attain a conformation with larger surface area i.e., unfolded state. Thus, the protein in the presence of such osmolytes gets destabilized.

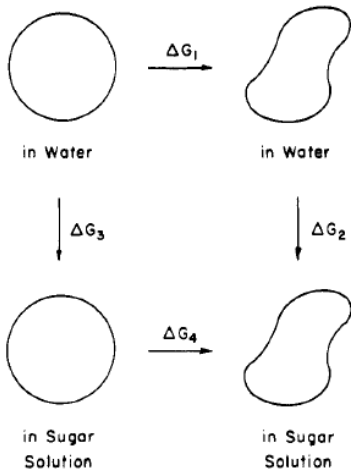

Scheme 8: Schematic representation of the phenomenon of unfolding of protein in osmolyte solution (taken from reference [43]).

Although Timasheff had satisfactorily presented the theory but fail to give a molecular insight over why osmolyte molecules distributes differently in the near vicinity of the protein relative to the bulk and why distribution depends on the type of osmolyte.

Later in 1995, Bolen's group came up with a reasonable insight over what happens at the molecular level that makes the osmolyte to distribute differently in the near vicinity and away from the protein surface and how this distribution varies depending on the type of osmolyte [44,45]. It has been observed that stabilizing and destabilizing osmolytes, both interact favourably with the protein and the difference has been created by the kind of interaction between the osmolyte and the protein surface specifically the protein backbone [44]. It has been proved experimentally that stabilizing osmolytes do have repulsive interaction with the protein backbone and thus these osmolyte distributes in a fashion where the concentration of osmolyte molecules is less at the surface relative to the bulk and vice-versa.

1.3.2 Limitations of the preferential interaction theory

At first glance, the theory seems to be perfect in defining the interaction between the osmolyte and the protein, but this theory fails to explain some common observations. Theory is based on purely surface tension phenomenon and technically it's impossible to directly measure the surface tension at the protein surface as the protein is very small in size. Researchers have used the air-water or water-oil interface as the most approximate model to mimic the protein-water interface to measure the surface tension [46–48]. They have observed that the osmolyte, glycerol thermally stabilizes the protein which is justified by the increase in the melting temperature (T_m) value of the protein and also signifies by $\Delta T_m > 0$, where ΔT_m is defined as the extent of thermal stability in osmolyte solution compared to water only system and is given as

$$\Delta T_m = (T_m)_{osmolyte} - (T_m)_{water}$$

where, T_m is an experimentally observed quantity and is defined as the temperature at which the folded and unfolded state are equally populated in the sample. Higher the T_m value greater is the thermally stability of the protein. According to the theory the observed thermal stability of protein in the presence of osmolyte must be the consequence of increased surface tension at the protein surface but at the air-water interface it has been observed that with increase in glycerol concentration there is a continuous decrease in surface tension[48] as shown in Figure 1.1 which is against the proposal of the theory. Similarly, there were several other observations that can't be explained by this theory.

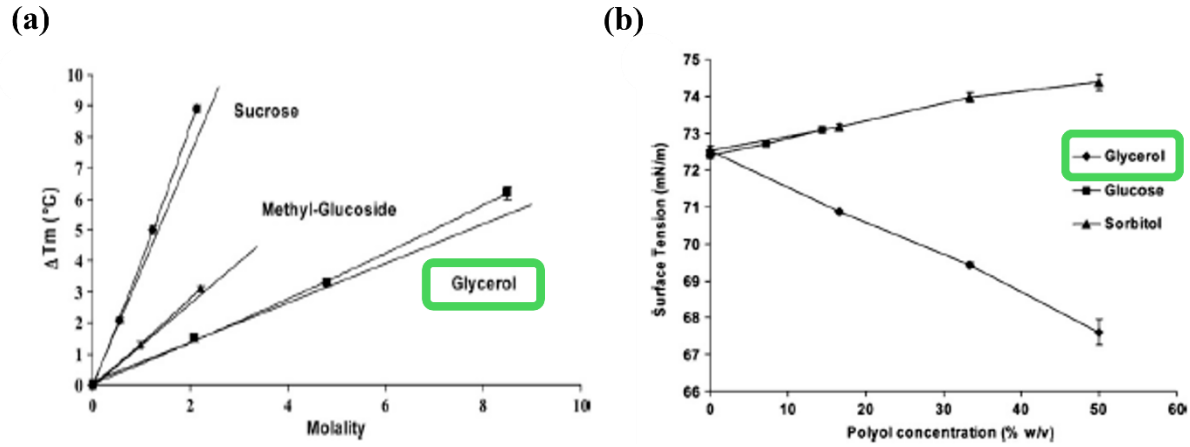

Figure 1.1: Modulation of the (a) extent of thermal stability of lysozyme and (b) surface tension with varying concentration of glycerol (taken from reference [48]).

1.3.3 Water Structure Modulation Theory

To explain the stabilizing effect of glycerol on thermal stability of protein, researchers explored the modulation in the properties of water on the addition of osmolyte. Self-diffusion ($\mathscr{D}_o$) coefficient is one such property of water that has been explored to observe the modulations in the dynamics and structure of water [47]. TMAO is a well-known protein stabilizer and with the increasing concentration of TMAO the thermal stability of protein enhances continuously. Researchers have found that on the addition of TMAO to water the self-diffusion coefficient of water molecules decreases continuously (Figure 1.2) confirmed by the relative self-diffusion coefficient ($\mathscr{D}/\mathscr{D}_o$) of water molecules [47]. Where $\mathscr{D}$ and $\mathscr{D}_o$ represents the self-diffusion coefficient of water molecules in neat water and in the presence of osmolyte. Value of relative self-diffusion coefficient of water molecules less than and greater than one represents slower and faster diffusion of water molecules in the presence of additive respectively [47,49]. Similar retardation in self-diffusion coefficient of water molecules in the presence of glycerol has also been observed a shown in Figure 1.2.

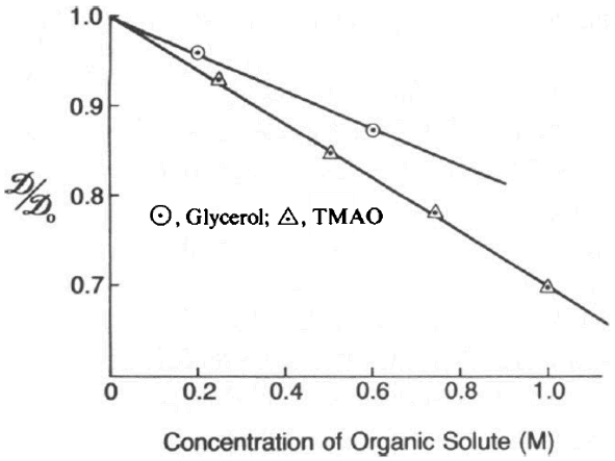

Figure 1.2: Modulation of the relative diffusion coefficient of water molecules in glycerol and TMAO (taken from reference [47]).

This retardation in self-diffusion coefficient of water has been linked with the thermal stabilization of protein by saying that the osmolyte stabilizes the protein by its structure making property of water. Similarly, the destabilizers are observed to show the water structure breaking property and by breaking the water structure these destabilizes the protein. Recently Hishida et al., probed the water dynamics around the osmolyte molecules by employing terahertz (THz) spectroscopy [50]. They successfully found a relation between the water dynamics and thermal stability of the protein, RNase A [50]. They have observed that the higher the retardation in the water dynamics around the osmolyte molecules, greater the thermal stabilization of the protein. In case of denaturants, they have observed the acceleration in the collective rotation dynamics of the water molecules. Whereas with other techniques researchers have observed opposite results. Rezus et al., employed polarization-resolved mid-infrared pump-probe spectroscopy to study the effect of urea on the structure and dynamics of water. They have observed that the orientational water dynamics in the presence of urea almost remains same as that in neat water [51]. Depending on the techniques the observations vary.

1.3.4 Limitations of the water structure modulation theory

Water structure modulation theory probes the water structure or dynamics directly to describe the effect of adding solute on the properties of water. This theory helps in understanding that osmolytes exert their effects on protein stability primarily through interactions mediated by water molecules, at least to a significant extent if not entirely. While this theory explicitly focuses on how added solutes affect water, it overlooks the protein's influence on water properties and its response to solute-induced changes [50–59]. This lack of perspective of protein in the theory prevents it from explaining the protein specific effects (described in chapters 3, 5 and 6 in detail) which includes, distinct response of protein towards same osmolyte, concentration dependent reversal of protein stabilization, protein dependent stabilization and destabilization in same osmolyte system[60] and so on.

However, despite its inability in describing the protein-osmolyte interactions completely, it successfully provides insights on the general effects of osmolyte mediated through modulation in water structure. To understand the protein-osmolyte interactions thoroughly the theory needs to be improved and must incorporate the perspective of proteins as well.

1.4 Associated water (Hydration Layer/ Biological water)

Water has always been found crucial for the existence of life. The folding of protein in a specific 3D structure has also been attributed to the involvement of water [61]. The water molecules attached to the protein surface are not free as these were in bulk [62]. The release of such water molecules in going from unfolded to folded conformation increases the entropy of the overall folding process and makes it thermodynamically favourable [61].

When a protein molecule comes into contact with water, it induces the formation of a structured layer composed of water molecules surrounding its surface. This layer, often referred to as the *hydration shell* or *associated water*, arises due to specific interactions between the polar, charged, and hydrophobic residues of the protein and the surrounding water molecules[63–65] as shown in Scheme 9.

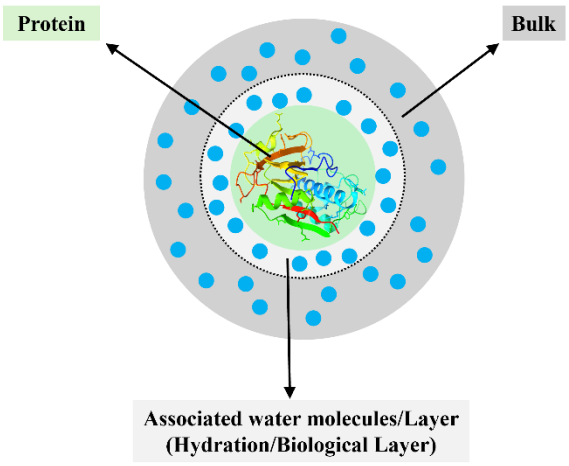

Scheme 9: Schematic representation of the associated water molecules/Layer around the protein surface.

The characteristics of this water layer is different than that of the bulk water. This water layer has already been shown to impact various aspects of protein among which the most important is the function of the protein. Hans Frauenfelder have shown experimentally that the binding of carbon monoxide (CO) molecule with myoglobin (Mb) is influenced by two types of motions of protein [66,67]. Former is the overall large-scale dynamics of protein which brings the CO molecule in the near vicinity of the active site and the latter is the small-scale fast dynamics of the protein around the active site controlled by the fluctuations in the hydration layer of the protein [67–69]. Later, Zhong has shown experimentally that the relaxation dynamics of water and protein are strongly coupled, and the fluctuations are predominantly governed by hydration water molecules on the picosecond timescale [70,71]. These are some crucial findings and there are plenty of other observations as well that supports the idea of water enslaved motions of protein [64,65,72–78].

The stability of the protein is also a crucial factor for its proper functioning. The bulk water is also observed to play an important role in defining the stability of protein in osmolyte system up to some extent. The lack of protein participation in the water structure modulation mechanism limits the ability of this model to fully explain protein–osmolyte interactions. Since it is well established that protein motions are influenced by the hydration layer, probing this layer in the presence of osmolytes could provide crucial insights into protein–osmolyte interactions as well. This forms the foundation of the present thesis, wherein the hydration layer, referred to as 'associated water' throughout, has been systematically investigated. The focus lies on understanding how osmolytes modulate the dynamics of this associated water. Particular attention is given to the protein interior, exploring how osmolyte-induced changes in associated water dynamics influence the core of the protein. This approach aims to reveal, at a molecular level, how such interactions ultimately affect the thermal stability of proteins in the presence of osmolytes. This theory has been referred as "*Associated Water Stabilization Mechanism*" and abbreviated as "*AWSM*". To the best of our knowledge, this work represents the first comprehensive investigation that offers molecular-level insights that encompass not only water dynamics but also the protein itself, advancing our understanding of their coupled dynamics in defining the protein-osmolyte interactions.

1.5 Limitations in the current understanding

As discussed, understanding protein–osmolyte interactions is crucial not only for elucidating biologically relevant mechanisms but also for advancing various industrial applications. The subject has remained a longstanding focus of research, with numerous studies dedicated to resolving the complexities involved. Yet, our understanding remains far from complete. The traditional theories generally fail to explain some of the key observations and that must be addressed to understand the mechanism completely.

1. The Necessity of a Unified Mechanism

The understanding of the protein-osmolyte interaction generally lacks a unified mechanism. Osmolytes are classified as stabilizing or destabilizing based on their effect on the thermal stability of proteins, those that enhance stability are termed as stabilizing osmolytes, while those that reduce it are considered destabilizing. Stabilizing osmolytes are generally believed to induce their effect on protein indirectly through water whereas the destabilizing osmolytes impart its destabilizing effect by directly interacting with the protein. Nevertheless, the fact that both stabilizing and destabilizing osmolytes influence water structure supports the notion of a common mechanistic framework.

2. **Protein dependent response of osmolyte**

It has been observed that the action of the osmolyte depends on the protein as well. The bromelain is observed to get destabilized whereas papain gets stabilized in the presence of sucrose which is not understandable by any of the traditional theories [79]. There are plenty of other examples where the protein is observed to get destabilized even in the presence of the stabilizing osmolyte and denaturants are observed to stabilize the protein in small concentrations which could not be explained by water structure modulation mechanism.

3. **Absence of molecular insights of the interior of the protein**

However, the water structure modulation hypothesis explains protein–osmolyte interactions based on the changes in water structure or dynamics induced by the presence of solutes. Yet, it lacks molecular-level insight into how these perturbations in water properties translate into changes in the thermal stability of proteins. This limitation represents a major drawback of the hypothesis, rendering it incomplete in fully describing protein–osmolyte interactions.

4. **Concentration dependent reversal of stabilization**

The stabilizing osmolytes strengthens the water structure which keeps on getting strengthened with increasing concentration and as per the water structure modulation hypothesis, the protein will also be get stabilized more with increasing concentration of osmolyte. But it has been observed that with some proteins the stability increases continuously with increase in concentration of osmolyte whereas with other proteins the stability first decreases and then increases. With some cases it has also been observed that the stability first increases and then deceases with higher concentration. Such observations are impossible to explain with water structure modulation hypothesis.

5. **Distinct response of proteins towards same osmolyte**

It has been observed that osmolytes can stabilize proteins; however, the extent of stabilization often varies depending on the specific protein. The traditional water structure modulation hypothesis claims that osmolytes influence water structure or dynamics in a manner that is independent of the protein. According to this view, the perturbation in water properties is determined solely by the nature and concentration of the osmolyte. Consequently, the theory predicts a uniform stabilizing effect across different proteins, regardless of their individual identity or characteristics. This is a general observation that appears to fall beyond the explanatory scope of the water structure modulation hypothesis.

6. **Counteraction effect of osmolytes by destabilizers**

It has been observed that destabilizing osmolytes (denaturants) can counteract or diminish the stabilizing effect of protective osmolytes on proteins [80–82]. This counteraction was initially attributed solely to direct interactions between the two types of osmolytes; however, this explanation has been challenged, as such interactions have been found to be weak and insufficient to account for the observed effects. Traditional theories also fall short in explaining these complex interactions. Considering the existing gaps in our current understanding of protein–osmolyte interactions, it becomes essential to seek for a comprehensive framework, one that

not only accounts for the phenomena explained by traditional theories but also addresses their inherent limitations.

1.6 Aim of the thesis

As previously noted, traditional theories fall short in describing protein-osmolyte interactions, either due to the technical limitations of the preferential interaction mechanism in probing surface tension at the protein-water interface, or because of the explicitly osmolyte-centric perspective adopted by the water structure modulation hypothesis. It is very well known that the osmolytes specially the stabilizing one imparts their effect on protein by staying away from the protein surface proved successfully by the preferential interaction mechanism. Water is the only component in the system that interact with both, the protein and the osmolyte, and thus the water structure modulation theory described the protein-osmolyte interaction in terms of the modulation in the properties of water where the water act as a mediator. Still the theory fails to explain the general protein-osmolyte interactions. Water obviously acts as a mediator here but to understand the interactions it must be the water that is influenced by both, the protein and the osmolyte.

Zewail, Bagchi, and Bhattacharyya proved independently that the surface of the protein is associated with a thin layer of water molecules, which is distinct in properties than that of the bulk. Later Frauenfelder observed the importance of this layer in describing the function of the protein. Zhong experimentally proved the notion of water enslaved motions of protein where the faster dynamics of the proteins are controlled by the dynamics of the water molecules in the hydration layer. These observations proved that the hydration layer is critical to the functioning of the protein and thus probing the hydration layer in the presence of osmolyte might help in understanding the protein osmolyte interaction in a better way as the water molecules in this hydration layer are in direct contact with the protein. The modulation in the water properties will be influenced by osmolyte and protein both. This approach may also offer molecular-level insights into how modulation of the

hydration layer (associated water) influences the thermal stability of proteins. Since protein dynamics are governed by the associated water, monitoring these dynamics can provide clues about how the protein interior responds to the presence of osmolytes. This approach can also help in understanding the observations that are not otherwise possible with traditional hypothesis.

The primary aim of this thesis is to develop a comprehensive understanding of protein-osmolyte interactions by focusing on the critical role of the hydration layer also known as associated water surrounding the protein surface. While traditional theories, such as the preferential interaction mechanism and the water structure modulation hypothesis, provide partial insights, they fall short in offering a unified molecular-level explanation. This work seeks to bridge that gap by investigating how osmolyte-induced perturbations in the hydration layer influence protein dynamics and thermal stability. By probing the dynamics of the associated water, which is jointly influenced by both the protein and the osmolyte, this thesis aims to unravel a more complete picture of the underlying mechanisms governing protein-osmolyte interactions, particularly those aspects that cannot be explained by existing models.

1.7 References

(1) Banani, S. F.; Lee, H. O.; Hyman, A. A.; Rosen, M. K. Biomolecular Condensates: Organizers of Cellular Biochemistry. *Nature Reviews Molecular Cell Biology*. Nature Publishing Group May 1, 2017, pp 285–298. https://doi.org/10.1038/nrm.2017.7.

(2) Klumpp, S. Transcription-Translation Coupling: Traveling a Road under Construction. *Biophysical Journal*. Biophysical Society January 3, 2023, pp 1–3. https://doi.org/10.1016/j.bpj.2022.12.006.

(3) Wolf, M. B. Whole Body Acid-Base and FLuid-Electrolyte Balance: A Mathematical Model. *Am J Physiol Renal Physiol* **2013**, *305*, 1118–1131. https://doi.org/10.1152/ajprenal.00195.2013.-A.

(4) Demling, R. H. *Nutrition, Anabolism, and the Wound Healing Process: An Overview*; 2009.

(5) Kirschning, A. On the Evolutionary History of the Twenty Encoded Amino Acids. *Chemistry - A European Journal*. John Wiley and Sons Inc October 4, 2022. https://doi.org/10.1002/chem.202201419.

(6) Spencer, P. S.; Barral, J. M. Genetic Code Redundancy and Its Influence on the Encoded Polypeptides. *Computational and Structural Biotechnology Journal*. Elsevier B.V. 2012, p e201204006. https://doi.org/10.5936/csbj.201204006.

(7) Eisenberg, D. *The Discovery of The-Helix and-Sheet, the Principal Structural Features of Proteins*; 2003. www.pnas.orgcgidoi10.1073pnas.2034522100.

(8) Yu, P. Protein Secondary Structures (α-Helix and β-Sheet) at a Cellular Level and Protein Fractions in Relation to Rumen Degradation Behaviours

of Protein: A New Approach. *British Journal of Nutrition* **2005**, *94* (5), 655–665. https://doi.org/10.1079/bjn20051532.

(9) Haider, T.; Akram, W.; Joshi, R.; Vishwakarma, M.; Saraf, S.; Soni, V.; Garud, N. Unlocking the Secrets: Structure-Function Dynamics of Plant Proteins. *Colloids and Surfaces B: Biointerfaces*. Elsevier B.V. October 1, 2025. https://doi.org/10.1016/j.colsurfb.2025.114791.

(10) Veenhoff, L. M.; Heuberger, E. H. M. L.; Poolman, B. *Quaternary Structure and Function of Transport Proteins*; 2002; Vol. 27. http://tibs.trends.com0968-0004/02/$-seefrontmatter.

(11) Janin, J.; Bahadur, R. P.; Chakrabarti, P. Protein-Protein Interaction and Quaternary Structure. *Quarterly Reviews of Biophysics*. May 2008, pp 133–180. https://doi.org/10.1017/S0033583508004708.

(12) Koehler Leman, J.; Szczerbiak, P.; Renfrew, P. D.; Gligorijevic, V.; Berenberg, D.; Vatanen, T.; Taylor, B. C.; Chandler, C.; Janssen, S.; Pataki, A.; Carriero, N.; Fisk, I.; Xavier, R. J.; Knight, R.; Bonneau, R.; Kosciolek, T. Sequence-Structure-Function Relationships in the Microbial Protein Universe. *Nat Commun* **2023**, *14* (1). https://doi.org/10.1038/s41467-023-37896-w.

(13) Lin, B.; Luo, X.; Liu, Y.; Jin, X. A Comprehensive Review and Comparison of Existing Computational Methods for Protein Function Prediction. *Briefings in Bioinformatics*. Oxford University Press July 1, 2024. https://doi.org/10.1093/bib/bbae289.

(14) Lombard, V.; Grudinin, S.; Laine, E. Explaining Conformational Diversity in Protein Families through Molecular Motions. *Sci Data* **2024**, *11* (1). https://doi.org/10.1038/s41597-024-03524-5.

(15) Morris, R.; Black, K. A.; Stollar, E. J. Uncovering Protein Function: From Classification to Complexes. *Essays in Biochemistry*. Portland Press Ltd August 1, 2022, pp 255–285. https://doi.org/10.1042/EBC20200108.

(16) Gambardella, G.; Notari, S.; Cavaterra, D.; Iavarone, F.; Castagnola, M.; Bocedi, A.; Ricci, G. The Anfinsen Dogma: Intriguing Details Sixty-Five Years Later. *Int J Mol Sci* **2022**, *23* (14). https://doi.org/10.3390/ijms23147759.

(17) Masson, P.; Lushchekina, S. Conformational Stability and Denaturation Processes of Proteins Investigated by Electrophoresis under Extreme Conditions. *Molecules*. MDPI October 1, 2022. https://doi.org/10.3390/molecules27206861.

(18) Ahmad, F. Protein Stability [Determination] Problems. *Front Mol Biosci* **2022**, *9*. https://doi.org/10.3389/fmolb.2022.880358.

(19) Kamerzell, T. J.; Middaugh, C. R. The Complex Inter-Relationships between Protein Flexibility and Stability. *J Pharm Sci* **2008**, *97* (9), 3494–3517. https://doi.org/10.1002/jps.21269.

(20) Soulages, J. L. Chemical Denaturation: Potential Impact of Undetected Intermediates in the Free Energy of Unfolding and m-Values Obtained from a Two-State Assumption. *Biophys J* **1998**, *75* (1), 484–492. https://doi.org/10.1016/S0006-3495(98)77537-X.

(21) Fersht, A. R.; Daggett, V. *Protein Folding and Unfolding at Atomic Resolution*; 2002; Vol. 108.

(22) Sosnick, T. R.; Baxa, M. C. Collapse and Protein Folding: Should We Be Surprised That Biothermodynamics Works So Well? **2025**, *53*, 44. https://doi.org/10.1146/annurev-biophys-080124.

(23) Pace, C. N.; Fu, H.; Fryar, K. L.; Landua, J.; Trevino, S. R.; Schell, D.; Thurlkill, R. L.; Imura, S.; Scholtz, J. M.; Gajiwala, K.; Sevcik, J.; Urbanikova, L.; Myers, J. K.; Takano, K.; Hebert, E. J.; Shirley, B. A.; Grimsley, G. R. Contribution of Hydrogen Bonds to Protein Stability. *Protein Science* **2014**, *23* (5), 652–661. https://doi.org/10.1002/pro.2449.

(24) Wang, M.; Wales, T. E.; Fitzgerald, M. C. *Conserved Thermodynamic Contributions of Backbone Hydrogen Bonds in a Protein Fold*; 2006; Vol. 103. www.pnas.orgcgidoi10.1073pnas.0508121103.

(25) Myers, J. K.; Pace, C. N. Hydrogen Bonding Stabilizes Globular Proteins. *Biophys J* **1996**, *71* (4), 2033–2039. https://doi.org/10.1016/S0006-3495(96)79401-8.

(26) Masson, P.; Lushchekina, S. Conformational Stability and Denaturation Processes of Proteins Investigated by Electrophoresis under Extreme Conditions. *Molecules* **2022**, *27* (20), 6861. https://doi.org/10.3390/molecules27206861.

(27) Bryngelson, J. D.; Onuchic, J. N.; Socci, N. D.; Wolynes, P. G. Funnels, Pathways, and the Energy Landscape of Protein Folding: A Synthesis. *Proteins: Structure, Function, and Bioinformatics* **1995**, *21* (3), 167–195. https://doi.org/10.1002/prot.340210302.

(28) Dobson, C. Protein Folding and Misfolding.

(29) Verkman, A. S. Aquaporins at a Glance. *J Cell Sci* **2011**, *124* (13), 2107–2112. https://doi.org/10.1242/jcs.079467.

(30) Singer, S. J.; Nicolson, G. L. *The Fluid Mosaic Model of the Structure of Cell Membranes*. https://www.science.org.

(31) Tirindelli, R.; Dibattista, M.; Pifferi, S.; Menini, A. From Pheromones to Behavior. **2009**. https://doi.org/10.1152/physrev.00037.2008.-In.

(32) Božič, B.; Zemljič Jokhadar, S.; Kristanc, L.; Gomišček, G. Cell Volume Changes and Membrane Ruptures Induced by Hypotonic Electrolyte and Sugar Solutions. *Front Physiol* **2020**, *11*. https://doi.org/10.3389/fphys.2020.582781.

(33) Ranklin, F.; Pstein, H. E.; Ichael, M.; Anus, M.; Hurchwell, E. B. C.; Trange, S. *MECHANISMS OF DISEASE REVIEW ARTICLES REGULATION OF CELL VOLUME IN HEALTH AND DISEASE*.

(34) Burg, M. B.; Ferraris, J. D. Intracellular Organic Osmolytes: Function and Regulation. *Journal of Biological Chemistry*. March 21, 2008, pp 7309–7313. https://doi.org/10.1074/jbc.R700042200.

(35) Yancey, P. H. Organic Osmolytes as Compatible, Metabolic and Counteracting Cytoprotectants in High Osmolarity and Other Stresses. *J. Exp. Biol*. August 2005, pp 2819–2830. https://doi.org/10.1242/jeb.01730.

(36) Khan, S.; Siraj, S.; Shahid, M.; Haque, M. M.; Islam, A. Osmolytes: Wonder Molecules to Combat Protein Misfolding against Stress Conditions. *Int. J. Biol. Macromol* **2023**, *234*, 123662. https://doi.org/10.1016/j.ijbiomac.2023.123662.

(37) Wlodarczyk, S. R.; Custódio, D.; Pessoa, A.; Monteiro, G. Influence and Effect of Osmolytes in Biopharmaceutical Formulations. *Eur. J. Pharm. Biopharm.* **2018**, *131* (June), 92–98. https://doi.org/10.1016/j.ejpb.2018.07.019.

(38) Timasheff, S. N. *THE CONTROL OF PROTEIN STABILITY AND ASSOCIATION BY WEAK INTERACTIONS WITH WATER: How Do Solvents Affect These Processes?*; 2025. www.annualreviews.org.

(39) Arakawa, T.; Timasheff, S. N. The Stabilization of Proteins by Osmolytes. *Biophys. J* **1985**, *47* (3), 411–414. https://doi.org/10.1016/S0006-3495(85)83932-1.

(40) Lee, J. C.; Timasheff, S. N. The Stabilization of Proteins by Sucrose. *J. Biol. Chem.* **1981**, *256* (14), 7193–7201. https://doi.org/10.1016/s0021-9258(19)68947-7.

(41) Timasheff, S. N. Water as Ligand: Preferential Binding and Exclusion of Denaturants in Protein Unfolding. *Biochemistry* **1992**, *31* (41), 9857–9864.

(42) Noelken, M. E.; Timasheff, S. N. Preferential Solvation of Bovine Serum Albumin in Aqueous Guanidine Hydrochloride. *J Biol Chem* **1967**, *242* (21), 5080–5085. https://doi.org/10.1016/s0021-9258(18)99478-0.

(43) Feeney, J.; Fisher, G. H.; Ryan, J. W.; Berryer, P.; Chung, A.; Kozlowski, H.; Formicka-Kozlowska, G.; Jezowska-Trze-Biatowska, B.; Lintner, K.; Fermandjian, S.; Regoli, D.; Barabe, J.; London, R. E.; Stewart, J. M.; Cann, J. R.; Matwiyoff, N. A.; Marlborough, D. L.; Felix, A. M.; Paiva, A. C. M.; Juliano, L.; Ptak, M.; Heitz, A.; Dreux, M. *Stabilization of Protein Structure by Sugars*; Elsevier, 1982; Vol. 21. https://pubs.acs.org/sharingguidelines.

(44) Bolen, D. W. The Peptide Backbone Plays a Dominant Role in Protein Stabilization by Naturally Occurring Osmolytes. *Biochemistry* **1995**, *34* (39), 12884–12891.

(45) Santoro, M.; Liu, Y.; A Khan, S. M.; Hou, L.-X.; Bolen, D. W. Increased Thermal Stability of Proteins in the Presence of Naturally Occurring Osmolytes. *Biochemistry* **1992**, *31* (23), 5278–5283.

(46) Lin' And, T.-Y.; Timasheff, S. N. *On the Role of Surface Tension in the Stabilization of Globular Proteins*; Cambridge University Press, 1996; Vol. 5.

(47) Clark, M. E.; Burnell, E. E.; Chapman, N. R.; Hinke, J. A. Water in Barnacle Muscle. IV. Factors Contributing to Reduced Self-Diffusion. *Biophys J* **1982**, *39* (3), 289–299. https://doi.org/10.1016/S0006-3495(82)84519-0.

(48) Kumar, V.; Chari, R.; Sharma, V. K.; Kalonia, D. S. Modulation of the Thermodynamic Stability of Proteins by Polyols: Significance of Polyol Hydrophobicity and Impact on the Chemical Potential of Water. *Int J Pharm* **2011**, *413* (1–2), 19–28. https://doi.org/10.1016/j.ijpharm.2011.04.011.

(49) Sacco, A.; Asciolla, A.; Matteolib, E.; Holz, M. *NMR Study of the Influence of Urea on the Self-Association of Propan-1-01 in Water and Comparison with Kirkwood-Buff Integral Results*.

(50) Hishida, M.; Anjum, R.; Anada, T.; Murakami, D.; Tanaka, M. Effect of Osmolytes on Water Mobility Correlates with Their Stabilizing Effect on Proteins. *J. Phys. Chem. B* **2022**, *126* (13), 2466–2475. https://doi.org/10.1021/acs.jpcb.1c10634.

(51) Rezus, Y. L. A.; Bakker, H. J. Effect of Urea on the Structural Dynamics of Water. *Proc. Natl. Acad. Sci* **2006**, *103* (49), 18417–18420.

(52) Hishida, M.; Anjum, R.; Anada, T.; Murakami, D.; Tanaka, M. Effect of Osmolytes on Water Mobility Correlates with Their Stabilizing Effect on Proteins. *Journal of Physical Chemistry B* **2022**, *126* (13), 2466–2475. https://doi.org/10.1021/acs.jpcb.1c10634.

(53) Higuchi, Y.; Saleh, M. A.; Anada, T.; Tanaka, M.; Hishida, M. Rotational Dynamics of Water near Osmolytes by Molecular Dynamics Simulations. *Journal of Physical Chemistry B* **2024**, *128* (20), 5008–5017. https://doi.org/10.1021/acs.jpcb.3c08470.

(54) Hishida, M.; Kaneko, A.; Yamamura, Y.; Saito, K. Contrasting Changes in Strongly and Weakly Bound Hydration Water of a Protein upon Denaturation. *J Phys Chem B* **2023**, *127* (28), 6296–6305. https://doi.org/10.1021/acs.jpcb.3c02970.

(55) Funkner, S.; Havenith, M.; Schwaab, G. Urea, a Structure Breaker? Answers from THz Absorption Spectroscopy. *J. Phys. Chem. B* **2012**, *116* (45), 13374–13380. https://doi.org/10.1021/jp308699w.

(56) Shukla, N.; Narayan Bhatt, A.; Aliverti, A.; Zanetti, G.; Bhakuni, V. Guanidinium Chloride-and Urea-Induced Unfolding of FprA, a Mycobacterium NADPH-Ferredoxin Reductase Stabilization of an Apo-Protein by GdmCl. *FEBS J* **2005**, *272* (9), 2216–2224. https://doi.org/10.1111/j.1742-4658.2005.04645.x.

(57) Batchelor, J. D.; Olteanu, A.; Tripathy, A.; Pielak, G. J. Impact of Protein Denaturants and Stabilizers on Water Structure. *J Am Chem Soc* **2004**, *126* (7), 1958–1961. https://doi.org/10.1021/ja039335h.

(58) Verma, P. K.; Lee, H.; Park, J. Y.; Lim, J. H.; Maj, M.; Choi, J. H.; Kwak, K. W.; Cho, M. Modulation of the Hydrogen Bonding Structure of Water by Renal Osmolytes. *J. Phys. Chem. Lett* **2015**, *6* (14), 2273–2279. https://doi.org/10.1021/acs.jpclett.5b01087.

(59) Heugen, U.; Schwaab, G.; Brü, E.; Heyden, M.; Yu, X.; Leitner, D. M.; Havenith, M. Solute-Induced Retardation of Water Dynamics Probed Directly by Terahertz Spectroscopy. *Proc. Natl. Acad. Sci. U. S. A.* **2006**, *103* (33), 12301–12306.

(60) Negi, K. S.; Das, N.; Khan, T.; Sen, P. Osmolyte Induced Protein Stabilization: Modulation of Associated Water Dynamics Might Be a Key Factor. *Phys. Chem. Chem. Phys* **2023**, *25* (47), 32602–32612. https://doi.org/10.1039/d3cp03357k.

(61) Rani, A.; Venkatesu, P. Changing Relations between Proteins and Osmolytes: A Choice of Nature. *Phys. Chem. Chem. Phys*. Royal Society of Chemistry 2018, pp 20315–20333. https://doi.org/10.1039/c8cp02949k.

(62) Nandi, N.; Bagchi, B. Dielectric Relaxation of Biological Water. *J Phys Chem B* **1997**, *101* (50), 10954–10961.

(63) Kumar, S.; Peon, J.; Zewail, A. H. Biological Water at the Protein Surface: Dynamical Solvation Probed Directly with Femtosecond Resolution. *Proc. Natl. Acad. Sci. U. S. A.* **2002**, *99* (4), 1763–1768.

(64) Bhattacharyya, S. M.; Wang, Z. G.; Zewail, A. H. Dynamics of Water near a Protein Surface. *J. Phys. Chem. B* **2003**, *107* (47), 13218–13228. https://doi.org/10.1021/jp030943t.

(65) Mukherjee, S.; Mondal, S.; Bagchi, B. Distinguishing Dynamical Features of Water inside Protein Hydration Layer: Distribution Reveals What Is Hidden behind the Average. *J. Chem. Phys* **2017**, *147* (2), 024901. https://doi.org/10.1063/1.4990693.

(66) Frauenfelder, H.; Chen, G.; Berendzen, J.; Fenimore, P. W.; Jansson, H.; McMahon, B. H.; Stroe, I. R.; Swenson, J.; Young, R. D. A Unified Model of Protein Dynamics. *Proc. Natl. Acad. Sci. U. S. A.* **2009**, *106* (13), 5129–5134. https://doi.org/10.1073/pnas.0900336106.

(67) McMahon, B. H.; Frauenfelder, H.; Fenimore, P. W. The Role of Continuous and Discrete Water Structures in Protein Function. *Eur. Phys. J. Spec. Top* **2014**, *223* (5), 915–926. https://doi.org/10.1140/epjst/e2014-02125-y.

(68) Frauenfelder, H.; Fenimore, P. W.; McMahon, B. H. Hydration, Slaving and Protein Function. *Biophys. Chem.* **2002**, *98* (1–2), 35–48. https://doi.org/10.1016/S0301-4622(02)00083-2.

(69) Fenimore, P. W.; Frauenfelder, H.; McMahon, B. H.; Young, R. D. Bulk-Solvent and Hydration-Shell Fluctuations, Similar to α- and β-Fluctuations in Glasses, Control Protein Motions and Functions. *Proc. Natl. Acad. Sci. U. S. A.* **2004**, *101* (40), 14408–14413. https://doi.org/10.1073/pnas.0405573101.

(70) Qin, Y.; Jia, M.; Yang, J.; Wang, D.; Wang, L.; Xu, J.; Zhong, D. Molecular Origin of Ultrafast Water-Protein Coupled Interactions. *Journal of Physical Chemistry Letters* **2016**, *7* (20), 4171–4177. https://doi.org/10.1021/acs.jpclett.6b01954.

(71) Qin, Y.; Wang, L.; Zhong, D. Dynamics and Mechanism of Ultrafast Water-Protein Interactions. *Proc Natl Acad Sci U S A* **2016**, *113* (30), 8424–8429. https://doi.org/10.1073/pnas.1602916113.

(72) Qiu, W.; Zhang, L.; Okobiah, O.; Yang, Y.; Wang, L.; Zhong, D.; Zewail, A. H. Ultrafast Solvation Dynamics of Human Serum Albumin: Correlations with Conformational Transitions and Site-Selected Recognition. *J. Phys. Chem. B* **2006**, *110* (21), 10540–10549. https://doi.org/10.1021/jp055989w.

(73) Zhang Luyuan; Wang Lijuan; Kao Ya-Ting; Qiu Weihong; Yang Yi; Okobiah Oghaghare; Zhong Dongping. Mapping Hydration Dynamics around a Protein Surface. *Proc. Natl. Acad. Sci. U. S. A.* **2007**, *104* (47), 18461–18466.

(74) Houston, P.; Macro, N.; Kang, M.; Chen, L.; Yang, J.; Wang, L.; Wu, Z.; Zhong, D. Ultrafast Dynamics of Water-Protein Coupled Motions around the Surface of Eye Crystallin. *J. Am. Chem. Soc.* **2020**, *142* (8), 3997–4007. https://doi.org/10.1021/jacs.9b13506.

(75) Nandy, A.; Chakraborty, S.; Nandi, S.; Bhattacharyya, K.; Mukherjee, S. Structure, Activity, and Dynamics of Human Serum Albumin in a Crowded Pluronic F127 Hydrogel. *J. Phys. Chem. B* **2019**, *123* (16), 3397–3408. https://doi.org/10.1021/acs.jpcb.9b00219.

(76) Sen, P.; Roy, D.; Sahu, K.; Mondal, S. K.; Bhattacharyya, K. Hydration Dynamics of a Protein in the Presence of Urea and Sodium Dodecyl Sulfate. *Chem Phys Lett* **2004**, *395* (1–3), 58–63. https://doi.org/10.1016/j.cplett.2004.07.052.

(77) Dutta, P.; Sen, P.; Halder, A.; Mukherjee, S.; Sen, S.; Bhattacharyya, K. Solvation Dynamics in a Protein-Surfactant Complex. *Chem Phys Lett* **2003**, *377* (1–2), 229–235. https://doi.org/10.1016/S0009-2614(03)01143-6.

(78) Sen, P.; Mukherjee, S.; Dutta, P.; Halder, A.; Mandal, D.; Banerjee, R.; Roy, S.; Bhattacharyya, K. Solvation Dynamics in the Molten Globule State of a Protein. *J. Phys. Chem. B* **2003**, *107* (51), 14563–14568. https://doi.org/10.1021/jp036277d.

(79) Habib, S.; Khan, M. A.; Younus, H. Thermal Destabilization of Stem Bromelain by Trehalose. *Protein J* **2007**, *26* (2), 117–124. https://doi.org/10.1007/s10930-006-9052-1.

(80) Lin, T.; Timasheff, S. N. Why Do Some Organisms Use a Urea-Methylamine Mixture as Osmolyte? Thermodynamic Compensation of Urea and Trimethylamine N-Oxide Interactions with Protein. *Biochemistry* **1994**, *33* (42), 12695–12701.

(81) Mondal, J.; Stirnemann, G.; Berne, B. J. When Does Trimethylamine N-Oxide Fold a Polymer Chain and Urea Unfold It? *J. Phys. Chem. B* **2013**, *117* (29), 8723–8732. https://doi.org/10.1021/jp405609j.

(82) Nasralla, M.; Laurent, H.; Baker, D. L.; Ries, M. E.; Dougan, L. A Study of the Interaction between TMAO and Urea in Water Using NMR Spectroscopy. *Phys. Chem. Chem. Phys* **2022**, *24* (35), 21216–21222. https://doi.org/10.1039/d2cp02475f.

Chapter 2

Experimental

- **Steady-State Absorption and Emission Spectra**
- **Circular Dichroism Spectroscopy**
- **TCSPC**
- **Fluorescence Up conversion**
- **Time-Resolved Emission Spectra**
- **Transient Absorption Spectroscopy**
- **Fluorescence Correlation Spectroscopy**
- **Bulk Viscosity**
- **Protein Tagging**
- **Some Control Experiments Related to Tagging**
- **Materials**
- **Sample Preparations**
- **References**

This page left blank intentionally

2.1 Steady-State Absorption and Emission Spectra:

All steady-state absorption measurements were carried out using a Shimadzu UV-2450 UV–Vis spectrophotometer (Japan). Emission spectra were acquired on a Fluoromax-4 spectrofluorometer (Horiba Jobin Yvon). The recorded emission intensities were corrected for the wavelength-dependent response of the detector and monochromator using the relation S1C/R1, where S1 represents the raw emission signal, C is the correction factor for the system response, and R1 corresponds to the lamp profile. Sample concentrations were optimized to maintain absorbance values below 0.2, thereby reducing potential inner filter effects and self-quenching. Control (blank) spectra were recorded and subtracted where necessary. For temperature-dependent measurements, a Peltier-based temperature controller (TCC-100, Shimadzu, Japan), offering ±0.5 °C accuracy, was employed in conjunction with the spectrophotometer and spectrofluorometer.

2.2. Circular Dichroism Spectroscopy

Circular dichroism (CD) spectra were recorded using a J-815 spectropolarimeter (Jasco, Japan) fitted with a quartz cuvette of 0.2 cm pathlength. A corresponding blank—containing all components except the protein—was used for baseline correction by subtracting it from the sample spectra. Each final spectrum represents an average of three accumulations to enhance signal reliability.

The principle of CD is based on the differential absorption of left- and right-circularly polarized light by chiral molecules, resulting in a characteristic CD signal[10]. This technique is particularly well-suited for investigating the secondary and tertiary structures of biomolecules, as distinct structural motifs—such as α-helices, β-sheets, and random coils—produce unique spectral signatures[11]. Specifically, α-helical structures show strong negative bands around 208 nm and 222 nm[12,13], while β-sheets are typically identified by a negative band at approximately 218 nm and a positive band near 195 nm[13,14]. Several computational approaches are

available to interpret CD spectra and estimate secondary structure content. In this thesis, the freely available CDNN software was used for deconvoluting the CD data and quantifying the relative amounts of different secondary structures[15]. Additionally, the temperature-dependent change in ellipticity at 222 nm was tracked to monitor variations in α-helical content, which served as a key indicator in the subsequent thermodynamic analyses.

2.3. Time-resolved fluorescence Measurement using Time-Correlated Single Photon Counting (TCSPC)

Time-resolved fluorescence techniques are employed to measure the average time a molecule spends in its excited state, known as the fluorescence lifetime. Various experimental approaches are available for determining this parameter, including time-correlated single-photon counting (TCSPC), fluorescence up-conversion, and streak camera methods. In this study, fluorescence lifetimes were primarily obtained using a TCSPC setup with an instrument response function (IRF) of approximately 75 picoseconds. Additionally, in one part of the work, femtosecond-resolved fluorescence up-conversion spectroscopy was employed, offering an IRF of ~300 femtoseconds for capturing ultrafast dynamics.

2.3.1. Brief Theory of TCSPC

Time-Correlated Single Photon Counting (TCSPC) is among the commonly employed techniques for time-resolved fluorescence analysis, and its theoretical and practical aspects are well documented in several specialized texts[16–18]. In TCSPC, the time delay (t) between the excitation pulse and the detection of the first emitted photon is measured. The probability of detecting a photon at a specific time point t directly corresponds to the fluorescence intensity at that moment.

Due to the inherently stochastic nature of fluorescence, photon emission occurs from various relaxation pathways following excitation to the Franck–Condon region,

resulting in a temporally distributed photon emission pattern referred to as the fluorescence decay. By collecting a large number of such single-photon detection events across many excitation cycles, a statistical decay curve is generated. This decay curve is subsequently analysed to estimate the average lifetime that a fluorophore spends in its electronically excited state.

2.3.2. Schematic Representation of the TCSPC Setup

A schematic overview of the Time-Correlated Single-Photon Counting (TCSPC) setup is provided in Scheme 2.3. This technique enables precise measurement of photon arrival times following excitation of the sample by a pulsed light source. Upon each excitation event, a trigger signal is generated and processed through a series of electronic modules. The constant fraction discriminator (CFD) first determines the exact timing of the excitation pulse, which then initiates the time-to-amplitude converter (TAC) by starting a linear voltage ramp on a capacitor. Meanwhile, fluorescence photons emitted from the sample are detected, and the arrival signal is also routed through the CFD, which stops the TAC ramp, capturing the time interval between excitation and emission.

The emitted photons are wavelength-selected using a monochromator (MC) and subsequently detected by a multichannel plate photomultiplier tube (MCP PMT), capable of registering single-photon events. One of the challenges in TCSPC is the timing uncertainty introduced by variations in signal amplitude and source jitter, which collectively broaden the instrument response function (IRF). To minimize this, the CFD separates the input signal into two parts one delayed and the other inverted and then recombines them. This configuration stabilizes the zero-crossing point and makes the timing signal largely independent of amplitude fluctuations[19].

To maintain the single photon counting regime, experimental conditions are adjusted so that, on average, one photon is detected for every 100 excitation pulses. The output voltage from the TAC proportional to the delay between excitation and

emissionis amplified and digitized by an analog-to-digital converter (ADC), with each digital value representing a single photon detection event. These events are categorized into time bins by a multichannel analyzer (MCA) according to their arrival times. The system used in this study accommodates up to 4096 channels, yielding a temporal resolution of 4.88 picoseconds per channel over a 20-nanosecond TAC range.

To determine fluorescence lifetimes with high precision, a decay histogram is constructed by plotting photon counts as a function of time delay. This decay curve reflects the time-resolved emission profile of the fluorophore. For accurate lifetime extraction, the emission polarizer is positioned at the magic angle (54.9°) relative to the excitation polarizer, ensuring elimination of rotational diffusion artifacts. All TCSPC measurements presented in this thesis were conducted using a commercial system (LifeSpec II, Edinburgh Instruments, U.K.).

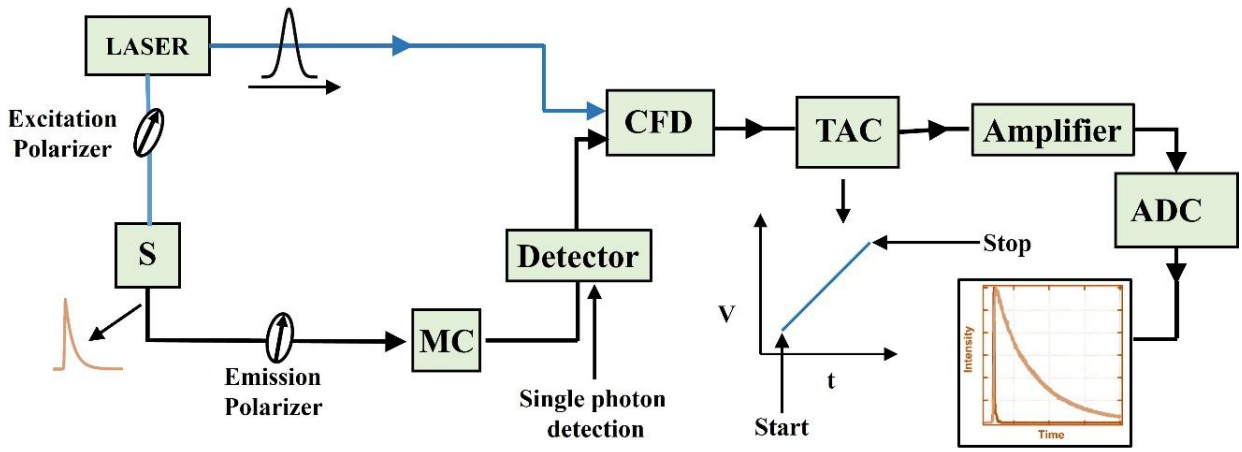

Scheme 2.3. A schematic representation of the TCSPC instrument. Abbreviations: CFD: Constant Fraction Discriminator, S: Sample holder, TAC: Time to Amplitude Converter, MC: Monochromator, ADC: Analogue to digital converter.

2.3.3. TCSPC data analysis

The time-resolved fluorescence decay profile obtained through TCSPC can be quantitatively analyzed using suitable mathematical models to extract the

fluorescence lifetime of a sample. Prior to this analysis, it is essential to account for contributions from the excitation laser pulse and the finite temporal resolution of the detection system. Although decay analysis typically assumes that the excitation pulse is a delta function, real-world laser pulses have a measurable duration.

To correct for these instrumental effects, the instrument response function (IRF) is recorded using a scatterer—commonly colloidal silica (Ludox) or diluted milk—which serves as a reference with effectively zero fluorescence lifetime. This IRF is then used during deconvolution to correct the raw fluorescence decay signal. The deconvolution approach treats the finite-width excitation pulse as a sequence of weighted delta functions. Accordingly, the observed fluorescence intensity at any time point *t* is modeled as the sum of the system's responses to each of these delta components, a process mathematically described in detail elsewhere[16,18].

$$N(t) = \int_0^t L(t')I(t-t')\,dt' \qquad (2.1)$$

where, $I(t-t')$ represents the fluorescence intensity of the sample at time t, resulting from an excitation pulse of amplitude $L(t')$ at time t'. This relationship, referred to as the convolution integral, serves as the foundation for extracting the most suitable decay function from the experimental data. While fitting a single-exponential decay is relatively simple and often sufficient, the use of multi-exponential models introduces additional complexity. Therefore, higher-order exponential fits should be employed only when lower-order models fail to adequately capture the characteristics of the measured decay profile.

The deconvolution process employs an iterative least-squares reconvolution method[16,17,19]. Once both the instrument response function (IRF) and the experimental fluorescence decay curve have been acquired, a theoretical decay model is convolved with the IRF to generate a simulated decay profile. This reconvoluted curve is then compared to the measured data, and the difference between the two is quantified using the χ^2 (chi-squared) statistic, which serves as a measure of the goodness of fit.

$$\chi^2 = \sum_{k=0}^{n} \frac{1}{\sigma_k^2} [F(t_k) - F_P(t_k)]^2 \quad (2.2)$$

where, $F(t_k)$ and $F_P(t_k)$ represent the experimental and projected fluorescence intensities at two different times, n is the number of data points and σ_k is the standard deviation of each data point. Since TCSPC follows Poisson statistics, the standard deviation is given by

$$\sigma_k = [N(t_k)]^{\frac{1}{2}} \quad (2.3)$$

Where, N is taken as the number of channels used for measurement.

The reconvolution process and χ^2 calculations continue iteratively until successive iterations yield negligible improvement. Once the fitting process converges, a reduced chi-square value (χ_r) is computed as:

$$\chi_r^2 = \frac{\chi^2}{n-f} = \frac{\chi^2}{\nu} \quad (2.4)$$

where ν is the degree of freedom, which is the difference between the number of data points (n) and the floating parameters (f). The software, FAST (provided by the instrument manufacturer), has been used in this thesis to analyze and extract the time components of the fluorescence transients measured by TCSPC.

2.4. Time-resolved fluorescence Measurement using Fluorescence Up-conversion Spectroscopy:

Femtosecond fluorescence up-conversion is a highly sensitive technique used to probe ultrafast photophysical and photochemical events. It enables the exploration of excited-state molecular dynamics with temporal resolution on the sub-picosecond scale, making it particularly valuable for investigating key processes such as energy transfer, charge separation, and relaxation pathways.

2.4.1. Basic principle of fluorescence up-conversion

The fundamental working principle of femtosecond fluorescence up-conversion is based on the nonlinear optical phenomenon known as sum-frequency generation[20–22]. In this technique, the sample is excited using the second harmonic output of a mode-locked Ti:Sapphire femtosecond laser operating at frequency ω_1[20–23]. The moment the excitation pulse interacts with the sample is designated as time zero, initiating fluorescence emission at frequency ω_2. This emitted light is then used in the sum-frequency mixing process for time-resolved detection.

A second pulse, derived from the fundamental laser output and known as the gate pulse, is introduced with a controlled temporal delay, arriving at the sample at time $t = \tau$. This delayed gate pulse is combined with the fluorescence emission from the sample, and the two pulses interact within a nonlinear optical medium typically a beta barium borate (BBO) crystal. Through this interaction, sum-frequency generation occurs, producing an up-converted signal at frequency ω_3, corresponding to a higher-energy photon that can be detected and analysed.

$$\omega_1 + \omega_2 = \omega_3 \tag{2.5}$$

The arrival time of the gate pulse at the nonlinear crystal is precisely controlled using a mechanical delay stage. Since fluorescence intensity varies over time according to the excited-state lifetime, the intensity of the emitted fluorescence and thus the intensity of the resulting sum-frequency signal is directly influenced by this temporal behavior. Mathematically, the intensity of the sum frequency light (I_{sum}) is proportional to both the intensity of the fluorescence (I_{fl}) and of the gate pulse (I_{gate}) as[22],

$$I_{sum} \propto \int_{-\infty}^{+\infty} I_{fl}(t) I_{gate}(t-\tau) dt \tag{2.6}$$

The sum frequency light is only generated when both the fluorescence and the gate pulse are present in the crystal.

2.4.2. Schematic Representation and a Brief Explanation of the Fluorescence Up-conversion Setup

A standard femtosecond fluorescence up-conversion setup consists of a femtosecond laser source, a mechanical delay stage for adjusting the time delay between the excitation and gate pulses, a nonlinear crystal for sum-frequency generation, and a detection unit—typically comprising a monochromator coupled with either a photomultiplier tube or a CCD camera (see scheme 2.4).

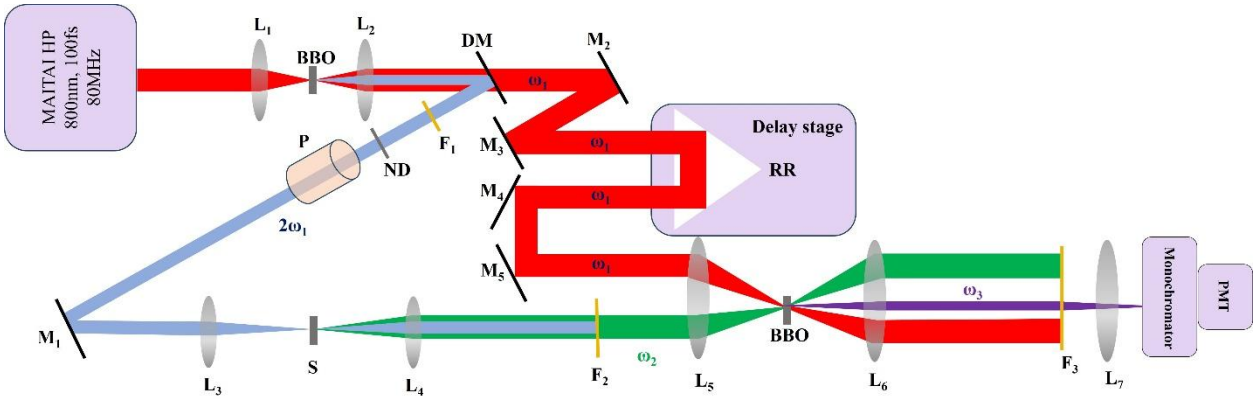

Scheme 2.4. A schematic representation of the fluorescence up-conversion instrument. Abbreviations: L_1, L_2, L_3, L_4, L_5, L_6, L_7: Lens, BBO: β-barium borate crystal, DM: Dichroic mirror/ Dichroic beamsplitter, M_1, M_2, M_3, M_4, M_5: Mirror, RR: roto reflector used to control delay, F_1, F_2, F_3: Filter to cut light of certain wavelength, ND: neutral density filter, P: Berek polarizer to adjust excitation light's polarization, S: Sample, PMT: Photomultiplier tube, ω_1: fundamental (excitation) light, ω_2: emitted light from the sample, ω_3: Sum frequency light.

The experimental setup is initiated using a mode-locked Ti:Sapphire laser (Mai-Tai HP, Spectra Physics, USA), which produces ultrafast pulses at a fundamental frequency (ω_1). Operating at an 80 MHz repetition rate with a pulse duration of 100 femtoseconds, this laser provides the high temporal resolution necessary for capturing rapid fluorescence dynamics. The fundamental beam (ω_1) is focused

through a lens (L1) onto a 0.2 mm thick β-barium borate (BBO) crystal, where second harmonic generation occurs, producing light at frequency $2\omega_1$. This frequency-doubled beam serves as the excitation source for the sample.

The $2\omega_1$. beam is directed through a lens (L2) and then reflected by a dichroic mirror (DM), which splits it into two components: the excitation and gate beams. The excitation beam is further processed through a cut-off filter (F_1) to eliminate residual fundamental light, a neutral density (ND) filter to control beam intensity, and a Berek compensator (P) to adjust the beam's polarization. This refined excitation light is then directed toward the rotating sample cell using a mirror (M_1) and focused via lens (L_3).

Upon absorbing the excitation pulse ($2\omega_1$), the sample transitions to an excited state and subsequently emits fluorescence at a longer wavelength (ω_2). This fluorescence is collected by lens (L_4) and passed through a second cut-off filter (F_2) to remove any remaining excitation light, ensuring only the emission signal is transmitted to the detection system.

The gate pulse (ω_1) is routed separately using mirrors (M_2 and M_3) toward a retro-reflector (RR) mounted on a computer-controlled mechanical delay stage. This configuration enables precise temporal control of the gate pulse, allowing it to overlap with the fluorescence emission at defined time intervals. Both the emitted fluorescence (ω_2) and the delayed gate pulse (ω_1) are then focused onto a second β-barium borate (BBO) crystal using lens L_5, where they undergo sum-frequency mixing—a nonlinear optical process that produces a new signal at frequency ω_3 ($\omega_1 + \omega_2$).

To isolate the up-converted signal (ω_3), the output beam is passed through lens L_6, a cut-off filter (F_3), and an iris (not shown in the schematic) to remove any residual components from the excitation and gate beams. The purified sum-frequency light is then focused into a monochromator via lens L_7, which spectrally selects the desired wavelength. The selected signal is subsequently directed to a photomultiplier

tube (PMT) connected to a photon-counting module for detection. Control of the monochromator, delay stage, and data acquisition is integrated and managed using LUMEX software (CDP Corp).

2.4.3. Data analysis of fluorescence up-conversion

Accurate determination of fluorescence lifetimes requires prior characterization of the instrument response function (IRF), which reflects the temporal resolution of the experimental setup. The IRF accounts for pulse broadening and timing distortions introduced by various optical and electronic components in the system.

The instrument response function (IRF) was determined using the Raman scattering signal of water, which appears at a spectral shift of approximately 3300 cm^{-1} from the excitation wavelength[23–25]. For this measurement, the sample cell was replaced with a cuvette containing pure water, and the system was configured to detect the IRF at a specific wavelength. Since Raman scattering occurs instantaneously, with no intrinsic delay, it serves as a suitable zero-time reference. By monitoring the sum-frequency signal generated from the interaction of the Raman-scattered light and the gate pulse, the combined temporal profile of the excitation and detection pulses was captured.

The resulting IRF was accurately modeled by a Gaussian function, characterized by a full-width at half-maximum (FWHM) of approximately 250 femtoseconds. Mathematically, the IRF is expressed as:

$$G(x) = \frac{1}{\sigma\sqrt{2\pi}} e^{-(x-\mu)^2 / 2\sigma^2} \quad (2.7)$$

Where, σ represents the width parameter of the Gaussian function, μ is the x-axis position (mean) of the function. The FWHM of this Gaussian function can be calculated as, $H = 2\sigma\sqrt{2\ ln2} \sim 2.3548\ \sigma$.

The excitation pulse is assumed to occur at zero time, so for data analysis, the function is simplified by setting $\mu = 0$.

In femtosecond fluorescence up-conversion spectroscopy, the experimentally recorded fluorescence decay does not directly reflect the intrinsic molecular relaxation dynamics. Instead, it is convoluted with the instrument response function (IRF), which has a finite temporal width. This convolution significantly influences the measured signal, especially when dealing with ultrafast processes on the sub-picosecond timescale. Therefore, to accurately determine fluorescence lifetimes, it is essential to apply deconvolution methods.

In this study, the experimental decay profiles were analysed by fitting a convolution of the IRF with a sum of exponential decay functions. This approach allows for precise extraction of decay parameters. The methodology can be readily extended to accommodate multi-exponential decays, enabling characterization of complex relaxation pathways.

The convolution function is,

$$I(t) = G(x) * S(x) \tag{2.8}$$

Where, $S(x) = \exp\left(-\frac{x}{\tau}\right)$, τ is the lifetime.

$$I(t) = \frac{1}{\sigma\sqrt{2\pi}} \int_0^\infty exp\left(-\frac{x}{t}\right) exp\left(-{(t-x)^2}/{2\sigma^2}\right) dx \tag{2.9}$$

$$\therefore I(t) = \frac{1}{\sigma\sqrt{2\pi}} \int_0^\infty exp\left(-\frac{\left(x^2 + t^2 + \frac{2\sigma^2 x}{\tau} - 2tx\right)}{2\sigma^2}\right) dx \tag{2.10}$$

Let's assume,

$$z = \frac{\left(x - \left(t - \frac{\sigma^2}{\tau}\right)\right)}{\sigma\sqrt{2}} \tag{2.11}$$

$$\therefore \frac{\left(x^2+t^2+\frac{2\sigma^2 x}{\tau}-2tx\right)}{2\sigma^2} = z^2 + \frac{1}{\tau}\left[t - \frac{\sigma^2}{2\tau}\right] \quad (2.12)$$

Using equations 2.11 and 2.12 in equation 2.10, we get,

$$I(t) = \frac{1}{\sqrt{\pi}} exp\left(\frac{\sigma^2}{2\tau^2} - \frac{t}{\tau}\right) \int_{-\left(\frac{t-\frac{\sigma^2}{\tau}}{\sigma\sqrt{2}}\right)}^{\infty} exp(-z^2)dz \quad (2.13)$$

The error function can be introduced as,

$$erf(x) = \frac{2}{\sqrt{\pi}}\int_0^x exp(-z^2)dz \quad (2.14)$$

Also, as error function is an odd function, $erf(-x) = -erf(x)$ can be written.

By introducing this error function in equation 2.13, we get,

$$I(t) = \frac{1}{\sqrt{\pi}} exp\left(\frac{\sigma^2}{2\tau^2} - \frac{t}{\tau}\right)\left(1 - erf\left(\frac{\sigma^2 - t\tau}{\sqrt{2}.\sigma t}\right)\right) \quad (2.15)$$

The above equation has been employed in this work to fit fluorescence transients recorded via femtosecond fluorescence up-conversion. While the presented form describes a mono-exponential decay, the actual data fitting was performed using a multi-exponential model to account for complex relaxation dynamics. Given that convolution is a linear operation, its distributive and additive properties were utilized to extend the fitting model. Specifically, Equation 2.15 was reformulated as a summation of multiple exponential decay components, each convolved with the same Gaussian instrument response function and weighted by corresponding amplitude coefficients. All transient fittings were carried out using the IGOR Pro software (WaveMetrics, Inc.).

2.5. Basics of Time-Resolved Emission Spectra (TRES)

Time-Resolved Emission Spectra (TRES) can be reconstructed indirectly by collecting fluorescence decay profiles at different emission wavelengths[16,19]. This approach relies on the principle that photoexcitation induces a significant alteration

in the dipole moment of the fluorescent probe [19]. In response, solvent molecules dynamically reorganize to stabilize the excited-state dipole. This solvent relaxation process manifests experimentally as a gradual red shift in the emission maximum over time—a phenomenon referred to as the time-dependent Stokes shift—which continues until equilibrium is achieved between the solute and its environment (refer to Scheme 2.5) [19,26].

To construct Time-Resolved Emission Spectra (TRES), fluorescence decay measurements are collected at various wavelengths spanning the steady-state emission range. These wavelength-resolved decay curves are then processed using the analytical techniques previously outlined. At any given time *t* and wavelength λ, the intensity of the TRES can be mathematically described as the product of two separate functions one dependent on time and the other on wavelength reflecting the assumption of temporal and spectral separability.

$$I(\lambda, t) = A(\lambda)B(t) \tag{2.16}$$

The steady-state fluorescence spectrum (I_{SS}) is obtained by integrating $I(\lambda, t)$ over time and can be written as,

$$I_{SS} = \int_0^\infty I(\lambda, t)dt \tag{2.17}$$

Substituting Equation 2.16 into Equation 2.17:

$$I_{SS} = \int_0^\infty A(\lambda)B(t)dt \tag{2.18}$$

Since A(λ) is independent of time, it can be taken out of the integral:

$$I_{SS} = A(\lambda) \int_0^\infty B(t)dt \tag{2.19}$$

Here, B(t) represents the fluorescence decay, which is typically modeled as a sum of exponentials. Therefore,

$$B(t) = \sum_i \alpha_i \exp\left(-\frac{t}{\tau_i}\right) \quad (2.20)$$

Where the pre-exponential factors satisfy the condition, $\sum_i a_i(\lambda) = 1$

we obtain,

$$I_{SS} = A(\lambda)\sum_i \alpha_i \tau_i \quad (2.21)$$

$$A(\lambda) = \frac{I_{SS}}{\sum_i \alpha_i \tau_i} \quad (2.22)$$

Therefore,

$$I(\lambda, t) = \frac{I_{SS}}{\sum_i \alpha_i \tau_i} \sum_i \alpha_i \exp\left(-\frac{t}{\tau_i}\right) \quad (2.23)$$

The above equation characterizes how fluorescence intensity is distributed over various wavelengths at a specific time point. A commonly adopted method for analyzing the temporal behavior of TRES involves tracking the evolution of the emission maximum over time—an effect known as the time-dependent Stokes shift. This spectral shift, denoted as ν(t), is typically modeled using a lognormal function, which captures the asymmetric broadening and red-shifting behavior of the emission profile during solvent relaxation.

$$g(\nu) = g_0 exp\left[-\ln(2)\left(\frac{\ln\left[1+\frac{2b(\nu-\nu_p)}{\Delta}\right]}{b}\right)^2\right] \quad (2.24)$$

for $\alpha > 1$, $g(\nu) = 0$ (2.25)

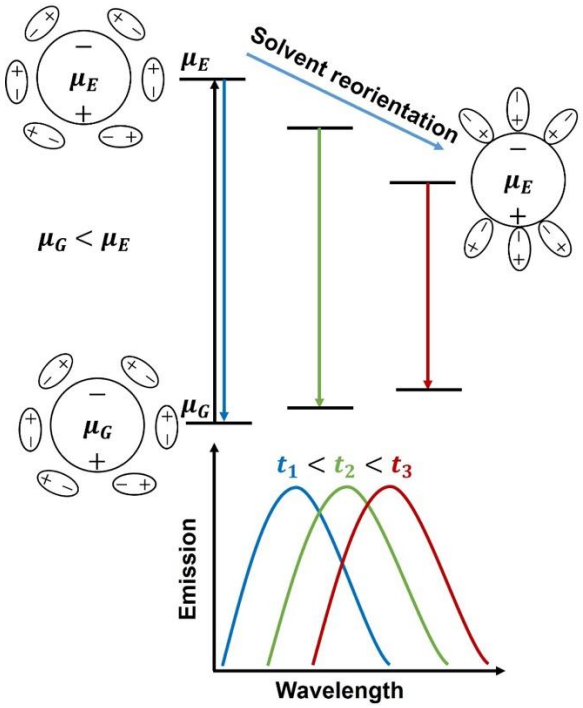

Scheme 2.5. The scheme illustrates the concept of solvation dynamics (upper panel) alongside the progression of time-resolved fluorescence Stokes shift (lower panel). Following optical excitation to the Franck–Condon (FC) state, and vibrational relaxation, the surrounding solvent begins to reorganize to accommodate the altered electronic distribution of the excited molecule because of the dipole moment difference between the ground (μ_G) and excited (μ_E) state. This relaxation with a more favorable solvent arrangement towards the excited state dipole leads to a decrease in the overall energy of the system. As a result, the emitted fluorescence undergoes a red shift over time, each corresponding to emission at different stages of solvent reorganization. The lower panel of the graph shows how the emission maximum shifts toward longer wavelengths (from t_1 to t_3), reflecting the time-dependent nature of the Stokes shift as solvation proceeds toward equilibrium.

for $\alpha < 1$, where $\alpha = \frac{2b(\nu - \nu_p)}{\Delta}$ (2.26)

To facilitate comparison, the peak frequency shift $\nu(t)$ is often converted into a solvent response (normalized) function $C(t)$ as,

$$C(t) = \frac{\nu(t)-\nu(\infty)}{\nu(0)-\nu(\infty)} \quad (2.16)$$

The function $C(t)$ is typically modeled using either a single exponential or a sum of exponentials to determine the average solvation time ($\langle\tau_s\rangle$).

2.6. Transient Absorption Spectroscopy (TA)

In this thesis, transient absorption (TA) spectroscopy has been employed to a limited extent. It was specifically used to probe the solvation dynamics of the buffer and various concentrations of hydrated deep eutectic solvents (DES) in the absence of protein. The relaxation times observed in these systems fall within the 1–30 picosecond range, which lies beyond the temporal resolution of Time-Correlated Single Photon Counting (TCSPC). Although femtosecond fluorescence up-conversion is, in principle, capable of capturing such fast dynamics, the TA setup used in this study provides a superior time resolution of approximately 70–80 femtoseconds—markedly faster than the ~300 fs instrument response of the available up-conversion system. Moreover, TA data processing is more streamlined, and solvation dynamics can be more readily extracted via the stimulated emission signals, which directly yield time-resolved emission spectra (TRES) without requiring the intricate deconvolution procedures necessary in fluorescence up-conversion.[27]

2.6.1. Fundamentals of TA

Transient absorption (TA) spectroscopy is a well-established pump–probe technique that facilitates the investigation of excited-state dynamics with femtosecond temporal resolution [28–30]. In this approach, an ultrafast excitation pulse—typically lasting tens of femtoseconds—initiates a non-equilibrium population in the sample. The resulting transient states are then monitored by a time-delayed probe pulse, which interrogates the system's evolution as a function of delay time [28–30]. When the excitation pulse duration is sufficiently short (e.g., ~50 fs), it becomes feasible to resolve early-stage processes in the excited-state manifold, capturing fundamental events that unfold on ultrafast timescales.

In the transient absorption experiments conducted for this study, the pump pulse was centered at 400 nm and was used to selectively excite a portion of the molecular population to the electronically excited state. A broadband white-light continuum, covering the 450–750 nm range in the visible spectrum, served as the probe. This probe beam intersected the same region of the sample at variable time delays, which were precisely controlled using a computer-operated mechanical delay stage. To avoid the introduction of nonlinear optical artifacts or multiphoton excitation, the intensity of the probe beam was deliberately kept low throughout all measurements (see Scheme 2.6).

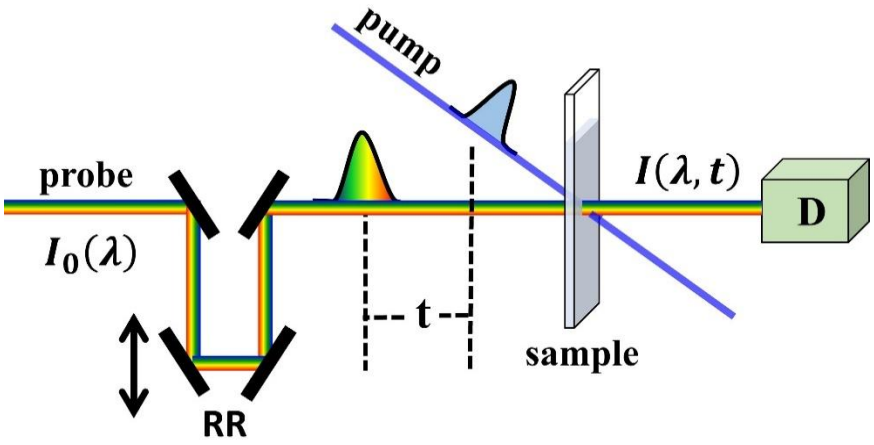

Scheme 2.6. Simplified illustration of the transient absorption spectroscopy setup.

At each selected delay time, detection is carried out spectrally across the full range of the probe beam, and this procedure is repeated for successive delays to generate a complete time-resolved dataset. Since transient absorption is an absorption-based technique, the underlying principles can be described using the Lambert-Beer law, which governs how the probe intensity is attenuated as it passes through the sample following photoexcitation.

$$I(\lambda, t) = I_0(\lambda) \times 10^{-\varepsilon(\lambda)N(t)l} \quad (2.17)$$

Where, $I_0(\lambda)$ is the initial probe intensity at a given wavelength and $I(\lambda, t)$ is the transmitted intensity at a time delay t. Note that the time zero corresponds to the point where the pump and probe pulses arrive at the sample simultaneously. $\varepsilon(\lambda)$ is the molar extinction coefficient at the wavelength λ, $N(t)$ denotes the time-dependent population of the absorbing state, and l is the optical path length of the sample.

From Equation 2.17, the absorbance $A(\lambda, t)$ at any wavelength and time can be expressed as,

$$A(\lambda, t) = log \frac{I_0(\lambda)}{I(\lambda,t)} = \varepsilon(\lambda)N(t)l \quad (2.18)$$

However, in transient absorption (TA) spectroscopy, the primary observable is the change in absorbance that occurs upon photoexcitation, reflecting the difference between the excited and ground (unexcited) states of the sample. This quantity, known as differential absorbance, is expressed as:

$$\Delta A(\lambda,t) = A(\lambda,t) - A(\lambda) \tag{2.19}$$

$$\Delta A(\lambda,t) = log\frac{I_0(\lambda)}{I(\lambda,t)} - log\frac{I_0(\lambda)}{I(\lambda)} = log\frac{I(\lambda)}{I(\lambda,t)} \tag{2.20}$$

Equation 2.20 indicates that the measurable parameter is the change in probe intensity with and without the excitation by the pump. Hence, it simplifies to,

$$\Delta A(\lambda,t) = log\frac{I^{probe}}{I^{probe}_{pump}} \tag{2.21}$$

In equation 2.21, the quantity I^{probe} represents the intensity measured when the pump is blocked (usually using a mechanical chopper). I^{probe}_{pump} is the intensity when both pump and probe interact with the sample.

As the excited-state population $N(t)$ evolves over time through various relaxation processes, the differential absorbance $\Delta A(\lambda,t)$ also changes accordingly. This time-dependent behavior of ΔA encodes the underlying excited-state dynamics of the system initiated by photoexcitation.

As an absorption-based technique, transient absorption spectroscopy is capable of monitoring both radiative and non-radiative relaxation pathways, depending on the spectral signatures under investigation [29,30]. This capability makes it a highly versatile method for exploring a broad spectrum of ultrafast photophysical and photochemical processes.

2.6.2. Insights from TA

Transient absorption (TA) spectroscopy enables the observation of multiple distinct photophysical processes, four of which are frequently detected in typical measurements. These processes are illustrated in Scheme 2.7 and are outlined below.

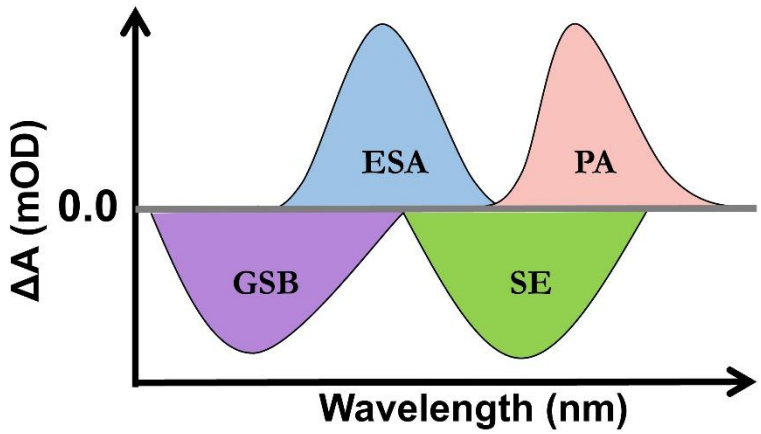

Scheme 2.7. Representative contributions of various transient signals observed in TA spectra.

Ground state bleaching (GSB): - Upon excitation by the pump pulse, a fraction of the molecular population is promoted from the ground electronic state to an excited state, resulting in a temporary depletion of the ground-state population. This reduction leads to diminished absorption of the probe light at wavelengths associated with ground-state transitions. Because the sample absorbs less probe light compared to its unexcited state (i.e., $I^{probe} < I^{probe}_{pump}$), the corresponding change in absorbance (ΔA) becomes negative. This negative signal, referred to as ground-state bleaching (GSB), gradually diminishes as the excited molecules return to the ground state through radiative or non-radiative relaxation pathways.

Stimulated Emission (SE):- Excited-state molecules can return to the ground state through the emission of photons. While spontaneous emission occurs without external influence, stimulated emission (SE) is triggered when the probe pulse contains photons with energies matching the electronic transition from the excited to the ground state. In such cases, the incident photons induce emission of additional photons that are coherent, traveling in the same direction and phase as the probe. This process enhances the transmitted probe intensity at those wavelengths, resulting in a negative ΔA signal, much like ground-state bleaching $I^{probe} < I^{probe}_{pump}$. The spectral profile of SE typically resembles the molecule's fluorescence spectrum and is red-shifted relative to the GSB band. The intensity of the SE signal decays over time as the excited-state population diminishes. To ensure accurate measurement of this feature without disturbing the system, the probe intensity is carefully maintained at a sufficiently low level to prevent significant perturbation of the excited-state dynamics.

Excited-state absorption (ESA)*:* - Following excitation by the pump pulse, a portion of the molecular population occupies an excited electronic state. From this state, the molecules can further absorb photons from the probe pulse, promoting them to higher-lying excited states—a process known as excited-state absorption (ESA). Since this additional absorption occurs only in the presence of prior excitation, the probe intensity transmitted through the sample decreases relative to the unexcited condition $I^{probe} > I^{probe}_{pump}$, resulting in a positive ΔA signal. The spectral features and temporal evolution of ESA bands provide valuable information about the structure and dynamics of higher excited states. This ability to probe non-emissive states and transitions is a major advantage of transient absorption spectroscopy, offering insights that are often inaccessible through fluorescence-based techniques.

After excitation by the pump, some molecules reside in an excited state, from which they may absorb additional photons from the probe pulse to reach higher electronic

states. This process leads to excited-state absorption. As the probe photons are absorbed only when the pump creates an excited state, the transmitted probe intensity decreases in the presence of pump excitation, and $I^{probe} > I^{probe}_{pump}$ in this case. This will result in a positive ΔA signal. The appearance and evolution of ESA bands provide insights into higher-lying excited-state structures and their dynamics. Finding this information is one of the strengths of transient absorption which was typically inaccessible through fluorescence methods.

Product absorption (PA): - Upon photoexcitation, molecules may undergo a range of secondary processes such as electron or proton transfer, structural reorganization, or photochemical reactions, leading to the generation of new transient species. These photoinduced intermediates often exhibit distinct absorption features and can interact with the probe pulse. Because these species are absent in the ground-state population, their absorption results in a reduced probe transmission in the excited-state condition compared to the unexcited sample $I^{probe} > I^{probe}_{pump}$, yielding a positive photoinduced absorption (PA) signal. The appearance and evolution of these features provide critical insights into the kinetics and mechanistic pathways of ultrafast photochemical and photophysical transformations.

The strength of transient absorption (TA) spectroscopy lies in its ability to simultaneously monitor multiple photophysical and photochemical processes within a single experimental framework, making it an invaluable tool in both physics and chemistry. However, several practical limitations must be acknowledged. These include the finite spectral range of the probe pulse, which may not cover all relevant transitions, and the temporal resolution constrained by the instrument response function. Additionally, the complexity of TA spectra often containing overlapping signals from various processes can pose challenges in disentangling individual contributions, potentially limiting the resolution of distinct dynamic events.

2.6.3. Instrumentation of TA setup

All transient absorption measurements presented in this work were performed using a commercially available femtosecond broadband TA system (Femto-Frame-II, IB Photonics, Bulgaria). The detailed optical layout is shown in Scheme 2.8. The system is driven by a Ti:Sapphire regenerative amplifier (Spitfire Pro XP, Spectra-Physics, USA), which generates pulses centered at 800 nm with a temporal width of approximately 80 femtoseconds and operates at a repetition rate of 1 kHz. The amplifier is optically pumped by a 20 W Q-switched Nd:YLF laser (Empower, Spectra-Physics) and seeded by a femtosecond oscillator (MaiTai SP, Spectra-Physics). The pulse duration was independently verified using a commercial autocorrelator.

The 800 nm output beam from the amplifier is divided into two components using a beamsplitter (BS_1). One arm is directed for pump generation, while the other is used to create the probe. The pump pulse is generated using a JANOS tripler module (IB Photonics), in which the incoming 800 nm beam first passes through a β-barium borate (BBO) crystal to produce the second harmonic at 400 nm. This 400 nm light, along with the residual fundamental, is passed through a half-wave plate and then into a second BBO crystal, where third harmonic generation (266 nm) takes place. The resulting 800, 400, and 266 nm beams are separated using dichroic mirrors, and depending on the experimental requirement, either the 400 nm or 266 nm output is selected for excitation using mirrors M_6 and M_7.

The other portion of the 800 nm light, following reflection from mirror M_5, is directed through mirrors M_{B1}–M_{B3} to a retroreflector (RR) mounted on a computer-controlled mechanical translation stage, enabling variable time delays up to 2 nanoseconds between pump and probe pulses. A small fraction of this beam is diverted by beamsplitter BS_2 onto a photodiode (PD), which synchronizes with a mechanical chopper for pump modulation. The main portion of the 800 nm probe beam is then attenuated using a neutral density filter (ND_1), spatially shaped using an iris, and tightly focused by lens L_4 onto a 0.3 mm sapphire crystal to generate a

white-light continuum (WLC) spanning ~450–750 nm. The generation of WLC is highly sensitive to beam quality and energy, which are carefully adjusted using the ND filter and iris. The resulting continuum is collected with a parabolic mirror (M_{B5}), filtered through two notch filters (N_1 and N_2) to remove residual 800 nm light, and redirected via mirrors M_{B6} and M_{B7}. The probe is then focused onto the sample by another parabolic mirror (M_{B10}).

Simultaneously, the pump beam passes through a mechanical chopper for modulation and a half-wave plate to control polarization, minimizing anisotropic contributions. Its intensity is adjusted using a rotating neutral density filter (ND_2), and the beam is directed onto the same sample location as the probe using lens L_3 and mirror M_{B12}. The typical excitation spot diameter at the sample ranges from 100–200 μm. The chopper alternately blocks and unblocks the pump beam to enable measurement of both pump-on and pump-off conditions, which are essential for calculating the differential absorbance (ΔA).

After interacting with the sample, the transmitted probe light is collected and focused onto a 200 μm fiber optic using mirror M_{B11}. An additional neutral density filter (ND_3) ensures that the light entering the detector remains within the optimal intensity range. Spectral detection is achieved using a CCD-based spectrograph, which disperses the probe light using a set of diffraction gratings. Due to a small angular separation between the pump and probe beams at the sample, only the probe reaches the detector.

Time-zero calibration was performed using a Coumarin 152 solution in ethanol by monitoring the rising edge of its known transient signal and adjusting the delay stage accordingly. The full setup is operated through a LabVIEW-based control interface. Throughout all measurements, the pump power was carefully maintained at 10–15 μW to avoid sample photodegradation. To confirm sample integrity, steady-state absorption spectra were recorded before and after each TA experiment.

The output beam at 800 nm is divided into two parts using a beamsplitter (BS1). One portion is directed to generate the pump pulse, while the other is used to produce the probe. Pump generation is carried out within a JANOS tripler module provided by the same manufacturer. The incoming 800 nm light first passes through a BBO crystal to generate the second harmonic at 400 nm. This 400 nm light, along with the residual 800 nm, passes through a half-wave plate and enters a second BBO crystal where third harmonic generation (266 nm) occurs. The three harmonics (800, 400, 266 nm) are then separated using dichroic mirrors, and depending on the requirement, either 400 nm or 266 nm is selected for sample excitation using mirrors M_6 and M_7. The other arm of the fundamental 800 nm light, after reflection off mirror M_5, is routed through a series of mirrors (M_{B1}–M_{B3}) into a retroreflector (RR) mounted on a mechanical translation stage. This stage allows for delay generation of up to 2 nanoseconds between the pump and probe pulses. A small fraction of this beam is deflected by BS_2 to fall onto a photodiode (PD), which regulates the mechanical chopper controlling pump modulation. The remaining portion of the 800 nm beam is attenuated via a neutral density filter (ND_1), shaped with an iris, and then focused by lens L_4 onto a 0.3 mm sapphire crystal to produce a white light continuum (WLC), covering ~450–750 nm. The characteristics of the WLC strongly depend on the incident beam profile and energy, which are tuned using the ND filter and iris. This continuum is collected using a parabolic mirror (M_{B5}), passed through two notch filters (N_1, N_2) to remove residual 800 nm light, and redirected via mirrors M_{B6} and M_{B7}. It is then focused onto the sample using another parabolic mirror (M_{B10}). Meanwhile, the pump pulse, after passing through a chopper for modulation, has its polarization adjusted with a half-wave plate to minimize anisotropic interference. The intensity is regulated by a rotating neutral density filter (ND_2), and the beam is focused onto the same location as the probe using lens L_3 and mirror M_{B12}. The typical excitation spot diameter at the sample position ranges from 100–200 μm. The chopper periodically blocks the pump to enable acquisition of both pump-on and pump-off conditions, essential for calculating differential absorbance. The probe light, after transmission through the sample, is focused onto a 200 μm

fiber optic cable using mirror M_{B11}. A final neutral density filter (ND_3) ensures the intensity reaching the detector is within operational limits. Detection is performed using a CCD-based spectrograph, where the dispersed probe beam is analyzed using a set of diffraction gratings. Due to a slight angular difference between the pump and probe beams at the sample, only the probe reaches the detection system. Time-zero calibration is carried out using a reference material (Coumarin 152 in ethanol) by monitoring the rise of the known signal and tuning the delay stage accordingly. The entire instrument is operated via software developed on the LabVIEW platform. Throughout the experiments, pump power was maintained around 10–15 μW to prevent photodegradation. To verify sample integrity, steady-state absorption spectra were recorded before and after each measurement session.

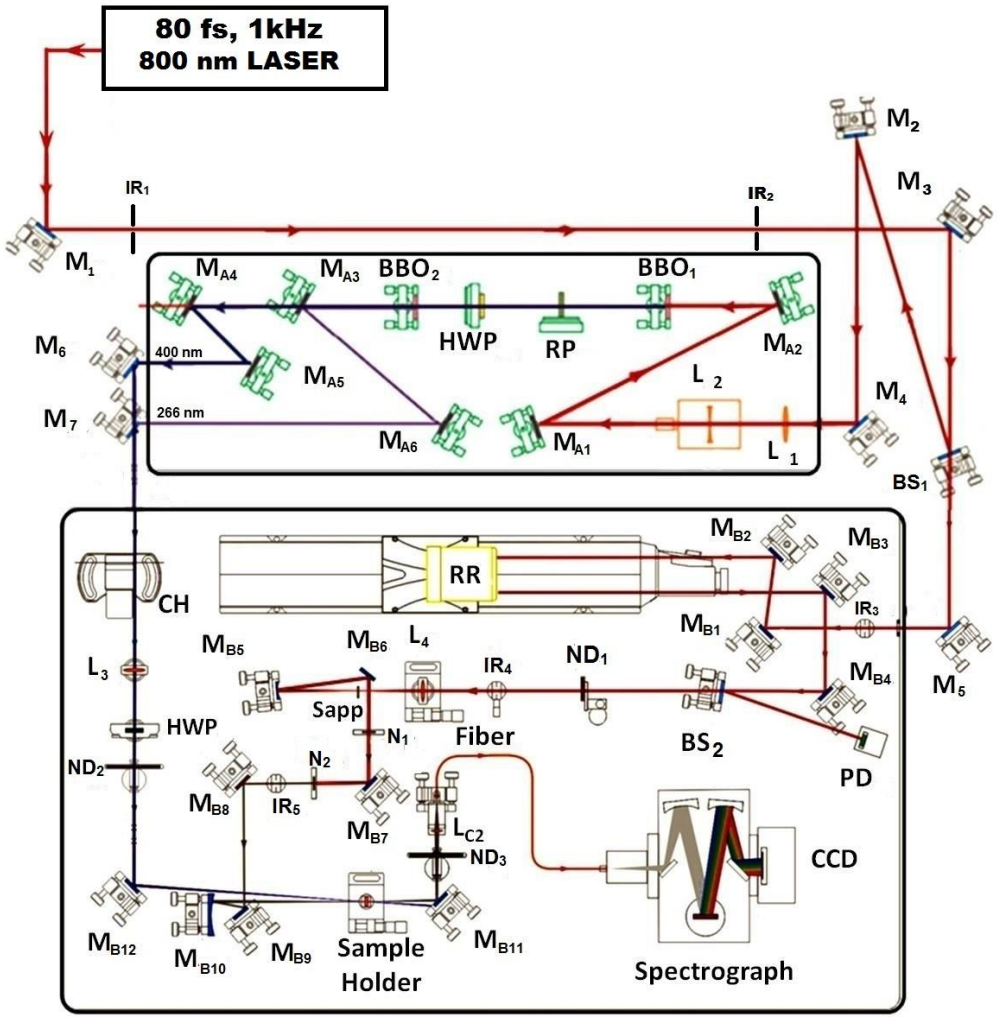

Scheme 2.8. Detailed optical schematic of the femtosecond transient absorption spectrometer.

2.6.4. TA data analysis

In this thesis, the use of transient absorption (TA) spectroscopy has been exclusively focused on investigating solvation dynamics [27]. The analysis was confined to the spectral window of 450–550 nm, where the differential absorbance spectra of C-343 in both buffer and osmolyte environments are dominated by stimulated emission (SE) signals. The selection of C-343 as a solvation probe was driven primarily by its good solubility in both buffer and hydrated osmolyte solutions, ensuring compatibility across all sample conditions examined.

In contrast to fluorescence lifetime techniques such as TCSPC and femtosecond fluorescence up-conversion where time-resolved emission spectra must be reconstructed from wavelength-dependent decay traces transient absorption (TA) spectroscopy provides the advantage of directly capturing time-resolved emission information through the evolution of the stimulated emission (SE) signal. This is particularly effective when the SE band is well-resolved and minimally affected by overlapping features such as excited-state absorption (ESA) or photoinduced absorption (PA). To accurately determine the SE peak position at each time delay, the corresponding ΔA spectra were individually fitted with a log-normal function, confined to the SE-dominated region. Tracking the temporal shift in these SE maxima allowed for the construction of the solvent response function, as described by Equation 2.16. The extracted solvent response curves were then analyzed using multiexponential fitting to determine the characteristic solvation times.

Due to the challenges associated with signal overlap—particularly interference from other transient features obscuring the stimulated emission (SE) band—and the limited accessibility of suitable instrumentation, the use of transient absorption (TA) spectroscopy for solvation dynamics studies has remained relatively restricted [27,30–

[35]. One of the earliest demonstrations of this approach was reported by Poizat et al. in 2002 [36]. Since then, only a modest number of studies have employed TA for probing solvation dynamics. Notably, recent work by Xia *et al.* [33] has shown strong agreement between solvation times obtained via TA and those reported by Maroncelli and colleagues using conventional time-resolved emission spectroscopy (TRES) [37]. These results highlight that, despite its limited adoption, TA when carefully executed and free from significant spectral interference can serve as a powerful and complementary method for investigating solvation dynamics.

2.7. Fluorescence Correlation Spectroscopy (FCS)

This thesis incorporates single-molecule fluorescence measurements to uncover insights that are often inaccessible through conventional ensemble-averaged techniques. Methods such as steady-state absorption, circular dichroism (CD), and time-resolved fluorescence spectroscopy are well-suited for homogeneous, isotropic systems; however, they tend to obscure critical information in systems exhibiting molecular heterogeneity. In scenarios where variations in molecular behavior or properties exist within the sample, ensemble measurements provide only an averaged view, potentially masking rare or functionally important subpopulations. Under such conditions, the ability to observe and analyze fluorescence from individual molecules becomes essential for capturing the true complexity of the system.

Certain dynamic and structural characteristics of biomolecules especially those involving conformational fluctuations can be meaningfully captured only through single-molecule techniques [38–42] Beyond their ability to resolve molecular heterogeneity, these methods offer a significant experimental advantage: they function efficiently at extremely low analyte concentrations, often in the nanomolar to picomolar range [43,44]. This low concentration requirement is particularly beneficial in cases where higher concentrations, typically in the micromolar range,

may promote protein aggregation, thereby complicating data interpretation in ensemble measurements.

2.7.1. A short theory of FCS

Fluorescence Correlation Spectroscopy (FCS) was first introduced by Elliot L. Elson, Douglas Magde, and Watt. W. Webb in the year 1972.[45–48] This technique is based on the analysis of time-dependent fluctuations in fluorescence intensity within a tightly focused optical volume[44,46,47]. These intensity fluctuations primarily result from the stochastic diffusion of fluorescent molecules in and out of the observation volume. However, additional contributions can arise from photophysical transitions, chemical reactions, or conformational changes that occur on timescales similar to or faster than molecular diffusion[43,44]. FCS quantifies these fluctuations using temporal correlation methods, such as autocorrelation and cross-correlation functions, enabling the extraction of kinetic and dynamic parameters associated with the fluorescent species under investigation[44].

2.7.2. Mathematical Foundation: Fluctuations and Correlation

'An Introduction to Fluorescence Correlation Spectroscopy' by Prof. Wohland, Maiti, and Machan has nicely covered this part. This part is essentially taken from that book[44].

2.7.2.1. Fluctuations

The primary objective of Fluorescence Correlation Spectroscopy (FCS) is to extract information about dynamic molecular processes occurring within a given system. This system can range from simple buffer solutions to complex biological environments such as protein mixtures, enzymes, living cells, or even entire

organisms [45,49–52]. These molecular processes consist of discrete events that result in changes to observable parameters. In the context of FCS, such changes manifest as temporal fluctuations in fluorescence intensity, which represent deviations from the mean signal within a highly confined detection volume. These fluctuations carry valuable information about the underlying kinetics and dynamics of the system being studied [44,45].

These fluctuations are caused by a) Brownian diffusion of molecules in and out of the observation volume, b) Photophysical transitions, such as triplet state blinking, c) Chemical reactions or conformational changes affecting fluorophore brightness.

If $F(t)$ is the fluorescence intensity at time t, then the fluctuation ($\delta F(t)$) is defined as:

$$\delta F(t) = F(t) - \langle F(t) \rangle \tag{2.22}$$

Average of the fluctuation,

$$\langle \delta F(t) \rangle = \langle F(t) - \langle F(t) \rangle \rangle = 0 \tag{2.23}$$

Even in systems that seem to be at equilibrium, molecular motions and reactions persist, giving rise to subtle fluctuations around the average state. These fluctuations are not merely random noise; rather, they contain meaningful information about the kinetics, diffusion behavior, and molecular interactions within the system. It is precisely this fluctuation-based signal that forms the basis of Fluorescence Correlation Spectroscopy (FCS), enabling it to probe dynamic processes with high sensitivity [44].

2.7.2.2. Idea of Correlation and Correlation Function

To understand how fluctuations in fluorescence intensity reveal molecular-level dynamics, it is important to first introduce the concept of correlation. In general terms, correlation describes the extent to which two variables are related—that is,

how the value of one variable depends on or is influenced by the other [44]. The strength of this relationship determines the degree of correlation. In the case of perfect correlation, knowing the value of one variable allows for the exact prediction of the other. A simple example is the linear relationship between mass and volume for a solid under standard conditions; any change in mass results in a proportional change in volume, illustrating a clear and predictable dependency [44].

To define correlation mathematically, let's consider two variables, a and b, each of which depends on some general coordinate or parameter u.

According to the mathematical definition, two variables are said to be correlated if the average of their product is equal to the product of their individual averages.[44] In other words:

$$\langle a(u).b(u)\rangle \neq \langle a(u)\rangle.\langle b(u)\rangle \tag{2.24}$$

The correlation coefficient is defined as,

$$g = \frac{\langle a(u).b(u)\rangle}{\langle a(u)\rangle.\langle b(u)\rangle} \tag{2.25}$$

Whenever, $g > 1$: the data is correlated, $g > 1$: the data is anti-correlated, and $g = 1$: the data is not correlated.[44]

At its core, correlation refers to the extent of similarity or association between two quantities. Within the context of this thesis, particular attention is given to the autocorrelation function, which quantifies the correlation of a signal with a time-shifted version of itself. Specifically, autocorrelation assesses how the value of a given variable at one point in time is related to its value at a later time, separated by a defined time lag. This temporal self-comparison forms the foundation of Fluorescence Correlation Spectroscopy (FCS), enabling the extraction of dynamic information from time-dependent fluctuations in fluorescence intensity [44].

In Fluorescence Correlation Spectroscopy (FCS), the primary variable of interest is the fluorescence intensity, which fluctuates over time as fluorescent molecules

diffuse into and out of a small, confocal detection volume [44]. This intensity reflects the number of photons emitted and detected from molecules transiently present within that confined space. When a fluorescent molecule enters the observation volume, its emission is efficiently collected by the detector; as it exits, its contribution to the signal ceases. These temporal fluctuations in photon count serve as the foundation for computing the autocorrelation function, enabling the analysis of molecular diffusion and dynamic behaviour with single-molecule sensitivity [44,50].

If $F(t)$ is the fluorescence intensity at time t, and if we want to write the autocorrelation function after a time $t + \tau$,

$$G(\tau) = \frac{\langle F(t).F(t+\tau)\rangle}{\langle F(t)\rangle.\langle F(t+\tau)\rangle} \quad (2.26)$$

We can simplify this equation as we measure only in an equilibrium condition (stationary process) i.e. process in which the time of measurement does not alter the observation or the average value of the observable, and thus, $\langle F(t)\rangle = \langle F(t+\tau)\rangle$

$$G(\tau) = \frac{\langle F(t).F(t+\tau)\rangle}{\langle F(t)\rangle^2} \quad (2.27)$$

This can be easily shown that autocorrelation function is an even function,

$G(\tau) = G(-\tau)$.

It is important to emphasize that the correlation function in Fluorescence Correlation Spectroscopy is fundamentally defined in terms of the fluorescence intensity, not the fluctuations themselves. This approach is appropriate because the experimentally recorded observable is the time-dependent fluorescence intensity, which is directly accessible for correlation analysis. However, since fluctuations represent deviations from the mean intensity, calculating them requires first determining the average fluorescence signal. Once the mean has been established, the autocorrelation function can be computed based on these deviations, providing insights into the temporal relationships within the fluctuating signal.

As the definition of fluctuation is deviation from the mean, fluctuation ($\delta F(t)$) can be written as[44],

$$\delta F(t) = F(t) - \langle F(t) \rangle \tag{2.28}$$

The average of the fluctuation is (from equation 2.28),

$$\langle \delta F(t) \rangle = \langle F(t) - \langle F(t) \rangle \rangle = \langle F(t) \rangle - \langle \langle F(t) \rangle \rangle = \langle F(t) \rangle - \langle F(t) \rangle = 0$$

From equation 2.28, we can express the signal $F(t)$ in terms of fluctuation,

$$F(t) = \delta F(t) + \langle F(t) \rangle \tag{2.29}$$

If we substitute this equation 2.29 into the autocorrelation function of the signal (equation 2.27),

$$G(\tau) = \frac{\langle (\delta F(t) + \langle F(t) \rangle)(\delta F(t+\tau) + \langle F(t+\tau) \rangle) \rangle}{\langle F(t) \rangle^2} \tag{2.30}$$

$$= \frac{\langle \delta F(t).\delta F(t+\tau) + \delta F(t).\langle F(t+\tau) \rangle + \langle F(t) \rangle.\delta F(t+\tau) + \langle F(t) \rangle.\langle F(t+\tau) \rangle \rangle}{\langle F(t) \rangle^2} \tag{2.31}$$

We have already shown the average over fluctuation $\langle \delta F(t) \rangle = 0$. Also, for the stationary processes, $\langle F(t) \rangle = \langle F(t+\tau) \rangle$.

That means,

$$\langle \delta F(t).\langle F(t+\tau) \rangle \rangle = \langle \delta F(t) \rangle.\langle F(t+\tau) \rangle = 0 \tag{2.32}$$

$$\langle \langle F(t) \rangle.\delta F(t+\tau) \rangle = \langle F(t) \rangle.\langle \delta F(t+\tau) \rangle = 0 \tag{2.33}$$

Thus, the equation 2.31 becomes,

$$G(\tau) = \frac{\langle \delta F(t).\delta F(t+\tau) + \langle F(t) \rangle.\langle F(t+\tau) \rangle \rangle}{\langle F(t) \rangle^2}$$

$$\therefore G(\tau) = \frac{\langle \delta F(t).\delta F(t+\tau) + \langle F(t) \rangle^2 \rangle}{\langle F(t) \rangle^2}$$

$$\therefore G(\tau) = \frac{\langle \delta F(t).\delta F(t+\tau) \rangle + \langle F(t) \rangle^2}{\langle F(t) \rangle^2}$$

$$\therefore G(\tau) = \frac{\langle \delta F(t).\delta F(t+\tau)\rangle}{\langle F(t)\rangle^2} + 1$$

That means we have proved that,

$$G(\tau) = \frac{\langle F(t).F(t+\tau)\rangle}{\langle F(t)\rangle^2} = \frac{\langle \delta F(t).\delta F(t+\tau)\rangle}{\langle F(t)\rangle^2} + 1 \quad (2.34)$$

From this analysis, it follows that the autocorrelation function (ACF) computed directly from the raw fluorescence signal and the one obtained from its fluctuations exhibits the same mathematical form, differing only by a constant offset of 1. This offset arises because the raw signal includes both the mean and the fluctuating components, whereas the fluctuation-based calculation isolates only the deviations from the mean. Consequently, apart from this additive constant, both approaches yield equivalent information regarding the underlying molecular dynamics of the system. By convention, the correlation function derived directly from the signal is denoted as $G(\tau)$, while the autocorrelation of the fluctuations is represented as $g(\tau)$.

$$\therefore G(\tau) = \frac{\langle F(t).F(t+\tau)\rangle}{\langle F(t)\rangle^2} = g(\tau) + 1 \quad (2.35)$$

$$\text{And, } g(\tau) = \frac{\langle \delta F(t)\delta F(t+\tau)\rangle}{\langle F(t)\rangle^2} \quad (2.36)$$

$$\text{At } \tau = 0,\ g(0) = \frac{\langle \delta F(t)^2\rangle}{\langle F(t)\rangle^2}$$

$$\text{And at any } \tau \neq 0,\ g(\tau) = \frac{\langle \delta F(t)\delta F(t+\tau)\rangle}{\langle F(t)\rangle^2}$$

$\langle \delta F(t)\rangle^2$ is always positive as it is a square term, however $\langle \delta F(t)\delta F(t+\tau)\rangle$ can be both larger and smaller than zero, which is expected for fluctuations.

Thus,

$\langle \delta F(t)^2\rangle \geq \langle \delta F(t)\delta F(t+\tau)\rangle$ as the term "$\langle \delta F(t)\delta F(t+\tau)\rangle$" will have negative contributions. Therefore, the correlation function (either signal or fluctuation) will have the highest value at $\tau = 0$. And at a very long time ($\tau \to \infty$) $g(\tau)$ will become

0. This means a plot of $g(\tau)$ versus τ will give us a decay curve of self-similarity with time.

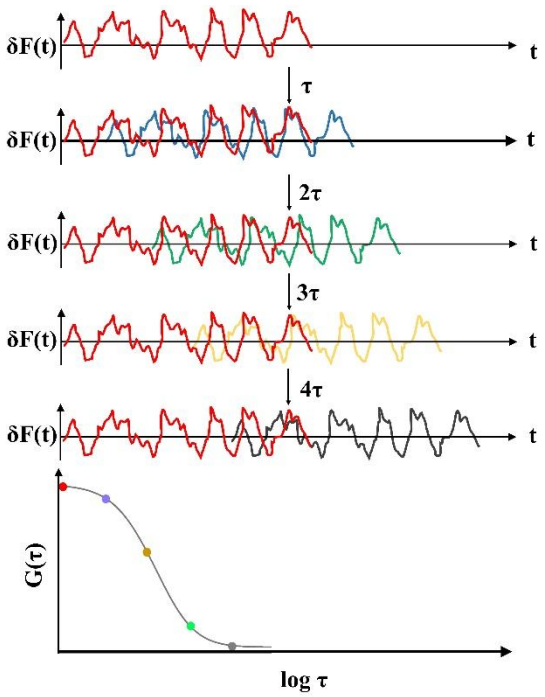

Scheme 2.9. Conceptual illustration of how the autocorrelation function is constructed. Autocorrelation quantifies the self-similarity of a fluctuating fluorescence signal over time. In this schematic, the same fluorescence fluctuation trace is compared with its time-shifted versions at increasing lag times ($\tau, 2\tau, 3\tau, 4\tau$). As the lag time increases, the overlap between the original and shifted traces decreases, leading to a reduction in correlation. Eventually, at large lag times, no meaningful similarity remains, and the autocorrelation value approaches zero. The plot at the bottom shows the decay of the autocorrelation function $g(\tau)$ as a function of lag time on a logarithmic scale.

Traditionally in FCS, fluorescence intensity or its fluctuations were recorded using a single detector, and the autocorrelation function was computed to extract dynamic information—most commonly, the free diffusion of fluorophores through the confocal detection volume[44]. With advancements in instrumentation, modern FCS setups often employ two detectors in combination with a 50:50 beam splitter. In this

configuration, the emitted fluorescence is evenly divided between the two optical paths and simultaneously detected by separate detectors. This dual-channel approach significantly enhances the signal-to-noise ratio by suppressing detector-specific noise, which is inherently uncorrelated between the two channels, thereby improving the reliability and sensitivity of the correlation analysis [44].

This allows the measurement of a cross-correlation function between the two independently recorded fluorescence signals, $F_1(t)$ and $F_2(t)$ as[44],

$$G_{12} = \frac{\langle F_1(t).F_2(t+\tau)\rangle}{\langle F_1(t)\rangle.\langle F_2(t+\tau)\rangle} \quad (2.37)$$

Scheme 2.9 visually demonstrates how the autocorrelation function decreases with increasing lag time. A similar decay profile is observed in cross-correlation measurements. However, to interpret this decay in a meaningful way especially in the context of molecular diffusion or other dynamic processes that contribute to fluorescence fluctuations and is crucial to have a precise understanding of both the optical detection volume and the characteristics of the system under investigation. The choice of the mathematical model for curve fitting plays a critical role; it must accurately reflect the physical processes responsible for the observed fluctuations. Only with an appropriately selected model can the fitting procedure yield reliable and physically meaningful parameters that describe the system's dynamic behavior.

2.7.3. Fitting Function of the Fluorescence Autocorrelation Function

In Fluorescence Correlation Spectroscopy (FCS), the analysis is based on recording a time-dependent fluorescence intensity trace, F(t), that originates from a confined observation volume. Several spatial and optical parameters influence the fluorescence signal detected at any given time. Let 'r' represent the position in space and 't' time. The key factors determining the signal include[44]:

(a) The excitation intensity distribution ($I(r,t)$), which describes how the excitation light is spatially distributed. For most practical cases in FCS, this intensity is considered time-independent, reducing to $I(r)$.

(b) The collection efficiency function (CEF) of the optical system, which reflects how effectively emitted photons are captured at different locations in space. In confocal FCS, this function is largely governed by the microscope's point spread function (PSF) and the geometry of the pinhole, which restricts out-of-focus light.

(c) The factor k which encompasses the molecular brightness of the fluorophore. This includes its absorption cross-section, quantum yield, and overall detection efficiency—accounting for photon losses through the optical path and the efficiency of the detector.

(d) $S(r)$, defines the spatial extent of the fluorescent sample being investigated.

(e) The spatiotemporal distribution of fluorophores, represented by $C(r,t)$ which varies as molecules diffuse through or react within the detection volume.

The intensity fluctuations, which are basically due to concentration fluctuation in the observation volume, can be defined as[44]

$$\delta F(t) = \int I(r).CEF(r).S(r).\delta C(r,t)dr \tag{2.38}$$

As we already know, from equation 2.36,

$$g(\tau) = \frac{k^2 \int\int I(r).I(r')CEF(r).CEF(r')S(r)S(r')\langle\delta C(r,t)\delta C(r',t+\tau)\rangle drdr'}{k^2\langle\int I(r).CEF(r).S(r).C(r,t)dr\rangle^2} \tag{2.39}$$

Assuming the sample is much larger than the observation volume, $S(r) = 1$. Also, in the denominator only the concentration term is affected by time, and a time integral over that concentration term will result in average concentration, $\langle C\rangle$. Thus, we can write,

$$\therefore g(\tau) = \frac{\int\int I(r).I(r')CEF(r).CEF(r')S(r)S(r')\langle\delta C(r,t)\delta C(r',t+\tau)\rangle drdr'}{\langle c\rangle^2\langle\int I(r).CEF(r).S(r).dr\rangle^2} \tag{2.40}$$

In confocal fluorescence correlation spectroscopy (FCS), the combined influence of the focused excitation beam and the spatial filtering introduced by the pinhole is commonly approximated by a three-dimensional Gaussian profile. This approximation is widely accepted, as it provides a close representation of the actual detection volume created by a tightly focused laser in a confocal setup. The Gaussian model simplifies analytical treatment while accurately capturing the spatial characteristics of the excitation-emission overlap region.

Let *P* represent the laser power. The spatial profile of the detection volume in fluorescence correlation spectroscopy, denoted as *W(r)*, is defined as the product of the excitation intensity distribution *I(r)* and the collection efficiency function *CEF(r)*[44]. This combined function represents the overall sensitivity of the system to fluorescence originating from a given spatial location *r*. Under the widely adopted three-dimensional Gaussian approximation, the detection profile *W(r)* can be expressed as [44]:

$$W(r) = I(r).CEF(r) = \frac{2P}{\pi w_0} e^{\frac{-2x^2}{{w_0}^2}.\frac{-2y^2}{{w_0}^2}.\frac{-2z^2}{{z_0}^2}} \quad (2.41)$$

For pure diffusion, the fluctuations in concentration can be written (the details can be found in the book [44] mentioned above) as,

$$\langle \delta C(r,t)\delta C(r',t+\tau)\rangle = \langle C\rangle.\frac{e^{\frac{-(x-x')^2+(y-y')^2+(z-z')^2}{4D\tau}}}{8(\pi D\tau)^{3/2}} \quad (2.42)$$

Replacing these equations (2.41, 2.42) into the autocorrelation function,

$g(\tau)$

$$= \frac{\int\int\int\int\int\int e^{\frac{-2\left(x^2+x'^2\right)}{w^2{}_0}} e^{\frac{-2\left(y^2+y'^2\right)}{w^2{}_0}} e^{\frac{-2\left(z^2+z'^2\right)}{z^2{}_0}} \cdot \frac{e^{\frac{-(x-x')^2+(y-y')^2+(z-z')^2}{4D\tau}}}{8(\pi D\tau)^{3/2}} dxdx'\,dydy'\,dzdz'}{\langle C\rangle\left(\int\int\int e^{\frac{-2x^2}{w^2{}_0}} e^{\frac{-2y^2}{w^2{}_0}} e^{\frac{-2z^2}{z^2{}_0}} dxdydz\right)^2}$$

(2.43)

Integrating and simplifying, we get,

$$g(\tau) = \frac{1}{\langle C\rangle \pi^{3/2} {w_0}^2 z_0}\left(1+\frac{4D\tau}{{w_0}^2}\right)^{-1/2}\left(1+\frac{4D\tau}{{w_0}^2}\right)^{-1/2}\left(1+\frac{4D\tau}{{z_0}^2}\right)^{-1/2} \quad (2.44)$$

Diffusion in each direction has one term in this equation 2.44. As the system is rotationally symmetric, the two terms coming from x and y direction are essentially the same, and thus the function becomes,

$$g(\tau) = \frac{1}{N}\left(1+\frac{\tau}{\tau_D}\right)^{-1}\left(1+\frac{\tau}{K^2\tau_D}\right)^{-1/2} \quad (2.45)$$

In this equation,

$N = \langle C\rangle \pi^{3/2} w_0^2 z_0 = \langle C\rangle . V_{eff}$,

$\tau_D = diffusion\ time = \frac{w_0^2}{4D}$; $K = structure\ factor = \frac{z_0}{w_0}$

Most importantly, the effective detection volume of the FCS (V_{eff}) is represented as,

$$V_{eff} = \pi^{3/2} w_0^2 z_0 \quad (2.46)$$

At $\tau = 0$, the equation 2.45 becomes, $g(0)$, which is the inverse of the average particle number in the observation volume and is expressed as,

$$g(0) = \frac{1}{N} = \frac{1}{V_{eff}\langle C \rangle} \tag{2.47}$$

So, equation 2.45 can be rewritten as,

$$g(\tau) = g(0) \cdot \left(1 + \left(\frac{\tau}{\tau_D}\right)\right)^{-1} \cdot \left(1 + \left(\frac{1}{K}\right)^2 \cdot \frac{\tau}{\tau_D}\right)^{-\frac{1}{2}} \tag{2.48}$$

In the case where $\tau = \tau_D$, the function (equation 2.48) will become,

$$g(\tau_D) = g(0) \cdot \left(1 + \left(\frac{\tau_D}{\tau_D}\right)\right)^{-1} \cdot \left(1 + \left(\frac{1}{K}\right)^2 \cdot \frac{\tau_D}{\tau_D}\right)^{-\frac{1}{2}}$$

$$\therefore g(\tau_D) = g(0).\frac{1}{2\sqrt{1+K^{-2}}}$$

Replacing a typical value of K in a confocal FCS setup, $K \sim 5$, in $g(\tau_D)$,

$$g(\tau_D) \approx \frac{g(0)}{2.04} \approx \frac{1}{2.04\ N}$$

So, τ_D is the time at which the amplitude of the correlation becomes half of its initial value. This simple way can be qualitatively used to estimate the comparative nature of diffusion, i.e., faster or slower than the other.

Thus far, the derivation of the autocorrelation function has been based on the assumption that fluctuations in fluorescence intensity arise solely from the translational diffusion of fluorophores through the confocal observation volume. However, under real experimental conditions, this assumption is often an oversimplification. Additional dynamic processes—such as photophysical transitions (e.g., intersystem crossing to the triplet state), chemical reactions, or conformational changes—can significantly contribute to the observed fluctuation

patterns. These non-diffusive events must be considered when interpreting the autocorrelation data to ensure accurate representation of the system's underlying dynamics [43,44,50].

To account for such non-diffusive contributions, an additional multiplicative factor is incorporated into the autocorrelation function. The total ACF is now expressed as,

$$g_{total}(\tau) = g_{total}(\tau) \cdot X_{kinetics}(\tau) \quad (2.49)$$

In cases where the fluorophore undergoes reversible transitions such as entering a non-fluorescent triplet state, the kinetic contribution can be modeled using a simple exponential decay function

$$X_R(\tau) = 1 - A + A \cdot e^{-\frac{\tau}{\tau_R}} \quad (2.50)$$

Where A is the fractional contribution of the photophysical process to the overall fluorescence fluctuation, τ_R is the characteristic time constant of the process (e.g., triplet lifetime). For convenience, this function can be normalized by the non-fluctuating component $(1 - A)$, leading to the simplified form

$$X_R(\tau) = 1 + a \cdot e^{-\frac{\tau}{\tau_R}} \quad (2.51)$$

Where, $a = {}^{A}/_{1-A}$.

When both diffusion and a reversible photophysical process contribute to fluorescence fluctuations, the final form of the autocorrelation function can be written as,

$$g(\tau) = \frac{1}{V_{eff}\langle C\rangle} \cdot \frac{1}{\left(1+\left(\frac{\tau}{\tau_D}\right)\right)} \cdot \frac{1}{\sqrt{1+\left(\frac{1}{K}\right)^2 \cdot \frac{\tau}{\tau_D}}} \cdot \left(1 + a \cdot e^{-\frac{\tau}{\tau_R}}\right)$$

$$\therefore g(\tau) = g(0) \cdot \left(1 + \left(\frac{\tau}{\tau_D}\right)\right)^{-1} \cdot \left(1 + \left(\frac{1}{K}\right)^2 \cdot \frac{\tau}{\tau_D}\right)^{-\frac{1}{2}} \cdot \left(1 + a \cdot e^{-\frac{\tau}{\tau_R}}\right) \qquad (2.52)$$

In some cases, anomalous diffusion (e.g., hindered or subdiffusive motion in crowded environments) must be considered.[53–55] This is accounted for by introducing an anomaly exponent α, modifying the autocorrelation function as[54,56],

$$g(\tau) = g(0) \cdot \left(1 + \left(\frac{\tau}{\tau_D}\right)^{\alpha}\right)^{-1} \cdot \left(1 + \left(\frac{1}{K}\right)^2 \cdot \left(\frac{\tau}{\tau_D}\right)^{\alpha}\right)^{-\frac{1}{2}} \qquad (2.53)$$

'α' is a measure of the extent of deviation from normal diffusion. The diffusion is referred to as subdiffusion for $0 < \alpha < 1$, normal diffusion for $\alpha = 1$, and super diffusion for $\alpha > 1$.[54,56]

For more than one particle diffusing normally (i.e. $\alpha = 1$), the ACF can be written as[44]

$$G(\tau) = \frac{1}{(\sum_i N_i)^2} \sum_i N_i D_i(\tau)\,;\; D_i(\tau) = \left(1 + \frac{\tau}{\tau_{D_i}}\right)^{-1} \left(1 + \frac{1}{K^2}\frac{\tau}{\tau_{D_i}}\right)^{-\frac{1}{2}} \qquad (2.54)$$

2.7.4. Structural Information Extraction employing FCS

Once the diffusion time (τ_D) is obtained by fitting the autocorrelation curves with suitable theoretical models (as discussed earlier), the translational diffusion coefficient (D_t) of the particle can be calculated. This, in turn, enables the extraction

of structural information—specifically, the hydrodynamic radius (r_H) by applying the Stokes–Einstein equation [57,58]. The Stokes–Einstein relation describes the Brownian motion of a spherical particle with hydrodynamic radius (r_H) as it diffuses through a viscous medium at constant temperature, linking the particle's size to its mobility in solution. The mathematical form of the equation is,

$$r_H = \frac{k_B T}{6\pi\eta D_t} \tag{2.55}$$

where k_B is the Boltzmann constant, T is the absolute temperature and η is the viscosity of the medium, D_t is the translational diffusion coefficient.

To calibrate the system and precisely estimate the confocal volume (parameterized by K), fluorescence correlation spectroscopy (FCS) measurements were conducted using Rhodamine 6G (R6G) dissolved in water across a range of concentrations. The resulting autocorrelation functions were subjected to global fitting, wherein K was determined by assuming a known diffusion coefficient for R6G in water, $D_t = 4.14 \times 10^{-6}\ cm^2 s^{-1}$ [59]. After this calibration step, the obtained value of K was held constant for fitting all subsequent experimental datasets belonging to the same series, regardless of the specific fitting model employed.

2.7.5. Accounting for Medium-induced Refractive Index and Viscosity Alterations

External perturbations—such as temperature variation, the introduction of deep eutectic solvents (DES), or the presence of macromolecular crowding agents—can notably influence both the viscosity and refractive index of the medium. To distinguish the specific contribution of viscosity from other factors like molecular size or structural changes, we conducted control measurements under each

experimental condition using Rhodamine 6G (R6G) as a reference fluorophore. Due to its small size and rigid structure, R6G remains structurally unaltered in response to environmental modifications, including DES addition, crowding, or thermal shifts. Therefore, any observed change in its diffusion time can be attributed exclusively to variations in the viscosity of the solution.

By utilizing the known hydrodynamic radius of Rhodamine 6G (R6G) in buffer and its experimentally determined diffusion time under identical conditions, we estimated the hydrodynamic radius of the protein or any other fluorescent dye at each experimental point using the following relationship:

$$r_H^{protein} = r_H^{R6G} \times \frac{\tau_D^{protein}}{\tau_D^{R6G}} \tag{2.56}$$

FCS is routinely used by researchers to monitor the conformational change of protein in the presence of various external perturbations like desaturating agents, heat, DES, crowder, confinement, and so forth.[40,51,52,60–67]

To account for variations in refractive index under different experimental conditions, the objective collar was carefully adjusted. At each condition, the collar was optimized to maximize the $G(0)$ value, thereby ensuring minimal effective observation volume and maintaining consistent optical alignment throughout all measurements.

2.7.6. FCS Setup

A major hurdle in single-molecule fluorescence detection is the suppression of background contributions, such as Raman scattering originating from the solvent [19]. This issue can be effectively addressed by confining the observation volume to the

femtoliter range, which significantly diminishes background interference and improves signal-to-noise ratio. Attaining such a highly restricted detection volume is a fundamental objective of Fluorescence Correlation Spectroscopy (FCS) instrumentation [19]. This confinement is typically achieved using one of two primary optical configurations: (i) confocal microscopy, or (ii) total internal reflection fluorescence (TIRF) geometry [44,68].

In this thesis, a home-built confocal FCS setup has been used for performing single molecular level fluorescence experiments (see scheme 2.10). The schematic diagram has been shown in scheme 2.10 and the photograph of the actual setup has been shown in Figure 2.1.

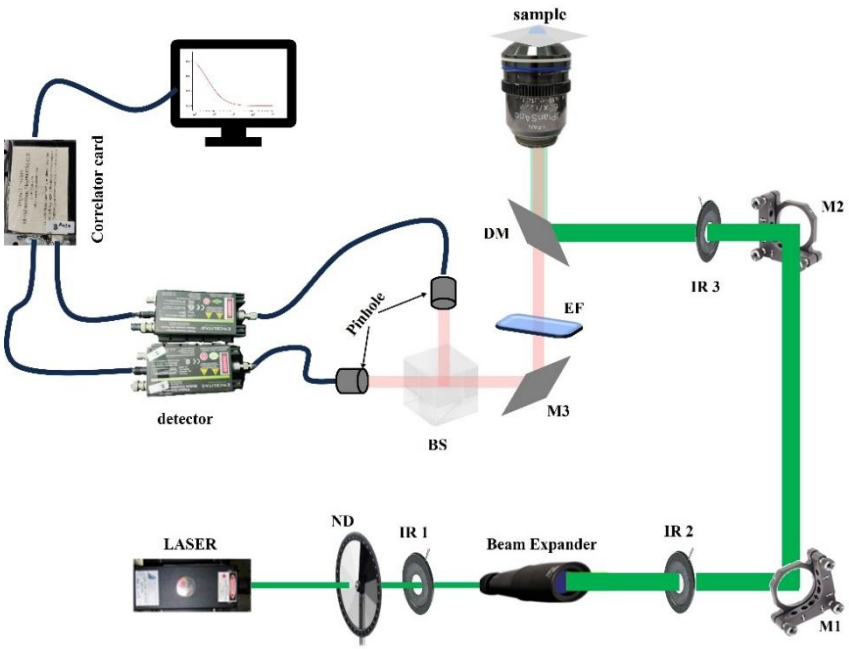

Scheme 2.10. A schematic diagram of a home-built FCS. (Abbreviations: IR, iris; M, mirror; DM, dichroic mirror; ND, neutral density filter; EF, emission filter). The sample cells are specially designed glass cells with a water jacket surrounding them. In the water jacket, there are one inlet and one outlet for water circulation. Labocon LLCB-202 temperature controller unit has been used to circulate water of a specific temperature through the water jacket to control the temperature of the sample cell.

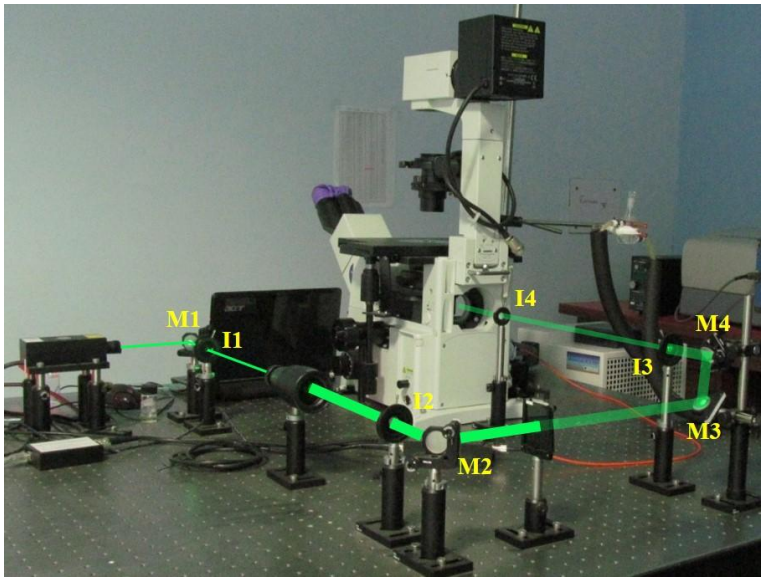

Figure 2.1. Image of home-built FCS setup.

To facilitate understanding, the entire setup is divided into three major functional components such as (a) excitation unit, (b) detection unit, and (c) data analysis unit, and they are discussed in the following paragraphs.

(a) Excitation unit: The excitation module consists of a laser source, a beam expander (telescope), a series of mirrors (M1–M4), and irises (I1–I4). The laser emits a collimated beam with an initial diameter of approximately 2.5 mm. To achieve a tightly focused spot at the sample plane, the beam is expanded nearly eightfold using the telescope, enabling efficient filling of the back aperture of the objective lens. The expanded beam is then guided into the microscope via a set of carefully aligned mirrors. A neutral density (ND) filter is introduced along the optical path to control the excitation intensity. Just before entering the microscope, an iris is used to fine-tune the beam diameter, which is maintained close to 10 mm to match the aperture size of the objective. The collimated beam subsequently encounters a dichroic mirror, which reflects the excitation light toward the objective

lens. The objective, a compound lens system, focuses the beam onto the sample, which is mounted on a clean coverslip positioned on the microscope stage.

(b) Detection unit: After excitation, the sample emits fluorescence, which is selectively collected by the same objective lens, but only from the portion of light directed back into it. This emitted light is collimated by the objective and passes through the dichroic mirror, followed by an emission filter that eliminates any residual excitation light. The filtered fluorescence signal then encounters a 50:50 cubic beamsplitter, which divides the light equally along two perpendicular detection paths. Each path leads to a pinhole, implemented using fiber tips, which serves as a spatial filter. These pinholes ensure that only photons originating from the defined focal volume are detected, while out-of-focus fluorescence is rejected preserving confocality. The size of the pinhole determines the extent of the effective observation volume, thus playing a crucial role in spatial resolution. (see Scheme 2.11 and Scheme 2.12 for illustration).

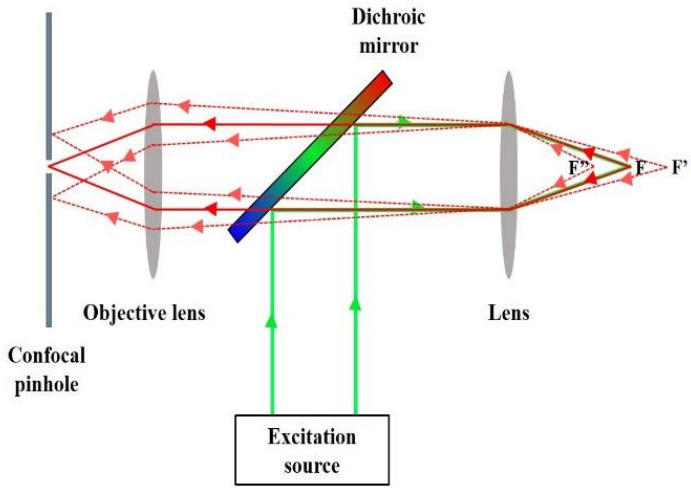

Scheme 2.11. Schematic representation of the confocal detection system.

The optical fiber, securely mounted on a five-axis positioner for precise alignment, channels the collected photons to a single-photon avalanche photodiode (APD),

where they are converted into electronic pulses suitable for time-resolved photon counting.

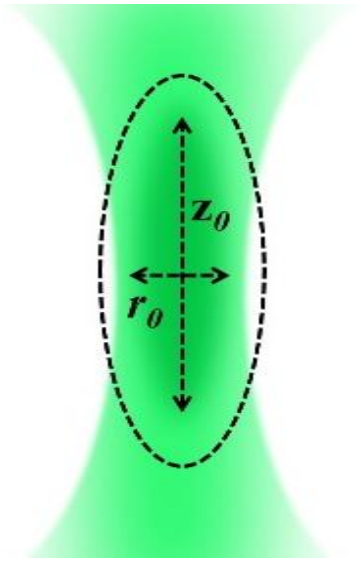

Scheme 2.12. Gaussian-shaped observation volume.

(c) Analysis unit: The fluorescence signal collected through the two pinholes and guided via optical fibers is registered as photon counts by the avalanche photodiodes (APDs). These signals are then transmitted to an autocorrelator card, which segments the intensity time traces into discrete time bins and calculates the cross-correlation between the two detection channels as a function of time delay (lag time). Individual autocorrelation curves from each APD can also be obtained by disabling the alternate detector.

To generate the correlation curve, the system first determines the average fluorescence intensity from one channel, $\langle F_1(t)\rangle$, and calculates its corresponding fluctuation profile, $\delta F_1(t)$. The fluctuation signal from the second channel, $\delta F_2(t)$), is then systematically time-shifted in increments defined by the time resolution of the correlator hardware. The correlation between the two fluctuation profiles is computed at each time lag to construct the full correlation function.

In our experimental setup, the correlator card offers a minimum lag time resolution of 0.2 microseconds, enabling detection of fluorescence fluctuations occurring on timescales as short as 0.2 µs. The system supports a maximum lag time of approximately 3,435,969,984 microseconds—equivalent to nearly one hour—allowing for the observation of slow dynamic processes over extended periods. Consequently, the spectrum of dynamic events that can be analyzed is intrinsically constrained by these lower and upper lag time limits.

After the correlation curve is generated, the output is transmitted to a LabVIEW-based graphical user interface, enabling real-time visualization of the data. Simultaneously, the correlation data is stored in ASCII format, allowing for seamless import into external analysis tools such as Igor Pro for detailed quantitative evaluation and model fitting.

2.7.6.1. Specification of the Components of the FCS setup

Laser: MGL-III-532-5mW (532 nm), CNI, China

Telescope: BE10M-A, Thorlabs, USA

Mirrors: KM100, Thorlabs, USA

Microscope: Inverted confocal microscope, IX-71, Olympus, Japan

Objective lens: 60X water immersion objective with numerical aperture 1.2, working distance 0.28 mm, Olympus.

Dichroic mirror: ZT532RDC, Chroma, USA.

Bandpass filters: ET605/70m

Neutral density filters: NDC-50C-4M - Mounted Continuously Variable ND Filter, Thorlabs, USA

Cubic Beam Splitter: BS010 - 50:50 Non-Polarizing Beamsplitter Cube, 400 - 700 nm, Thorlabs, USA

Fibre patch chord: M43L01, M42L01, M67L01, Thorlabs, USA

Detector: SPCM-AQRH-13-FC-24420, Excelitas technologies

Correlator card: Flex 990EM-12E,

Opto-mechanics: Post, rods, iris, and holders are from Thorlabs, USA, and Holmarc, India.

2.7.6.2. Calibration of the Instrument

Analyzing the experimental auto- and cross-correlation curves provides the diffusion time of molecules as they traverse the detection volume. However, this diffusion time is not an intrinsic property; it is affected by parameters such as the size of the observation volume and the viscosity of the surrounding medium, classifying it as an extensive property [43,44]. To derive accurate, size-specific information from the measured diffusion times, it is therefore necessary to calibrate the focal volume. Moreover, the theoretical frameworks applied in FCS analysis assume of a Gaussian intensity profile of the excitation beam. As a result, thorough system calibration is a critical prerequisite prior to acquiring any experimental data.

2.7.6.3. Alignment of the Detector:

The fiber patch cord, which simultaneously serves as the confocal pinhole, must be accurately positioned at the focal point of the emitted fluorescence to ensure efficient detection of photons originating from the defined Gaussian observation volume. This precise alignment is accomplished using a five-axis positioner, enabling translational adjustments along the x, y, and z axes, as well as angular tilts in two orthogonal planes. The alignment procedure is carried out as follows:

(i) Initial Alignment: A concentrated dye solution is placed in the sample chamber, and the fiber is coarsely aligned until the fluorescence becomes visible at the fiber's output.

(ii) Fine Alignment: A dilute dye solution (~1–5 nM) is then used, and the fiber position is adjusted carefully using the screws of five-axis to maximize photon count at the detector, ensuring that it is perfectly aligned with the focused emission path.

Before taking any data for an unknown sample, the photon count from a standard dye like rhodamine 6G (R6G) is checked. If the signal is lower than expected, the alignment and calibration procedure is repeated.

2.7.6.4. Achieving the minimal Detection Volume

After achieving optimal alignment, the subsequent step is to minimize the excitation volume, which is essential for enhancing both spatial resolution and the signal-to-noise ratio. The diameter of the excitation beam is a critical parameter influencing the size of the focal volume—wider beam diameters lead to more tightly confined focal spots (refer to Scheme 2.13). Calibration is performed by measuring the diffusion time of a dilute dye solution (typically 1–5 nM) while systematically adjusting the objective collar and fine-tuning the focal plane height relative to the coverslip surface.

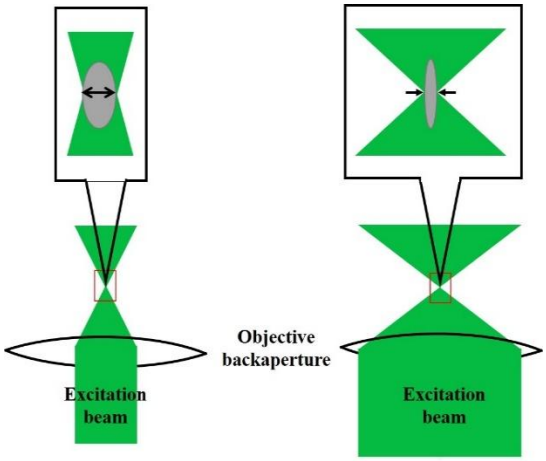

Scheme 2.13. Illustration of focal volume control via excitation beam diameter and objective overfilling.

The objective's collar ring serves to compensate for spherical aberrations arising from refractive index mismatches among the immersion medium, cover glass, and sample. Identifying the optimal collar setting is crucial for each combination of refractive index and excitation wavelength to ensure accurate focusing and minimal optical distortion. Figure 2.2 demonstrates the dependence of Rhodamine 6G diffusion time in aqueous solution on the objective collar position, highlighting the importance of proper adjustment.

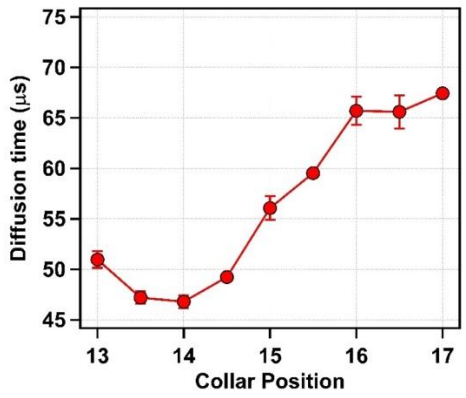

Figure 2.2. Dependence of rhodamine 6G diffusion time on the objective collar setting.

As evident from the figure, the shortest diffusion time is attained at collar position ~13.5-14, indicating optimal alignment and minimal focal volume.

Vertical positioning of the focal plane (z-axis control) is achieved using a rotary knob integrated into the microscope, which allows precise adjustment of the objective's height relative to the sample. The positions of the upper and lower surfaces of the coverslip can be identified by a sharp increase in detected photon counts, indicating the optical interfaces. To maintain consistency and minimize optical artifacts, the focal plane is typically set approximately 40 µm above the coverslip surface, a distance that has proven optimal for the instrumentation used in this study.

2.7.6.5. Measurement of the dimension of the observation volume

The observation volume, which generally exhibits a Gaussian profile (see Scheme 2.12), is characterized using a reference dye—commonly Rhodamine 6G (R6G) with a known diffusion coefficient. To determine this volume, multiple autocorrelation curves are acquired at varying dye concentrations (Figure 2.3). The geometric parameter '*K*', defined as the ratio of the axial to radial dimensions of the focal volume, quantifies its shape and remains constant across all concentrations. Only the average number of fluorescent molecules within the observation volume changes with concentration. The resulting autocorrelation curves are globally fitted starting from 1 µs using a one-component diffusion model that includes an additional exponential term to account for the known triplet-state dynamics of rhodamine dyes. Since the characteristic timescale of this photophysical process in buffer lies within ~1–2 µs, fitting the data from 10 µs onward effectively excludes any contribution from triplet-state kinetics, allowing the use of a simple one-component diffusion model. Notably, the extracted observation volume parameters remain consistent between both fitting approaches.

The global fitting yields the diffusion time (which is independent of the concentration and hence the same for all the curves) and the instrumental parameter

'K' which is the ratio of the axial and radial diameters of the observation volume, $K = \frac{z_0^2}{w_0^2}$.

The known diffusion coefficient of R6G dye in the buffer is 4.14 x 10^{-6} cm^2 sec^{-1} [59]. The value of the transverse radius (r) is can then be calculated using the equation, $D = \frac{w_0^2}{4\tau_D}$. By employing another equation, $V_{eff} = \pi^{3/2} w_0^2 z_0$, the effective observation volume of our setup was estimated to be ~ 0.7-0.9 fL.

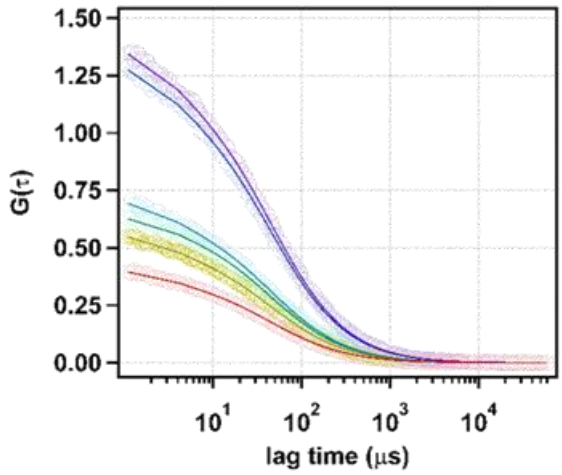

Figure 2.3. Global fitting of autocorrelation curves using equation 2.52 in order to measure the dimensions of the observation volume.

2.7.6.6. Checking the effect of power

Fluorescence Correlation Spectroscopy (FCS) is extremely sensitive to temporal fluctuations in fluorescence intensity. However, at higher excitation powers, additional fluctuation sources—such as photobleaching and population of non-emissive triplet states—can introduce distortions in the signal, thereby complicating quantitative analysis. To mitigate these artifacts, it is essential to optimize and carefully adjust the excitation power before commencing data acquisition.

To identify the optimal excitation power, an initial power-dependence assessment is performed. The sample is subjected to a range of laser intensities, and the corresponding fluorescence autocorrelation curves are recorded for comparison. Photostable fluorophores such as Rhodamine 6G typically tolerate high excitation powers without significant alterations in their correlation profiles. In contrast, more sensitive systems such as fluorescently tagged proteins exhibit deviations in the autocorrelation curves once the excitation power exceeds a critical threshold. For these less stable systems, all subsequent measurements are carried out at a laser power slightly below this threshold, ensuring minimal photophysical artifacts while preserving sufficient signal intensity for reliable data acquisition.

2.8. Bulk Viscosity

Viscosity measurements were carried out using a commercially available viscometer (VISCO Package E, Atago, Japan) equipped with an integrated temperature control unit. All measurements were conducted at a constant temperature of 298 K.

2.9. Protein Tagging

In this thesis, two proteins, Papain and Bromelain, were studied. Site-specific fluorescent tagging was carried out to probe distinct structural and dynamical features of these proteins. Both proteins were tagged following previously published reports.[69–73]

Both proteins, papain and bromelain possess a single free cysteine at their catalytic site located at residue number 25 and 26 respectively (Scheme 2.12). This thiol group served as a labeling site, and CPM was employed for site-specific conjugation.

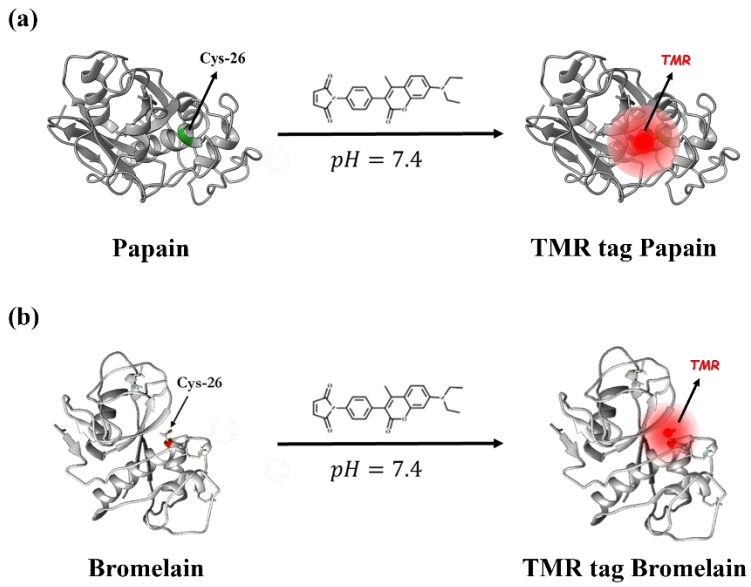

Scheme 2.12. Schematic representation of labeling of (a) Cys-25 of papain, and (b) Cys-26 of bromelain by TMR fluorophore.

I have employed TMR-tagged proteins for the FCS study. However, for the time-resolved emission, I have employed CPM tagged proteins where the dye has been changed but the location of tagging remains the same i.e., free cysteine.

Labeling of Papain and Bromelain

Papain (PDB ID: 9PAP) and bromelain (PDB ID: 1W0Q) were site-specifically labeled at their sole free cysteine residue (position 25) using the thiol-reactive fluorophore 7-diethylamino-3-(4-maleimidophenyl)-4-methylcoumarin (CPM), following established protocols [69]. These CPM-labeled proteins were employed in time-resolved fluorescence experiments, leveraging the solvatochromic properties of CPM. For fluorescence correlation spectroscopy (FCS) studies, papain and bromelain were instead conjugated with the thiol-specific dye tetramethylrhodamine-5-maleimide (TMR). Control experiments confirmed that fluorophore tagging did not perturb the native structure of the proteins.

Tagging efficiency was determined by calculating the molar ratio of protein to fluorophore, using extinction coefficients $\epsilon_{papain}^{280} = 57600\ M^{-1}cm^{-1}$, $\epsilon_{bromelain}^{280} = 63500\ M^{-1}cm^{-1}$, $\epsilon_{papain}^{CPM} = 33000\ M^{-1}cm^{-1}$ *and* $\epsilon_{papain}^{TMR} = 75000\ M^{-1}cm^{-1}$ [69].

2.10. Some Control Experiments Related to Tagging:

2.10.1. Confirmation, Site-selectivity, and Perturbation Related to Tagging of Fluorophores to Papain and Bromelain:

CPM is a solvatochromic fluorophore, meaning it is sensitive to the polarity of its local environment. In aqueous buffer, CPM exhibits weak fluorescence; however, upon covalent attachment to a protein, a marked enhancement in fluorescence intensity is observed (Figure 2.4(a) and Figure 2.5(a)). This enhancement is likely due to restricted intramolecular rotation of the dye within the protein matrix, which reduces non-radiative decay pathways. When excited at its absorption maximum of 393 nm, the CPM-labelled protein displays an emission maximum around 479 nm, whereas the free dye in buffer emits at approximately 481 nm (Figure 2.4(b)). The observed blue shift upon tagging suggests that the fluorophore is localized within a relatively hydrophobic region of the protein. These spectral changes collectively confirm successful conjugation of CPM to the protein.

In contrast, tetramethyl rhodamine (TMR) is not solvatochromic, rendering emission-based confirmation of tagging ineffective. Therefore, Fluorescence Correlation Spectroscopy (FCS) was used to evaluate the diffusion behaviour of TMR-labelled samples. TMR-tagged papain exhibited a significantly slower diffusion time (130 µs) compared to free TMR dye (39 µs) when measured within the same observation volume (~0.5 fL), confirming successful protein labelling (Figure 2.4(c)). Additionally, no significant changes were observed in the circular dichroism (CD) spectra or the intrinsic fluorescence emission profile (λ_{ex} = 295 nm)

of papain upon tagging with either CPM or TMR (Figures 2.4(d)), indicating that the protein's secondary structure remains largely unaltered following dye conjugation.

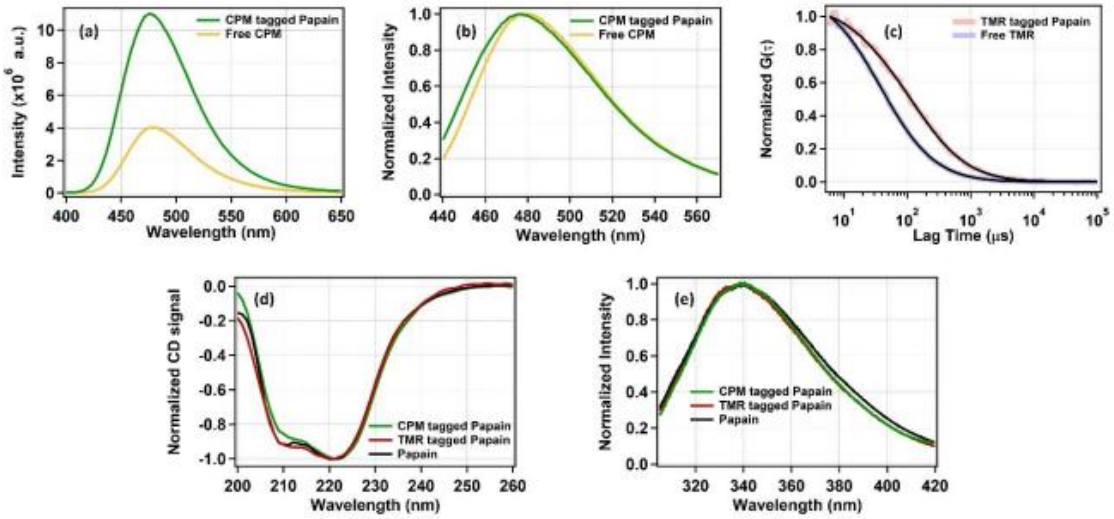

Figure 2.4. (a) Emission of CPM before and after tagging. (b) Normalized emission spectra of free CPM and CPM-tagged papain on excitation at 390 nm. (c) Normalized autocorrelation traces for free TMR dye and TMR tagged papain. The fitting line for each trace is shown in black. (d) Normalized CD spectra of papain, CPM tagged papain, TMR tagged papain. (e) Normalized emission spectra of papain, CPM tagged papain, TMR tagged papain (λ_{ex}=295nm).

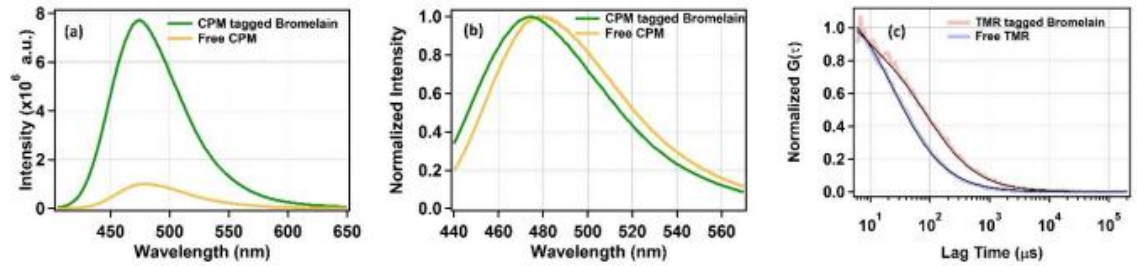

Figure 2.5. (a) Emission of CPM before and after tagging, (b) Normalized emission spectra of CPM tagged bromelain on excitation at 390 nm, (c) Normalized autocorrelation traces for free TMR dye and TMR tagged bromelain, and here the fitting line for each trace is shown in black.

An increase in fluorescence intensity accompanied by a blue shift of approximately 6 nm in the emission spectrum further confirms successful tagging of CPM to bromelain (Figure 2.5(b)). Additionally, the slower diffusion time of TMR-labeled bromelain (114 μs), as shown in Figure 2.5(c), relative to that of free TMR dye, provides further evidence of effective conjugation. As structural integrity of bromelain upon CPM and TMR tagging has already been demonstrated previously, those results are not reiterated here.

2.11. Materials Used

We have purchased papain (from papaya latex), bromelain (from the pineapple stem), 7-diethylamino-3-(4-maleimidophenyl)-4-methylcoumarin (CPM) (≥90%), tetramethylrhodamine-5-maleimide (TMR) (≥85%), urea (≥99%), guanidine hydrochloride (≥99%), sucrose (≥99.5%), d-sorbitol (≥98%), d-(+)-trehalose (≥99%), and d-(+)-glucose (≥99.5%) from Sigma-Aldrich and used them as received. Glycine (≥99%) was purchased from S.D. Fine Chemicals Ltd, India and purified as per the procedure given in the literature before use. HPLC grade dimethyl sulfoxide (DMSO) was also purchased from S.D. Fine Chemicals Ltd, India and used after distillation. Trimethyl amine *N*-oxide dihydrate (TMAO) (≥98%) was purchased from the Tokyo Chemical Company, Japan and used as received. The dialysis membrane (14 kDa cutoff) was purchased from Sigma-Aldrich and used after washing according to the procedure given by Sigma-Aldrich. We have purchased analytical grade disodium hydrogen phosphate (≥99%) and sodium dihydrogen phosphate (≥98%) from Merck, India and used them directly to prepare 50 mM buffer (pH 7.4). Centrifugal filtration units (10 kDa cutoff, Amicon Ultra) have been purchased from Merck Millipore, Germany.

2.12. Sample Preparation

Untagged proteins were dissolved in 50 mM phosphate buffer of pH 7.4 and then centrifuged using Amicon Ultra-4 centrifugal filtration units (cutoff 10 kDa) and all

the experiments are then performed using the supernatant. Samples were then prepared by mixing the required amount of filtered papain/bromelain (tagged/untagged according to requirements) with the required amount of freshly prepared osmolyte stock solution in 50 mM phosphate buffer (pH 7.4). Samples were incubated for 12 hours before performing any experiment. Protein concentration was maintained as 10 μM for steady-state, time-resolved fluorescence measurements and 25 μM for the CD experiment. For FCS measurements, the protein concentration was kept as 5 nM.

2.13. References

(1) Demchenko, A. P. The Red-Edge Effects: 30 Years of Exploration. *Luminescence*. 2002, pp 19–42. https://doi.org/10.1002/bio.671.

(2) Demchenko, A. P. Weber's Red-Edge Effect That Changed the Paradigm in Photophysics and Photochemistry. **2016**, 95–141. https://doi.org/10.1007/4243_2016_14.

(3) Azumi, T.; Itoh, K. I.; Shiraishi, H. Shift of Emission Band upon the Excitation at the Long Wavelength Absorption Edge. III. Temperature Dependence of the Shift and Correlation with the Time Dependent Spectral Shift. *J Chem Phys* **1976**, *65* (7), 2550–2555. https://doi.org/10.1063/1.433440.

(4) Itoh, K. I.; Azumi, T. Shift of the Emission Band upon Excitation at the Long Wavelength Absorption Edge. II. Importance of the Solute-Solvent Interaction and the Solvent Reorientation Relaxation Process. *J Chem Phys* **1975**, *62* (9), 3431–3438. https://doi.org/10.1063/1.430977.

(5) Nelson, D. L.; Cox, M. M.; Hoskins, A. A. *Lehninger Principles of Biochemistry*; Macmillan Learning: New York, USA, 2021.

(6) Das, N.; Khan, T.; Sen, P. The Shift of Excitation Spectra at Blue Edge of Emission (BEEmS) as a New Methodology to Probe Heterogeneity. *Chem Phys* **2024**, *577*, 112138. https://doi.org/10.1016/J.CHEMPHYS.2023.112138.

(7) Chattopadhyay, A.; Haldar, S. Dynamic Insight into Protein Structure Utilizing Red Edge Excitation Shift. *Acc Chem Res* **2014**, *47* (1), 12–19. https://doi.org/10.1021/ar400006z.

(8) More, S. R.; Jha, S. K. Multi-Site Red-Edge Excitation Shift Reveals the Residue-Specific Solvation Dynamics during the Native to Amyloid-like Transition of an Amyloidogenic Protein. *Journal of Physical Chemistry B* **2024**. https://doi.org/10.1021/acs.jpcb.4c07067.

(9) Brahma, R.; Raghuraman, H. Novel Insights in Linking Solvent Relaxation Dynamics and Protein Conformations Utilizing Red Edge Excitation Shift Approach. *Emerg Top Life Sci* **2021**, *5* (1), 89–101. https://doi.org/10.1042/ETLS20200256.

(10) Whitmore, L.; Wallace, B. A. Protein Secondary Structure Analyses from Circular Dichroism Spectroscopy: Methods and Reference Databases. *Biopolymers* **2008**, *89* (5), 392–400. https://doi.org/10.1002/BIP.20853,.

(11) Johnson, W. C. Secondary Structure of Proteins through Circular Dichroism Spectroscopy. *Annu Rev Biophys Biophys Chem* **1988**, *17*, 145–166. https://doi.org/10.1146/ANNUREV.BB.17.060188.001045,.

(12) Wei, Y.; Thyparambil, A. A.; Latour, R. A. Protein Helical Structure Determination Using CD Spectroscopy for Solutions with Strong Background Absorbance from 190-230 Nm. *Biochim Biophys Acta* **2014**, *1844* (12), 2331. https://doi.org/10.1016/J.BBAPAP.2014.10.001.

(13) Greenfield, N. J. Using Circular Dichroism Spectra to Estimate Protein Secondary Structure. *Nat Protoc* **2007**, *1* (6), 2876–2890. https://doi.org/10.1038/nprot.2006.202.

(14) Greenfield, N.; Fasman, G. D. Computed Circular Dichroism Spectra for the Evaluation of Protein Conformation. *Biochemistry* **1969**, *8* (10), 4108–4116. https://doi.org/10.1021/BI00838A031/ASSET/BI00838A031.FP.PNG_V03.

(15) Bohm, G.; Muhr, R.; Jaenicke, R. Quantitative Analysis of Protein Far UV Circular Dichroism Spectra by Neural Networks. *Protein Eng* **1992**, *5* (3), 191–195.

(16) Fleming, G. R. *Chemical Applications of Ultrafast Spectroscopy*; Oxford University Press: New York, 1986.

(17) Becker, W. *Advanced Time-Correlated Single Photon Counting Techniques*; Castleman, A. W., Toennies, J. P., Zinth, W., Eds.; Springer Series in Chemical Physics; Springer Berlin Heidelberg: Berlin, Heidelberg, 2005; Vol. 81. https://doi.org/10.1007/3-540-28882-1.

(18) O' Connor, D. V.; Phillips, D. *Time Correlated Single Photon Counting*; Academic Press, New York, USA: New York, 1984.

(19) Lakowicz, J. R. *Principles of Fluorescence Spectroscopy*; Springer, 2006; pp 1–954. https://doi.org/10.1007/978-0-387-46312-4.

(20) Hallidy, L. A.; Topp, M. R. Picosecond Luminescence Detection Using Type-II Phase-Matched Frequency Conversion. *Chem Phys Lett* **1977**, *46* (1), 8–14. https://doi.org/10.1016/0009-2614(77)85153-1.

(21) Chosrowjan, H.; Taniguchi, S.; Tanaka, F. Ultrafast Fluorescence Upconversion Technique and Its Applications to Proteins. *FEBS J* **2015**, *282* (16), 3003–3015. https://doi.org/10.1111/FEBS.13180.

(22) Kahlow, M. A.; Jarzęba, W.; DuBruil, T. P.; Barbara, P. F. Ultrafast Emission Spectroscopy in the Ultraviolet by Time-gated Upconversion. *Review of Scientific Instruments* **1988**, *59* (7), 1098–1109. https://doi.org/10.1063/1.1139734.

(23) Xu, J.; Knutson, J. R. Ultrafast Fluorescence Spectroscopy via Upconversion: Applications to Biophysics. *Methods Enzymol* **2008**, *450*, 159–183. https://doi.org/10.1016/S0076-6879(08)03408-3.

(24) Y.R., S. *The Principles of Nonlinear Optics*; John Wiley, New York, 1984.

(25) Zernike, F.; Midwinter, J. E. *Applied Nonlinear Optics*; John Wiley & Sons, Ltd., 1973.

(26) Fleming, G. R.; Gijzeman, O. L. J.; Freed, K. F.; Lin, S. H. Theory for Time Resolved Emission Spectra. *Journal of the Chemical Society, Faraday Transactions 2: Molecular and Chemical Physics* **1975**, *71*, 773–780. https://doi.org/10.1039/F29757100773.

(27) Changenet-Barret, P.; Choma, C. T.; Gooding, E. F.; Degrado, W. F.; Hochstrasser, R. M. Ultrafast Dielectric Response of Proteins from Dynamics Stokes Shifting of Coumarin in Calmodulin. *J. Phys. Chem. B* **2000**, *104* (39), 9322–9329. https://doi.org/10.1021/jp001634v.

(28) *Femtosecond Laser Pulses*; Rullière, C., Ed.; Advanced Texts in Physics; Springer New York: New York, NY, 2005. https://doi.org/10.1007/B137908.

(29) Ruckebusch, C.; Sliwa, M.; Pernot, P.; de Juan, A.; Tauler, R. Comprehensive Data Analysis of Femtosecond Transient Absorption Spectra: A Review. *Journal of Photochemistry and Photobiology C: Photochemistry Reviews* **2012**, *13* (1), 1–27. https://doi.org/10.1016/J.JPHOTOCHEMREV.2011.10.002.

(30) Berera, R.; van Grondelle, R.; Kennis, J. T. M. Ultrafast Transient Absorption Spectroscopy: Principles and Application to Photosynthetic Systems. *Photosynth Res* **2009**, *101* (2–3), 105–118. https://doi.org/10.1007/s11120-009-9454-y.

(31) Buzády, A.; Savolainen, J.; Erostyák, J.; Myllyperkiö, P.; Somogyi, B.; Korppi-Tommola, J. Femtosecond Transient Absorption Study of the Dynamics of Acrylodan in Solution and Attached to Human Serum Albumin. *J. Phys. Chem. B* **2003**, *107* (5), 1208–1214. https://doi.org/10.1021/jp027107o.

(32) McGregor, S. K. M.; Govind, C.; Wood, M. K. R.; Shukla, A.; Lim, H.; Lepage, R. J.; Krenske, E. H.; K. N., N. U.; Ajayaghosh, A.; Karunakaran, V.; Namdas, E. B.; Lo, S.-C. Structural Integration of Carbazole and Tetraphenylethylene: Ultrafast Excited-State Relaxation Dynamics and Efficient Electroluminescence. *Adv Photonics Res* **2021**, *2* (4), 2000144. https://doi.org/10.1002/adpr.202000144.

(33) Zhu, H.; Li, M.; Hu, J.; Wang, X.; Jie, J.; Guo, Q.; Chen, C.; Xia, A. Ultrafast Investigation of Intramolecular Charge Transfer and Solvation Dynamics of Tetrahydro[5]-Helicene-Based Imide Derivatives. *Sci Rep* **2016**, *6*, 24313. https://doi.org/10.1038/srep24313.

(34) Chowdhury, P. K.; Halder, M.; Sanders, L.; Calhoun, T.; Anderson, J. L.; Armstrong, D. W.; Song, X.; Petrich, J. W. Dynamic Solvation in Room-Temperature Ionic Liquids. *J. Phys. Chem. B* **2004**, *108* (29), 10245–10255. https://doi.org/10.1021/jp0376828.

(35) Gupta, S.; Rafiq, S.; Sen, P. Dynamics of Solvent Response in Methanol-Chloroform Binary Solvent Mixture: A Case of Synergistic Solvation. *J. Phys. Chem. B* **2015**, *119* (7), 3135–3141. https://doi.org/10.1021/jp5120338.

(36) Tan, X.; Gustafson, T. L.; Lefumeux, C.; Burdzinski, G.; Buntinx, G.; Poizat, O. Solvation Dynamics Probed by Femtosecond Transient Absorption Spectroscopy: Vibrational Cooling and Conformational Relaxation in S1 Trans-4,4′-Diphenylstibene. *J. Phys. Chem. A* **2002**, *106* (14), 3593–3598. https://doi.org/10.1021/jp013176b.

(37) Horng, M. L.; Gardecki, J. A.; Papazyan, A.; Maroncelli, M. Subpicosecond Measurements of Polar Solvation Dynamics: Coumarin 153 Revisited. *J. Phys. Chem.* **1995**, *99* (48), 17311–17337. https://doi.org/10.1021/J100048A004.

(38) Schuler, B. Single-Molecule FRET of Protein Structure and Dynamics - a Primer. *J Nanobiotechnology* **2013**, *11(suppl 1)* (S2), 1–17. https://doi.org/10.1186/1477-3155-11-S1-S2.

(39) Petrášek, Z.; Hoege, C.; Mashaghi, A.; Ohrt, T.; Hyman, A. A.; Schwille, P. Characterization of Protein Dynamics in Asymmetric Cell Division by Scanning Fluorescence Correlation Spectroscopy. *Biophys J* **2008**, *95* (11), 5476–5486. https://doi.org/10.1529/biophysj.108.135152.

(40) Yadav, R.; Sengupta, B.; Sen, P. Conformational Fluctuation Dynamics of Domain i of Human Serum Albumin in the Course of Chemically and Thermally Induced Unfolding Using Fluorescence Correlation Spectroscopy. *J. Phys. Chem. B* **2014**, *118* (20), 5428–5438. https://doi.org/10.1021/jp502762t.

(41) Sengupta, B.; Acharyya, A.; Sen, P. Elucidation of the Local Dynamics of Domain-III of Human Serum Albumin over the Ps–Ms Time Regime Using a New Fluorescent Label. *Phys. Chem. Chem. Phys.* **2016**, *18* (41), 28548–28555. https://doi.org/10.1039/C6CP05743H.

(42) Quast, R. B.; Margeat, E. Studying GPCR Conformational Dynamics by Single Molecule Fluorescence. *Mol Cell Endocrinol* **2019**, *493*, 110469. https://doi.org/10.1016/j.mce.2019.110469.

(43) Rigler, R.; Elson, E. S. *Fluorescence Correlation Spectroscopy*; Springer Series in Chemical Physics; Springer Berlin Heidelberg: Berlin, Heidelberg, 2001; Vol. 65. https://doi.org/10.1007/978-3-642-59542-4.

(44) Wohland, T.; Maiti, S.; Macháň, R. *An Introduction to Fluorescence Correlation Spectroscopy*; IOP Publishing, 2020. https://doi.org/10.1088/978-0-7503-2080-1.

(45) Elson, E. L. Fluorescence Correlation Spectroscopy: Past, Present, Future. *Biophys J* **2011**, *101* (12), 2855–2870. https://doi.org/10.1016/j.bpj.2011.11.012.

(46) Magde, D.; Elson, E.; Webb, W. W. Thermodynamic Fluctuations in a Reacting System—Measurement by Fluorescence Correlation Spectroscopy. *Phys Rev Lett* **1972**, *29* (11), 705. https://doi.org/10.1103/PhysRevLett.29.705.

(47) Magde, D.; Elson, E. L.; Webb, W. W. Fluorescence Correlation Spectroscopy. II. An Experimental Realization. *Biopolymers* **1974**, *13* (1), 29–61. https://doi.org/10.1002/BIP.1974.360130103,.

(48) Maiti, S.; Haupts, U.; Webb, W. W. Fluorescence Correlation Spectroscopy: Diagnostics for Sparse Molecules. *Proc Natl Acad Sci U S A* **1997**, *94* (22), 11753. https://doi.org/10.1073/PNAS.94.22.11753.

(49) Krieger, J. W.; Singh, A. P.; Bag, N.; Garbe, C. S.; Saunders, T. E.; Langowski, J.; Wohland, T. Imaging Fluorescence (Cross-) Correlation Spectroscopy in Live Cells and Organisms. *Nature Protocols 2015 10:12* **2015**, *10* (12), 1948–1974. https://doi.org/10.1038/nprot.2015.100.

(50) Macháň, R.; Wohland, T. Recent Applications of Fluorescence Correlation Spectroscopy in Live Systems. *FEBS Lett* **2014**, *588* (19), 3571–3584. https://doi.org/10.1016/J.FEBSLET.2014.03.056.

(51) Das, N.; Sen, P. Structural, Functional, and Dynamical Responses of a Protein in a Restricted Environment Imposed by Macromolecular Crowding. *Biochemistry* **2018**, *57* (42), 6078–6089. https://doi.org/10.1021/acs.biochem.8b00599.

(52) Das, N.; Sen, P. Shape-Dependent Macromolecular Crowding on the Thermodynamics and Microsecond Conformational Dynamics of Protein Unfolding Revealed at the Single-Molecule Level. *J. Phys. Chem. B* **2020**, *124* (28), 5858–5871. https://doi.org/10.1021/acs.jpcb.0c03897.

(53) Feder, T. J.; Brust-Mascher, I.; Slattery, J. P.; Baird, B.; Webb, W. W. Constrained Diffusion or Immobile Fraction on Cell Surfaces: A New Interpretation. *Biophys J* **1996**, *70* (6), 2767–2773. https://doi.org/10.1016/S0006-3495(96)79846-6.

(54) Höfling, F.; Franosch, T. Anomalous Transport in the Crowded World of Biological Cells. *Reports on Progress in Physics* **2013**, *76* (4), 046602. https://doi.org/10.1088/0034-4885/76/4/046602.

(55) Banks, D. S.; Tressler, C.; Peters, R. D.; Höfling, F.; Fradin, C. Characterizing Anomalous Diffusion in Crowded Polymer Solutions and Gels over Five Decades in Time with Variable-Lengthscale Fluorescence Correlation Spectroscopy. *Soft Matter* **2016**, *12* (18), 4190–4203. https://doi.org/10.1039/c5sm01213a.

(56) Tabatabaei, F.; Lenz, O.; Holm, C. Simulational Study of Anomalous Tracer Diffusion in Hydrogels. *Colloid Polym Sci* **2011**, *289* (5–6), 523–534. https://doi.org/10.1007/S00396-011-2393-0/FIGURES/11.

(57) Einstein, A. Über Die von Der Molekularkinetischen Theorie Der Wärme Geforderte Bewegung von in Ruhenden Flüssigkeiten Suspendierten Teilchen. *Ann Phys* **1905**, *322* (8), 549–560. https://doi.org/10.1002/ANDP.19053220806.

(58) Das, N.; Sen, P. Dynamic Heterogeneity and Viscosity Decoupling: Origin and Analytical Prediction. *Phys. Chem. Chem. Phys.* **2021**, *23* (29), 15749–15757. https://doi.org/10.1039/d1cp01804c.

(59) Müller, C. B.; Loman, A.; Pacheco, V.; Koberling, F.; Willbold, D.; Richtering, W.; Enderlein, J. Precise Measurement of Diffusion by Multi-Color Dual-Focus Fluorescence Correlation Spectroscopy. *EPL* **2008**, *83* (4), 46001. https://doi.org/10.1209/0295-5075/83/46001.

(60) Das, N.; Sen, P. Macromolecular Crowding: How Shape and Interaction Affect the Structure, Function, Conformational Dynamics and Relative Domain Movement of a Multi-Domain Protein. *Phys. Chem. Chem. Phys.* **2022**, *24* (23), 14242–14256. https://doi.org/10.1039/D1CP04842B.

(61) Khan, T.; Das, N.; Negi, K. S.; Bhowmik, S.; Sen, P. Understanding the Intricacy of Protein in Hydrated Deep Eutectic Solvent: Solvation Dynamics, Conformational Fluctuation Dynamics, and Stability. *Int. J. Biol. Macromol.* **2023**, *253*, 127100. https://doi.org/10.1016/j.ijbiomac.2023.127100.

(62) Hossain, S. S.; Paul, S.; Samanta, A. Structural Stability and Conformational Dynamics of Cytochrome c in Hydrated Deep Eutectic Solvents. *J. Phys. Chem. B* **2021**, *125* (22), 5757–5765. https://doi.org/10.1021/acs.jpcb.1c01975.

(63) Pabbathi, A.; Ghosh, S.; Samanta, A. FCS Study of the Structural Stability of Lysozyme in the Presence of Morpholinium Salts. *J. Phys. Chem. B* **2013**, *117* (51), 16587–16593. https://doi.org/10.1021/jp409842d.

(64) Sengupta, B.; Das, N.; Sen, P. Elucidation of Ms Dynamics of Domain-III of Human Serum Albumin during the Chemical and Thermal Unfolding: A Fluorescence Correlation Spectroscopic Investigation. *Biophys Chem* **2017**, *221*, 17–25. https://doi.org/10.1016/j.bpc.2016.11.006.

(65) Sengupta, B.; Chaudhury, A.; Das, N.; Sen, P. Single Molecular Level Probing of Structure and Dynamics of Papain Under Denaturation. *Prot. Pep. Lett.* **2017**, *24* (11), 1073–1081. https://doi.org/10.2174/0929866524666170811145838.

(66) Sengupta, B.; Das, N.; Singh, V.; Thakur, A. K.; Sen, P. Fluorescence Correlation Spectroscopy as a Tool to Investigate the Directionality of Proteolysis. *Int. J. Biol. Macromol.* **2020**, *164*, 2524–2534. https://doi.org/10.1016/j.ijbiomac.2020.08.103.

(67) Halder, B.; Ghosh, S.; Khan, T.; Pal, S.; Das, N.; Sen, P. Tracking Heterogenous Protein Aggregation at Nanoscale through Fluorescence Correlation Spectroscopy. *Photochem Photobiol* **2024**, *100*, 989–999. https://doi.org/10.1111/php.14004.

(68) White, D. S.; Smith, M. A.; Chanda, B.; Goldsmith, R. H. Strategies for Overcoming the Single-Molecule Concentration Barrier. *ACS Measurement Science Au* **2023**, *3* (4), 239. https://doi.org/10.1021/ACSMEASURESCIAU.3C00002.

(69) Das, N.; Khan, T.; Subba, N.; Sen, P. Correlating Bromelain's Activity with Its Structure and Active-Site Dynamics and the Medium's Physical Properties in a Hydrated Deep Eutectic Solvent. *Phys. Chem. Chem. Phys.* **2021**, *23* (15), 9337–9346. https://doi.org/10.1039/d1cp00046b.

(70) Das, N.; Yadav, S.; Negi, K. S.; Tarif, E.; Sen, P. Does Microsecond Active-Site Dynamics Primarily Control Proteolytic Activity of Bromelain? Clues from Single Molecular Level Study with a Denaturant, a Stabilizer and a

Macromolecular Crowder. *BBA Advances* **2022**, *2*, 100041. https://doi.org/10.1016/j.bbadva.2022.100041.

(71) Das, N.; Sahu, S.; Khan, T.; Sen, P. Site-Specific Heterogeneity of Multi-Domain Human Serum Albumin and Its Origin: A Red Edge Excitation Shift Study. *Photochem Photobiol* **2023**, *99* (2), 538–546. https://doi.org/10.1111/php.13712.

(72) Das, N.; Tarif, E.; Dutta, A.; Sen, P. Associated Water Dynamics Might Be a Key Factor Affecting Protein Stability in the Crowded Milieu. *J. Phys. Chem. B* **2023**, *127* (14), 3151–3163. https://doi.org/10.1021/acs.jpcb.2c09043.

(73) Das, N.; Sen, P. Size-Dependent Macromolecular Crowding Effect on the Thermodynamics of Protein Unfolding Revealed at the Single Molecular Level. *Int J Biol Macromol* **2019**, *141*, 843–854. https://doi.org/10.1016/j.ijbiomac.2019.09.029.

(74) Subba, N.; Sahu, P.; Das, N.; Sen, P. Rational Design, Preparation and Characterization of a Ternary Non-Ionic Room-Temperature Deep Eutectic Solvent Derived from Urea, Acetamide, and Sorbitol. *Journal of Chemical Sciences* **2021**, *133* (1), 25. https://doi.org/10.1007/s12039-020-01866-2.

Chapter 3

Osmolyte induced Protein Stabilization: Modulation of Associated Water might be a Key Factor

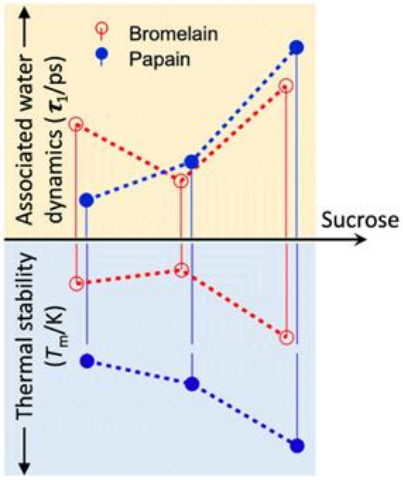

Kuldeep Singh Negi, Nilimesh Das, Tanmoy Khan, and Pratik Sen

Phys. Chem. Chem. Phys., **2023**, *25*, 32602-32612

Abstract:

The mechanism of protein stabilization by osmolyte remains one of the most important and long-standing puzzles. The traditional explanation of osmolyte-induced stability through the preferential exclusion of osmolytes from the protein surface has been seriously challenged by the observations like the concentration-dependent reversal of osmolyte-induced stabilization/destabilization. The more modern explanation of protein stabilization/destabilization by osmolyte considers an indirect effect due to osmolyte-induced distortion of the water structure. It provides a general mechanism, but there are numerous examples of protein-specific effects, i.e., a particular osmolyte might stabilize one protein, but destabilize the other, that could not be rationalized through such an explanation. Herein, we hypothesized that osmolyte-induced modulation of associated water might be a critical factor in controlling protein stability in such a medium. Taking different osmolytes and papain as a protein, we proved that our proposal could explain protein stability in osmolytes. Stabilizing osmolytes rigidify associated water structures around the protein, whereas destabilizing osmolytes make it flexible. The strong correlation between stability and the associated water dynamics, and the fact that such dynamics are very much protein specific, established the importance of considering the modulation of associated water structure in explaining osmolyte-induced stabilization/destabilization of proteins. More interestingly, we took another protein, bromelain, for which traditionally stabilizing osmolyte sucrose acts as a stabilizer at higher concentrations but as a destabilizer at lower concentrations. Our proposal successfully explains such observations, which is probably impossible by any known mechanisms. We believe this report will trigger much research in this area.

3.1. Introduction

3.1.1. Osmolytes are essential for keeping protein active and stable in living cells: Proteins are responsible for countless phenomena occurring throughout the life span of a living system. The native structure of a protein can be perturbed under stressed conditions created through changes in its environment, such as the presence of additives, pressure, salinity, temperature, etc. The protein in perturbed conditions may lose its quaternary, tertiary and secondary structure. Alternatively, it may assume an intermediate conformation or aggregate into accumulating β-amyloid fibrils, which have been observed to exhibit toxicity towards cells.[1] Nevertheless, the Nature is well-equipped with many defense mechanisms to combat the deleterious effect of these perturbates, and osmolytes play an important role in this process. The osmolytes are small natural organic molecules, which are accumulated in the cell while in stress to protect proteins and enzymes.[2] Osmolytes are usually stabilizing, and crudely can be of four types: sugars, polyols, amino acids, and methyl amines (and their derivatives). Surprisingly, there are some osmolytes (like urea) which generally destabilizes a protein.[3] One of the longstanding and most debated topics of biophysics is how these osmolytes stabilizes/destabilizes a protein,[4] though the molecular-level understanding is far from complete. In this report, we attempted to provide a unique mechanistic view of osmolyte-induced stabilization/destabilization of proteins.

3.1.2. Various theories to explain osmolytes induced protein stability and their drawbacks: There are broadly two hypotheses (Scheme 1) on the action of osmolytes on proteins, but none explains the phenomenon entirely. First is the direct mechanism, which is also known as the preferential interaction mechanism and osmophobic theory.[5] According to this theory, the stabilizing osmolytes are preferentially excluded from the protein surface because of unfavorable interactions, which shifts the equilibrium towards the native state (i.e., the state with less surface area) due to the excluded volume effect by the osmolytes.[6,7] On the other hand, denaturants preferentially get bound to the protein surface due to favorable

interaction, and the equilibrium is shifted to the denatured state with larger number of active binding centers.[6] This theory has been widely accepted for a long time.[5–7] Because of its simplicity, it remains the go-to theory to explain protein stability in the presence of added solutes. However, several experimental and computational observations did not parallel the preferential interaction hypothesis.[8–14] For example, Cremer *et al.* showed that trimethylamine N-oxide (TMAO) stabilizes the hydrophobic collapse of an elastin-like polypeptide (ELP) by accumulating at the surface of the protein[8] and L-proline also stabilizes protein by accumulating at its surface.[9] In addition to these observations, there are ample examples where the direct interaction theory fails to explain the stabilization of proteins by osmolytes, especially in a concentration-dependent manner.[15–18]

These observations clearly indicate that something is still missing in the preferential interaction theory. Bruzdziak *et al.* studied a series of stabilizing osmolytes and their derivatives towards the thermal stability of hen egg white lysozyme. They found that the stability of lysozyme follows the order water < TMAO < betaine < glycine <N-dimethyl glycine < N-methyl glycine, which correlates directly with the oxygen–oxygen distance of water molecules in the presence of the osmolytes.[19] This observation suggests the involvement of water in osmolyte-induced protein stabilization and gives a clue for that missing component, which leads to the indirect mechanism hypothesis.[19]

In the indirect mechanism hypothesis, the effect of osmolyte on protein is considered to be mediated through water. Here, osmolytes are believed to change the arrangement and/or strength of the hydrogen bond of water molecules, which influences the stability of the protein.[20–26] A change in water arrangement or strength is generally probed by the change in the dynamics of water,[20–32] which is expected to be altered in the presence of osmolytes. Earlier, many theoretical and simulation studies tried to explain the protein stability with added solutes or cosolvents through water structure modulation. However, it is not easy to measure the change of water structure in presence of added solutes.[33] Also, the interacting water molecules (with protein) constitute only a little fraction of the total water but play a major role in

controlling protein behavior. Therefore, even if there are some attempts to correlate protein stability and water structure modulation with osmolytes, those are not very successful. For example, using pressure perturbation calorimetry and exploiting basic thermodynamics Pielak and co-workers examine the impact of several protein stabilizers and destabilizers on the water structure.[33,34] They did not notice any correlation between a solute's impact on water structure and stability.[33] However, recently, with progress in NMR and its residue-level resolution, there have been some successes in relating protein stability and water structure.[34–36] There are some efforts by terahertz spectroscopy as well to study the modulation of associated water structure with added osmolytes. For example, Havenith and co-workers showed that disaccharide modulates water more strongly than monosaccharides.[37] It might explain the generally higher stabilizing ability of sucrose than glucose. Recently Hishida *et al.* showed that the stabilization of ribonuclease-A by osmolytes is associated with slowing down water dynamics, whereas, faster water dynamics accompanying destabilization.[27] However, this theory could not predict the protein-specific nature of osmolyte action.[27,38] This raises a question on the acceptance of the indirect mechanism.[27,28]

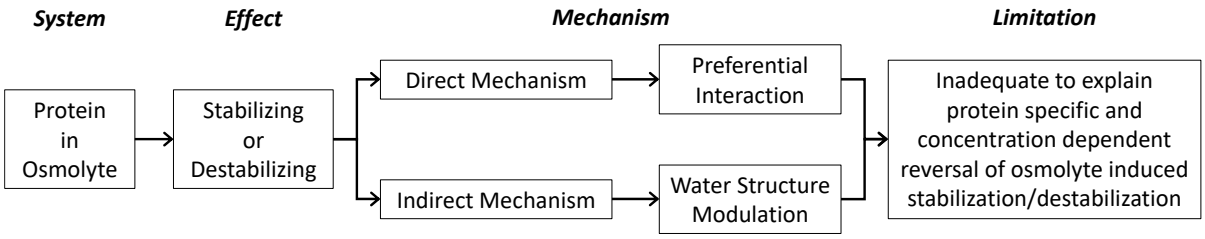

Scheme 1. Known mechanisms of protein stabilization by osmolytes and their limitation.

3.1.3. Our hypothesis: Protein-specific effect involving associated water:

Both the direct and indirect mechanism hypothesis provide valuable insights into the protein stabilization/destabilization by osmolytes, but none is absolute. Several experimental and computational observations portray that both mechanisms might operate simultaneously. As a result, there is a need for better theories.

In the indirect mechanism, the change in the water structure is not only important for osmolytes, but can go far beyond in protein folding problem.[39–42] However, this theory generally considers the effect of added solute on the water structure modulation either in the near vicinity of the concerned solute or over the whole water structure, ignoring the water around the protein (known as biological water, or protein hydration layer, or protein associated water).[29–32,38,43,44] This associated water is known to be the controlling factor of protein behavior.[45–49] It is well established that such water is very much different from bulk water, as it has much retarded dynamics than bulk water.[50–53] Moreover, how much different this water is from the bulk water depends on the nature of the protein surface and thus varies from protein to protein. Overall, water structure modulation might be significant; however, as this associated water directly interacts with the protein surface, these should profoundly affect the protein stability. Herein, we propose that osmolyte-induced modulation of associated water structure might be a key factor in controlling protein stability.

To establish our hypothesis, we have taken different osmolytes and tried to correlate protein stability and the perturbation in the associated water dynamics. In the past, numerous techniques, e.g., terahertz spectroscopy,[20,21,26] time-resolved infrared (IR) spectroscopy,[22,23] nuclear magnetic resonance (NMR),[24,25] time-dependent fluorescence Stokes shift (TDFSS),[50,54–56] molecular dynamic (MD) simulation,[26,57,58] etc. were employed to measure the associated water dynamics. Among these, the TDFSS technique is superior to others in terms of its better temporal and spatial resolution,[51,52] which we have used in our study. Note that it is very likely that a change in the water structure around the osmolyte or protein surface (i.e., associated water) will be suppressed in the presence of a colossal concentration of bulk water if one cannot probe the associated water selectively. The unmatched spatial resolution of TDFSS technique overcomes this issue. Our results suggest that protein stabilization is associated with the slower dynamics of associated water, whereas faster dynamics destabilize the protein. Further, we proved the protein specificity by taking two different proteins. We showed that for a particular

osmolyte, the effect might be stabilizing or destabilizing depending on the protein, and for a specific protein, the effect of osmolyte on protein stability might be stabilizing/destabilizing depending on the concentration of osmolyte but could be explained through our proposition. It provides a step forward in understanding protein stabilization by osmolytes.

3.2. Results and Discussion

3.2.1. Thermal stability of papain in buffer and with various osmolytes:

Five tryptophan residues present in papain are used as a fluorescent marker to track the changes of its stability against thermal perturbation in buffer and different aqueous osmolyte media. Emission spectra are recorded at different temperatures after exciting at 295 nm and emission maxima is chosen as a representative of overall structure. The measured emission spectra and the change in the emission maxima of papain in buffer with raise in the medium temperature are shown in figures 1a and 1b, respectively.

The choices of osmolytes and their concentrations are based on the retention of the conformational structure of papain as associated water dynamics can also be influenced by the protein's conformation (see Section 3.3). At each temperature, fraction of denatured/unfolded protein (f_D) in the sample is calculated using equation 3.2.1 and stability curve is created by plotting f_D with corresponding temperature, as illustrated in figure 1c for the buffer case.

$$f_D = \frac{\lambda_i(T) - \lambda_N}{\lambda_D - \lambda_N} \qquad (3.2.1)$$

In the above equation, λ_N and λ_D represent the emission maximum of the native and fully denatured state of papain (λ_{ex} = 295 nm), respectively, which are taken as the lowest (340 nm) and highest (348 nm) value of the emission maxima in the thermal denaturation experiment. $\lambda_i(T)$ are the emission maxima at a given temperature. This data could be used to represent the stability of papain in terms of its melting

temperature (T_m). T_m corresponds to the temperature at which the value of f_D is 0.5, i.e., temperature at which fraction of native and denatured

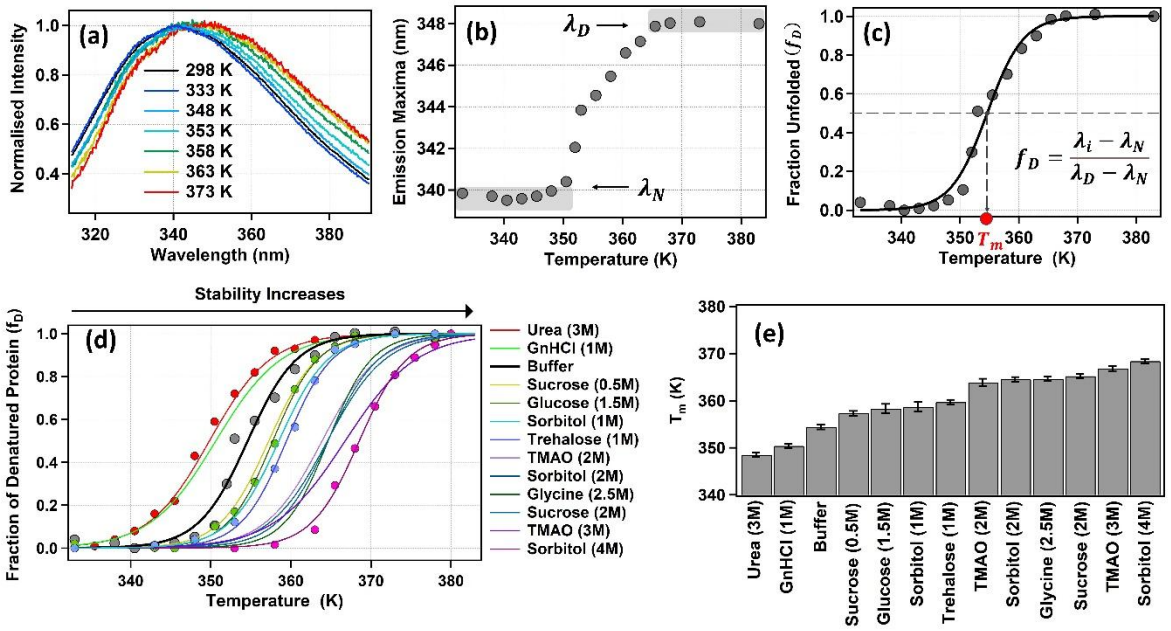

Figure 1. (a) Normalized intrinsic emission spectra of papain (λ_{ex} = 295 nm) in buffer as a function of temperature. (b) Variation of emission maxima of papain as a function of temperature. Emission maxima at 340 nm and 348 nm are taken as the signature of the native (λ_N) and denatured state (λ_D), respectively. (c) Variation of the fraction denatured, f_D, (Equation 3.2.1) of papain in buffer as a function of temperature. The data has been fitted to a sigmoidal function to determine the melting temperature, T_m. (d) Variation of fraction denatured, f_D, of papain in the presence of various osmolytes, and in buffer. (e) Variation of melting temperature of papain in the presence of various osmolytes compared to in buffer. The error bar represents the standard deviation of the mean of three independent experiments.

protein become equal and give a measure of thermal stability of the protein (see figure 1c for papain in buffer). Stability profile and melting temperature of papain in buffer and other osmolyte solutions are shown in figures 1d and 1e, respectively. The corresponding melting temperatures are also tabulated in table 1.

The result depicts that the melting temperature of papain in the buffer is ~354 K, which matches well with the previous report.[59] With the added osmolytes, melting temperature changes significantly (see figure 1e). The traditional stabilizing osmolytes (e.g., glucose, sucrose, sorbitol, TMAO, etc.) increase the melting

temperature. This suggests that these osmolytes impart stabilization to papain. On the other hand, with urea and GnHCl, melting temperature of papain decreases, suggesting destabilization of papain with these two destabilizing osmolytes.

Table 1. Melting point of papain in buffer and other osmolyte solution. (Error bar represents the standard deviation of the mean of three independent experiments.)

Osmolyte	T_m**(K)**
Urea (3M)	349.8±0.5
GnHCl (1M)	350.4 ±0.5
Buffer	354.4 ±0.5
Sucrose (0.5M)	357.3 ±0.5
Glucose (1.5M)	358.3 ±1.0
Sorbitol (1M)	358.7 ±1.0
Trehalose (1M)	359.7 ±0.5
TMAO (2M)	363.9 ±0.7
Sorbitol (2M)	364.5 ±0.5
Glycine (2.5M)	364.6 ±0.5
Sucrose (2M)	365.2 ±0.5
TMAO (3M)	366.8 ±0.5
Sorbitol (4M)	368.4 ±0.5

3.2.2. Associated water dynamics around papain in buffer and other osmolyte solutions:

We have measured the solvation dynamics of papain by tagging it site selectively (at cys-25) with solvatochromic CPM dye as per the procedure mentioned in the experimental section. See figure 2a and 2b for the TRES and the variation of

emission maxima of CPM-tagged papain in buffer, as a function of time. The constructed solvent response functions, S(t), through equation 3.2.2, are shown in figure 2c for buffer and in figure 2d for osmolyte solutions.

$$S(t) = \frac{\bar{\nu}(t) - \bar{\nu}(\infty)}{\bar{\nu}(0) - \bar{\nu}(\infty)} \qquad (3.2.2)$$

S(t) has been fitted well with a bi-exponential function and yielded two distinct time constants for buffer as well as for each osmolyte solution, out of which one is in the picosecond (ps), and another is in the nanosecond (ns) regime. The fitting parameters are tabulated in table 2, and variations in the time components are depicted in figures 2e and 2f. In the case of CPM-tagged papain in buffer, the two components of the solvent response function are found to be 70 ps and 130 ps, respectively, with an average time constant of 110 ps. Interestingly, with stabilizing osmolytes, the time scale of fast solvation component increases with increase in the stabilizing power, and with the destabilizing osmolytes, it decreases, as evident in figure 2e. However, the slower time component does not show such a trend (figure 2f).

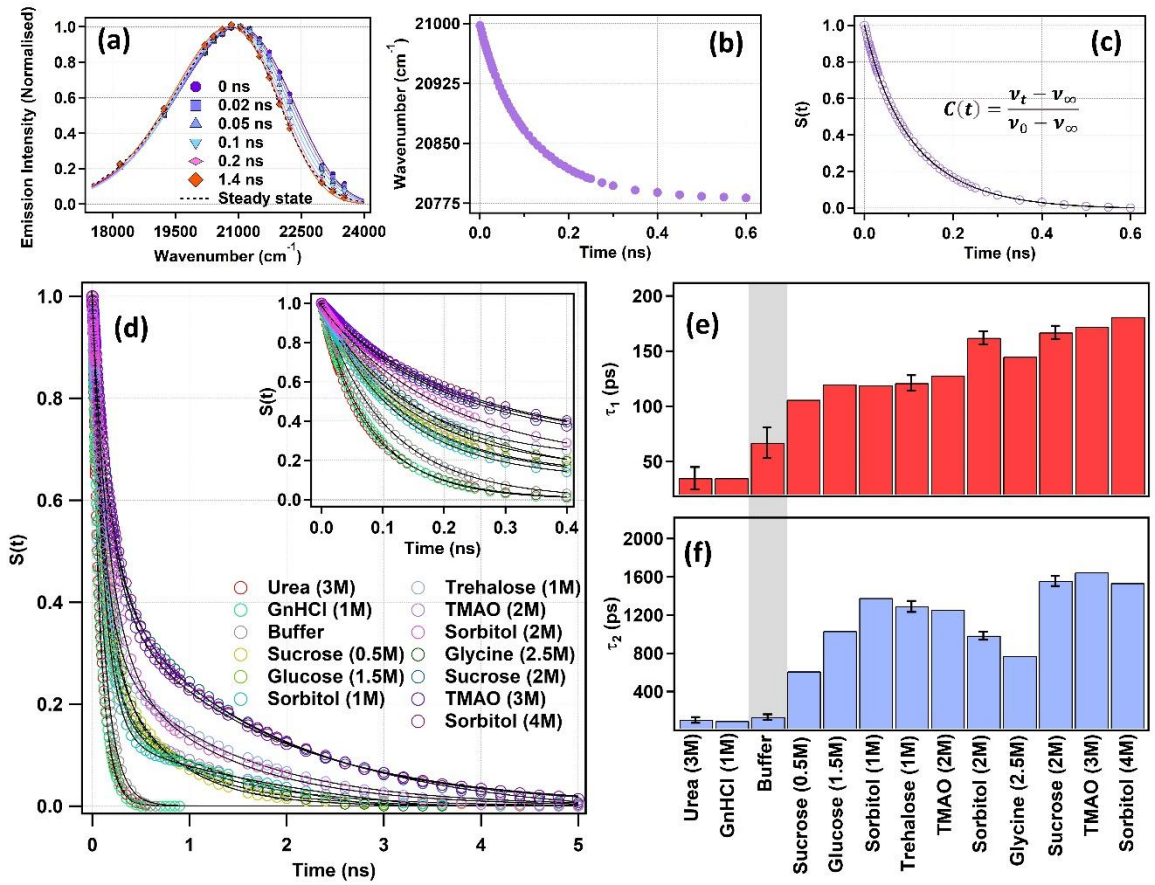

Figure 2. (a) Normalized time resolved emission spectra (TRES) and (b) the variation of emission maxima (in cm^{-1}) of papain in buffer as a function of time. (c) Solvent response function for papain in buffer is constructed using equation 3.2.2. (d) Solvent response function for papain in presence of various osmolytes is presented and compared with the same in buffer. Solid black lines are the fittings to a bi-exponential function. The results are tabulated in table 2. Variation of the (e) the fast component, and (f) the slow component of solvation time in papain in the presence of various osmolytes are compared with that in buffer. The error bar represents the standard deviation of the mean of three independent experiments. All the solvation experiments have been performed at 298 K.

Table 2. Relaxation time constants and their relative weightage in solvation dynamics study of papain in buffer and other aqueous osmolyte solution. (Error bar represents the standard deviation of the mean of three independent experiments.)

Osmolyte	a_1	τ_1 **(ps)**	a_2	τ_2 **(ps)**	τ_{avg} **(ps)**
Urea (3M)	0.30±0.10	30±10	0.70±0.22	100 ±30	79 ±28

GnHCl (1M)	0.17	30	0.83	90	80
Buffer	0.31±0.15	70 ±14	0.69±0.25	130±31	110 ±20
Sucrose (0.5M)	0.64	110	0.36	610	290
Glucose (1.5M)	0.80	120	0.20	1030	300
Sorbitol (1M)	0.84	120	0.16	1380	320
Trehalose (1M)	0.68±0.02	120±7	0.32±0.01	1290±58	490 ±31
TMAO (2M)	0.82	130	0.18	1260	330
Sorbitol (2M)	0.63±0.01	160±6	0.37±0.01	980±43	460±20
Glycine (2.5M)	0.74	150	0.26	770	310
Sucrose (2M)	0.56±0.01	170±6	0.44±0.01	1560±53	780±27
TMAO (3M)	0.59	170	0.41	1650	830
Sorbitol (4M)	0.54	180	0.46	1540	800

3.2.3. Protein conformation change does not play key role in the modulation of associated water:

It is well known from the literature that not only the associated water but also the polar moieties, including the protein side chain, present in the system might contribute to the solvation process.[21,60,61] Therefore, a change in the protein conformation might also modulate the measured dynamics. Thus, to comment anything on the relationship between associated water dynamics and stability of a protein, it is necessary to check if the applied perturbation has any significant effect on the protein conformation. Only if the change in conformation is minimal, it is possible to draw a relationship.

Herein, we have used three independent measurements, (i) steady-state emission of CPM-tag papain to examine the environment around the probe (figure 3a), (ii) circular dichroism signal to probe the secondary structure (figure 3b). The secondary

structural content of papain is estimated from the measured CD spectrum using CDNN software (figure 3d) and (iii) hydrodynamic radii to investigate the overall conformation (figure 3c) of papain in the presence of various osmolytes. Our experiments clearly reveal that there is almost no change in protein conformation in the presence of chosen osmolytes. This study confirms that protein conformational change does not modulate the associated water dynamics significantly. This gives the opportunity to examine if there is any correlation between associated water dynamics and protein stability.

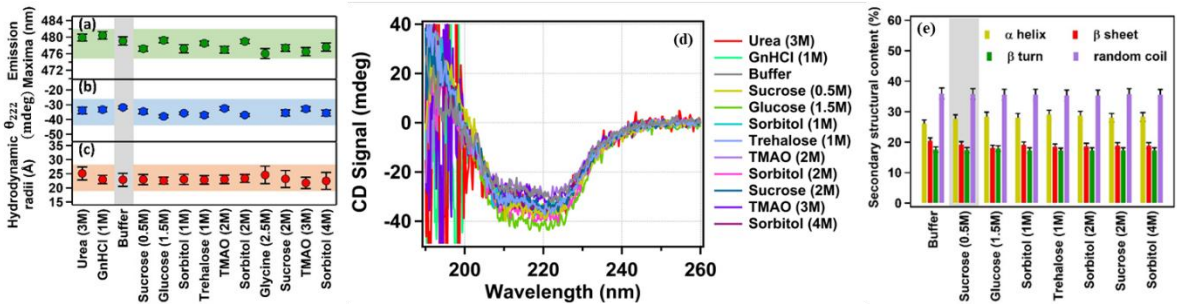

Figure 3. Variation of (a) emission maxima of CPM-tag papain (λ_{ex} = 375 nm), (b) CD signal (θ_{222}) of papain, (c) hydrodynamic radii of papain, (d) Raw CD spectrum corresponding to each osmolyte system and (e) secondary structural content of papain in the presence of various osmolytes and buffer. Every experimental point is the average of three independent measurements, and the error bar represents the standard deviation. All the experiments have been performed at 298 K.

3.2.4. Correlating the thermodynamic stability with associated water dynamics of protein:

Before going into the correlation between the thermodynamic stability with associated water dynamics of protein we want to make one point clear. Due to our instrumental resolution (IRF~150 ps), we cannot detect events occurring in a time scale faster than 30 ps. It also poses a concern about the confidence level of the fast time component (~100 ps). For this, we measured the solvation dynamics of CPM-tag papain in buffer using the femtosecond fluorescence up-conversion technique in combination with the TCSPC measurement[62] to get the information on whole range from fs to ns relaxation processes involved in protein solvation, where the lifetime

traces over the whole steady state emission spectrum of CPM tag papain are acquired which are further processed similarly as is done while performing solvation experiment using TCSPC to produce TRES as is shown in figure 4(a). The wavenumber maxima corresponding to each time resolved emission spectrum is plotted against the representative time. Following the procedure, we have merged the time dependent wavenumber maxima shift obtained from fs-fluorescence up conversion and TCSPC (shown in figure 4b which is then normalized using equation 2 as shown in figure 4c.

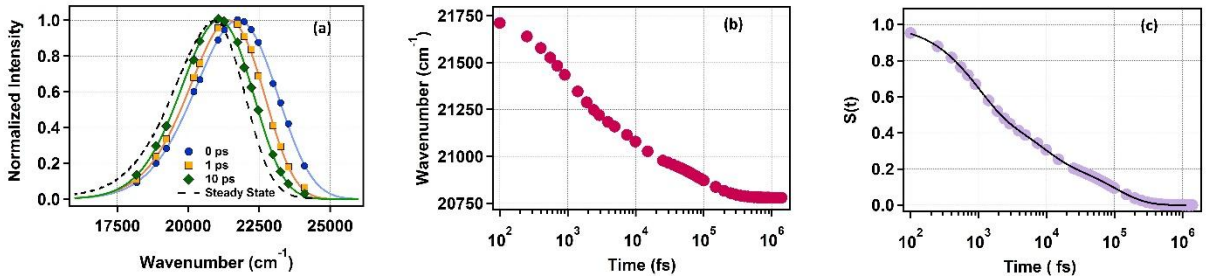

Figure 4. (a) Normalized time resolved emission spectra of papain in buffer (TRES) (b) variation of emission maxima (wavenumber) of papain in buffer with time. Emission maxima are obtained by employing TRES. (c) solvent response function (S(t)) for papain in buffer. Experiments have been performed at 298 K.

On fitting S(t) (shown in figure 4c) obtained from time dependent wavenumber maxima shift we got 4-time constants as 905 fs (47 %), 7.8 ps (27 %) ps, 77.6 ps (13 %), 135 ps (13 %).

From literature we know that fs component is coming from bulk water as the probe is at the surface of protein thus can sense bulk water, fast ps component is coming from water reorientation in PHL, moderately slow ps component is coming from restructured water in the vicinity of protein with coupled motions of side chain, and slowest ps component is coming from internal motions of protein itself. Since we are interested in the event associated with the time scale of 70±14 ps which is slow enough to capture using TCSPC alone. Although we are unable to get the first two-time components, the other two slower components match well with the time-components obtained from the TCSPC measurement. This experiment gives us the confidence to correlate the measured associated water dynamics using TCSPC setup

with the stability. In figure 5, we showed how the fast and slow component of associated water dynamics around the active site of papain is related to its stability. Although one could find an obvious correlation between the stability and solvation time (individual components) of papain, the extent of correlation is not same for the two cases. The correlation of the slower component of solvation time with the stability is not very strong (adjusted R^2 is 0.69). The strongest associated water dynamics – stability correlation (adjusted R^2 ~ 0.95) is observed for the faster component of solvation dynamics.

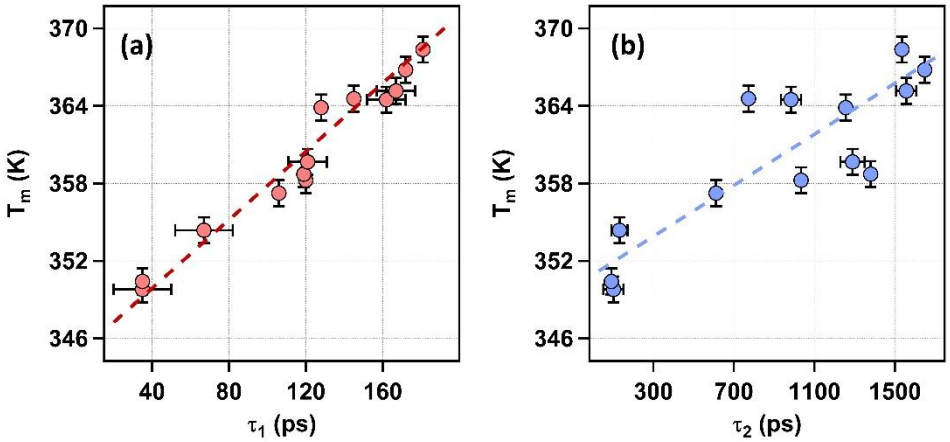

Figure 5. Plot of melting temperature with (a) faster time component, and (b) slower time component of solvation dynamics in papain in the presence of various osmolytes and in buffer. Dashed lines represent fitting to a straight line.

To understand why the time components, correlate differently with stability, it is essential to know the origin of the components in solvation dynamics measurement. Although there is a debate, the most prominent and accepted explanation was given by Bagchi and coworkers.[49,51,53] According to them, the 1-8 ps component originates from the reorientation dynamics of water molecules in the hydration layer. We have not observed this time component due to the temporal resolution of our setup. The 20-200 ps component arises due to the restructuring of the associated water.[27,54,63–66] In the present report, this time component varies between 30-180 ps. The ~1000 ps (90-1650 ps in the present study) component mainly originates from the protein's internal motions.[67] Several experimental studies, notably from Zewail, Zhong and Bhattacharyya group establishes these relaxation timescales.[50,52,54,56,64,66,68]

However, a clear separation and identification of these time components are experimentally tricky due to the overlap of time constants. Nevertheless, in the present case, the two time-constants are somewhat well distinguished, and the problem of overlapping is minimal. Thus, individual time components could be used for the assignment of the associated event.

After understanding the origin of the two time-components, it is logical that the correlation of the two-time components with the stability would be different. Following our proposal of protein stability modulation through the associated water dynamics, the faster time component (30-180 ps) is expected to correlate better with the stability of papain, which has been observed experimentally (Figure 4b). At this point, it is difficult to ascertain why there is an unexpected correlation between longer component of solvation dynamics and the stability of papain, which is weak but obvious. There might be several reasons for it. The mixing of time components of solvation, exchange between associated water and bulk layer, dependency of protein internal motion might be some of them. In the future, we will investigate this aspect critically.

3.2.5. Further discussion in the context of previous literature:

Over the past decade, researchers have dedicated significant efforts to investigate the modulation of water dynamics in the presence of osmolytes.[19,21,39,60] However, there is a limited number of papers that concurrently assess and compare the modulation of water structure and stability of protein.[27,69,70] The most comprehensive report came very recently, where the authors examined the water structure modulation with 20 osmolytes and compared that to the stability of ribonuclease-A.[27] They found a definitive, but not so very strong correlation between water structure modulation and protein stability. The component analysis of solvation in the present study where we specifically can observe the associated water of protein, probably provides a better way to investigate the problem. Stangret and coworkers recently showed that hydration water is significantly strengthened with stabilizing osmolytes. Hydration structure does not change much with destabilizing

osmolytes, but it now contains more water molecules.[28,71] There are indeed a few efforts to address the correlation between water structure modulation and protein stabilization by TDFSS. Zewail and coworkers showed that associated water dynamics around (domain-II of) HSA is slowest at pH 4.2, followed by at pH 7.0, 2.9, and 11.0.[55,72] Interestingly, domain-II of HSA is most structured at 4.2, followed by at pH 7.0, 2.9 and 11.0.[73] Generally, more compact the protein conformation is, more stability it has. In fact, there are several studies, including that from our group, show that solvation time around protein decreases upon denaturation.[68,72,74–76] Therefore, our result follows the expected trend. However, as exchange is the primary channel between associated and bulk water, any structural modulation will have a prominent effect not only on protein stability, but to water structure also. Therefore, it is impossible to confidently relate the faster dynamics of such states to their decreased stability. However, in the present case, we have shown that protein conformation is almost not altered with the osmolyte addition.

This study is one of the few systematic studies where the protein stability and the modulation of water dynamics is experimentally measured together. Notably, one of our most recent studies proved that associated water dynamics is the key factor affecting protein stability in crowded milieu.[69] Crudely speaking, our result is in line with the previous literature: "slowing down of water stabilizes protein".[69] However, proper control experiment and component analysis of solvation provide some unique information. Overall, our results indicate that modulation of associated water dynamics can explain protein stability in osmolytes equally well as that of the existing direct and indirect mechanisms.

3.2.6. Concentration-dependent reversal and protein-specific effect of osmolyte-induced stability: Our proposal can explain it successfully, which previous theories cannot:

The nature of associated water is protein specific, and thus the effect of added perturbation should also be protein specific. This advantage could be exploited in explaining the concentration-dependent reversal of protein stability with a particular

osmolyte[15,17,77–83] and/or protein-specific stabilization/destabilization by an osmolyte,[84] which cannot be explained either by the direct or the indirect mechanisms.

To verify this, it is necessary to have a protein that would be stabilized by a particular osmolyte at some concentration but would be destabilized by the same osmolyte at a different concentration. Several proteins are known to show concentration-dependent stabilization reversal by denaturants like GnHCl or urea.[18,82,85] However, generally, protein structure changes significantly with GnHCl or urea, rendering these useless to prove our point. We also require an osmolyte, which will stabilize a protein at some concentration but destabilize another protein at the same concentration. Fortunately, it was previously reported that sucrose might unexpectedly destabilize bromelain, which is a protease of the papain family.[18,84] Thus, the sucrose-bromelain/papain pair gives us the opportunity to check if our hypothesis can explain concentration dependent reversal of protein stability and the protein-specific stabilization/destabilization by osmolytes.

We first checked the stability of bromelain in buffer and with 0.5 M and 2 M sucrose (Figure 5a). The melting temperature of bromelain in the buffer is ~336 K. It decreases to ~334 K with 0.5 M sucrose but increases to ~344 K with 2 M sucrose. The melting temperature values are given represented in table 3.

Table 3: Melting point of papain in buffer and other osmolyte solution. (Error bar represents the standard deviation of the mean of three independent experiments.)

Osmolyte	T_m **(K)**
Buffer	336.4 ±0.5
Sucrose (0.5M)	334.1 ±0.5
Sucrose (2M)	344.5 ±1.0

We have observed that the environment around the tag remains similar confirmed by the almost similar values of emission maxima of CPM tag bromelain as shown in figure 6a, the value of θ_{222} remains almost same confirming the similar secondary structure of bromelain in the absence and presence of sucrose as shown in figure 6b and is further confirmed by the quantitative analysis of secondary structure where the amount of all the four structural contents remains almost similar as shown in figure 6d. The hydrodynamic radii of bromelain in presence and absence of sucrose remains within the error limit which confirms no significant perturbation in the overall structure of bromelain as shown in figure 6c. From figure 6, it is verified that there is no significant perturbation in the overall structure of bromelain by sucrose.

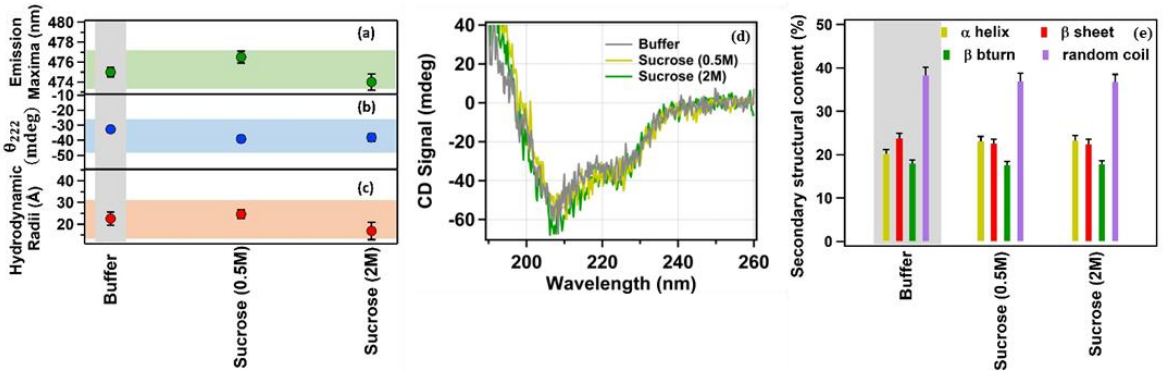

Figure 6. Bromelain conformation with added osmolytes. (a). variation of emission maxima of CPM tagged papain (ex. 375 nm) (b). Secondary structural (θ_{222}) variation of bromelain. (c). Size variation of TMR tagged papain in buffer and other osmolyte solution. (d). Raw CD spectrum corresponding to each osmolyte system. (e). variation of the secondary structural content of bromelain in presence and absence of sucrose. Error bar represents the standard deviation of the mean of three independent experiments. Experiments have been performed at 298 K.

The result indicates that sucrose acts as a destabilizer at a lower concentration (0.5 M) whereas it is a stabilizer at a higher concentration (2M). If this stabilizing effect were only osmolyte dependent, then (i) destabilization at lower concentration and stabilization at higher concentration of sucrose is objectionable according to the direct mechanism, and (ii) papain would have also shown destabilization and stabilization in presence of 0.5 M and 2 M sucrose, respectively. But it is not the case, as is evident from figure 5c. In the case of papain, experimentally observed

melting temperatures are ~354 K, ~357 K and ~365 K in buffer, 0.5 M and 2 M sucrose, respectively. In this case, stability increases with an increase in sucrose concentration.

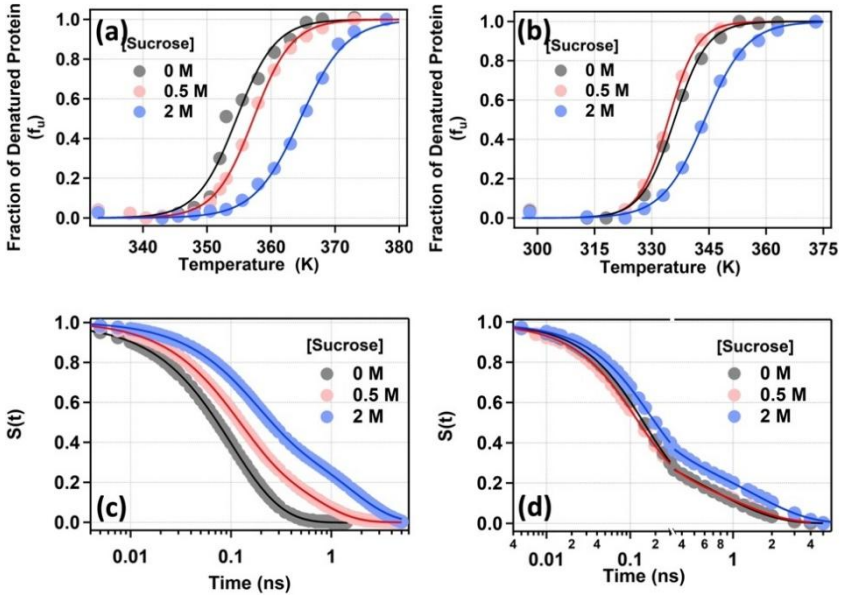

Figure 7. Variation of the fraction denatured, f_D, of (a) papain and (b) bromelain in the absence and presence of sucrose as a function of temperature. The data has been fitted with sigmoidal function to determine the melting temperature (see section S5 of the ESI for details). Solvent response function along with its fitting for (c) CPM-tag papain and (d) CPM-tag bromelain in buffer, 0.5 M and 2 M sucrose. The fitting results are shown in section S7 of the ESI. All the solvation experiments have been performed at 298 K.

If our proposal holds true, we expect that (i) with 0.5 M sucrose bromelain hydration layer becomes somewhat flexible, but with 2M sucrose, it becomes somewhat rigid compared to in buffer, and (ii) the modulation of associated water dynamics would be just opposite for papain and bromelain at 0.5 M sucrose. To our delight, our expectation goes well with the prediction, as is evident from figure 5b and 5d. (a) The fast component of associated water dynamics in the hydration layer of bromelain

Table 4. Relaxation time constants and their relative weightage in solvation dynamics study of bromelain in buffer and other aqueous osmolyte solutions. (Error bar represents the standard deviation of the mean of three independent experiments.)

Osmolyte	a_1	τ_1 (ps)	a_2	τ_2 (ps)	τ_{avg} (ps)
Buffer	0.68±0.13	130±10	0.32±0.20	980±35	400±22
Sucrose (0.5M)	0.61	100	0.39	0.81	0.38
Sucrose (2M)	0.59±0.02	150±8	0.41±0.01	1440±50	680±31

is measured to be 130 ps, 100 ps and 150 ps in buffer, 0.5 M, and 2 M sucrose, respectively. Fitting values are provided in table 4.

Whereas, for papain, there is a monotonous increase in the fast time component of the associated water dynamics with an increase in sucrose concentration, i.e., 70 ps, 110 ps and 170 ps in buffer, 0.5 M, and 2 M sucrose, respectively. (b) The fast component of the associated water dynamics for bromelain and papain modulates oppositely in 0.5 M sucrose i.e., for bromelain it decreases by 23%, and for papain it increases by 57% compared to buffer (Figure 8).

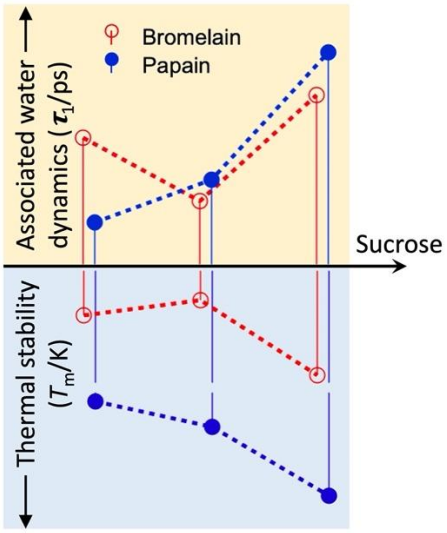

Figure 8. Osmolyte induced modulation of associated water could explain the protein-specific effect and concentration dependent reversal of stabilization.

3.3. Conclusion:

In this paper, we have presented and successfully proved a hypothesis that gives a better insight into the mechanism of osmolyte-induced stabilization/destabilization

of a protein through modification of its associated water. Using the ultrafast fluorescence method and taking papain as a model protein, we have shown that destabilizing osmolytes make the associated water flexible. In contrast, the stabilizing osmolytes rigidify the associated water compared to the buffer. More interestingly, a comparison with another protein, bromelain, which is stabilized by sucrose at a higher concentration and destabilized at a lower concentration, successfully captures, and explains the concentration and protein-specific effect. To the best of our knowledge, these observations could not be explained by any known mechanism. Of course, the nanoscopic view of how dynamics control stability is yet to be explored.

3.4. References:

(1) Masson, P.; Lushchekina, S. Conformational Stability and Denaturation Processes of Proteins Investigated by Electrophoresis under Extreme Conditions. *Molecules* **2022**, *27* (20), 6861. https://doi.org/10.3390/molecules27206861.

(2) Steeves, C. L.; Hammer, M.-A.; Walker, G. B.; Rae, D.; Stewart, N. A.; Baltz, J. M. The Glycine Neurotransmitter Transporter GLYT1 Is an Organic Osmolyte Transporter Regulating Cell Volume in Cleavage-Stage Embryos. *J. Cell. Physiol* **2005**, *204* (1), 273–279.

(3) Yancey, P. H. Organic Osmolytes as Compatible, Metabolic and Counteracting Cytoprotectants in High Osmolarity and Other Stresses. *J. Exp. Biol.* August 2005, pp 2819–2830. https://doi.org/10.1242/jeb.01730.

(4) Khan, S.; Siraj, S.; Shahid, M.; Haque, M. M.; Islam, A. Osmolytes: Wonder Molecules to Combat Protein Misfolding against Stress Conditions. *Int. J. Biol. Macromol* **2023**, *234*, 123662. https://doi.org/10.1016/j.ijbiomac.2023.123662.

(5) Street, T. O.; Wayne Bolen, D.; Rose, G. D.; Jenkins, T. C. A Molecular Mechanism for Osmolyte-Induced Protein Stability. *Proc. Natl. Acad. Sci. U. S. A.* **2006**, *103*, 13997–14002.

(6) Bolen, D. W. The Peptide Backbone Plays a Dominant Role in Protein Stabilization by Naturally Occurring Osmolytes. *Biochemistry* **1995**, *34* (39), 12884–12891.

(7) Arakawa, T.; Timasheff, S. N. The Stabilization of Proteins by Osmolytes. *Biophys. J* **1985**, *47* (3), 411–414. https://doi.org/10.1016/S0006-3495(85)83932-1.

(8) Liao, Y. T.; Manson, A. C.; DeLyser, M. R.; Noid, W. G.; Cremer, P. S. Trimethylamine N-Oxide Stabilizes Proteins via a Distinct Mechanism Compared with Betaine and Glycine. *Proc. Natl. Acad. Sci* **2017**, *114* (10), 2479–2484. https://doi.org/10.1073/pnas.1614609114.

(9) Bruździak, P.; Adamczak, B.; Kaczkowska, E.; Czub, J.; Stangret, J. Are Stabilizing Osmolytes Preferentially Excluded from the Protein Surface? FTIR and MD Studies. *Phys. Chem. Chem. Phys* **2015**, *17* (35), 23155–23164. https://doi.org/10.1039/c5cp03065j.

(10) Rani, A.; Venkatesu, P. Changing Relations between Proteins and Osmolytes: A Choice of Nature. *Phys. Chem. Chem. Phys*. Royal Society of Chemistry 2018, pp 20315–20333. https://doi.org/10.1039/c8cp02949k.

(11) Mukherjee, M.; Mondal, J. Heterogeneous Impacts of Protein-Stabilizing Osmolytes on Hydrophobic Interaction. *J. Phys. Chem. B* **2018**, *122* (27), 6922–6930. https://doi.org/10.1021/acs.jpcb.8b04654.

(12) Schroer, M. A.; Michalowsky, J.; Fischer, B.; Smiatek, J.; Grübel, G. Stabilizing Effect of TMAO on Globular PNIPAM States: Preferential Attraction Induces Preferential Hydration. *Phys. Chem. Chem. Phys* **2016**, *18* (46), 31459–31470. https://doi.org/10.1039/c6cp05991k.

(13) Mukherjee, M.; Mondal, J. Unifying the Contrasting Mechanisms of Protein-Stabilizing Osmolytes. *J. Phys. Chem. B* **2020**, *124* (30), 6565–6574. https://doi.org/10.1021/acs.jpcb.0c04757.

(14) Mondal, J.; Stirnemann, G.; Berne, B. J. When Does Trimethylamine N-Oxide Fold a Polymer Chain and Urea Unfold It? *J. Phys. Chem. B* **2013**, *117* (29), 8723–8732. https://doi.org/10.1021/jp405609j.

(15) Romero, C. M.; Albis, A.; Lozano, J. M.; Sancho, J. Thermodynamic Study of the Influence of Polyols and Glucose on the Thermal Stability of Holo-Bovine α-Lactalbumin. *J Therm Anal Calorim* **2009**, *98* (1), 165–171. https://doi.org/10.1007/s10973-009-0138-9.

(16) S Knapp; R Ladenstein; E A Galinski. Extrinsic Protein Stabilization by the Naturally Occuring Osmolyte Beta-Hydroxyectoine and Betaine. *Extremophiles* **1999**, *3*, 191–198.

(17) Santoro, M.; Liu, Y.; A Khan, S. M.; Hou, L.-X.; Bolen, D. W. Increased Thermal Stability of Proteins in the Presence of Naturally Occurring Osmolytes. *Biochemistry* **1992**, *31* (23), 5278–5283.

(18) Das, N.; Yadav, S.; Negi, K. S.; Tarif, E.; Sen, P. Does Microsecond Active-Site Dynamics Primarily Control Proteolytic Activity of Bromelain? Clues from Single Molecular Level Study with a Denaturant, a Stabilizer and a Macromolecular Crowder. *BBA Advances* **2022**, *2*, 100041. https://doi.org/10.1016/j.bbadva.2022.100041.

(19) Bruździak, P.; Panuszko, A.; Stangret, J. Influence of Osmolytes on Protein and Water Structure: A Step to Understanding the Mechanism of Protein Stabilization. *J. Phys. Chem. B* **2013**, *117* (39), 11502–11508. https://doi.org/10.1021/jp404780c.

(20) Funkner, S.; Havenith, M.; Schwaab, G. Urea, a Structure Breaker? Answers from THz Absorption Spectroscopy. *J. Phys. Chem. B* **2012**, *116* (45), 13374–13380. https://doi.org/10.1021/jp308699w.

(21) Wirtz, H.; Schäfer, S.; Hoberg, C.; Havenith, M. Differences in Hydration Structure Around Hydrophobic and Hydrophilic Model Peptides Probed by THz Spectroscopy. *J. Infrared Millim. Terahertz Waves* **2018**, *39* (9), 816–827. https://doi.org/10.1007/s10762-018-0478-2.

(22) Rezus, Y. L. A.; Bakker, H. J. Effect of Urea on the Structural Dynamics of Water. *Proc. Natl. Acad. Sci* **2006**, *103* (49), 18417–18420.

(23) Rezus, Y. L. A.; Bakker, H. J. Destabilization of the Hydrogen-Bond Structure of Water by the Osmolyte Trimethylamine N-Oxide. *J. Phys. Chem. B* **2009**, *113* (13), 4038–4044. https://doi.org/10.1021/jp805458p.

(24) Nasralla, M.; Laurent, H.; Baker, D. L.; Ries, M. E.; Dougan, L. A Study of the Interaction between TMAO and Urea in Water Using NMR Spectroscopy. *Phys. Chem. Chem. Phys* **2022**, *24* (35), 21216–21222. https://doi.org/10.1039/d2cp02475f.

(25) Palmer, H. R.; Bedford, J. J.; Leader, J. P.; Smith, R. A. J. 31P and 1H NMR Studies of the Effect of the Counteracting Osmolyte Trimethylamine-N-Oxide on Interactions of Urea with Ribonuclease A. *J. Biol. Chem* **2000**, *275* (36), 27708–27711. https://doi.org/10.1074/jbc.M003550200.

(26) Heugen, U.; Schwaab, G.; Brü, E.; Heyden, M.; Yu, X.; Leitner, D. M.; Havenith, M. Solute-Induced Retardation of Water Dynamics Probed Directly by Terahertz Spectroscopy. *Proc. Natl. Acad. Sci. U. S. A.* **2006**, *103* (33), 12301–12306.

(27) Hishida, M.; Anjum, R.; Anada, T.; Murakami, D.; Tanaka, M. Effect of Osmolytes on Water Mobility Correlates with Their Stabilizing Effect on

Proteins. *J. Phys. Chem. B* **2022**, *126* (13), 2466–2475. https://doi.org/10.1021/acs.jpcb.1c10634.

(28) Stasiulewicz, M.; Panuszko, A.; Bruździak, P.; Stangret, J. Mechanism of Osmolyte Stabilization-Destabilization of Proteins: Experimental Evidence. *J. Phys. Chem. B* **2022**, *126* (16), 2990–2999. https://doi.org/10.1021/acs.jpcb.2c00281.

(29) Verma, P. K.; Lee, H.; Park, J. Y.; Lim, J. H.; Maj, M.; Choi, J. H.; Kwak, K. W.; Cho, M. Modulation of the Hydrogen Bonding Structure of Water by Renal Osmolytes. *J. Phys. Chem. Lett* **2015**, *6* (14), 2273–2279. https://doi.org/10.1021/acs.jpclett.5b01087.

(30) Hunger, J.; Tielrooij, K. J.; Buchner, R.; Bonn, M.; Bakker, H. J. Complex Formation in Aqueous Trimethylamine-N-Oxide (TMAO) Solutions. *J. Phys. Chem. B* **2012**, *116* (16), 4783–4795. https://doi.org/10.1021/jp212542q.

(31) Bennion, B. J.; Daggett, V. The Molecular Basis for the Chemical Denaturation of Proteins by Urea. *Proc. Natl. Acad. Sci* **2003**, *100* (9), 5142–5147.

(32) Groot, C. C. M.; Bakker, H. J. A Femtosecond Mid-Infrared Study of the Dynamics of Water in Aqueous Sugar Solutions. *Phys. Chem. Chem. Phys* **2015**, *17* (13), 8449–8458. https://doi.org/10.1039/c4cp05431h.

(33) Batchelor, J. D.; Olteanu, A.; Tripathy, A.; Pielak, G. J. Impact of Protein Denaturants and Stabilizers on Water Structure. *J Am Chem Soc* **2004**, *126* (7), 1958–1961. https://doi.org/10.1021/ja039335h.

(34) Crilly, C. J.; Eicher, J. E.; Warmuth, O.; Atkin, J. M.; Pielak, G. J. Water's Variable Role in Protein Stability Uncovered by Liquid-Observed Vapor Exchange NMR. *Biochem* **2021**, *60* (41), 3041–3045. https://doi.org/10.1021/acs.biochem.1c00552.

(35) Brom, J. A.; Petrikis, R. G.; Pielak, G. J. How Sugars Protect Dry Protein Structure. *Biochem* **2023**, *62* (5), 1044–1052. https://doi.org/10.1021/acs.biochem.2c00692.

(36) Huang, K. Y.; Kingsley, C. N.; Sheil, R.; Cheng, C. Y.; Bierma, J. C.; Roskamp, K. W.; Khago, D.; Martin, R. W.; Han, S. Stability of Protein-Specific Hydration Shell on Crowding. *J Am Chem Soc* **2016**, *138* (16), 5392–5402. https://doi.org/10.1021/jacs.6b01989.

(37) Heyden, M.; Bründermann, E.; Heugen, U.; Niehues, G.; Leitner, D. M.; Havenith, M. Long-Range Influence of Carbohydrates on the Solvation Dynamics of Water - Answers from Terahertz Absorption Measurements and Molecular Modeling Simulations. *J Am Chem Soc* **2008**, *130* (17), 5773–5779. https://doi.org/10.1021/ja0781083.

(38) Soper, A. K.; Castner, E. W.; Luzar, A. Impact of Urea on Water Structure: A Clue to Its Properties as a Denaturant? *Biophys. Chem.* **2003**, *105*, 649–666. https://doi.org/10.1016/S0301-4622Ž03.00095-4.

(39) Bellissent-Funel, M. C.; Hassanali, A.; Havenith, M.; Henchman, R.; Pohl, P.; Sterpone, F.; Van Der Spoel, D.; Xu, Y.; Garcia, A. E. Water Determines the Structure and Dynamics of Proteins. *Chem. Rev* **2016**, *116* (13), 7673–7697. https://doi.org/10.1021/acs.chemrev.5b00664.

(40) Sen, S.; Voorheis, H. P. Protein Folding: Understanding the Role of Water and the Low Reynolds Number Environment as the Peptide Chain Emerges from the Ribosome and Folds. *J. Theor. Biol* **2014**, *363*, 169–187. https://doi.org/10.1016/j.jtbi.2014.07.025.

(41) Rhee, Y. M.; Sorin, E. J.; Jayachandran, G.; Lindahl, E.; Pande, V. S. Simulations of the Role of Water in the Protein-Folding Mechanism. *Proc. Natl. Acad. Sci* **2004**, *101* (17), 6456–6461.

(42) Levy, Y.; Onuchic, J. N. Water and Proteins: A Love-Hate Relationship. *Proc. Natl. Acad. Sci* **2004**, *101* (10), 3325–3326.

(43) Rg Rö, J.; Pettitt, B. M.; Bolen, D. W. Protein Folding, Stability, and Solvation Structure in Osmolyte Solutions. *Biophys J* **2005**, *89* (5), 2988–2997. https://doi.org/10.1529/biophsyj.105.067330.

(44) Rezus, Y. L. A.; Bakker, H. J. Effect of Urea on the Structural Dynamics of Water. *Proc. Natl. Acad. Sci. U. S. A.* **2006**, *103* (49), 18417–18420.

(45) Hummer, G.; Tokmakoff, A. Preface: Special Topic on Biological Water. *J. Chem. Phys* **2014**, *141* (22), 22D101. https://doi.org/10.1063/1.4901337.

(46) Zhong, D.; Pal, S. K.; Zewail, A. H. Biological Water: A Critique. *Chem. Phys. Lett.* **2011**, *503* (1–3), 1–11. https://doi.org/10.1016/j.cplett.2010.12.077.

(47) Ball, P. Water as an Active Constituent in Cell Biology. *Chem. Rev.* January 2008, pp 74–108. https://doi.org/10.1021/cr068037a.

(48) Levy, Y.; Onuchic, J. N. Water Mediation in Protein Folding and Molecular Recognition. *Annu. Rev. Biophys.* **2006**, *35* (1), 389–415. https://doi.org/10.1146/ANNUREV.BIOPHYS.35.040405.102134.

(49) Bagchi, B. *Water in Biological and Chemical Processes: From Structure and Dynamics to Function*; Cambridge University Press, 2013. https://doi.org/10.1017/CBO9781139583947.

(50) Kumar, S.; Peon, J.; Zewail, A. H. Biological Water at the Protein Surface: Dynamical Solvation Probed Directly with Femtosecond Resolution. *Proc. Natl. Acad. Sci. U. S. A.* **2002**, *99* (4), 1763–1768.

(51) Mukherjee, S.; Mondal, S.; Bagchi, B. Distinguishing Dynamical Features of Water inside Protein Hydration Layer: Distribution Reveals What Is

Hidden behind the Average. *J. Chem. Phys* **2017**, *147* (2), 024901. https://doi.org/10.1063/1.4990693.

(52) Bhattacharyya, K. Nature of Biological Water: A Femtosecond Study. *Chem Commun.* Royal Society of Chemistry 2008, pp 2848–2857. https://doi.org/10.1039/b800278a.

(53) Mondal, S.; Mukherjee, S.; Bagchi, B. On the Origin of Diverse Time Scales in the Protein Hydration Layer Solvation Dynamics: A Molecular Dynamics Simulation Study. *J. Chem. Phys* **2017**, *147*, 154901.

(54) Peon, J.; Pal, K.; Zewail, A. H. Hydration at the Surface of the Protein Monellin: Dynamics with Femtosecond Resolution. *Proc. Natl. Acad. Sci* **2002**, *99* (17), 10964–10969.

(55) Qiu, W.; Zhang, L.; Okobiah, O.; Yang, Y.; Wang, L.; Zhong, D.; Zewail, A. H. Ultrafast Solvation Dynamics of Human Serum Albumin: Correlations with Conformational Transitions and Site-Selected Recognition. *J. Phys. Chem. B* **2006**, *110* (21), 10540–10549. https://doi.org/10.1021/jp055989w.

(56) Sen, P.; Roy, D.; Sahu, K.; Kumar Mondal, S.; Bhattacharyya, K. Hydration Dynamics of a Protein in the Presence of Urea and Sodium Dodecyl Sulfate. *Chem Phys Lett* **2004**, *395* (1–3), 58–63. https://doi.org/10.1016/j.cplett.2004.07.052.

(57) Lushchekina, S. V.; Inidjel, G.; Martinez, N.; Masson, P.; Trovaslet-Leroy, M.; Nachon, F.; Koza, M. M.; Seydel, T.; Peters, J. Impact of Sucrose as Osmolyte on Molecular Dynamics of Mouse Acetylcholinesterase. *Biomolecules* **2020**, *10* (12), 1–19. https://doi.org/10.3390/biom10121664.

(58) Shao, Q.; Gao, Y. Q. Water Plays an Important Role in Osmolyte-Induced Hairpin Structure Change: A Molecular Dynamics Simulation Study. *J. Chem. Phys* **2012**, *137* (14), 145101. https://doi.org/10.1063/1.4757419.

(59) Sathish, H. A.; Kumar, P. R.; Prakash, V. Mechanism of Solvent Induced Thermal Stabilization of Papain. *Int J Biol Macromol* **2007**, *41* (4), 383–390. https://doi.org/10.1016/j.ijbiomac.2007.05.009.

(60) Samanta, N.; Das Mahanta, D.; Choudhury, S.; Barman, A.; Kumar Mitra, R. Collective Hydration Dynamics in Some Amino Acid Solutions: A Combined GHz-THz Spectroscopic Study. *J. Chem. Phys* **2017**, *146* (12), 125101. https://doi.org/10.1063/1.4978900.

(61) Qiao, B.; Jiménez-Ángeles, F.; Nguyen, T. D.; De La Cruz, M. O. Water Follows Polar and Nonpolar Protein Surface Domains. *Proc. Natl. Acad. Sci* **2019**, *116* (39), 19274–19281. https://doi.org/10.1073/pnas.1910225116.

(62) Mukherjee, P.; Das, A.; Sen, P. Solvation Dynamics in SDS Micelle Revisited with Femtosecond Time Resolution to Reveal the Probe and Concentration Dependence. *Chem. Phys* **2018**, *513*, 141–148. https://doi.org/10.1016/j.chemphys.2018.07.034.

(63) Zhang Luyuan; Wang Lijuan; Kao Ya-Ting; Qiu Weihong; Yang Yi; Okobiah Oghaghare; Zhong Dongping. Mapping Hydration Dynamics around a Protein Surface. *Proc. Natl. Acad. Sci. U. S. A.* **2007**, *104* (47), 18461–18466.

(64) Bhattacharyya, S. M.; Wang, Z. G.; Zewail, A. H. Dynamics of Water near a Protein Surface. *J. Phys. Chem. B* **2003**, *107* (47), 13218–13228. https://doi.org/10.1021/jp030943t.

(65) Nandi, N.; Bagchi, B. Dielectric Relaxation of Biological Water †. *J Phys Chem B* **1997**, *101* (50), 10954–10961.

(66) Houston, P.; Macro, N.; Kang, M.; Chen, L.; Yang, J.; Wang, L.; Wu, Z.; Zhong, D. Ultrafast Dynamics of Water-Protein Coupled Motions around the Surface of Eye Crystallin. *J. Am. Chem. Soc.* **2020**, *142* (8), 3997–4007. https://doi.org/10.1021/jacs.9b13506.

(67) Khodadadi, S.; Curtis, J. E.; Sokolov, A. P. Nanosecond Relaxation Dynamics of Hydrated Proteins: Water versus Protein Contributions. *J. Phys. Chem. B* **2011**, *115* (19), 6222–6226. https://doi.org/10.1021/jp1122213.

(68) Sen, P.; Mukherjee, S.; Dutta, P.; Halder, A.; Mandal, D.; Banerjee, R.; Roy, S.; Bhattacharyya, K. Solvation Dynamics in the Molten Globule State of a Protein. *J. Phys. Chem. B* **2003**, *107* (51), 14563–14568. https://doi.org/10.1021/jp036277d.

(69) Das, N.; Tarif, E.; Dutta, A.; Sen, P. Associated Water Dynamics Might Be a Key Factor Affecting Protein Stability in the Crowded Milieu. *J. Phys. Chem. B* **2023**, *127* (14), 3151–3163. https://doi.org/10.1021/acs.jpcb.2c09043.

(70) Hishida, M.; Kaneko, A.; Yamamura, Y.; Saito, K. Contrasting Changes in Strongly and Weakly Bound Hydration Water of a Protein upon Denaturation. *J Phys Chem B* **2023**, *127* (28), 6296–6305. https://doi.org/10.1021/acs.jpcb.3c02970.

(71) Panuszko, A.; Wojciechowski, M.; Bruździak, P.; Rakowska, P. W.; Stangret, J. Characteristics of Hydration Water around Hen Egg Lysozyme as the Protein Model in Aqueous Solution. FTIR Spectroscopy and Molecular Dynamics Simulation. *Phys. Chem. Chem. Phys* **2012**, *14* (45), 15765–15773. https://doi.org/10.1039/c2cp42229h.

(72) Kamal, J. K. A.; Zhao, L.; Zewail, A. H. Ultrafast Hydration Dynamics in Protein Unfolding: Human Serum Albumin. *Proc. Natl. Acad. Sci* **2004**, *101* (37), 13411–13416.

(73) Dockal, M.; Carter, D. C.; Rü, F. Conformational Transitions of the Three Recombinant Domains of Human Serum Albumin Depending on PH*. *J. Biol. Chem* **2000**, *275* (5), 3042–3050.

(74) Das, N.; Sen, P. Structural, Functional, and Dynamical Responses of a Protein in a Restricted Environment Imposed by Macromolecular Crowding. *Biochem* **2018**, *57* (42), 6078–6089. https://doi.org/10.1021/acs.biochem.8b00599.

(75) Mohan, V.; Sengupta, B.; Das, N.; Banerjee, I.; Sen, P. Domain-Specific Stabilization of Structural and Dynamic Responses of Human Serum Albumin by Sucrose. *Protein Pept Lett* **2019**, *26* (4), 287–300. https://doi.org/10.2174/0929866526666190122115702.

(76) Jha, A.; Ishii, K.; Udgaonkar, J. B.; Tahara, T.; Krishnamoorthy, G. Exploration of the Correlation between Solvation Dynamics and Internal Dynamics of a Protein. *Biochemistry* **2011**, *50* (3), 397–408. https://doi.org/10.1021/bi101440c.

(77) Granata, V.; Palladino, P.; Tizzano, B.; Negro, A.; Berisio, R.; Zagari, A. The Effect of the Osmolyte Trimethylamine N-Oxide on the Stability of the Prion Protein at Low PH. *Biopolymers* **2006**, *82* (3), 234–240. https://doi.org/10.1002/bip.20481.

(78) Singh Laishram R; Poddar Nitesh Kumar; Dar Tanveer Ali; Kumar Raj; Ahmad Faizan. Protein and DNA Destabilization by Osmolytes: The Other Side of the Coin. *Life Sci.* **2011**, *88* (3–4), 117–125.

(79) Olsson, C.; Jansson, H.; Swenson, J. The Role of Trehalose for the Stabilization of Proteins. *J. Phys. Chem. B* **2016**, *120* (20), 4723–4731. https://doi.org/10.1021/acs.jpcb.6b02517.

(80) Shukla, N.; Narayan Bhatt, A.; Aliverti, A.; Zanetti, G.; Bhakuni, V. Guanidinium Chloride-and Urea-Induced Unfolding of FprA, a Mycobacterium NADPH-Ferredoxin Reductase Stabilization of an Apo-Protein by GdmCl. *FEBS J* **2005**, *272* (9), 2216–2224. https://doi.org/10.1111/j.1742-4658.2005.04645.x.

(81) Gull, N.; Sen, P.; Kabir-ud-Din; Khan, R. H. Effect of Physiological Concentration of Urea on the Conformation of Human Serum Albumin. *J Biochem* **2007**, *141* (2), 261–268. https://doi.org/10.1093/jb/mvm027.

(82) Bhuyan, A. K. Protein Stabilization by Urea and Guanidine Hydrochloride. *Biochemistry* **2002**, *41* (45), 13386–13394. https://doi.org/10.1021/bi020371n.

(83) Mayr, L. M.; Schmid, F. X. Stabilization of a Protein by Guanidinium Chloride* 1". *Biochemistry* **1993**, *32*, 7994–7998.

(84) Habib, S.; Khan, M. A.; Younus, H. Thermal Destabilization of Stem Bromelain by Trehalose. *Protein J* **2007**, *26* (2), 117–124. https://doi.org/10.1007/s10930-006-9052-1.

(85) Sathish, H. A.; Kumar, R.; Prakash, V. Effect of Urea at Lower Concentration on the Structure of Papain-Formation of a Stable Molten Globule and Its Characterization. *Indian J. Biochem. Biophys* **2002**, *39* (3), 155–162.

This page left blank intentionally

Chapter 4

Interplay between Protein Fluctuation and Associated Water Dynamics on the Osmolyte induced Protein Stabilization

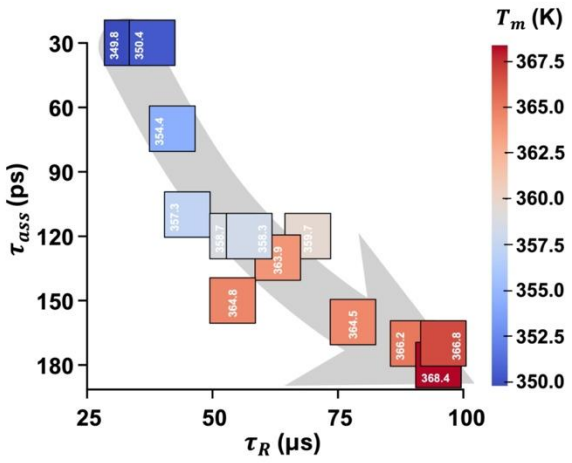

Kuldeep Singh Negi, Subhajit Rana, Tanmoy Khan, Dipankar Mondal, and Pratik Sen

Biophys. J., ***2025***, *124, 2082 – 2091*

Abstract

The mechanism behind osmolyte-induced protein stabilization remains elusive despite extensive research. Amongst various hypotheses, the associated water modulation hypothesis has proven to be the most effective in explaining osmolyte-induced stabilization effects. Earlier we had demonstrated that osmolytes that slow down associated water dynamics enhance protein thermal stability, whereas those that accelerate it, promote destabilization. However, the molecular basis of this correlation remains unclear. Using fluorescence correlation spectroscopy, we observe that osmolyte-induced changes in the associated water dynamics directly affect the internal flexibility of the protein, which is assessed through conformational fluctuation dynamics, serving as a tool to measure the protein's internal flexibility. The osmolytes that induce retardation in the associated water dynamics make the interior of the protein more rigid, as reflected by the slowed conformational fluctuation dynamics of the protein, leading to enhanced thermal stabilization. The destabilizers induce effects that are exactly opposite to stabilizers. These findings provide new insights into the interplay of associated water dynamics, protein flexibility, and stability, contributing to a deeper understanding of osmolyte induced protein stabilization.

4.1 Introduction

Proteins are indispensable for the proper functioning of living organisms. They are composed of amino acid residues that fold into a specific three-dimensional structure, referred to as the native state. The native conformation is critical for the biological activity of proteins. Even a marginal alteration in the environment, like a change in the temperature, pressure, pH, and salt concentration, can change the native state conformation and may modify protein's functional efficacy. Osmolytes, a class of small organic molecules including sugars, polyols, and amino acids, play a critical role in preserving protein structural integrity under diverse environmental conditions [1–3]. These molecules are broadly categorized based on their effects on protein stability: stabilizing osmolytes, such as sucrose and trimethylamine N-oxide (TMAO), enhance the structural robustness of proteins, whereas destabilizing osmolytes (known as denaturants), e.g. urea and guanidine hydrochloride (GnHCl), promote protein unfolding [4,5]. Due to their ability to modulate protein stability, osmolytes have significant applications in the pharmaceutical industry, where they are employed to prolong the shelf life of biopharmaceutical products, thereby ensuring their stability and efficacy over extended periods [6,7].

Over the past few decades, extensive research has focused on understanding osmolyte-protein interactions due to their significance in both fundamental science and applications [7–13]. While substantial progress has been made (Scheme 1), a concise understanding of these interactions remains elusive. Timasheff's group first proposed a model based on the phenomenon of surface tension, specifically the excess surface free energy of water molecules at the protein-water interface [10,14,15]. This model differentiates between stabilizing osmolytes (such as sucrose) and destabilizing osmolytes (like urea) by introducing a parameter known as preferential interaction coefficient (Γ), which quantifies the interactions among the protein, osmolyte, and solvent. Stabilizing osmolytes have a negative preferential interaction coefficient (Γ) and promote a compact protein conformation by being excluded from the protein surface. On the other hand, destabilizing osmolytes have a positive preferential interaction coefficient (Γ) and tend to accumulate at the protein surface,

which stabilizes an extended conformation [14–16]. Later, Bolen's group expanded this model by demonstrating that interactions between osmolytes and the protein backbone are crucial to these observations [17]. Stabilizing osmolytes favour the compact state because the native state has a smaller, less exposed surface area, resulting in fewer repulsive interactions. In contrast, destabilizing osmolytes favour the extended state, as the denatured protein presents a larger surface area, allowing for more attractive interactions with the osmolyte. This model is known as the preferential or direct interaction mechanism [18]. This model emphasizes on the role of water molecules in the phenomenon of osmolyte-protein interaction. Further developments examined the role of water structure in detail. Studies suggest that osmolytes alter the hydrogen-bonding network of water, which contributes to protein thermal stability - a concept referred to as the indirect mechanism or water modulation theory [19–24]. The osmolytes which rigidifies the water structure or dynamics are expected to thermally stabilize the protein and vice-versa. Although these theories provide valuable insights into protein-osmolyte interaction, they often struggle to account for protein-specific effects [25–28] and osmolyte's concentration dependent reversal of the protein stability [25,28].

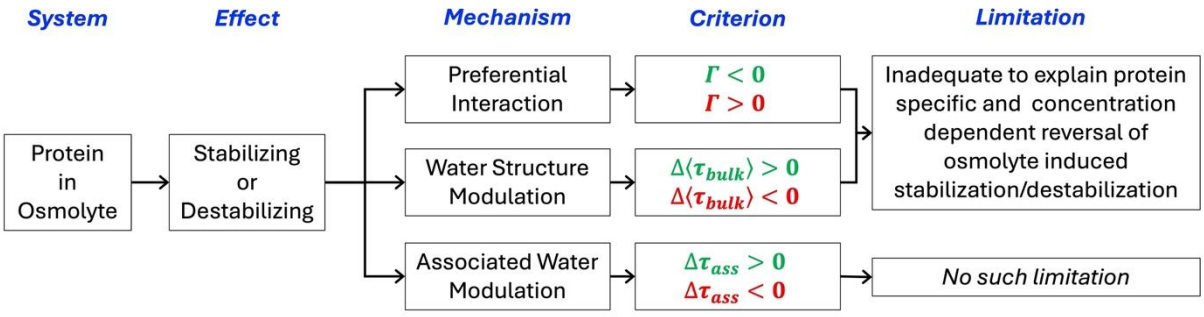

Scheme 1. Known mechanisms of protein stabilization by osmolytes and their limitations. The conditions written in green and red are for stabilizing and destabilizing osmolytes, respectively. Preferential interaction mechanism employs a parameter termed as preferential interaction coefficient (Γ) to describe the osmolyte protein interaction, which quantifies the interactions among the protein, osmolyte, and water. Osmolyte with $\Gamma < 0$ and $\Gamma > 0$ are considered as stabilizing and destabilizing osmolytes, respectively. In water structure modulation hypothesis, stabilizing and destabilizing osmolytes retards ($\Delta\langle\tau_{bulk}\rangle > 0$) and accelerates ($\Delta\langle\tau_{bulk}\rangle > 0$) the bulk

water dynamics, respectively, where, $\Delta\langle\tau_{bulk}\rangle = \langle\tau_{bulk}\rangle_{osmolyte} - \langle\tau_{bulk}\rangle_{buffer}$. In associated water modulation hypothesis, stabilizing and destabilizing osmolytes retards $\Delta\tau_{ass} > 0$ and accelerates $\Delta\tau_{ass} < 0$ the associated water dynamics, respectively, where, $\Delta\tau_{ass} = (\tau_{ass})_{osmolyte} - (\tau_{ass})_{buffer}$.

To address this, the water hypothesis has been modified to incorporate changes in water near the protein surface (known in the literature as biological water, hydration layer or associated water) upon the addition of osmolytes, aiming to explain the specific effects observed with different proteins [28]. This layer of water is distinctly different from bulk water in terms of its characteristics [29–32]. Recently, we argued that the modulation of the associated water structure is linked to protein thermal stability through our experimental findings [28,33–35]. However, the exact way how the changes in the associated water dynamics contribute to protein stability remain unclear and have yet to be explored.

Additionally, both experimental and computational studies have shown that the fast dynamics of protein side chains are influenced by the dynamics of the associated water molecules, a phenomenon referred to as water-slaved motions of the protein [36–39]. The research history is rich with studies demonstrating the relationship between protein flexibility and hydration water [40–46]. Recently, Li *et al.* using nuclear magnetic resonance (NMR) spectroscopy and molecular dynamics simulations have shown that the addition of osmolytes leads to a shortening of the protein backbone hydrogen bonds influenced by the modulation in associated water structure [47]. In short, water in biological systems often appears inactive and random but plays a crucial role in regulating protein properties (Scheme 2). Motivated by these findings, we hypothesized a significant connection between the associated water structure and the flexibility of the protein side chain. To verify our hypothesis, we have used papain as a model protein and employ fluorescence correlation spectroscopy (FCS) to probe the conformational fluctuation dynamics of papain in the presence of different stabilizing and denaturing osmolytes. In our previous study, using the same protein in the presence of different osmolytes we have shown that associated water dynamics correlates well with the thermal stability of the protein [28]. In the present

study, we investigated the possible correlation of the conformational fluctuations dynamics (indirect measure of internal protein flexibility) with associated water dynamics, aiming to uncover the dominant factors driving osmolyte induced changes in protein stability. Our findings provide deeper insights into the intricate relationship between protein dynamics and solvent interactions, shedding light on the fundamental principles governing protein folding and stability.

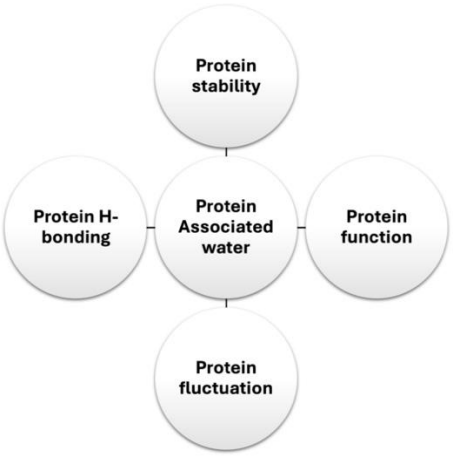

Scheme 2. Role of protein associated water in regulating protein properties.

4.2. Results and Discussion

Proteins exist in a dynamic equilibrium between their native and denatured states under specific environmental conditions. Any external perturbation, such as changes in temperature, pressure, or pH, can shift this equilibrium [48]. In this study, we have investigated the effect of temperature as a perturbant to assess the protective role of osmolytes against thermal denaturation. Upon the application of heat, the equilibrium shifts toward the unfolded state, favoring protein denaturation. The temperature at which the fractions of the unfolded and native states are equal (i.e., 0.5) is defined as the melting temperature (T_m), a widely used parameter to evaluate the thermal stability of proteins [49,50]. A higher T_m indicates greater thermal stability, whereas a lower T_m signifies reduced stability.

Various techniques can be employed to study protein thermal stability, among which fluorescence spectroscopy is particularly advantageous due to its sensitivity to

environmental changes surrounding fluorescent probes. In this study, we utilized the intrinsic fluorescence of tryptophan residues in papain, leveraging their solvatochromic properties. In the native state, the tryptophan residues are buried within the hydrophobic core of the protein. Upon unfolding, these residues become exposed to the polar aqueous environment, resulting in a red shift of the emission maximum. This shift serves as a reliable indicator of protein unfolding.

In a recent publication, we investigated the thermal denaturation of papain in the presence of various osmolytes using the same fluorescence-based approach [28]. The melting temperatures from that study have been reproduced here in figure 1a. T_m of papain in buffer is 354 K. Osmolytes that increase the T_m of a protein are classified as stabilizing, whereas those that lower T_m are considered destabilizing. As depicted in figure 1a, the thermal stability of papain varies significantly depending on the osmolyte present. Destabilizing osmolytes such as 1M guanidine hydrochloride (GnHCl) and 3M urea lead to a reduction in T_m, indicating enhanced thermal denaturation. Conversely, the other osmolytes exhibit a stabilizing effect to varying degrees, as reflected in the increased T_m values. We also measured the associated water dynamics (τ_{ass}) of papain in the presence of various osmolytes (Figure 1b) [28]. τ_{ass} of papain in buffer was measured to be ~70 ps, which varies significantly in presence of osmolytes. Destabilizing osmolytes like 1M GnHCl and 3M urea decrease τ_{ass} representing an increase in flexibility, whereas the stabilizing osmolytes increases τ_{ass} signifying an increase in the rigidity. As expected, we found that T_m and τ_{ass} correlates very well (Figure 1c) [28]. This observation affirms our proposal of the modulation of the thermal stability of papain in osmolyte solutions due to the modulation of protein-associated water structure/dynamics in the presence of osmolytes [28]. Increased rigidity of the water network enhances protein stability against thermal agitation, whereas increased water flexibility leads to thermal destabilization.

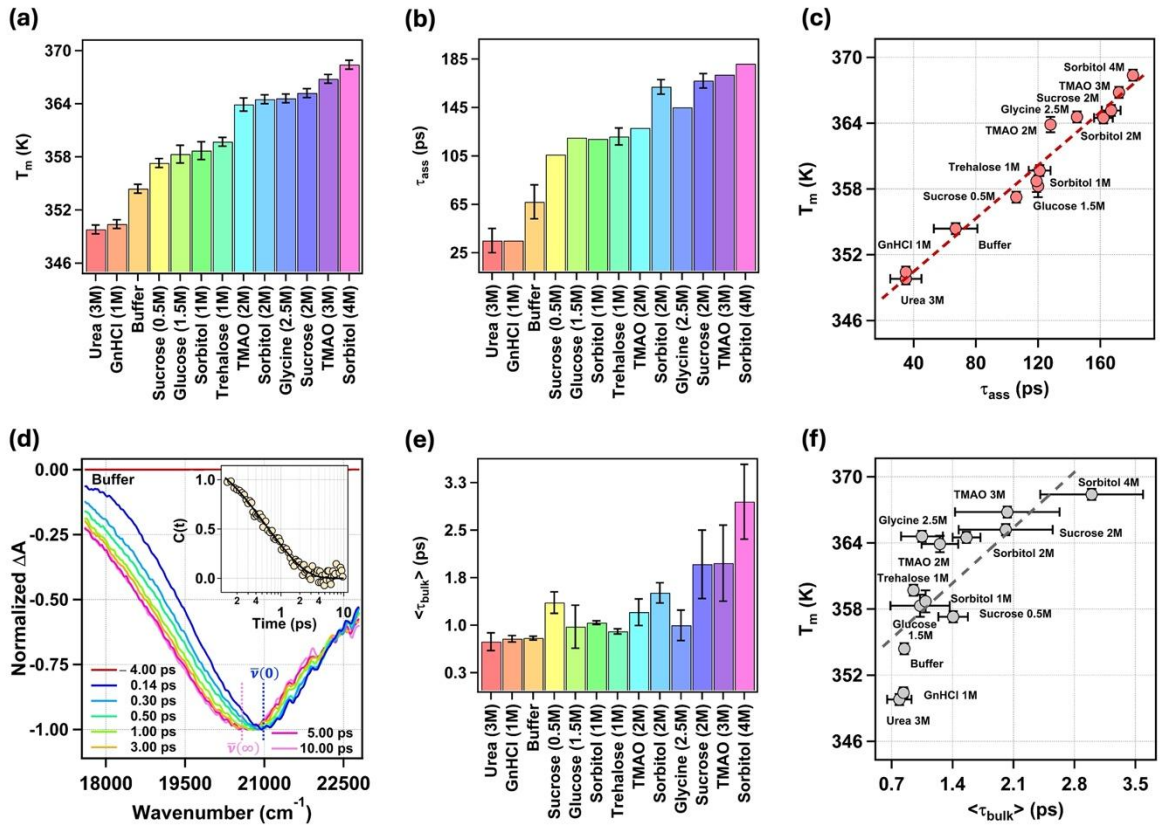

Figure 1. Modulation of (a) melting temperature (T_m) and (b) associated water dynamics of papain with added osmolyte and their (c) correlation with Adj. R^2 = 0.95. Data taken from *Phys. Chem. Chem. Phys.* 2023, 25:32602. (d) Stimulated emission of coumarin 343 in buffer at different times from the excitation at 298 K. The solvent response function, C(t), for buffer derived from the stimulated emission maxima following equation 1 is shown in the inset along with the bi-exponential fitting. The fitting parameters are given in table 1. The average solvation time for buffer is calculated to be 0.8 ps using equation 3. (e) A comparison of the average solvation time of buffer and osmolyte solutions under investigation at 298 K. Error in the measurements are estimated from the standard deviation of three independent measurements. (f) The plot of the melting temperature (T_m) of papain against bulk solvation dynamics in the presence of osmolytes shows a week correlation with Adj. R^2 =0.54. All the experiments except melting have been performed at 298 K.

To further testify to the proposal, we have investigated the bulk water dynamics of the osmolyte solutions, by monitoring the stimulated emission of solvatochromic probe C343. For C343 in buffer, the transient absorption spectra in the stimulated emission region are shown in figure 1d. The stimulated emission maximum against the corresponding time is processed to obtain the solvent response function $C(t)$

using equation 1, which has been fitted with equation 2 (inset of Figure 1d). The average bulk solvation dynamics, $\langle\tau_{Bulk}\rangle$, in buffer is determined using equation 3, and found to be ~0.8 ps, which is consistent with reported literature values [51].

$$C(t) = \frac{\bar{\nu}(t)-\bar{\nu}(\infty)}{\bar{\nu}(0)-\bar{\nu}(\infty)} \quad (1.2.1)$$

$$C(t) = \sum_i b_i e^{-\frac{t}{\tau_i}} \text{ where } \sum_i b_i = 1 \quad (1.2.2)$$

$$\langle\tau_s\rangle = \sum_i b_i \tau_i \quad (1.2.3)$$

In the above equations, $\bar{\nu}(t)$, $\bar{\nu}(0)$, and $\bar{\nu}(\infty)$ are the peak wavenumbers at times t, 0, and ∞, respectively.

In presence of osmolytes under investigation, all the raw data, the associated solvent response functions, $C(t)$ along with biexponential fitting are shown in figure 2 and figure 3 respectively. The corresponding fitting parameters are provided in table 1.

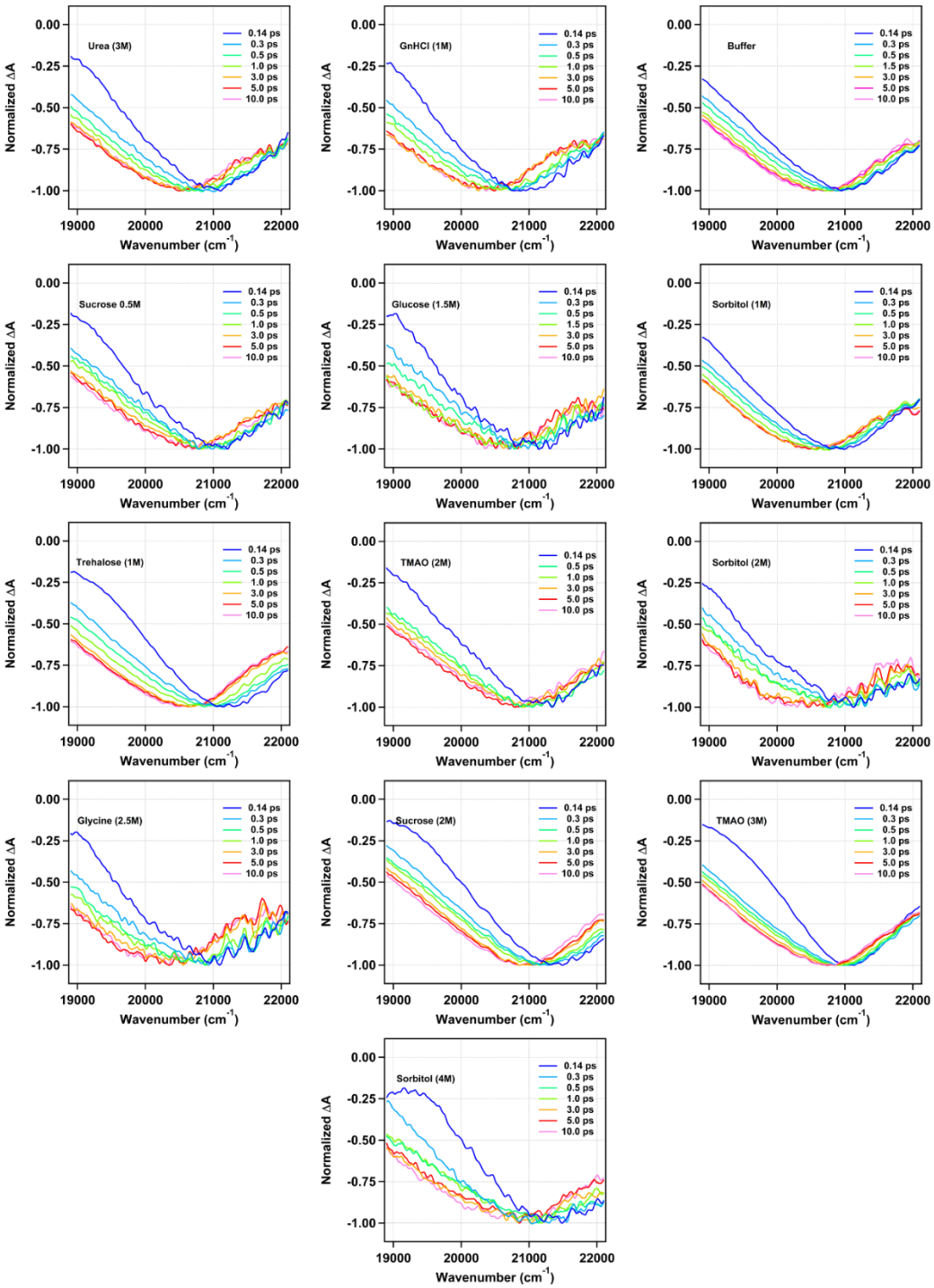

Figure 2: Shift in the stimulated emission traces of C-343 with time in buffer and other osmolyte solution. All the solvation experiments have been performed at 298 K.

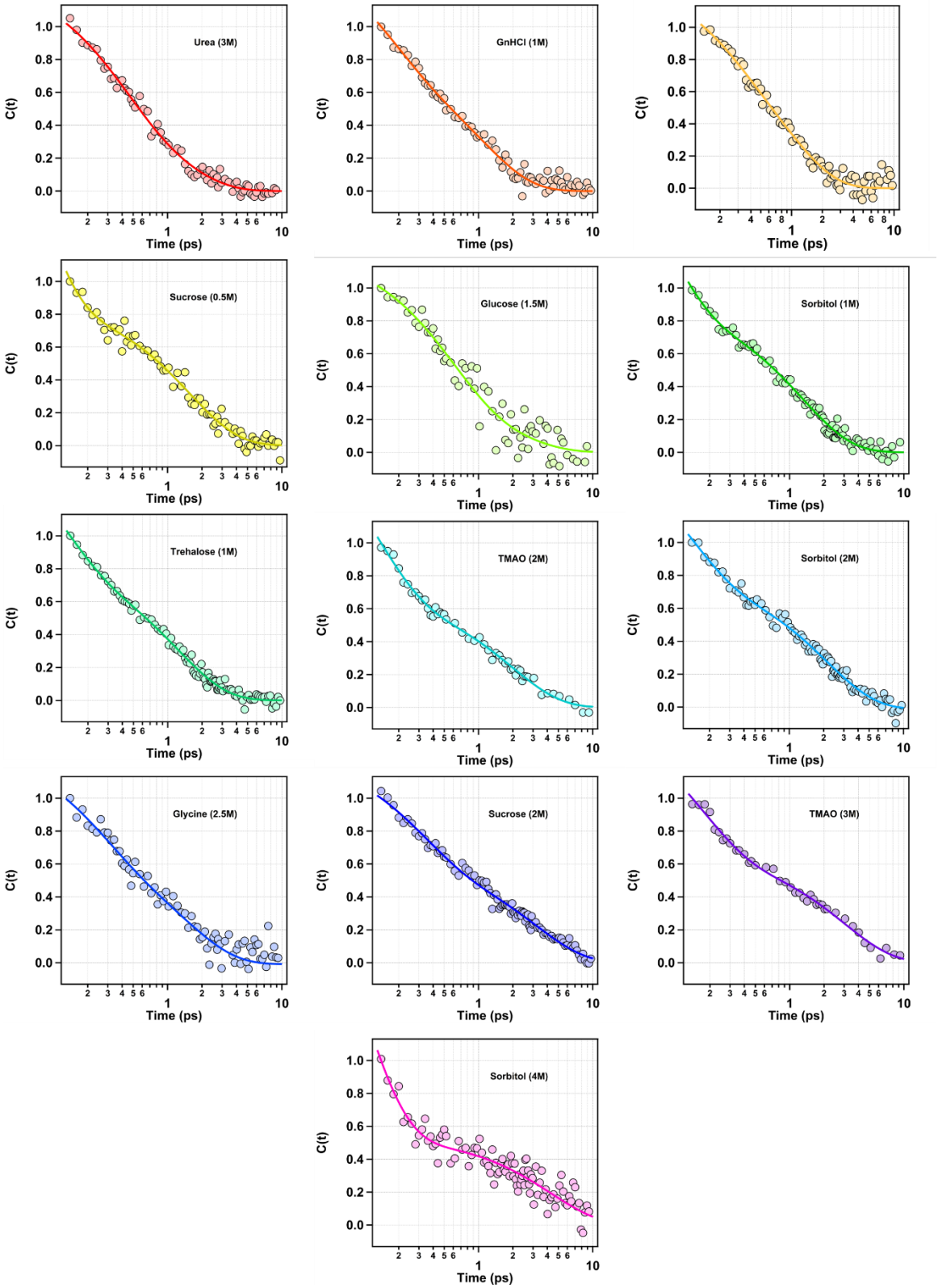

Figure 3: Fitting of solvent correlation function (c(t)) for C-343 in buffer and other osmolyte solution. All the solvation experiments have been performed at 298 K.

Table 1: Relaxation time constants and their relative weightage in solvation dynamics study of C-343 in buffer and other aqueous osmolyte solution.

Osmolyte (Concentration)	a_1	τ_1(ps)	a_2	τ_2(ps)	τ_{avg}(ps)
Urea (3M)	0.54±0.13	0.370±0.070	0.46±0.13	1.280±0.630	0.780±0.140
GnHCl (1M)	0.27±0.03	0.150±0.030	0.73±0.03	1.090±0.100	0.830±0.050
Buffer	0.23±0.06	0.230±0.070	0.77±0.060.	1.030±0.090	0.840±0.030
Sucrose (0.5M)	0.28±0.06	0.240±0.120	0.72±0.06	1.860±0.330	1.410±0.170
Glucose (1.5M)	0.69±0.11	0.540±0.150	0.31±0.11	2.110±0.420	1.030±0.340
Sorbitol (1M)	0.21±0.01	0.110±0.030	0.79±0.01	1.340±0.030	1.090±0.030
Trehalose (1M)	0.24±0.01	0.100±0.020	0.76±0.01	1.220±0.060	0.950±0.040
TMAO (2M)	0.38±0.03	0.120±0.060	0.62±0.03	1.950±0.420	1.260±0.210
Sorbitol (2M)	0.28±0.01	0.120±0.060	0.72±0.01	2.120±0.240	1.560±0.160
Glycine (2.5M)	0.34±0.11	0.230±0.100	0.66±0.11	1.470±0.570	1.050±0.240
Sucrose (2M)	0.41±0.05	0.300±0.130	0.59±0.05	3.200±1.090	2.010±0.540
TMAO (3M)	0.37±0.02	0.170±0.070	0.63±0.02	3.120±1.020	2.030±0.600
Sorbitol (4M)	0.47±0.02	0.150±0.050	0.53±0.05	5.470±0.870	2.990±0.590

The addition of stabilizing osmolytes resulted in a slight slowdown of solvation dynamics, suggesting enhanced hydrogen bonding among water molecules. Conversely, the addition of destabilizing osmolytes appeared to weaken intermolecular hydrogen bonding, though these changes remained within the experimental error margin. The average bulk solvation dynamics of various osmolyte solutions along with buffer are presented in figure 1e. A plot of T_m of

papain in presence of osmolyte against $\langle \tau_{Bulk} \rangle$ of the respective osmolyte solution show a weak correlation (Figure 1f) compared to the correlation of T_m with τ_{ass} (Figure 1c). The findings indicate that while bulk water modulation may influence protein thermal stability, it cannot serve as the sole explanation for the phenomenon. Furthermore, our previous observation that bromelain is destabilized in a 0.5 M sucrose solution, whereas papain remains stabilized in the same environment [28,52], cannot be elucidated by the modulation of bulk water dynamics as it remains same in 0.5M sucrose solution irrespective of protein and depends solely on the osmolyte and its concentration. Importantly, our hypothesis concerning the involvement of associated water dynamics has effectively accounted for these protein-specific effects.

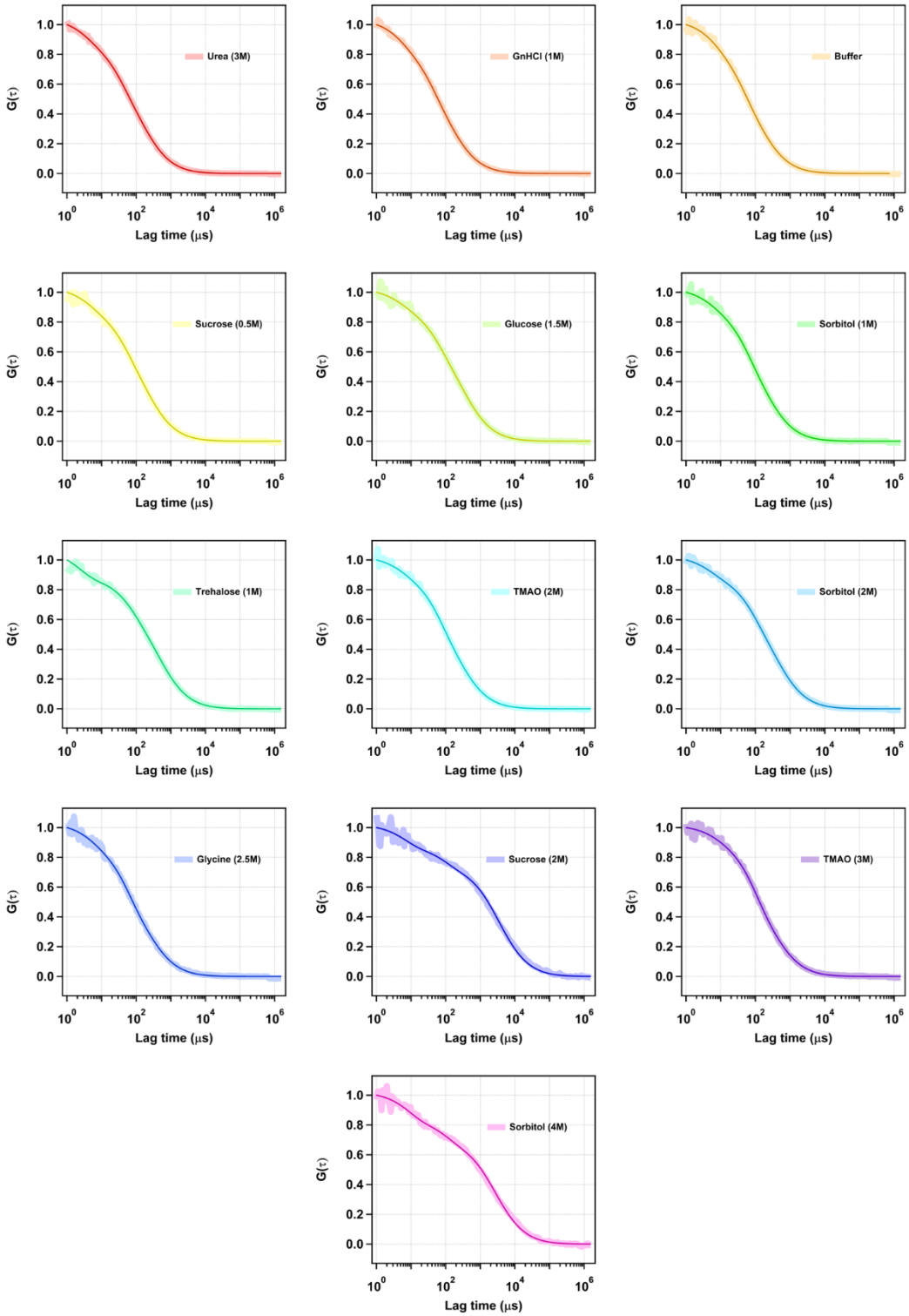

Figure 4: Normalized traces of FCS cross-correlation curves of TMR-tag papain in mentioned osmolyte. Black colored line represents the fitting line. All the FCS experiments have been performed at 298 K.

Though a correlation between the melting temperature (T_m) of papain and the associated water dynamics (τ_{ass}) is observed; the mechanism by which osmolytes influence protein thermal stability is still illusive. This raises the question - How does osmolyte-induced modulation of associated water dynamics affects protein stability at a molecular level? Given the absence of significant structural alterations of papain in presence and absence of osmolytes as confirmed by the almost similar hydrodynamic radii in buffer and other osmolyte solutions shown in figure 5 (the raw FCS correlation traces are shown in figure 4 along with the fitting line) and the fitting parameters are provided in table 2, it is unlikely that changes in the water dynamics directly modulate the thermodynamics of protein denaturation. This notion is particularly challenging in the case of stabilizing osmolytes, which, due to repulsive interactions, remain excluded from the protein surface.

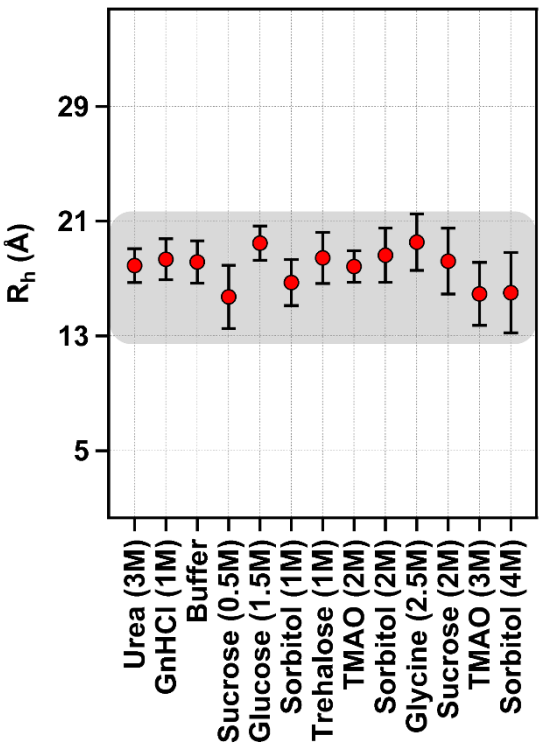

Figure 5: Modulation of the hydrodynamic radii (Å) of protein in buffer and other osmolyte solution. FCS experiments have been performed at 298 K.

Since there is a coupling between the associated water and the protein side chain, the associated water is believed to control their dynamics, which have a significant

role in defining their function [29,31,32,40,53,54]. It is reasonable to expect that osmolyte-induced changes in water dynamics may influence the internal environment of the protein. This modulation could be sufficient to alter the strength of intermolecular interactions, such as interaction among amino acid residues, without significantly perturbing the overall protein structure. Recent NMR

Table 2: Variation of time scales of diffusion, triplet state, conformational fluctuation dynamics and hydrodynamic radii of TMR-papain in buffer and other aqueous osmolyte solution.

Osmolyte (Concentration)	$\tau_d(\mu s)$	$\tau_T(\mu s)$ (p)	$\tau_R(\mu s)$ (a_R)	R_h(Å)
Urea (3M)	136.3±10.5	3.3±1.0 (0.12)	33.0±8.2 (0.19)	17.9±1.2
GnHCl (1M)	120.9±10.6	4.7±1.4 (0.13)	37.6±7.6 (0.18)	18.3±1.4
Buffer	119.2±7.5	5.8±0.8 (0.13)	41.8±3.3 (0.20)	18.3±1.0
Sucrose (0.5M)	180.1±29.1	4.1±0.5 (0.12)	45.2±6.9 (0.17)	15.7±2.2
Glucose (1.5M)	297.0±21.1	4.7±0.4 (0.1)	54.8±5.1 (0.19)	19.5±1.2
Sorbitol (1M)	174.1±19.2	4.7±0.9 (0.1)	54.5±5.4 (0.19)	16.7±1.6
Trehalose (1M)	431.7±48.6	2.3±0.1 (0.18)	68.8±3.1 (0.15)	18.4±1.8

TMAO (2M)	221.8±15.8	4.7±0.9 (0.1)	63.3±2.6 (0.22)	17.8±1.1
Sorbitol (2M)	372.1±43.8	4.6±0.5 (0.12)	78.3±9.5 (0.18)	18.6±1.9
Glycine (2.5M)	195.5±23.1	4.7±1.8 (0.12)	54.0±6.9 (0.42)	19.5±2.0
Sucrose (2M)	3435.7±326.7	6.3±3.3 (0.14)	90.2±6.0 (0.13)	18.2±1.5
TMAO (3M)	286.6±45.7	6.5±1.8 (0.07)	96.2±8.5 (0.27)	15.9±2.2
Sorbitol (4M)	2689.5±310.3	8.2±2.9 (0.17)	94.9±5.3 (0.14)	16.0±1.6

studies by Li *et al.* have demonstrated that osmolytes can shorten protein backbone hydrogen bonds, a phenomenon further supported by molecular dynamics simulations [47]. Such modifications in the protein interior could reshape the energy landscape, thereby affect its internal thermodynamics and ultimately influence its thermal stability. To gain a deeper understanding of how osmolytes influence protein stability through the interplay between associated water modulation and the altered protein interior, we aimed to study the modulation in the protein interior in presence of osmolytes.

Studying the interior of proteins is inherently challenging due to their structural complexity. The presence of diverse amino acid residues engaged in various interactions further complicate residue-specific investigations. Probing a specific amino acid residue or any specific interaction would be erroneous to portray the modification in the interior of the protein. In the present study, we have measured

conformational fluctuation dynamics employing fluorescence correlation spectroscopy (FCS) for probing the interior of papain in presence of osmolytes, as conformational fluctuation dynamics is not limited by any specific interactions. Notably, we have probed the active site of the protein, for which the associated water dynamics was measured.

FCS was utilized to indirectly assess the conformational fluctuations [55–57], using tetramethylrhodamine (TMR)-tagged to papain. FCS requires only a fluorescent tag within the system, making it an effective tool for tracking intensity fluctuations on timescales shorter than the molecular diffusion time but longer than the instrument's resolution limit (Figure 11a). To investigate conformational fluctuation dynamics or breathing motions in the microsecond regime, we leveraged the proximity of the tryptophan residue to the TMR-tag in papain. Given the interaction of π-cloud of tryptophan with TMR, fluorescence quenching is expected to occur in conjunction with the protein's dynamic motions [55,58,59]. The resulting cross-correlation traces were fitted to extract dynamical parameters. Since three distinct dynamic components (triplet state lifetime, conformational fluctuation and translational diffusion) were anticipated in the system, we employed a fitting model incorporating two exponential reaction terms and one diffusion component (equation 4), which yielded three-time components of ~6 μs, ~40 μs and ~120 μs for papain in buffer.

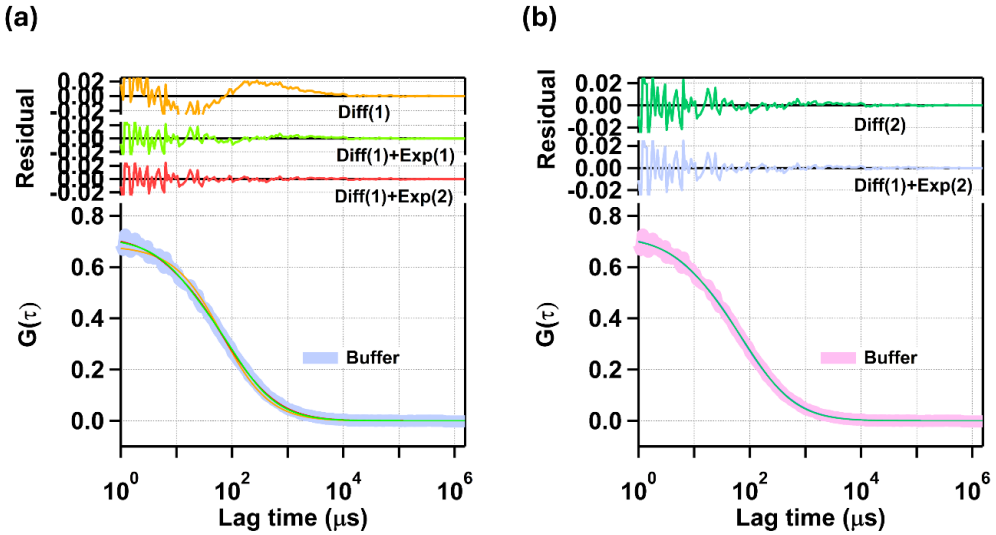

Figure 6: Fitting of FCS cross-correlation trace of TMR-papain in buffer with different fitting models. Residuals are given for each fitting model used (encircled area represents the part of the correlation traces that gets affected the most with the change in the fitting function). FCS experiments have been performed at 298 K.

$$G(\tau) = \frac{1}{N}\left(1+\frac{\tau}{\tau_D}\right)^{-1}\left(1+\frac{\tau}{\omega^2\tau_D}\right)^{-\frac{1}{2}}\left(1+K\,exp\left(-\frac{\tau}{\tau_R}\right)\right)\left(1+\frac{p}{1-p}\,exp\left(-\frac{\tau}{\tau_T}\right)\right) \qquad (1.2.4)$$

Control fitting analyses were performed using alternative models, including single-exponent with diffusion, single-diffusion, and dual-diffusion equations, to ensure robustness in data interpretation as shown in figure 6. From the residuals describing the goodness of fitting with different models in figure 6a clearly depicts that the model with single diffusion and two exponents fits the best among all the possible models. The residual for function with two diffusion components shown in figure 6b also seems promising but gives the value of one component too small ($\sim 14\mu s$) which is not even comparable to the diffusion time of the free ($\sim 50\mu s$) dye. Which rules out the possibility of having the second component arising out of the free dye present in the sample of TMR-papain. Figure 6 ensures that the model with single diffusion and two exponents is the most appropriate and matches well with the expected number of events possible with our system.

The longest time constant has been designated to the diffusion of papain in buffer and the smallest time constant is assigned to the triplet-state dynamics of TMR

tagged to papain, following previous reports [60,61]. The second time component has been assigned to papain's conformational fluctuation dynamics. To validate our assignment and to ensure these are not just experimental artifacts, we conducted the following two control experiments. First, we varied the incident photon flux. Since triplet-state dynamics are power-dependent, an increase in photon flux should increase the fraction of molecules in triplet state (p) without altering the time constant (τ_T), which has been confirmed experimentally as shown in figure 8 (raw fcs correlation traces are shown in figure 7) and the fitting values are provided in table 3.

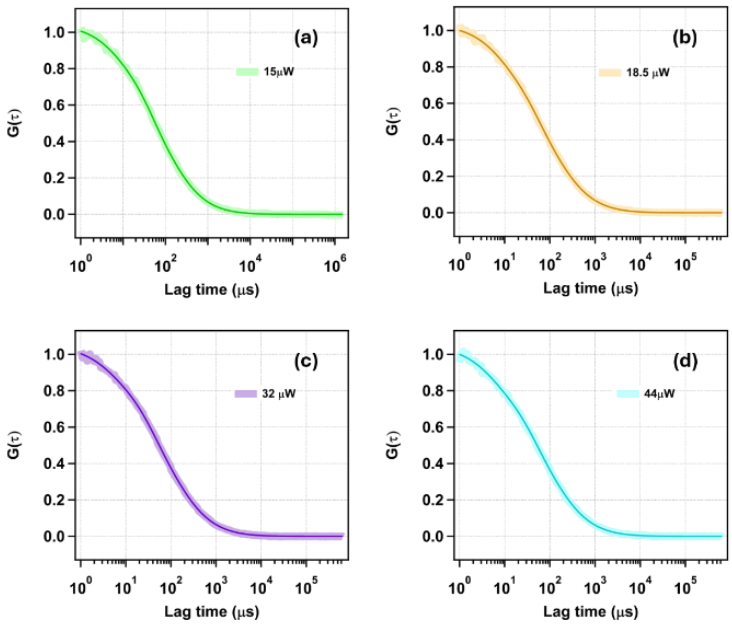

Figure 7: Normalized traces of FCS cross-correlation curves of TMR-tag papain at different power. Dark line represents the fitting line. FCS experiments have been performed at 298 K.

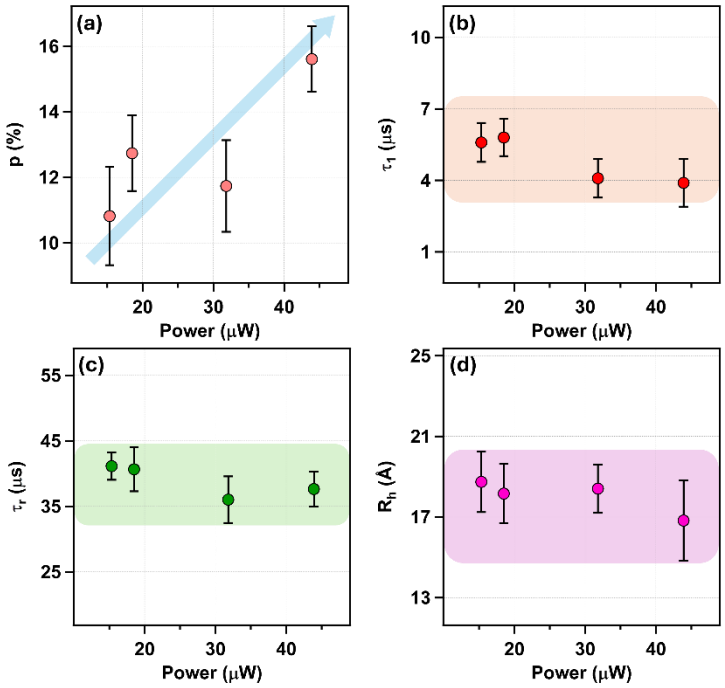

Figure 8: Variation of (a) fastest time constant (triplet state dynamics, τ_1), its (b) contribution (a_1) and (c) the second fastest time constant (conformational dynamics, τ_r) (d) size of the protein with power using optical fiber of diameter 50μm. Experiments have been performed at 298 K.

Table 3: Variation of time scales of diffusion, triplet state, conformational fluctuation dynamics and hydrodynamic radii of TMR-papain with variable laser power.

Power (μW)	$\tau_d(\mu s)$	$\tau_T(\mu s)$ (p)	$\tau_R(\mu s)$ (a_R)	R_h(Å)
44.0	112.7±13.2	3.9±1.0 (0.16)	37.7±2.7 (0.19)	16.8±1.7
32.0	120.6±9.1	4.1±0.8 (0.12)	36.1±3.6 (0.21)	18.4±1.2
18.5	119.2±7.5	5.8±0.8 (0.13)	41.8±3.3 (0.20)	18.3±1.0

15.0	113.1±10.5	5.6±0.8 (0.11)	41.1±2.1 (0.20)	18.7±1.5

Second, to confirm the second time constant corresponds to protein conformational fluctuations (τ_R), we tested its dependence on excitation power and observation volume. As expected, τ_R remains unchanged across different power levels and observation volumes as shown in figure 8c and figure 10 (raw fcs correlation traces are shown in figure 9) respectively, confirming its origin in protein internal dynamics. The corresponding fitting parameters are shown in table 4.

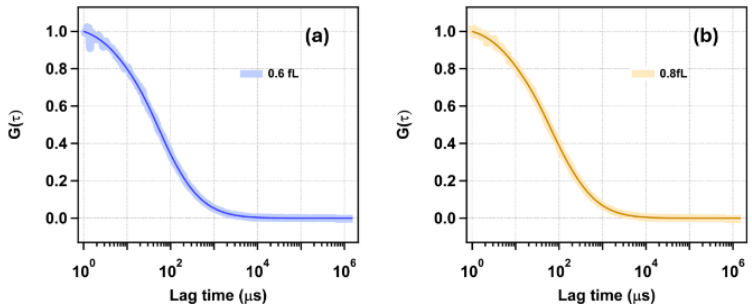

Figure 9: Normalized traces of FCS cross-correlation curves of TMR-tag papain at different observation volume. Dark line represents the fitting line. Experiments have been performed at 298 K.

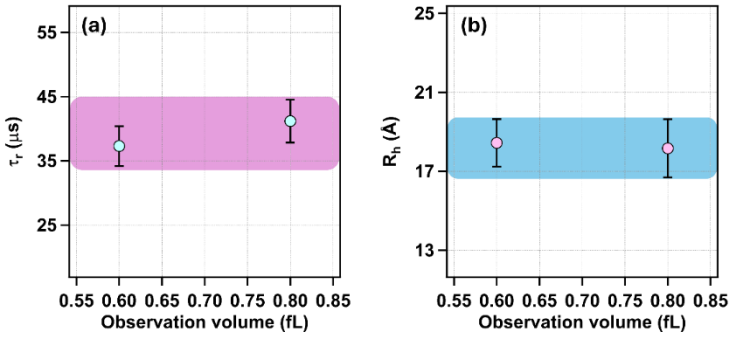

Figure 10: Variation of the (a) conformational fluctuation dynamics (τ_r) and (b) hydrodynamic radii (R_h) of TMR-tagged papain with change in the observation volume.

Table 4: Variation of time scales of diffusion, triplet state, conformational fluctuation dynamics and hydrodynamic radii of TMR-papain with variable observation volume.

Observation Volume (fL)	$\tau_d(\mu s)$	$\tau_T(\mu s)$ (p)	$\tau_R(\mu s)$ (a_R)	R_h(Å)
0.6	82.8±6.2	4.7±1.0 (0.1)	37.3±3.1 (0.16)	18.4±1.2
0.8	119.2±7.5	5.8±0.8 (0.13)	41.8±3.3 (0.20)	18.3±1.0

We determined the conformational fluctuation time of papain in presence of osmolytes under study to understand modulation in the interior of the protein, which are depicted in figure 11c. Papain in buffer displays a conformational fluctuation with time constant of ~40 μs. It gets reduced upto ~30 μs in the presence of denaturants and increased upto ~100 μs in the presence of stabilizing osmolytes under investigation. It can be concluded that the denaturants make the interior of the protein more flexible and the stabilizing osmolytes makes the protein interior rigid. As per our hypothesis, the modulation in the conformational fluctuation dynamics must be influenced by the modulation in the associated water dynamics, which is tested by plotting associated water dynamics against the conformational fluctuation dynamics of the papain in figure 2d, where we have observed a strong correlation. The osmolytes, which retards the associated water dynamics of papain are found to increase the timescale of conformational fluctuation dynamics of papain reflecting greater rigidity in the protein interior, as seen with stabilizing osmolytes. Conversely, osmolytes that increase water flexibility correspond to a decrease in the conformational fluctuation time, signifying enhanced internal flexibility, as observed with destabilizing osmolytes. We have found this correlation at the active site of papain and a similar correlation is expected if the probing site is mapped around the protein. These experimental findings align well with our proposed hypothesis. As expected, we also have observed a very strong correlation between

thermal stability and conformational fluctuation dynamics of papain as shown in figure 11e.

$$G(\tau) = \frac{1}{N}\left(1+\frac{\tau}{\tau_D}\right)^{-1}\left(1+\frac{\tau}{\omega^2\tau_D}\right)^{-1/2} \quad (1.2.5)$$

$$G(\tau) = \frac{1}{N}\left(1+\frac{\tau}{\tau_D}\right)^{-1}\left(1+\frac{\tau}{\omega^2\tau_D}\right)^{-1/2}\left(1+K\,exp\left(-\frac{\tau}{\tau_R}\right)\right) \quad (1.2.6)$$

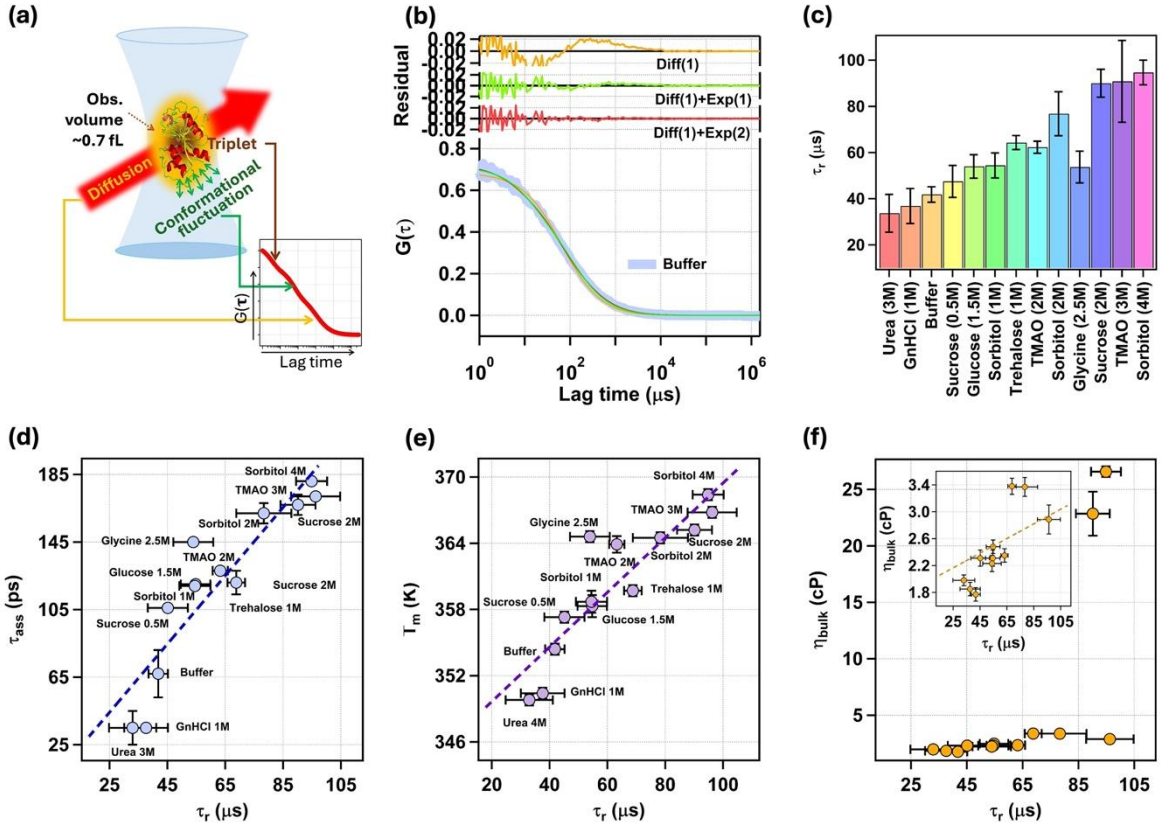

Figure 11. (a) Schematic representation of triplet state dynamics, conformational fluctuation dynamics and diffusion of TMR-tagged papain in the observation volume of a fluorescence correlation spectroscopy (FCS) setup. The standard observation volume (~0.7 fL) represented here is just a depiction. (b) Fluorescence intensity cross-correlation traces of TMR-tagged papain in buffer at 298 K along with its fitting with equations 5 (yellow), 6 (green), and 4 (red). (c) Modulation of the conformational fluctuation dynamics (τ_R) of TMR-tagged papain in buffer and other osmolyte solutions. Correlation of (d) associated water dynamics (τ_{ass}) with the conformational fluctuation dynamics (τ_R) of papain (Adj. R^2 =0.80), and (e) melting temperature (T_m) with conformational fluctuation dynamics (τ_R) of papain (Adj. R^2 =0.77). (f) Plot of the bulk viscosity of the osmolyte solution (η_{bulk}) against the conformational fluctuation dynamics of papain (τ_R) showing a very week correlation (Adj. R^2 =0.37). The correlation improves marginally (Adj. R^2 =0.60) as shown in the inset, when the two

extreme high viscosity osmolytes are excluded. All experiments except melting have been performed at 298 K.

Previous studies suggest that solution viscosity can influence protein dynamics [43,62,63]. While our data demonstrates a strong correlation between associated water dynamics and conformational fluctuation dynamics, it is essential to determine whether this relationship is intrinsic or merely an effect of bulk viscosity changes induced by osmolytes. To address this, we measured the bulk viscosity of each osmolyte solution and is provided in table 5.

Table 5: Viscosity of buffer and other aqueous osmolyte solutions.

Osmolyte	**Viscosity (cP)**
Urea (3M)	1.98±0.08
GnHCl (1M)	1.85±0.10
Buffer	1.77±0.10
Sucrose (0.5M)	2.31±0.12
Glucose (1.5M)	2.48±0.10
Sorbitol (1M)	2.31±0.12
Trehalose (1M)	3.38±0.12
TMAO (2M)	2.35±0.10
Sorbitol (2M)	3.37±0.14
Glycine (2.5M)	2.23±0.12
Sucrose (2M)	22.85±1.95
TMAO (3M)	2.89±0.22
Sorbitol (4M)	26.58±0.47

A plot of bulk viscosity against conformational fluctuation dynamics (Figure 11f) shows no significant correlation. Even after excluding the extreme viscosity values for 2M sucrose and 4M sorbitol, the revised correlation (inset of figure 11f) remains weak compared to the strong relationship observed between associated water dynamics and protein conformational fluctuations dynamics. These findings further support our hypothesis that conformational fluctuation dynamics of papain is modulated dominantly by the modulation in the associated water dynamics by the added osmolyte, and their interplay decides the thermal stability of papain.

4.3. Conclusion

This study reveals that the presence of osmolytes significantly alters the internal dynamics of proteins, as demonstrated by the modulated conformational fluctuation dynamics of papain in presence of osmolytes. Stabilizing osmolytes enhance the rigidity of the protein structure, while destabilizing osmolytes induce flexibility, as evidenced by the corresponding changes in the conformational fluctuation dynamics of papain. Furthermore, conformational fluctuation of papain is observed to get retarded in the presence of stabilizing osmolytes, where associated water dynamics also gets retarded. An opposite effect is observed with destabilizing osmolytes. A striking correlation is also identified between the thermal stability of papain and the conformational fluctuation dynamics in presence of osmolyte, suggesting a direct connection between water structure and protein dynamics in defining the thermal stability of papain in osmolyte solution. These findings indicate that osmolyte-induced modifications in associated water dynamics influence the protein's internal structure, which possibly affects its thermodynamic properties and thus the thermal stability (Scheme 3). Although a precise quantification of these effects remains a challenge, the study provides a conceptual understanding of how osmolytes modulate protein stability through changes in internal structural flexibility and associated water dynamics, offering directions for future research in the field.

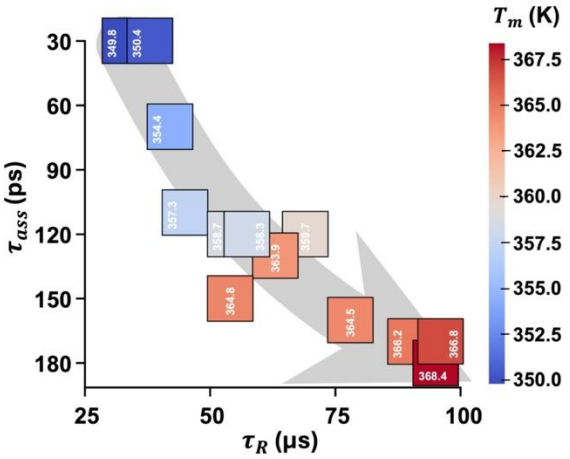

Scheme 3. Intricate relation between associated water dynamics (τ_{ass}) and conformational fluctuation dynamics (τ_R) in influencing the thermal stability (T_m) of papain in the presence of osmolytes. The melting point of papain in the presence of each osmolytes is written in each marker (square box).

4.4 References

(1) Steeves, C. L.; Hammer, M.-A.; Walker, G. B.; Rae, D.; Stewart, N. A.; Baltz, J. M. The Glycine Neurotransmitter Transporter GLYT1 Is an Organic Osmolyte Transporter Regulating Cell Volume in Cleavage-Stage Embryos. *J. Cell. Physiol* **2005**, *204* (1), 273–279.

(2) Boob, M. M.; Sukenik, S.; Gruebele, M.; Pogorelov, T. V. TMAO: Protecting Proteins from Feeling the Heat. *Biophys J* **2023**, *122* (7), 1414–1422. https://doi.org/10.1016/j.bpj.2023.03.008.

(3) Tadeo, X.; López-Méndez, B.; Castaño, D.; Trigueros, T.; Millet, O. Protein Stabilization and the Hofmeister Effect: The Role of Hydrophobic Solvation. *Biophys J* **2009**, *97* (9), 2595–2603. https://doi.org/10.1016/j.bpj.2009.08.029.

(4) Yancey, P. H. Organic Osmolytes as Compatible, Metabolic and Counteracting Cytoprotectants in High Osmolarity and Other Stresses. *J. Exp. Biol.* August 2005, pp 2819–2830. https://doi.org/10.1242/jeb.01730.

(5) Canchi, D. R.; Garciá, A. E. Backbone and Side-Chain Contributions in Protein Denaturation by Urea. *Biophys J* **2011**, *100* (6), 1526–1533. https://doi.org/10.1016/j.bpj.2011.01.028.

(6) Wlodarczyk, S. R.; Custódio, D.; Pessoa, A.; Monteiro, G. Influence and Effect of Osmolytes in Biopharmaceutical Formulations. *Eur. J. Pharm. Biopharm.* **2018**, *131* (June), 92–98. https://doi.org/10.1016/j.ejpb.2018.07.019.

(7) Wang, W.; Ohtake, S. Science and Art of Protein Formulation Development. *Int. J. Pharm.* **2019**, *568* (July), 118505. https://doi.org/10.1016/j.ijpharm.2019.118505.

(8) Pepelnjak, M.; Velten, B.; Näpflin, N.; von Rosen, T.; Palmiero, U. C.; Ko, J. H.; Maynard, H. D.; Arosio, P.; Weber-Ban, E.; de Souza, N.; Huber, W.; Picotti, P. In Situ Analysis of Osmolyte Mechanisms of Proteome Thermal Stabilization. *Nat. Chem. Biol.* **2024**, *20* (8), 1053–1065. https://doi.org/10.1038/s41589-024-01568-7.

(9) Miotto, M.; Warner, N.; Ruocco, G.; Tartaglia, G. G.; Scherman, O. A.; Milanetti, E. Osmolyte-Induced Protein Stability Changes Explained by Graph Theory. *Comput. Struct. Biotechnol. J.* **2024**, *23* (October), 4077–4087. https://doi.org/10.1016/j.csbj.2024.10.014.

(10) Lin, T.; Timasheff, S. N. Why Do Some Organisms Use a Urea-Methylamine Mixture as Osmolyte? Thermodynamic Compensation of Urea and Trimethylamine N-Oxide Interactions with Protein. *Biochemistry* **1994**, *33* (42), 12695–12701.

(11) Canchi, D. R.; García, A. E. Cosolvent Effects on Protein Stability. *Annu. Rev. Phys. Chem* **2013**, *64*, 273–293. https://doi.org/10.1146/annurev-physchem-040412-110156.

(12) Kamerzell, T. J.; Esfandiary, R.; Joshi, S. B.; Middaugh, C. R.; Volkin, D. B. Protein-Excipient Interactions: Mechanisms and Biophysical Characterization Applied to Protein Formulation Development. *Adv. Drug Deliv. Rev.* **2011**, *63* (13), 1118–1159. https://doi.org/10.1016/j.addr.2011.07.006.

(13) Schüle, S.; Schulz-Fademrecht, T.; Garidel, P.; Bechtold-Peters, K.; Frieß, W. Stabilization of IgG1 in Spray-Dried Powders for Inhalation. *Eur. J. Pharm. Biopharm.* **2008**, *69* (3), 793–807. https://doi.org/10.1016/j.ejpb.2008.02.010.

(14) Arakawa, T.; Timasheff, S. N. The Stabilization of Proteins by Osmolytes. *Biophys. J* **1985**, *47* (3), 411–414. https://doi.org/10.1016/S0006-3495(85)83932-1.

(15) Timasheff, S. N. Water as Ligand: Preferential Binding and Exclusion of Denaturants in Protein Unfolding. *Biochemistry* **1992**, *31* (41), 9857–9864.

(16) Lee, J. C.; Timasheff, S. N. The Stabilization of Proteins by Sucrose. *J. Biol. Chem.* **1981**, *256* (14), 7193–7201. https://doi.org/10.1016/s0021-9258(19)68947-7.

(17) Bolen, D. W. The Peptide Backbone Plays a Dominant Role in Protein Stabilization by Naturally Occurring Osmolytes. *Biochemistry* **1995**, *34* (39), 12884–12891.

(18) Street, T. O.; Wayne Bolen, D.; Rose, G. D.; Jenkins, T. C. A Molecular Mechanism for Osmolyte-Induced Protein Stability. *Proc. Natl. Acad. Sci. U. S. A.* **2006**, *103*, 13997–14002.

(19) Funkner, S.; Havenith, M.; Schwaab, G. Urea, a Structure Breaker? Answers from THz Absorption Spectroscopy. *J. Phys. Chem. B* **2012**, *116* (45), 13374–13380. https://doi.org/10.1021/jp308699w.

(20) Rezus, Y. L. A.; Bakker, H. J. Effect of Urea on the Structural Dynamics of Water. *Proc. Natl. Acad. Sci. U. S. A.* **2006**, *103* (49), 18417–18420.

(21) Rezus, Y. L. A.; Bakker, H. J. Destabilization of the Hydrogen-Bond Structure of Water by the Osmolyte Trimethylamine N-Oxide. *J. Phys. Chem. B* **2009**, *113* (13), 4038–4044. https://doi.org/10.1021/jp805458p.

(22) Nasralla, M.; Laurent, H.; Baker, D. L.; Ries, M. E.; Dougan, L. A Study of the Interaction between TMAO and Urea in Water Using NMR Spectroscopy. *Phys. Chem. Chem. Phys* **2022**, *24* (35), 21216–21222. https://doi.org/10.1039/d2cp02475f.

(23) Wirtz, H.; Schäfer, S.; Hoberg, C.; Havenith, M. Differences in Hydration Structure Around Hydrophobic and Hydrophilic Model Peptides Probed by THz Spectroscopy. *J. Infrared Millim. Terahertz Waves* **2018**, *39* (9), 816–827. https://doi.org/10.1007/s10762-018-0478-2.

(24) Heugen, U.; Schwaab, G.; Brü, E.; Heyden, M.; Yu, X.; Leitner, D. M.; Havenith, M. Solute-Induced Retardation of Water Dynamics Probed Directly by Terahertz Spectroscopy. *Proc. Natl. Acad. Sci. U. S. A.* **2006**, *103* (33), 12301–12306.

(25) Hishida, M.; Anjum, R.; Anada, T.; Murakami, D.; Tanaka, M. Effect of Osmolytes on Water Mobility Correlates with Their Stabilizing Effect on Proteins. *J. Phys. Chem. B* **2022**, *126* (13), 2466–2475. https://doi.org/10.1021/acs.jpcb.1c10634.

(26) Stasiulewicz, M.; Panuszko, A.; Bruździak, P.; Stangret, J. Mechanism of Osmolyte Stabilization-Destabilization of Proteins: Experimental Evidence. *J. Phys. Chem. B* **2022**, *126* (16), 2990–2999. https://doi.org/10.1021/acs.jpcb.2c00281.

(27) Soper, A. K.; Castner, E. W.; Luzar, A. Impact of Urea on Water Structure: A Clue to Its Properties as a Denaturant? *Biophys. Chem.* **2003**, *105*, 649–666. https://doi.org/10.1016/S0301-4622Ž03.00095-4.

(28) Negi, K. S.; Das, N.; Khan, T.; Sen, P. Osmolyte Induced Protein Stabilization: Modulation of Associated Water Dynamics Might Be a Key Factor. *Phys. Chem. Chem. Phys* **2023**, *25* (47), 32602–32612. https://doi.org/10.1039/d3cp03357k.

(29) Kumar, S.; Peon, J.; Zewail, A. H. Biological Water at the Protein Surface: Dynamical Solvation Probed Directly with Femtosecond Resolution. *Proc. Natl. Acad. Sci. U. S. A.* **2002**, *99* (4), 1763–1768.

(30) Mukherjee, S.; Mondal, S.; Bagchi, B. Distinguishing Dynamical Features of Water inside Protein Hydration Layer: Distribution Reveals What Is Hidden behind the Average. *J. Chem. Phys* **2017**, *147* (2), 024901. https://doi.org/10.1063/1.4990693.

(31) Bhattacharyya, K. Nature of Biological Water: A Femtosecond Study. *Chem Commun.* Royal Society of Chemistry 2008, pp 2848–2857. https://doi.org/10.1039/b800278a.

(32) Mondal, S.; Mukherjee, S.; Bagchi, B. On the Origin of Diverse Time Scales in the Protein Hydration Layer Solvation Dynamics: A Molecular Dynamics Simulation Study. *J. Chem. Phys* **2017**, *147*, 154901.

(33) Hirai, M.; Ajito, S.; Sugiyama, M.; Iwase, H.; Takata, S. ichi; Shimizu, N.; Igarashi, N.; Martel, A.; Porcar, L. Direct Evidence for the Effect of Glycerol on Protein Hydration and Thermal Structural Transition. *Biophys J* **2018**, *115* (2), 313–327. https://doi.org/10.1016/j.bpj.2018.06.005.

(34) Khan, T.; Das, N.; Bhowmik, S.; Negi, K. S.; Sen, P. Critical Role of Water beyond the Media to Maintain Protein Stability and Activity in Hydrated

Deep Eutectic Solvent. *J. Phys. Chem. B* **2025**, *129* (1), 162–175. https://doi.org/10.1021/acs.jpcb.4c07039.

(35) Khan, T.; Halder, B.; Das, N.; Sen, P. Role of Associated Water Dynamics on Protein Stability and Activity in Crowded Milieu. *J. Phys. Chem. B* **2024**, *128* (36), 8672–8686. https://doi.org/10.1021/acs.jpcb.4c04337.

(36) Zhong, D.; Pal, S. K.; Zewail, A. H. Biological Water: A Critique. *Chem. Phys. Lett.* **2011**, *503* (1–3), 1–11. https://doi.org/10.1016/j.cplett.2010.12.077.

(37) Ball, P. Water as an Active Constituent in Cell Biology. *Chem. Rev.* January 2008, pp 74–108. https://doi.org/10.1021/cr068037a.

(38) Levy, Y.; Onuchic, J. N. Water Mediation in Protein Folding and Molecular Recognition. *Annu. Rev. Biophys.* **2006**, *35* (1), 389–415. https://doi.org/10.1146/ANNUREV.BIOPHYS.35.040405.102134.

(39) Hummer, G.; Tokmakoff, A. Preface: Special Topic on Biological Water. *J. Chem. Phys* **2014**, *141* (22), 22D101. https://doi.org/10.1063/1.4901337.

(40) Frauenfelder, H.; Fenimore, P. W.; McMahon, B. H. Hydration, Slaving and Protein Function. *Biophys. Chem.* **2002**, *98* (1–2), 35–48. https://doi.org/10.1016/S0301-4622(02)00083-2.

(41) Jha, A.; Ishii, K.; Udgaonkar, J. B.; Tahara, T.; Krishnamoorthy, G. Exploration of the Correlation between Solvation Dynamics and Internal Dynamics of a Protein. *Biochemistry* **2011**, *50* (3), 397–408. https://doi.org/10.1021/bi101440c.

(42) Fenimore, P. W.; Frauenfelder, H.; McMahon, B. H.; Young, R. D. Bulk-Solvent and Hydration-Shell Fluctuations, Similar to α- and β-Fluctuations in Glasses, Control Protein Motions and Functions. *Proc. Natl. Acad. Sci. U.*

S. A. **2004**, *101* (40), 14408–14413. https://doi.org/10.1073/pnas.0405573101.

(43) Frauenfelder, H.; Chen, G.; Berendzen, J.; Fenimore, P. W.; Jansson, H.; McMahon, B. H.; Stroe, I. R.; Swenson, J.; Young, R. D. A Unified Model of Protein Dynamics. *Proc. Natl. Acad. Sci. U. S. A.* **2009**, *106* (13), 5129–5134. https://doi.org/10.1073/pnas.0900336106.

(44) McMahon, B. H.; Frauenfelder, H.; Fenimore, P. W. The Role of Continuous and Discrete Water Structures in Protein Function. *Eur. Phys. J. Spec. Top* **2014**, *223* (5), 915–926. https://doi.org/10.1140/epjst/e2014-02125-y.

(45) Abriata, L. A.; Spiga, E.; Peraro, M. D. Molecular Effects of Concentrated Solutes on Protein Hydration, Dynamics, and Electrostatics. *Biophys J* **2016**, *111* (4), 743–755. https://doi.org/10.1016/j.bpj.2016.07.011.

(46) Vagenende, V.; Trout, B. L. Quantitative Characterization of Local Protein Solvation to Predict Solvent Effects on Protein Structure. *Biophys J* **2012**, *103* (6), 1354–1362. https://doi.org/10.1016/j.bpj.2012.08.011.

(47) Li, J.; Chen, J.; An, L.; Yuan, X.; Yao, L. Polyol and Sugar Osmolytes Can Shorten Protein Hydrogen Bonds to Modulate Function. *Commun Biol* **2020**, *3* (1), 1–8. https://doi.org/10.1038/s42003-020-01260-1.

(48) Masson, P.; Lushchekina, S. Conformational Stability and Denaturation Processes of Proteins Investigated by Electrophoresis under Extreme Conditions. *Molecules* **2022**, *27* (20), 6861. https://doi.org/10.3390/molecules27206861.

(49) Sanfelice, D.; Temussi, P. A. Cold Denaturation as a Tool to Measure Protein Stability. *Biophys. Chem.* **2016**, *208*, 4–8. https://doi.org/10.1016/j.bpc.2015.05.007.

(50) Miotto, M.; Olimpieri, P. P.; Di Rienzo, L.; Ambrosetti, F.; Corsi, P.; Lepore, R.; Tartaglia, G. G.; Milanetti, E. Insights on Protein Thermal Stability: A Graph Representation of Molecular Interactions. *Bioinform* **2019**, *35* (15), 2569–2577. https://doi.org/10.1093/bioinformatics/bty1011.

(51) Das, N.; Tarif, E.; Dutta, A.; Sen, P. Associated Water Dynamics Might Be a Key Factor Affecting Protein Stability in the Crowded Milieu. *J. Phys. Chem. B* **2023**, *127* (14), 3151–3163. https://doi.org/10.1021/acs.jpcb.2c09043.

(52) Habib, S.; Khan, M. A.; Younus, H. Thermal Destabilization of Stem Bromelain by Trehalose. *Protein J* **2007**, *26* (2), 117–124. https://doi.org/10.1007/s10930-006-9052-1.

(53) Houston, P.; Macro, N.; Kang, M.; Chen, L.; Yang, J.; Wang, L.; Wu, Z.; Zhong, D. Ultrafast Dynamics of Water-Protein Coupled Motions around the Surface of Eye Crystallin. *J. Am. Chem. Soc.* **2020**, *142* (8), 3997–4007. https://doi.org/10.1021/jacs.9b13506.

(54) Zhang Luyuan; Wang Lijuan; Kao Ya-Ting; Qiu Weihong; Yang Yi; Okobiah Oghaghare; Zhong Dongping. Mapping Hydration Dynamics around a Protein Surface. *Proc. Natl. Acad. Sci. U. S. A.* **2007**, *104* (47), 18461–18466.

(55) Chattopadhyay, K.; Saffarian, S.; Elson, E. L.; Frieden, C. Measurement of Microsecond Dynamic Motion in the Intestinal Fatty Acid Binding Protein by Using Fluorescence Correlation Spectroscopy. *Proc. Natl. Acad. Sci. U. S. A.* **2002**, *99* (22), 14171–14176. https://doi.org/10.1073/pnas.172524899.

(56) Chattopadhyay, K.; Saffarian, S.; Elson, E. L.; Frieden, C. Measuring Unfolding of Proteins in the Presence of Denaturant Using Fluorescence Correlation Spectroscopy. *Biophys J* **2005**, *88* (2), 1413–1422. https://doi.org/10.1529/biophysj.104.053199.

(57) Sherman, E.; Itkin, A.; Kuttner, Y. Y.; Rhoades, E.; Amir, D.; Haas, E.; Haran, G. Using Fluorescence Correlation Spectroscopy to Study Conformational Changes in Denatured Proteins. *Biophys J* **2008**, *94* (12), 4819–4827. https://doi.org/10.1529/biophysj.107.120220.

(58) Sasmal, D. K.; Mondal, T.; Sen Mojumdar, S.; Choudhury, A.; Banerjee, R.; Bhattacharyya, K. An FCS Study of Unfolding and Refolding of CPM-Labeled Human Serum Albumin: Role of Ionic Liquid. *J. Phys. Chem. B* **2011**, *115* (44), 13075–13083. https://doi.org/10.1021/jp207829y.

(59) Nandy, A.; Chakraborty, S.; Nandi, S.; Bhattacharyya, K.; Mukherjee, S. Structure, Activity, and Dynamics of Human Serum Albumin in a Crowded Pluronic F127 Hydrogel. *J. Phys. Chem. B* **2019**, *123* (16), 3397–3408. https://doi.org/10.1021/acs.jpcb.9b00219.

(60) Krichevsky, O.; Bonnet, G. Fluorescence Correlation Spectroscopy: The Technique and Its Applications. *Rep. Prog. Phys.* **2002**, *65* (2), 251–297. https://doi.org/10.1088/0034-4885/65/2/203.

(61) Basak, S.; Chattopadhyay, K. Studies of Protein Folding and Dynamics Using Single Molecule Fluorescence Spectroscopy. *Phys. Chem. Chem. Phys.* **2014**, *16* (23), 11139–11149. https://doi.org/10.1039/c3cp55219e.

(62) Ansari, A.; Jones, C. M.; Henry, E. R.; Hofrichter, J.; Eaton, W. A. The Role of Solvent Viscosity in the Dynamics of Protein Conformational Changes. *Science (1979)* **1992**, *256* (5065), 1796–1798. https://doi.org/10.1126/science.1615323.

(63) Finkelstein, I. J.; Massari, A. M.; Fayer, M. D. Viscosity-Dependent Protein Dynamics. *Biophys J* **2007**, *92* (10), 3652–3662. https://doi.org/10.1529/biophysj.106.093708.

This page left blank intentionally

Chapter 5

Mechanistic insights deciphering the distinct response of proteins towards osmolyte: An associated water stabilization mechanism (AWSM) perspective

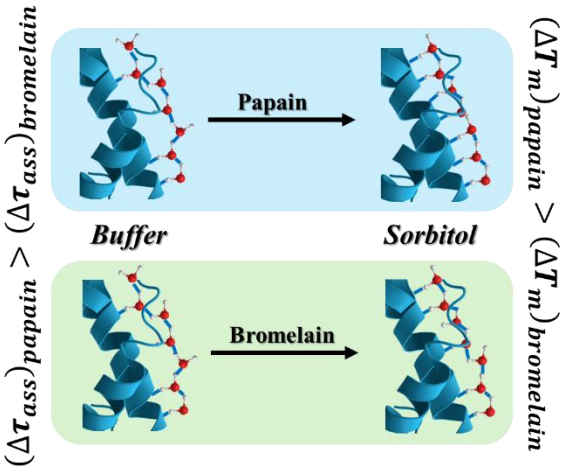

Kuldeep Singh Negi, Harshit Karnwal, Tanmoy Khan and Pratik Sen

Manuscript under preparation

Abstract

The unresolved puzzle of protein-osmolyte interaction is proved to have the significant role of water. The traditional theories revolve around water but fail to explain the protein-osmolyte interaction, especially where the effect varies with the protein. The properties of a protein against a particular osmolyte vary depending on the protein itself. One such property is its thermal stabilization in osmolyte solution where the extent of stabilization varies with protein. We have employed bromelain and papain as model proteins and sorbitol as model osmolyte. Melting, solvation dynamics and conformational dynamics studies have been performed to gather information on the modulation in the thermal stability, hydration layer and the interior of protein (bromelain and papain) respectively in the presence of osmolyte (sorbitol). Associated Water Stabilization Mechanism (AWSM) explains the protein-osmolyte interactions better, where the thermal stabilization of protein in osmolyte is shown to be an outcome of the strengthened interior (retarded conformational dynamics) of the protein caused by the osmolyte strengthened water-residue and water-water bonding (retarded associated water dynamics) at the protein surface. Both the proteins follow the mechanism individually whereas the better thermal stabilization of papain over bromelain needs a different approach within the same framework as AWSM which could be understood by considering the changes in the absolute values relative to their buffer counterpart rather than the comparison of absolute values in the presence of sorbitol in case of each protein. The higher extent of retardation in associated water dynamics of papain makes the extent of retardation in conformational dynamics higher implying greater strengthening of the interior of the protein and thus the papain gets better thermal stabilization than bromelain.

5.1 Introduction

Proteins are the crucial universal working machinery in living systems which function as sensors, transporters and so on. The three-dimensional (3D) structure of the protein plays an important role in defining the functionality of the protein. Under the influence of modified environmental conditions like variations in pH, salt concentration, temperature etc., these may undergo drastic changes in the structure that might even modify the function of the protein and in most cases lower down the functional efficacy [1,2]. Small organic solutes like sugars, polyols, amino acids and their derivatives are known to stabilize these macromolecules against the perturbing stress [3]. This aspect of preservation of biomacromolecules by osmolytes has been harnessed in biotechnology and pharmaceutical industries during storage and transport [4]. Therefore, a comprehensive understanding of protein-osmolyte interactions is vital, given their biological relevance and industrial utility. Although several theories have been proposed to explain the protein-osmolyte interactions, the mechanism of the protein osmolyte interaction is still not fully understood and needs to be revisited in more detail because of its importance [5,6]. To understand such interactions theory was forwarded by Timasheff and coworkers initially [6]. It was sugar proposed that protein will be get stabilized if the concentration of the solute is less on its surface compared to bulk and vice-versa based on purely surface tension phenomenon [5–10]. Bolen and coworkers supported this observation by giving a logical explanation backed by experimental findings, where it has been observed that the stabilizing osmolyte have repulsive interactions with the protein surface and vice-versa [11,12]. This theory is known by preferential interaction/direct interaction theory and since the direct measurement of surface tension at the protein–solvent interface remains technically challenging, limiting its broader application [13]. Apart from this, a new theory was introduced where it was believed that water even after being present in enormous amount can’t stay just as a spectator. People have observed the increased stability of protein in an osmolyte solution where either the water structure gets enhanced, or the hydrogen bond among the water molecules gets

strengthened [13]. This theory is commonly known by water structure modulation hypothesis or Indirect mechanism. Hishida et. al. observed an insightful correlation where the stability of the protein goes parallel with the enhanced water structure around the osmolyte molecules and vice versa [14–16]. This hypothesis explains the effect of osmolyte on the thermal stability of protein quite well but fails to explain protein specific effects in general [17]. These water structure-modulation based hypothesis are osmolyte centric and are thus not capable enough to explain the effects that are based on proteins [18]. One such effect is the different extent of stabilization of different proteins in a specific concentration of any osmolyte. According to water structure-related theories, protein stabilization depends on water modulation by the osmolyte, which is determined by its type and concentration. Since both are the same here, the extent of stabilization should be identical, regardless of the protein used. To explain such effects water structure theory should be modelled in a way where some weightage must be given to the protein. One such theory is the "Associated Water Stabilization Mechanism" (AWSM) [19–24]. This theory stands as a bridge between the two traditional theories described above. The water structure at the protein surface (associated water) is probed here directly unlike the measurement of the surface tension by mimicking the most appropriate model [10] for protein-water interface as is done in preferential interaction mechanism. We have shown this explicitly in our recent publication where the thermal stabilization of protein is caused by the strengthening of the interior of the protein which is brought up by the osmolyte induced strengthening of the water structure near the protein surface [24]. We here, tested the flexibility of the hypothesis to explain the thermal stabilization effects on different proteins individually in the presence of osmolyte [21,24]. Further we have tested the hypothesis to understand the distinct stabilization of proteins in the presence of same osmolyte by employing a new approach while keeping the framework of the theory same. Here, to test the hypothesis we have taken two different proteins bromelain and papain with sorbitol as the model osmolyte. The findings of this study might foster the research and understanding in the field of

protein science which might be useful in exploring the uncovered avenues related to the biomacromolecules as well.

5.2 Results and Discussion

5.2.1. Thermal stability of bromelain and papain in the presence of Sorbitol:

Proteins are dynamic entities. These are very sensitive to their immediate environment. Any kind of disturbance (temperature, pressure, pH, salinity etc.) in their surroundings can modulate the characteristics of the protein. Generally, under any perturbation the protein changes its conformation and the equilibrium between the folded (native) and unfolded (denatured) population shifts and known as denaturation [25,26]. Under the application of heat the protein unfolds, and the equilibrium shifts to the right favoring more protein molecules to unfold. Here, thermal study of proteins is carried out by employing fluorescence spectroscopy. Solvatochromic nature of inherently fluorescent amino acid residues (tryptophan) of the proteins is used here [27,28]. The interior of the protein is hydrophobic, and the surroundings are hydrophilic due to the presence of highly polar water media [29]. On the application of heat the protein unfolds and the buried tryptophan residues came out in the contact of the more polar water molecules [28]. Thus, owing to the positive solvatochromic nature of the tryptophan the emission spectrum of the protein shifts toward the higher wavelength as shown in figure 1(a). On increasing the temperature, the emission spectrum of the protein (excited at 295 nm) shifts and is illustrated in figure 1(b). Emission maximum is used as a representative of the individual emission spectrum and is plotted against the corresponding temperature as shown in figure 1(c) to produce a melting curve. The thermal stability of the protein is quantified by the parameter, melting temperature (T_m) and is defined as the temperature at which the population (where the fraction of the denatured state is 0.5) of the folded and unfolded proteins becomes equal. T_m is evaluated by normalizing the melting curve by employing equation 5.2.1 followed by fitting by

employing the sigmoidal function given by equation 5.2.2 as shown in figure 1(d) [21].

$$f_D = \frac{\lambda_i - \lambda_N}{\lambda_D - \lambda_N} \quad (5.2.1)$$

where λ_i, represents the emission maximum corresponding to any temperature i, λ_N represents the emission maximum representative of the native state and λ_D represents the emission maximum representative of the denatured state of the protein under thermal study. The denaturation of protein is considered as a cooperative phenomenon and thus the denaturation pathway is expected to follow the sigmoidal nature. Keeping this in mind, here the denaturation plot is fitted with a sigmoidal function given by equation 5.2.2,

$$y = a + b/(1 + \exp\,(x\_half - x))/d)) \quad (5.2.2)$$

Where "a" represents the value of lower asymptote which is taken as 0 and signifies native state ($i.e.,\ f_N = 0$), "b" represents the distance from 'a' to the upper asymptote which is taken as 1 and signifies the denatured state ($i.e.,\ f_D = 1$), "x_half" represents the inflection point and signifies the melting temperature (T_m) and "d" represents the distance from x_half of the zone of compliance.

Higher T_m value signifies the higher thermal stability of the protein and vice versa. With the increase in sorbitol concentration the melting curve of bromelain shifts towards the higher temperature values signifying enhanced thermal stability as depicted by the melting curve for buffer (violet) in the leftmost in the lowest temperature regime, followed by 1M (pink) and 2M (green) sorbitol with region of inflexion of the melting curve further shifts to higher temperature regime and the shift increases with increase in concentration of sorbitol as shown in figure 1(e) for bromelain. The same results have also been observed for papain in the presence of sorbitol as shown in figure 1(f). In case of papain the shift in inflexion region with increase in the sorbitol concentration relative to buffer is more compared to bromelain signifying higher thermal stabilization of papain over bromelain with

increase in sorbitol content. T_m value for bromelain in buffer only system is ~ 336 K which compliments the literature [17,21]. As observed qualitatively by examining the melting curves, on the addition of sorbitol bromelain gets thermal stabilization and quantitatively, the T_m value increases to ~ 338 K and ~ 340 K with continuous increase in concentration from 1M to 2M respectively as shown in figure 1(g). A similar increment in T_m has also been witnessed in the case of papain where the T_m in buffer is experimentally observed as ~ 354 K and matches well with the literature [21], which enhances to ~ 359 K and ~ 364 K with 1M and 2M sorbitol concentration as shown in figure 1(h). The melting temperature values for bromelain and papain in buffer and sorbitol are organized in table 1. The observed extent of thermal stabilization (ΔT_m) for bromelain and papain is ~ 2 K, ~ 4 K with 1M sorbitol respectively and ~ 4 K, ~ 10 K with 2M sorbitol respectively as shown in figure 1(i), where the extent of thermal stabilization is defined as,

$$\Delta T_m(Osmolyte) = T_m(Osmolyte) - T_m(Buffer) \quad (5.2.3)$$

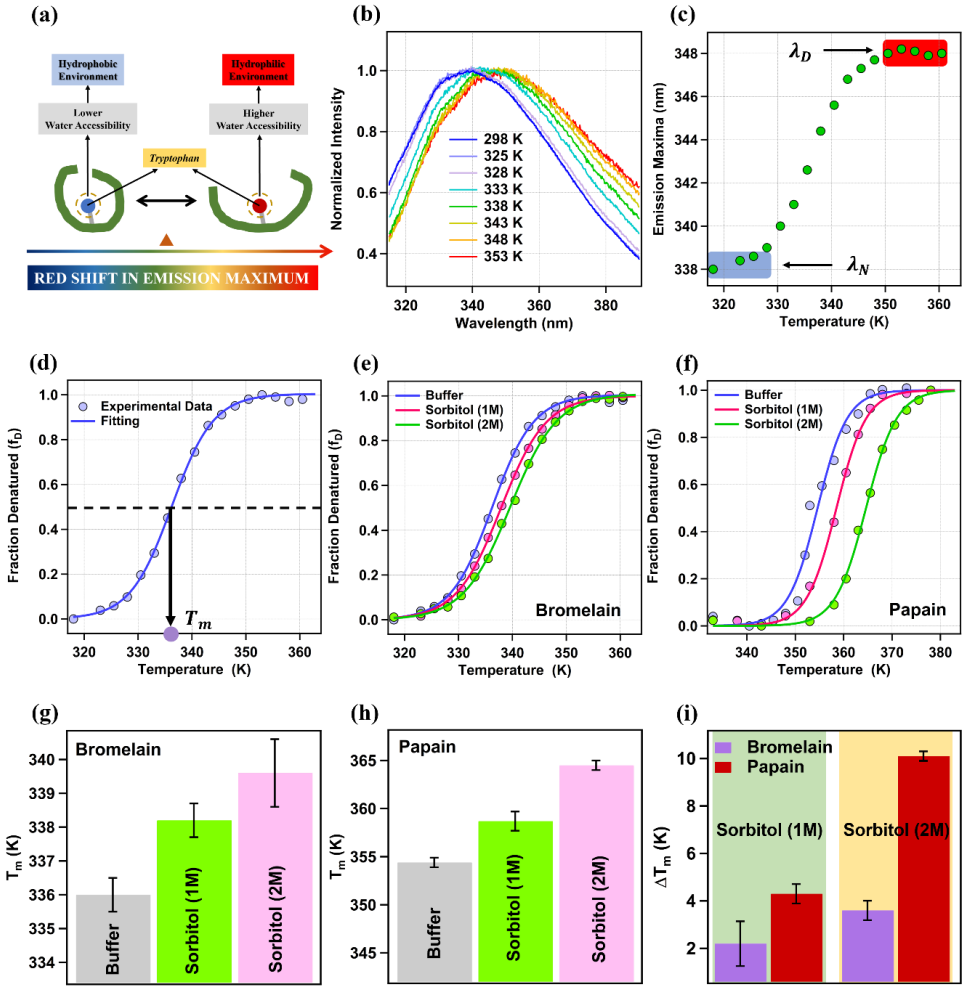

Figure 1: (a) Schematic representation of modulation of emission wavelength representative of specific distribution of population between native and denatured conformations during protein unfolding in thermal stability study. Modulation in the (b) normalized emission spectra and (c) emission maxima corresponding to the emission spectra of bromelain (excited at 295nm) in buffer with temperature where, $\lambda_N = 338\,nm$ and $\lambda_D = 348\,nm$ are the signature wavelength for the native and the denatured state of bromelain in buffer respectively. (d) Normalized plot representing the fraction of denatured bromelain at corresponding temperature fitted with a sigmoidal function represented by equation 5.2.2 to determine the melting temperature (T_m). Fraction of denatured (f_D) (e) bromelain and (f) papain at corresponding temperature in the presence of buffer (violet), 1M (pink) and 2M (green) concentration of sorbitol along with the fitting line. Variation of the melting temperature (T_m) of (g) bromelain and (h) papain in the presence of buffer (grey), 1M (green) and 2M (pink) of sorbitol. (i) Increament in the melting temperature (ΔT_m) of bromelain (violet) and papain (red) in 1M (green) and 2M (yellow) concentration of sorbitol.

Table 1: Variation of the melting temperature (T_m) of bromelain and papain in buffer and sorbitol solution

[Sorbitol] (M)	Bromelain		Papain	
	$T_m(K)$	$\Delta T_m(K)$	$T_m(K)$	$\Delta T_m(K)$
0	336.0±0.5	-	354.4±0.5	-
1	338.2±1.0	2.2±0.4	358.7±0.5	4.3±0.9
2	339.6±0.5	3.6±0.2	364.5±1.0	10.1±0.4

5.2.2 Bulk water dynamics in controlling protein stability:

The observed extent of thermal stabilization is distinct for the two proteins employed here in the presence of sorbitol and is a general observation for most of the osmolytes/additives. Here in the case of bromelain and papain with sorbitol the extent of thermal stabilization is less for bromelain relative to papain in each of the concentration of sorbitol used. Both the known theories (preferential interaction mechanism and water structure modulation theory) to explain protein-osmolyte interaction directly or indirectly revolves around the impact of water arrangement or interaction around protein molecules. Previously, we have reported the bulk solvation dynamics of the buffer and the osmolyte solutions in the absence of proteins by employing transient Absorption (TA) spectroscopy [19,20,24]. It provides information indirectly on the arrangement or the strength of the bonding between the water molecules in the bulk solution in the absence and presence of co-solute by harnessing the solvatochromic property of coumarin (C343).

Average bulk solvation dynamics (τ_{bulk}) in buffer only system has been reported around ~ 0.8 ps and it increased monotonically with the addition of sorbitol [20,24]. τ_{bulk} gets enhanced to a value of ~1.1 and ~1.6 with 1M and 2M sorbitol as shown in figure 2 (a). The data for bulk solvation is taken directly from our previous report and given in Table 2 for ready reference [24]. With the retardation in average bulk

solvation dynamics (increase in the value of τ_{bulk}), both the proteins (papain and bromelain are represented with red and violet color respectively) get thermal stabilization as evident from the straight line fit of the correlation plot between T_m and τ_{bulk} in figure 2(b). It signifies some role of water in modulating the thermal stabilization of proteins in the presence of osmolyte molecules. In figure 2(c), the extent of thermal stabilization (ΔT_m) is plotted against the change in average bulk solvation dynamics ($\Delta\tau_{bulk}$) to understand if the extent of modulation in bulk solvation can explain the distinct thermal stabilization of different proteins in same osmolyte. $\Delta\tau_{bulk}$ is evaluated as,

$$\Delta\tau_{bulk}\,(Osmolyte) = \tau_{bulk}\,(Osmolyte) - \tau_{bulk}\,(Buffer) \qquad (5.2.4)$$

From figure 2(c), it is evident that for the increment in the value of $\Delta\tau_{bulk}$ on the addition of 1M and 2M sorbitol the extent of thermal stabilization for papain and bromelain is different, confirmed individually by the green (1M) and the yellow (2M) strips in the same figure.

Table 2: Variation in the relaxation time constant, their relative weightage and average relaxation in solvation dynamics study of C-343 in buffer and sorbitol solution

[Sorbitol] (M)	a_1	τ_1 **(ps)**	a_2	τ_2 **(ps)**	τ_{avg} **(ps)**
0	0.23±0.06	0.230±0.070	0.77±0.060	1.030±0.090	0.840±0.030
1	0.21±0.01	0.110±0.030	0.79±0.01	1.340±0.030	1.090±0.030
2	0.28±0.01	0.120±0.060	0.72±0.01	2.120±0.240	1.560±0.160

*All the data for bulk solvation dynamics study has been procured from our previous work [24].

While bulk water may contribute to osmolyte-induced protein stabilization, it alone cannot account for the thermal stabilization of the two proteins by different extent. This is clear from the analysis of Figure 2(c), suggesting the involvement of additional factors beyond bulk water modulation. Bulk water includes effects from osmolyte but doesn't incorporate protein-induced effects on water modulation. Thus, Figure 2(c) confirms that protein-specific observations might not be explained by exploring bulk water behaviour alone.

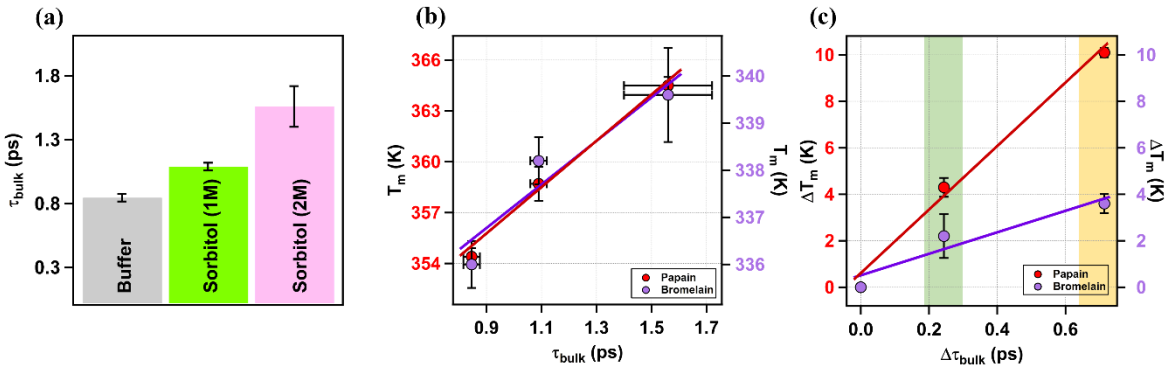

Figure 2: (a) Measurement of the bulk solvation dynamics (τ_{bulk}) in buffer, 1M and 2M sorbitol shown in grey, green and pink color respectively. Correlation plot showing the variation of (b) melting temperature (T_m) with bulk solvation dynamics (τ_{bulk}) and (c) extent of change in melting temperature (ΔT_m) with extent of change in bulk solvation dynamics ($\Delta\tau_{bulk}$) in the presence of 1M (green strip) and 2M (yellow) concentration of sorbitol for bromelain (violet) and papain (red). Experiments were performed at 298 K.

5.2.3. Associated water dynamics modulation in the presence of sorbitol:

To further investigate why two different proteins exhibit distinct levels of thermal stabilization in similar concentrations of the same osmolyte, we examine how the added osmolyte modulates the water that is directly associated with the protein, commonly termed as the associated water or biological water, which reflects influences from both the protein and the osmolyte, unlike bulk solvation dynamics that lack this level of specificity [30–33]. This water layer is special as it is known to have characteristics different than the bulk water and known to vary from protein to protein [34]. Apart from the unique behavior of the associated water, it is already

evident that this layer also plays a crucial role in defining the properties of the protein [35,36]. It has been shown how the modulation in the associated water dynamics modulates the activity of the protein in the presence of different co-solutes [20,23]. Thermal stabilization of the protein in the presence of different co-solutes is also reported to be influenced by the modulation of the associated water dynamics [20,21,23,24,37]. Our group reported that the osmolyte modifies the thermal stability of papain by modulating its associated water dynamics [21,24]. The osmolyte that retards the associated water dynamics thermally stabilizes the protein and vice versa.

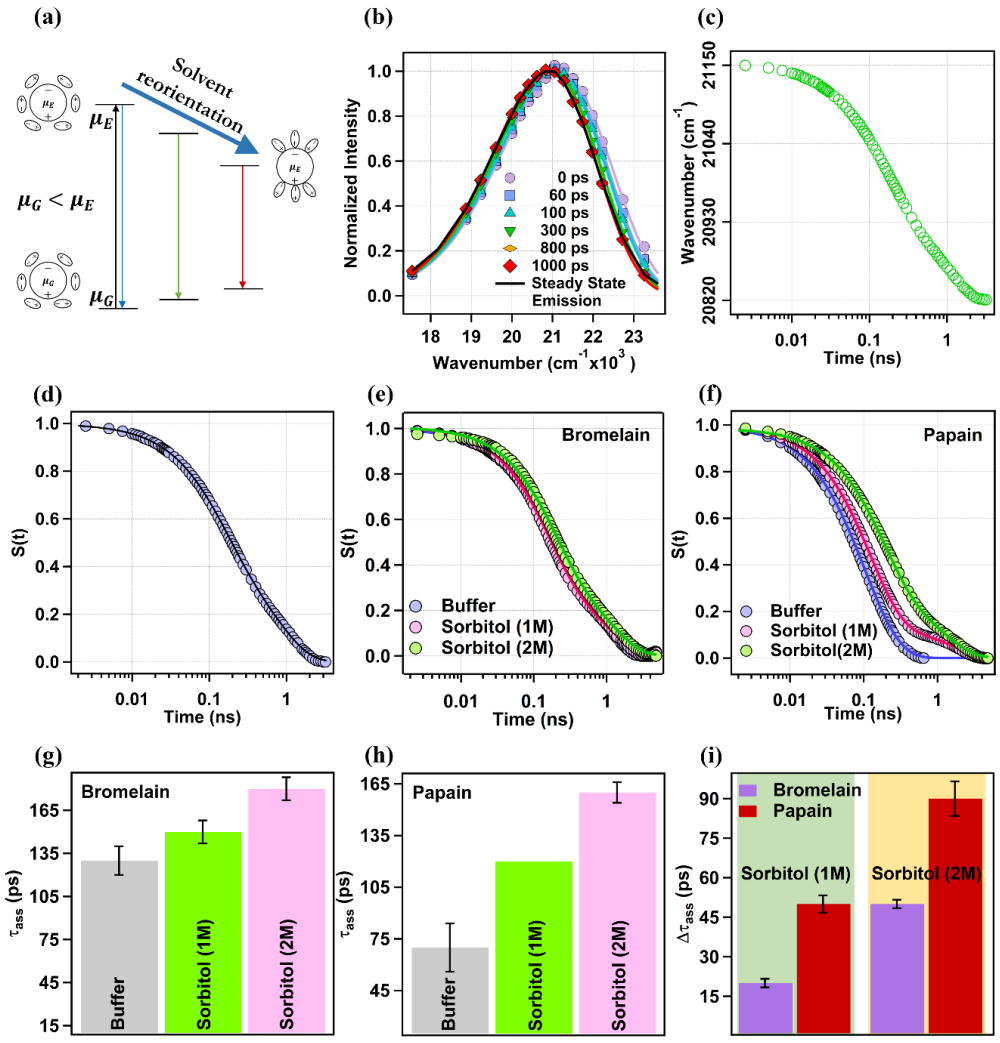

Figure 3: (a) Schematic representation of phenomenon of solvation. (b) The normalized time resolved emission spectra (TRES) for bromelain in buffer. The relaxation of the excited state represented by the (c) variation of the corresponding wavenumber maximum of the representative emission spectra with time and is normalized using the equation 2 to get the (d) solvent correlation function S(t) along with the fitting line obtained by employing the biexponential function. Solvent correlation function, S(t) for

(e) CPM tag bromelain and (f) CPM tag papain in buffer, 1M and 2M concentration of sorbitol represented in violet, pink and green respectively. Variation of the associated water dynamics (τ_{ass}) of (g) CPM tag bromelain and (h) CPM tag papain in buffer (grey), 1M (green) and 2M (pink) sorbitol solution. (i) Increament in the associated water dynamics ($\Delta\tau_{ass}$) of bromelain (violet) and papain (red) in 1M (green) and 2M (yellow) concentration of sorbitol. Experiments were performed at 298 K.

To test the credibility of this hypothesis which we termed as "Associated Water Stabilization Mechanism" (AWSM) to explain the distinct effect of osmolyte on the thermal stabilization of different proteins we have performed solvation experiments on both proteins individually, in the presence and absence of sorbitol, to investigate for the changes in their associated water dynamics. In the solvation experiment, excitation was carried out using a laser pulse ($\lambda_{ex} = 375nm$) which excited the fluorophore CPM covalently attached to the protein. During this excitation process the dipole moment of CPM molecules changes and is higher in the excited state compared to the ground state [38]. As this process is instantaneous, the arrangement of the surrounding solvent molecules in the excited state around the dipole remains the same as that in the ground state which makes it a thermodynamically unstable arrangement [39]. To regain stability, the surrounding solvent molecules reorient their dipoles to accommodate the new excited-state dipole of the fluorophore, a process known as solvent relaxation, as illustrated in Figure 3(a). This dynamic rearrangement was captured using time-resolved fluorescence measurements, yielding a series of emission spectra at different time points during relaxation, collectively known as Time-Resolved Emission Spectra (TRES) [21,31]. The normalized TRES for the CPM-labeled bromelain in buffer is shown in Figure 3(b). The emission maxima of representative emission spectra are plotted against the corresponding time as depicted in figure 3(c) and is normalized to generate the solvent response function S(t) by employing equation 5.2.5 as shown in figure 3(d).

$$S(t) = \frac{\bar{\nu}(t) - \bar{\nu}(\infty)}{\bar{\nu}(0) - \bar{\nu}(\infty)} \qquad (5.2.5)$$

S(t) is fitted using the biexponential equation as shown in figure 3(d). S(t) for bromelain and papain in the presence and absence of sorbitol along with the fitting lines are shown in figure 3(e) and figure 3(f). To test the feasibility of the bi-exponential model over single exponential model, the solvent response function in each case is fitted with both the models for comparative study. The TRES with fittings by employing single and bi-exponential functions for CPM tag bromelain and papain are presented in figure 4 and 5 respectively. The fitting values for bi-exponential fit for CPM tag bromelain and papain are provided in table 3 and 4.

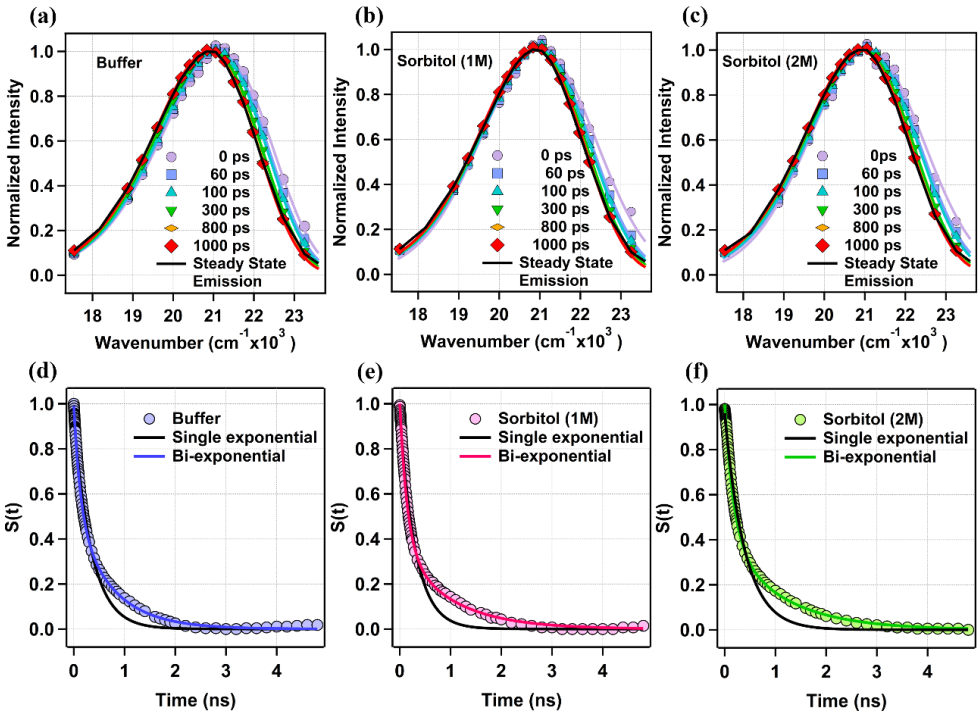

Figure 4: Time resolved emission spectra (TRES) of CPM tag bromelain in (a) buffer, (b) 1M and (c) 2M of sorbitol. Solvent correlation function along with the fitting lines for CPM tag bromelain in (d) buffer, (e) 1M and (f) 2M of sorbitol. Experiments were performed at 298 K.

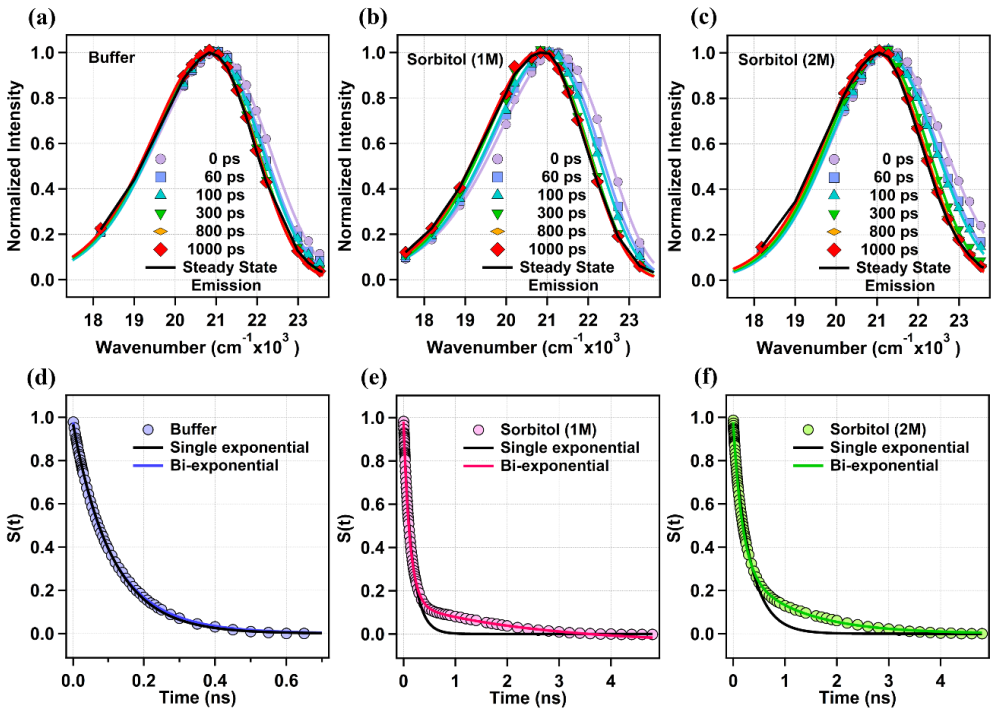

Figure 5: Time resolved emission spectra (TRES) of CPM tag papain in (a) buffer, (b) 1M and (c) 2M of sorbitol. Solvent correlation function along with the fitting lines for CPM tag papain in (d) buffer, (e) 1M and (f) 2M of sorbitol. Experiments were performed at 298 K.

Table 3: Variation in the relaxation time constant, their relative weightage and average relaxation in solvation dynamics study of CPM tag bromelain in buffer and sorbitol solution.

[Sorbitol] (M)	a_1	τ_1 (ps)	a_2	τ_2 (ps)	τ_{avg} (ps)
0	0.49±0.02	130±5	0.51±0.02	730±19	440±3
1	0.64±0.02	150±6	0.36±0.02	990±47	450±4
2	0.60±0.02	180±7	0.40±0.02	1100±39	550±5

Table 4: Variation in the relaxation time constant, their relative weightage and average relaxation in solvation dynamics study of CPM tag papain in buffer and sorbitol solution.

[Sorbitol] (M)	a_1	τ_1 (ps)	a_2	τ_2 (ps)	τ_{avg} (ps)
0	0.31±0.15	70 ±14	0.69±0.25	130±31	110±20
1	0.84±0.02	120±6	0.16±0.02	1380±176	320±10
2	0.56±0.01	170±6	0.44±0.01	1560±53	780±27

*All the data for solvation dynamics study of CPM tag papain has been procured from our previous work.

Proteins generally show a broad spectrum of solvation events in the picosecond (ps) to nanosecond (ns) range, where the event with time scale of ~1ps comes from the water motions in the bulk [30,31,33,40,41]. The relaxation in the time range ~ 5ps is from the relaxation of the water molecules in the protein hydration layer. The dynamics in the range ~ 20ps – 200ps originates from the concerted motions of the protein side chains and the water molecules attached to these side chains on the protein surface [31,42]. These motions are known to be initiated by the overall network movement of the water molecules in the hydration layer [42–45]. To distinguish this slow motion originating from the water network from the faster motions of the water molecules in the hydration layer, the dynamics linked with these motions are entitled as associated water dynamics. The dynamics >200ps comes from the various protein motions. As we have already mentioned that we are interested in probing the associated water layer and specifically we are more interested in probing the type of motions in which the water and protein both participate. From the description of the type of motions a protein undergoes, it's clear that our search matches with the associated water dynamics of the protein which are in the range ~20-200ps and the instrument used here i.e., TCSPC (with an IRF ~75ps and detection capability of dynamics as fast as ~30ps with precision) is suitable for observing dynamics in this range provided the protein shows the associated water dynamics (τ_{ass}) in the range ≥30ps. For the proteins, bromelain and papain, the τ_{ass} is observed experimentally

around 130ps (figure 3(g)) and 70ps (figure 3(h)) respectively in buffer only system. The value of τ_{ass} in case of bromelain has been observed to be around 150ps with 1M sorbitol which further increase to 180ps with increase in concentration of sorbitol to 2M as shown in figure 3(g). With the increase in the concentration of sorbitol the associated water dynamics of bromelain get retarded as is evident by the increase in the value of τ_{ass} shown in figure 3(g) and the same trend has also been observed in papain as well which is evident in figure 3(h). In the case of papain, the value of τ_{ass} increase from 70ps to 110ps on the addition of 1M sorbitol to buffer which increases continuously with increase in concentration of sorbitol and reaches to 150ps with 2M sorbitol as shown in figure 3(h). Researchers have emphasized the direct involvement of the associated water dynamics in influencing the thermal stabilization of the proteins in various systems. Das *et al.,* observed the modulation in the thermal stabilization of human serum albumin (HSA) in the presence of the macromolecular crowder by the modulation in the associated water dynamics mediated through the modulation of the entropy and enthalpy of the overall system [20]. Similar observations have been reported by Khan *et al.* for the thermal stabilization of bromelain in the presence of Ficoll-70k and deep eutectic solvents [20,23,37]. Even the altered thermal stabilization of papain in the presence of different osmolytes is found to be directly correlated with the modulation in the associated water dynamics of the enzyme [21]. Collectively, these studies suggest that the modulation in the associated water dynamics in the presence of added co-solute controls the thermal stabilization of the protein. To validate our hypothesis (AWSM) in explaining the thermal stabilization of bromelain and papain in the presence of increasing sorbitol concentration we have plotted the T_m against the τ_{ass} in the presence and absence of sorbitol as shown in Figure 6(a) for both the proteins. In Figure 6(a), it can be observed that with an increase in the concentration of sorbitol the value of τ_{ass} and T_m for bromelain (represented in violet) and the papain (represented in red) increases with sorbitol content and thus both the proteins follow the hypothesis justified by the straight line fit as where the associated water dynamics gets retarded (increased τ_{ass}) the protein get thermally stabilized

(increased T_m). Both the proteins, individually, follow the hypothesis, but it appears that with the basic approach of the theory it is hard to comment on the different stabilization of proteins in similar environmental conditions. To explore this, we extended our approach with a slightly different perspective by shifting focus from absolute values of the parameters to the extent of change, aiming to better capture the relative stabilization effects of osmolytes on different proteins.

As the concentration of sorbitol is increased the associated water dynamics for both the employed proteins increase but the extent of retardation in the dynamics ($\Delta\tau_{ass}$) is observed to be different for the two and is given by,

$$\Delta\tau_{ass}(Osmolyte) = \tau_{ass}(Osmolyte) - \tau_{ass}(Buffer) \quad (5.2.6)$$

The extent of retardation in the associated water dynamics for bromelain is observed to be ~ 20ps and ~ 50ps with subsequent increase in concentration from 1M to 2M sorbitol as shown by violet bars in figure 3(i). Whereas the extent of retardation for papain has seemed to increase from ~50ps to ~90ps with increase in sorbitol concentration from 1M to 2M shown by red bars in figure 3(i). On comparing the extent of retardation for the two proteins with individual concentration of the sorbitol we found out that the extent of retardation for bromelain and papain (green strips in figure 3(i)) in 1M sorbitol is ~20ps and ~50ps respectively. For 2M sorbitol the extent of retardation is ~50ps and ~90ps with bromelain and papain (yellow strips in figure 3(i)) respectively. With each of the concentration of sorbitol employed here the extent of retardation is less in case of bromelain relative to papain. Similar observation has also been observed where we have discussed the extent of thermal stabilization suggested weaker stabilization of bromelain rover papain. The results for the extent of thermal stabilization and retardation in associated water dynamics for the proteins in the employed concentration of sorbitol could be summarized as,

$$(\Delta T_m)_{[X],Bromelain} < (\Delta T_m)_{[X],Papain} \quad (5.2.7)$$

$$(\Delta\tau_{ass})_{[X],Bromelain} < (\Delta\tau_{ass})_{[X],Papain} \quad (5.2.8)$$

where, $[X]$ is the concentration of the sorbitol used in this study. The ΔT_m is plotted against $\Delta\tau_{ass}$ to search for any correlation between the two. In case of each of the proteins (violet for bromelain and red for papain), with the increase in sorbitol concentration, $\Delta\tau_{ass}$ increases which is correlated by the almost straight line relation with the ΔT_m which imply that with the increase in extent of retardation in associated water dynamics, each of the employed protein gets higher thermal stabilization as shown in Figure 6(b). The extent of retardation in the associated water dynamics and the extent of thermal stabilization for bromelain is less than that of papain with each of the sorbitol concentration. So, finally it can be concluded from Figure 6(b) that where the extent of retardation in associative water dynamics is more, the protein will get thermal stabilization by greater extent.

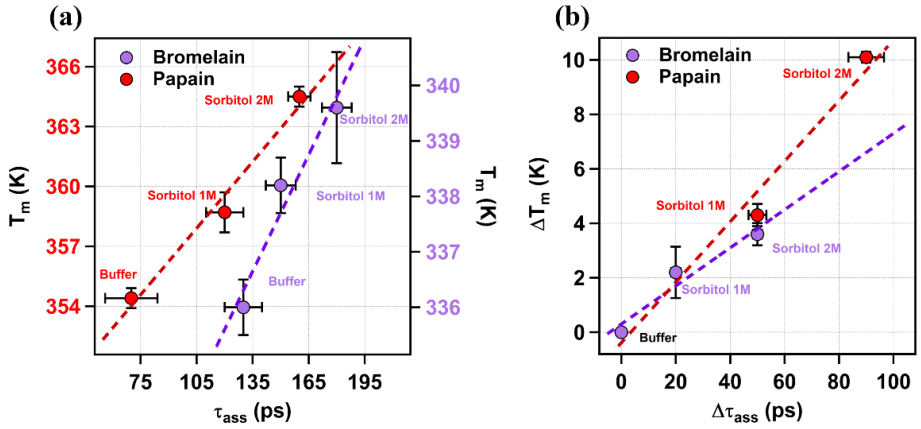

Figure 6: Correlation plot showing the variation in the (a) melting temperature (T_m) with the associated water dynamics (τ_{ass}) and (b) extent of change in melting temperature (ΔT_m) with extent of change in associated water dynamics ($\Delta\tau_{ass}$) for bromelain (violet) and papain (red) in the presence and absence of sorbitol. Experiments were performed at 298 K.

5.2.4. Microsecond conformational fluctuation dynamics measurement:

The correlation between the associative water dynamics and melting temperature of protein describes the thermal stabilization of bromelain and papain individually in the presence of sorbitol and the correlation between the extent of retardation in associated water dynamics with the extent of increment in melting temperature describes the higher thermal stabilization of papain over bromelain in sorbitol. However, the insight into how this correlation comes into play is still unclear.

Since water molecules in the hydration layer directly interact with the protein surface, changes in their dynamics may influence both residue–water interactions and intra-protein residue bonding [46]. These altered interactions could reshape the protein's thermodynamics, ultimately impacting its thermal stability. In our recent study, we provide mechanistic insight into this phenomenon by establishing a strong link between associated water modulation and conformational fluctuation dynamics in the presence of osmolytes [24]. This suggests that to understand the molecular events involved in processing the modulation in the associated water dynamics in the presence of sorbitol to directly reflect in the altered thermal stabilization we must probe the interior of the protein.

Dimension of the proteins is generally measured in terms of hydrodynamic radii (R_h) which spans in the Angstrom (Å) range. Since these are too small to be observed and thus hard to track directly any subtle changes these might undergo. Therefore, the interior of the protein must be probed indirectly. For this indirect measurement, we have employed fluorescence correlation spectroscopy (FCS) as a tool where an observation volume in femtolitre dimension (0.8 fl in our case shown in figure 7(a)) is created using the optical setup with the help of laser beam [47–49] ($\lambda_{ex} = 532\,nm$) and the fluctuations in the emission intensity of the fluorophore with time is recorded as shown in the upper panel of figure 7(b). The time traces of the emission intensity measured in two different detectors are correlated by giving a lag in time between the two to produce a cross-correlation function ($G(\tau)\ vs\ time$).

The dynamics of any event that induces the changes in the intensity of the fluorophore can be probed here as exemplified in the lower panel of figure 7(b), provided the dynamics must not be slower than the diffusion dynamics of the fluorophore in the observation volume and should not be faster than the detection limit of the overall FCS setup [49]. Here we have employed TMR attached to bromelain (CYS 26) and papain (CYS 25) for the FCS study [24,50]. The TMR tagged to bromelain and papain is surrounded by five tryptophan residues positioned at distinct locations from the free cysteine residue to which the TMR dye is attached. The fluorescence intensity of tagged TMR is expected to be quenched by the interaction of the π cloud of the tryptophan residues which is evident in other studies as well [51–53]. As the interaction depends on the distance of the quencher from the fluorophore, the quenching is expected to be dominated with the nearest tryptophan residue (TRP 27 and TRP 26 in bromelain and papain respectively). The quenching will be influenced by other relatively distant tryptophan residues as well, as all are within the proximity of the attached TMR dye owing to the small size of the bromelain $(R_h = \sim 22\ \text{Å})$ and papain $(R_h = \sim 18\ \text{Å})$. As per the literature the free (untagged) TMR dye shows a triplet state dynamics in the microsecond time scale [48,54]. On being attached covalently to the free cysteine of the bromelain, the inherent microsecond triplet state dynamics of the TMR dye is expected to be observed in the case of TMR tagged bromelain and papain as well with a slight modulation in the absolute value. As per the discussion the TMR tagged bromelain and papain are expected to show three different kinds of dynamical events namely, diffusion dynamics, conformational dynamics because of the quenching of TMR fluorescence by the nearby tryptophan residues and the inherent triplet state dynamics of the attached TMR dye.

For bromelain, the cross-correlation function, $G(\tau)$ for buffer only system is provided in figure 7(c) which has been fitted with equation 5.2.9 comprises of two exponential and one diffusion term [24,54].

$$G(\tau) = \frac{1}{N}\left(1+\frac{\tau}{\tau_D}\right)^{-1}\left(1+\frac{\tau}{\omega^2\tau_D}\right)^{-\frac{1}{2}}\left(1+K\ exp\left(-\frac{\tau}{\tau_R}\right)\right)\left(1+\frac{p}{1-p}\ exp\left(-\frac{\tau}{\tau_T}\right)\right) \qquad (5.2.9)$$

The normalized cross-correlation plot for bromelain in buffer with fitting is shown in figure 7(d). Although we have checked for the other equations as well, the cross-correlation fits best with the employed equation as shown in figure 8.

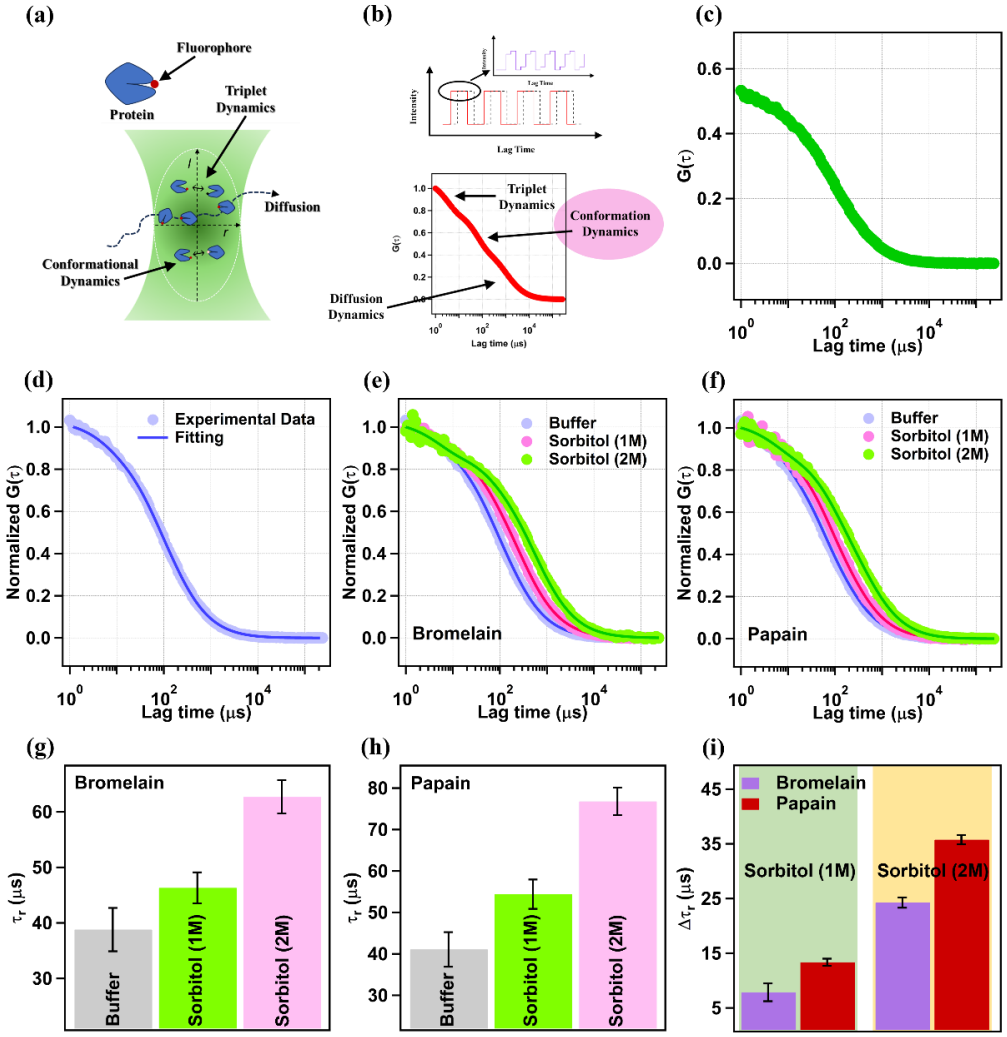

Figure 7: Schematic representation of the (a) possible processes of fluorophore attached protein within the observation volume of the FCS setup and (b) the processing of the fluctuations in the emission intensity of the attached fluorophore observed by two detectors (upper panel) to generate the cross-correlation function, $G(\tau)$ (lower panel). (c) Cross-correlation function for bromelain in buffer and (d) normalized cross-correlation function for bromelain with the fitting line by employing equation 5.

Normalized cross-corrleation function for (e) TMR tag bromelain and (f) TMR tag papain in buffer, 1M and 2M sorbitol concentration represented in violet, pink and green. Variation in the conformational dynamics (τ_r) of (g) TMR tag bromelain and (h) TMR tag papain in buffer, 1M and 2M concentration of sorbitol shown in grey, green and pink color respectively. (i) Increament in the conformational dynamics ($\Delta\tau_r$) of bromelain (violet) and papain (red) in 1M (green) and 2M (yellow) concentration of sorbitol. Experiments were performed at 298 K.

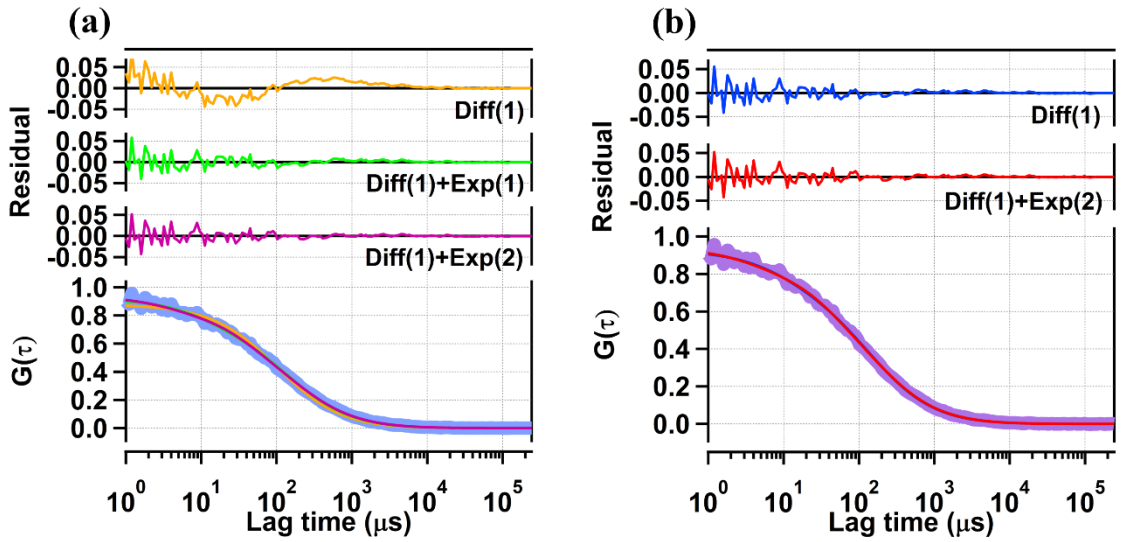

Figure 8: Fitting of FCS cross-correlation trace of TMR-bromelain in buffer with different fitting models. Residuals are given for each fitting model used. Experiments were performed at 298 K.

Control fitting analyses were performed using alternative models, including single-exponent with diffusion, single-diffusion, and dual-diffusion equations, to ensure robustness in data interpretation as shown in figure 8. From the residuals describing the goodness of fitting with different models in figure 8a clearly depicts that the model with single diffusion and two exponents fits the best among all the possible models. The residual for function with two diffusion components shown in figure 6b also seems promising but gives the value of one component too small ($\sim 14\mu s$) which is not even comparable to the diffusion time of the free ($\sim 50\mu s$) dye. Which rules out the possibility of having the second component arising out of the free dye present in the sample of TMR-papain. Figure 8 ensures that the model with single

diffusion and two exponents is the most appropriate and matches well with the expected number of events possible with our system.

The diffusion term is for the movement of the TMR tagged bromelain through the observation volume and must be the dynamics with slowest time scale. We must cross check for the source of the other two exponential components as the origin of the event might be the internal dynamics of the dye or the conformational fluctuation of the protein or an artifact of the device. Here in the case of TMR tagged bromelain we have got three events with time constants ~ $5\mu s$, ~ $38\mu s$ and ~ $140\mu s$. The event with the slowest time constant i.e., of $140\mu s$ is ascribed to the diffusion dynamics of the TMR tagged bromelain. For the other two faster time constants we are left with two possibilities that are internal dynamics of the dye and the conformational dynamics of the protein.

We have performed power dependent FCS experiment to confirm the event arising out of the inherent triplet state dynamics of the dye. We have observed the rise in the percentage of population of the dye molecules (p) in the triplet state with an increase in power whereas the associated time constant of ~ $5\mu s$ remains almost the same irrespective of the laser power used as shown in Figure 10. Raw data has been provided in Figure 9.

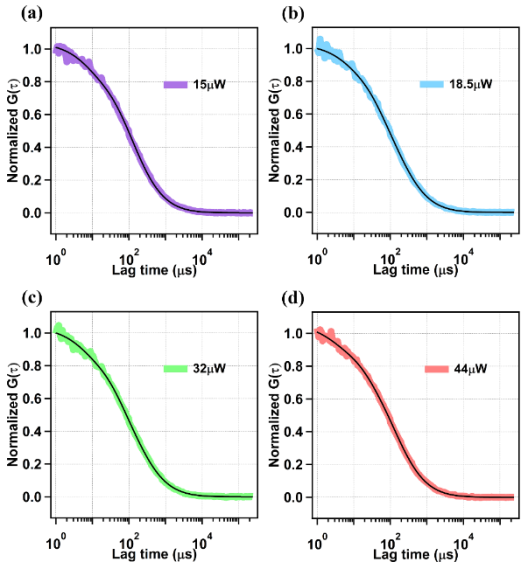

Figure 9: Normalized traces of FCS cross-correlation curves of TMR-tag bromelain at different power. Dark line represents the fitting line. Experiments were performed at 298 K.

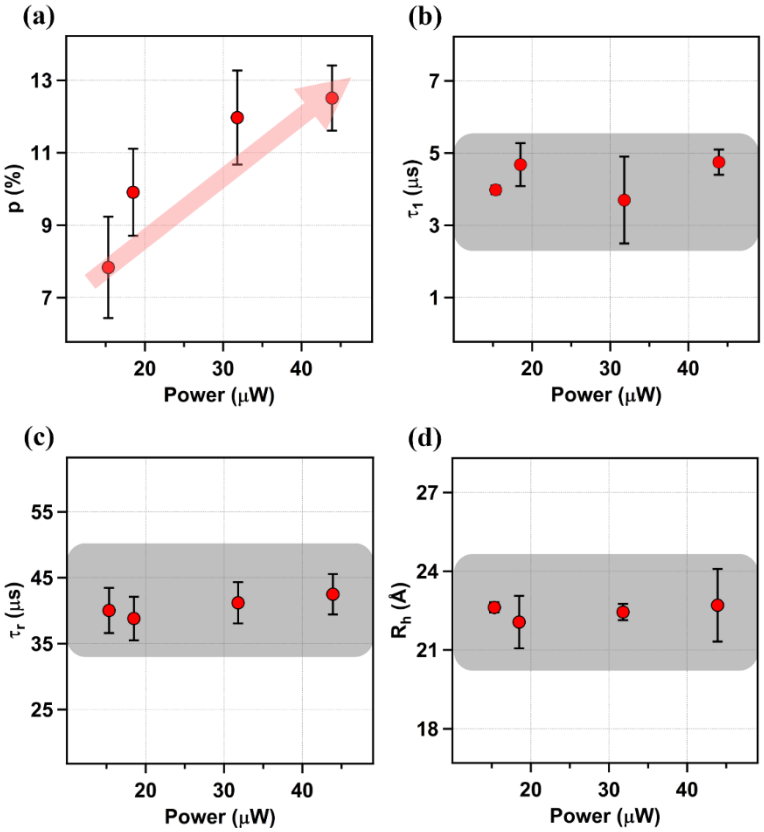

Figure 10: Variation of the (a) population of the dye molecules in the triplet state (p), (b) fastest time constant (triplet state dynamics, τ_T), (c) the second fastest time constant (conformational dynamics, τ_r), and (d) hydrodynamic radii (R_h) of the bromelain with power using optical fiber of diameter 50μm. Experiments were performed at 298 K.

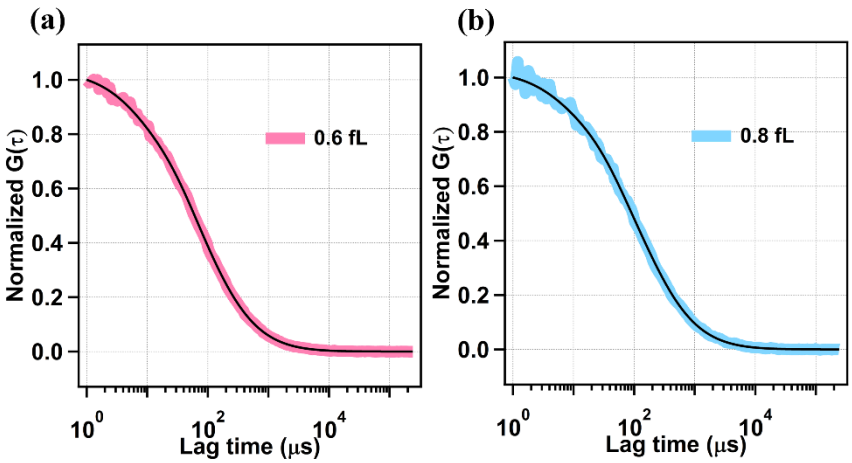

Figure 11: Normalized traces of FCS cross-correlation curves of TMR-tag bromelain at different observation volume. Dark line represents the fitting line. Experiments were performed at 298 K.

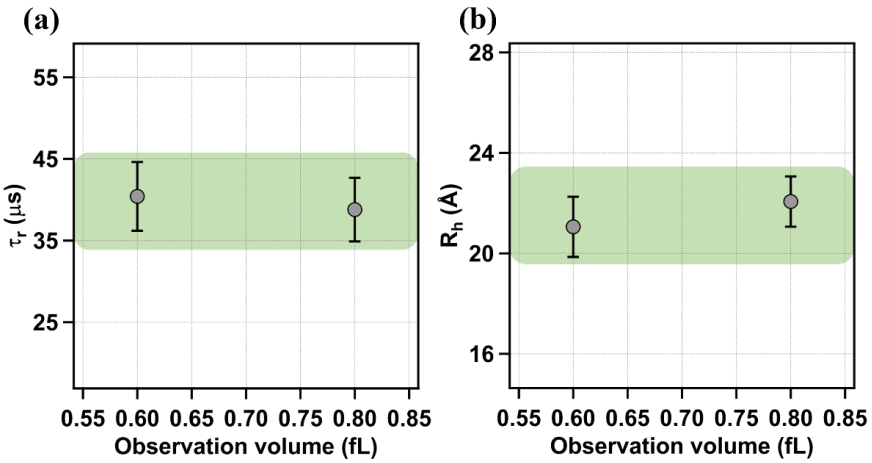

Figure 12: Variation of the (a) conformational fluctuation dynamics (τ_r) and (b) hydrodynamic radii (R_h) of TMR-tagged bromelain with change in the observation volume. Experiments were performed at 298 K.

This confirms the association of the dynamics with time scale ~ $5\mu s$ with the inherent triplet state dynamics of the dye. Further we have studied the variation in the time constant of dynamics by modulating the observation volume of the device through employing optical fibers with different dimensions to confirm that the dynamics in the range ~ $38\mu s$ is having protein origin and not originating from the dye itself [51]. We have observed almost similar time constant (~ $38\mu s$) associated with this event irrespective of the observation volume of the device shown in Figure 12, which justifies our assumption of having this event arising out of the conformational dynamics or the breathing motion of protein (raw data has been provided in Figure 11). As the protein papain shares a lot of similarities with bromelain and thus shows similar events. Papain shows a diffusion dynamics, conformational dynamics and triplet state dynamics with time constant of ~ $120\mu s$, ~ $41\mu s$ and ~ $6\mu s$ respectively. The similar control experiments for the assignment of events with different dynamic processes observed during FCS study of TMR tag papain have already been proved somewhere else [24].

The normalized cross-correlation plots for TMR tag bromelain and TMR tag papain in the presence and absence of sorbitol are shown in Figure 7(e) and Figure 7(f) respectively. In the case of both the proteins, with increase in the sorbitol content the

cross-correlation plot decays more slowly as evident by the violet color plot for buffer followed by pink for 1M and green for 2M sorbitol respectively in Figure 7(e) and 7(f). The time constant associated with the conformational dynamics (τ_R) of bromelain is ~ $38\mu s$. On the addition of sorbitol, the value of τ_R increases to ~ $46\mu s$ which further increases to ~ $63\mu s$ with 2M sorbitol as shown in Figure 7(g). For papain, the value of τ_R is observed experimentally around ~ $41\mu s$ which increases to ~ $54\mu s$ and ~ $77\mu s$ with increase in sorbitol concentration to 1M and 2M respectively as shown in Figure 7(h). All the fitting data has been provided in table 5 and 6 for TMR tag bromelain and papain respectively.

Table 5: Variation of time scales of triplet state dynamics, conformational dynamics, diffusion dynamics and hydrodynamic radii of bromelain in buffer and sorbitol solution

[Sorbitol] (M)	$\tau_T(\mu s)$	$\tau_R(\mu s)$	$\tau_D(\mu s)$	R_h(Å)
0	4.7±0.1	38.8±3.9	135.9±6.0	22.1±1.0
1	4.3±0.3	46.3±2.8	244.0±10.9	20.1±0.9
2	3.5±0.6	62.7±3.0	548.4±28.8	20.2±1.0

Table 6: Variation of time scales of triplet state dynamics, conformational dynamics, diffusion dynamics and hydrodynamic radii of papain in buffer and sorbitol solution

[Sorbitol] (M)	$\tau_T(\mu s)$	$\tau_R(\mu s)$	$\tau_D(\mu s)$	R_h(Å)
0	5.9±0.2	41.1±4.2	119.2±5.0	19.4±0.8
1	3.0±0.2	54.4±3.5	220.1±10.9	18.1±0.9
2	4.6±0.1	76.8±3.6	492.2±31.0	18.2±1.2

The continuous increase in the value of τ_R with the sorbitol content for both the proteins implies retardation in the conformational dynamics or slowness in the inherent motions of the proteins. The observed retardation in protein conformational dynamics can be attributed to two primary factors: an increase in bulk solution viscosity and the modulation of associated water dynamics due to osmolyte addition. This idea is supported by the work of protein science pioneer Hans Frauenfelder, who demonstrated that large-scale protein motions are governed by solvent viscosity, while small-scale motions are influenced by the properties of water molecules directly interacting with the protein surface what we refer to as associated water [35,55,56]. Both factors might impact the conformational dynamics of the protein in the microsecond regime. In our recent report, we have shown a pronounced impact of associated water dynamics on conformational dynamics in the microsecond regime over the viscosity [24].

Now, to see the influence of modulation of associated water on the modulation of the interior of the protein, we have plotted τ_{ass} against τ_r. As the value of τ_{ass} increases with the addition of sorbitol, the value of τ_r also increases as evident in Figure 13(a) by a straight line fit for both the proteins. With the addition of sorbitol, the bonding among the water molecules and water-surface amino acid residues get strengthened confirmed by the retardation in the associated water dynamics. This alteration in the bonding also makes an impact on the internal energetics of the protein (bonding between the amino acid residues within the protein) as the surface residues, water attached to the surface residues and the inner amnio acid residues are internally connected through the physical forces like hydrogen bonds and thus the conformational dynamics of the proteins also got changed as suggested by the correlation. The retardation in the conformational dynamics of the proteins on the addition of sorbitol points towards the strengthening of the bonding among the amino acid residues and thus both the proteins employed here get thermally stabilized.

This correlation between τ_{ass} and τ_r in the case of each protein gives insights into how the modulation in the associated water dynamics in the presence of sorbitol modulates the interior of the protein to reflect the ultimate effect on the thermal stabilization of the protein in presence of sorbitol. But this correlation doesn't provide any useful insights into how the two proteins get thermally stabilized by different extent in the presence of the same concentrations of sorbitol. To seek for a reasonable insight into the interior of the protein in the presence of sorbitol we have determined the extent ($\Delta\tau_r$) by which the interior of the protein gets perturbed on the addition of sorbitol with respect to the buffer counterpart in case of each protein by employing the equation,

$$\Delta\tau_r(Osmolyte) = \tau_r(Osmolyte) - \tau_r(Buffer) \qquad (5.2.10)$$

It has been observed that the value of $\Delta\tau_r$ for bromelain comes around ~ $8\mu s$ and ~ $24\mu s$ with 1M and 2M sorbitol respectively. For papain it appears around ~ $13\mu s$ and ~ $36\mu s$ for the sorbitol concentration of 1M and 2M respectively. Based on the comparative analysis for $\Delta\tau_r$

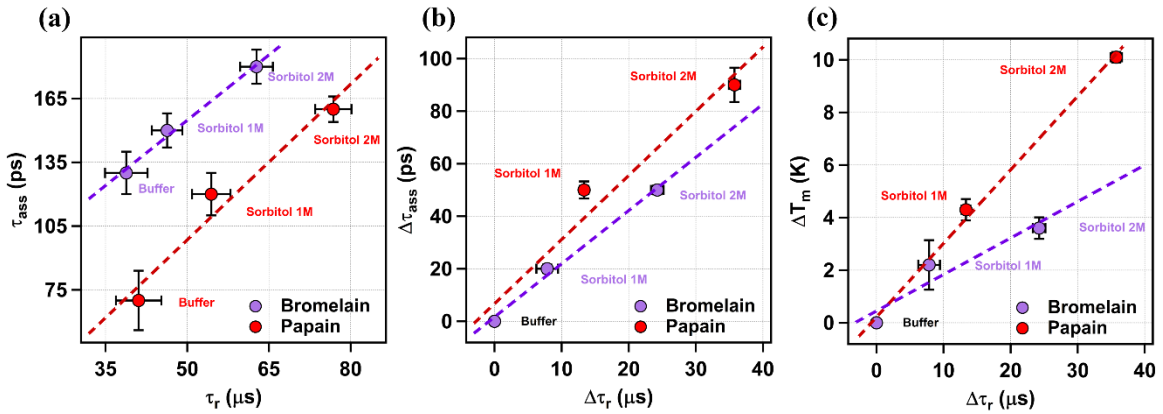

Figure 13: Correlation plot of the (a) variation in the associatd water dynamics (τ_{ass}) with conformational dynamics (τ_r), (b) extent of change in the associated water dynamics ($\Delta\tau_{ass}$) with the extent of change in the conformational dynamics ($\Delta\tau_r$) and (c) the extent of change in the melting temperature (ΔT_m) with the extent of change in the conformational dynamics ($\Delta\tau_r$) of bromelain and papain represented in violet and red color respectively. Experiments were performed at 298 K.

between bromelain and papain, it can be deduced that the extent of retardation in conformational dynamics is less for bromelain relative to papain with each

representative concentration of sorbitol used here in the study as is evident from Figure 7(i) and can be summarized as,

$$(\Delta\tau_r)_{[X],Bromelain} < (\Delta\tau_r)_{[X],Papain} \quad (5.2.11)$$

To explore how internal perturbations in proteins influence their melting thermodynamics, we plotted $\Delta\tau_{ass}$ against $\Delta\tau_r$ as shown in Figure 13(b). Upon sorbitol addition, bromelain showed a smaller retardation in both associated water dynamics and conformational dynamics, while papain exhibited greater retardation in both, as shown in Figure 6b. This suggests that the higher thermal stabilization of papain compared to bromelain in sorbitol arises from a stronger impact on its internal structure (Figure 13c), driven by stronger internal bonding and arrangement of water molecules in its associated water layer.

5.3 Conclusion

Protein responses to osmolyte-induced perturbations vary significantly across different proteins, an observation not adequately explained by traditional water structure modulation theories. In this study, we revisited the problem through the lens of the Associated Water Stabilization Mechanism (AWSM), using bromelain and papain as model systems and sorbitol as the osmolyte. Our findings demonstrate that sorbitol thermally stabilizes both proteins by modulating the dynamics of the associated water layer at the protein surface. This modulation strengthens water-water and water–residue interactions, which in turn influence the protein's internal bonding network, leading to enhanced conformational rigidity. However, the degree of stabilization differs between the two proteins. Comparing absolute values of associated water dynamics (τ_{ass}) and conformational dynamics (τ_r) in sorbitol is insufficient to explain this disparity. Instead, the extent of change relative to the buffer ($\Delta\tau_r, \Delta\tau_{ass}$) proves to be more insightful. Papain exhibits greater extent of retardation in both associated water dynamics ($\Delta\tau_{ass}$) and conformational dynamics

($\Delta\tau_r$), resulting in stronger internal stabilization and thus higher thermal stabilization than bromelain. Sorbitol strengthens the bonding between water molecules and between water-surface amino acid residues more in case of papain which strengthens the internal bonding in papain more and thus the papain gets better thermal stabilization compared to bromelain. These results validate the AWSM framework and offer a deeper, protein-specific understanding of osmolyte-induced stabilization. We believe this perspective provides a more mechanistic view of protein-osmolyte interactions and could open new avenues for exploring protein stability in complex biological and industrial settings.

5.4 References

(1) Yadav, R.; Sengupta, B.; Sen, P. Conformational Fluctuation Dynamics of Domain i of Human Serum Albumin in the Course of Chemically and Thermally Induced Unfolding Using Fluorescence Correlation Spectroscopy. *J. Phys. Chem. B* **2014**, *118* (20), 5428–5438. https://doi.org/10.1021/jp502762t.

(2) Janin, J.; Bahadur, R. P.; Chakrabarti, P. Protein-Protein Interaction and Quaternary Structure. *Quarterly Reviews of Biophysics*. May 2008, pp 133–180. https://doi.org/10.1017/S0033583508004708.

(3) Yancey, P. H. Organic Osmolytes as Compatible, Metabolic and Counteracting Cytoprotectants in High Osmolarity and Other Stresses. *J. Exp. Biol*. August 2005, pp 2819–2830. https://doi.org/10.1242/jeb.01730.

(4) Wang, W. Protein Aggregation and Its Inhibition in Biopharmaceutics. *International Journal of Pharmaceutics*. January 31, 2005, pp 1–30. https://doi.org/10.1016/j.ijpharm.2004.11.014.

(5) Lee, J. C.; Timasheff, S. N. The Stabilization of Proteins by Sucrose. *J. Biol. Chem.* **1981**, *256* (14), 7193–7201. https://doi.org/10.1016/s0021-9258(19)68947-7.

(6) Feeney, J.; Fisher, G. H.; Ryan, J. W.; Berryer, P.; Chung, A.; Kozlowski, H.; Formicka-Kozlowska, G.; Jezowska-Trze-Biatowska, B.; Lintner, K.; Fermandjian, S.; Regoli, D.; Barabe, J.; London, R. E.; Stewart, J. M.; Cann, J. R.; Matwiyoff, N. A.; Marlborough, D. L.; Felix, A. M.; Paiva, A. C. M.; Juliano, L.; Ptak, M.; Heitz, A.; Dreux, M. *Stabilization of Protein Structure by Sugars*; Elsevier, 1982; Vol. 21. https://pubs.acs.org/sharingguidelines.

(7) Timasheff, S. N. Water as Ligand: Preferential Binding and Exclusion of Denaturants in Protein Unfolding. *Biochemistry* **1992**, *31* (41), 9857–9864.

(8) Arakawa, T.; Timasheff, S. N. The Stabilization of Proteins by Osmolytes. *Biophys. J* **1985**, *47* (3), 411–414. https://doi.org/10.1016/S0006-3495(85)83932-1.

(9) Noelken, M. E.; Timasheff, S. N. Preferential Solvation of Bovine Serum Albumin in Aqueous Guanidine Hydrochloride. *J Biol Chem* **1967**, *242* (21), 5080–5085. https://doi.org/10.1016/s0021-9258(18)99478-0.

(10) Lin' And, T.-Y.; Timasheff, S. N. *On the Role of Surface Tension in the Stabilization of Globular Proteins*; Cambridge University Press, 1996; Vol. 5.

(11) Bolen, D. W. The Peptide Backbone Plays a Dominant Role in Protein Stabilization by Naturally Occurring Osmolytes. *Biochemistry* **1995**, *34* (39), 12884–12891.

(12) Santoro, M.; Liu, Y.; A Khan, S. M.; Hou, L.-X.; Bolen, D. W. Increased Thermal Stability of Proteins in the Presence of Naturally Occurring Osmolytes. *Biochemistry* **1992**, *31* (23), 5278–5283.

(13) Kumar, V.; Chari, R.; Sharma, V. K.; Kalonia, D. S. Modulation of the Thermodynamic Stability of Proteins by Polyols: Significance of Polyol Hydrophobicity and Impact on the Chemical Potential of Water. *Int J Pharm* **2011**, *413* (1–2), 19–28. https://doi.org/10.1016/j.ijpharm.2011.04.011.

(14) Hishida, M.; Kaneko, A.; Yamamura, Y.; Saito, K. Contrasting Changes in Strongly and Weakly Bound Hydration Water of a Protein upon Denaturation. *J Phys Chem B* **2023**, *127* (28), 6296–6305. https://doi.org/10.1021/acs.jpcb.3c02970.

(15) Hishida, M.; Anjum, R.; Anada, T.; Murakami, D.; Tanaka, M. Effect of Osmolytes on Water Mobility Correlates with Their Stabilizing Effect on Proteins. *Journal of Physical Chemistry B* **2022**, *126* (13), 2466–2475. https://doi.org/10.1021/acs.jpcb.1c10634.

(16) Higuchi, Y.; Saleh, M. A.; Anada, T.; Tanaka, M.; Hishida, M. Rotational Dynamics of Water near Osmolytes by Molecular Dynamics Simulations. *Journal of Physical Chemistry B* **2024**, *128* (20), 5008–5017. https://doi.org/10.1021/acs.jpcb.3c08470.

(17) Habib, S.; Khan, M. A.; Younus, H. Thermal Destabilization of Stem Bromelain by Trehalose. *Protein J* **2007**, *26* (2), 117–124. https://doi.org/10.1007/s10930-006-9052-1.

(18) Kaushik, J. K.; Bhat, R. *Thermal Stability of Proteins in Aqueous Polyol Solutions: Role of the Surface Tension of Water in the Stabilizing Effect of Polyols*; 1998. https://pubs.acs.org/sharingguidelines.

(19) Das, N.; Tarif, E.; Dutta, A.; Sen, P. Associated Water Dynamics Might Be a Key Factor Affecting Protein Stability in the Crowded Milieu. *J. Phys. Chem. B* **2023**, *127* (14), 3151–3163. https://doi.org/10.1021/acs.jpcb.2c09043.

(20) Khan, T.; Halder, B.; Das, N.; Sen, P. Role of Associated Water Dynamics on Protein Stability and Activity in Crowded Milieu. *J. Phys. Chem. B* **2024**, *128* (36), 8672–8686. https://doi.org/10.1021/acs.jpcb.4c04337.

(21) Negi, K. S.; Das, N.; Khan, T.; Sen, P. Osmolyte Induced Protein Stabilization: Modulation of Associated Water Dynamics Might Be a Key Factor. *Phys. Chem. Chem. Phys* **2023**, *25* (47), 32602–32612. https://doi.org/10.1039/d3cp03357k.

(22) Khan, T.; Das, N.; Bhowmik, S.; Negi, K. S.; Sen, P. Critical Role of Water beyond the Media to Maintain Protein Stability and Activity in Hydrated Deep Eutectic Solvent. *J. Phys. Chem. B* **2025**, *129* (1), 162–175. https://doi.org/10.1021/acs.jpcb.4c07039.

(23) Khan, T.; Das, N.; Bhowmik, S.; Negi, K. S.; Sen, P. Critical Role of Water beyond the Media to Maintain Protein Stability and Activity in Hydrated Deep Eutectic Solvent. *J. Phys. Chem. B* **2024**, *129*, 162–175. https://doi.org/10.1021/acs.jpcb.4c07039.

(24) Negi, K. S.; Rana, S.; Khan, T.; Mondal, D.; Sen, P. Interplay of Protein Fluctuation and Associated Water Dynamics in Osmolyte-Induced Stabilization. *Biophys J* **2025**, *124* (12), 2082–2091. https://doi.org/10.1016/j.bpj.2025.05.006.

(25) Das, N.; Sen, P. Structural, Functional, and Dynamical Responses of a Protein in a Restricted Environment Imposed by Macromolecular Crowding. *Biochem* **2018**, *57* (42), 6078–6089. https://doi.org/10.1021/acs.biochem.8b00599.

(26) Möller, J.; Schroer, M. A.; Erlkamp, M.; Grobelny, S.; Paulus, M.; Tiemeyer, S.; Wirkert, F. J.; Tolan, M.; Winter, R. The Effect of Ionic Strength, Temperature, and Pressure on the Interaction Potential of Dense Protein Solutions: From Nonlinear Pressure Response to Protein

Crystallization. *Biophys. J.* **2012**, *102* (11), 2641–2648. https://doi.org/10.1016/j.bpj.2012.04.043.

(27) Mohan, V.; Sengupta, B.; Das, N.; Banerjee, I.; Sen, P. Domain-Specific Stabilization of Structural and Dynamic Responses of Human Serum Albumin by Sucrose. *Protein Pept Lett* **2019**, *26* (4), 287–300. https://doi.org/10.2174/0929866526666190122115702.

(28) Moon, C. P.; Fleming, K. G. Using Tryptophan Fluorescence to Measure the Stability of Membrane Proteins Folded in Liposomes. In *Methods in Enzymology*; Academic Press Inc., 2011; Vol. 492, pp 189–211. https://doi.org/10.1016/B978-0-12-381268-1.00018-5.

(29) Dill, K. A. *Biochemistry © Perspectives in Biochemistry Dominant Forces in Protein Folding*; 1990. https://pubs.acs.org/sharingguidelines.

(30) Peon, J.; Pal, K.; Zewail, A. H. Hydration at the Surface of the Protein Monellin: Dynamics with Femtosecond Resolution. *Proc. Natl. Acad. Sci* **2002**, *99* (17), 10964–10969.

(31) Kumar, S.; Peon, J.; Zewail, A. H. Biological Water at the Protein Surface: Dynamical Solvation Probed Directly with Femtosecond Resolution. *Proc. Natl. Acad. Sci. U. S. A.* **2002**, *99* (4), 1763–1768.

(32) Bhattacharyya, S. M.; Wang, Z. G.; Zewail, A. H. Dynamics of Water near a Protein Surface. *J. Phys. Chem. B* **2003**, *107* (47), 13218–13228. https://doi.org/10.1021/jp030943t.

(33) Mukherjee, S.; Mondal, S.; Bagchi, B. Distinguishing Dynamical Features of Water inside Protein Hydration Layer: Distribution Reveals What Is Hidden behind the Average. *J. Chem. Phys* **2017**, *147* (2), 024901. https://doi.org/10.1063/1.4990693.

(34) Bhattacharyya, K. Nature of Biological Water: A Femtosecond Study. *Chem Commun.* Royal Society of Chemistry 2008, pp 2848–2857. https://doi.org/10.1039/b800278a.

(35) Frauenfelder, H.; Fenimore, P. W.; McMahon, B. H. Hydration, Slaving and Protein Function. *Biophys. Chem.* **2002**, *98* (1–2), 35–48. https://doi.org/10.1016/S0301-4622(02)00083-2.

(36) Frauenfelder, H.; Chen, G.; Berendzen, J.; Fenimore, P. W.; Jansson, H.; McMahon, B. H.; Stroe, I. R.; Swenson, J.; Young, R. D. A Unified Model of Protein Dynamics. *Proc. Natl. Acad. Sci. U. S. A.* **2009**, *106* (13), 5129–5134. https://doi.org/10.1073/pnas.0900336106.

(37) Khan, T.; Das, N.; Negi, K. S.; Bhowmik, S.; Sen, P. Understanding the Intricacy of Protein in Hydrated Deep Eutectic Solvent: Solvation Dynamics, Conformational Fluctuation Dynamics, and Stability. *Int. J. Biol. Macromol.* **2023**, *253* (P5), 127100. https://doi.org/10.1016/j.ijbiomac.2023.127100.

(38) Horng, M. L.; Gardecki, J. A.; Papazyan, A.; Maroncelli, M. Subpicosecond Measurements of Polar Solvation Dynamics: Coumarin 153 Revisited. *J. Phys. Chem* **1995**, *99* (48), 17311–17337. https://doi.org/10.1021/j100048a004.

(39) Maroncelli, M.; Fleming, G. R. Picosecond Solvation Dynamics of Coumarin 153: The Importance of Molecular Aspects of Solvation. *J Chem Phys* **1987**, *86* (11), 6221–6239. https://doi.org/10.1063/1.452460.

(40) Kamal, J. K. A.; Zhao, L.; Zewail, A. H. Ultrafast Hydration Dynamics in Protein Unfolding: Human Serum Albumin. *Proc. Natl. Acad. Sci* **2004**, *101* (37), 13411–13416.

(41) Nandi, N.; Bagchi, B. Dielectric Relaxation of Biological Water. *J Phys Chem B* **1997**, *101* (50), 10954–10961.

(42) Qin, Y.; Wang, L.; Zhong, D. Dynamics and Mechanism of Ultrafast Water-Protein Interactions. *Proc Natl Acad Sci U S A* **2016**, *113* (30), 8424–8429. https://doi.org/10.1073/pnas.1602916113.

(43) Qin, Y.; Jia, M.; Yang, J.; Wang, D.; Wang, L.; Xu, J.; Zhong, D. Molecular Origin of Ultrafast Water-Protein Coupled Interactions. *Journal of Physical Chemistry Letters* **2016**, *7* (20), 4171–4177. https://doi.org/10.1021/acs.jpclett.6b01954.

(44) Houston, P.; Macro, N.; Kang, M.; Chen, L.; Yang, J.; Wang, L.; Wu, Z.; Zhong, D. Ultrafast Dynamics of Water-Protein Coupled Motions around the Surface of Eye Crystallin. *J. Am. Chem. Soc.* **2020**, *142* (8), 3997–4007. https://doi.org/10.1021/jacs.9b13506.

(45) Buchenberg, S.; Schaudinnus, N.; Stock, G. Hierarchical Biomolecular Dynamics: Picosecond Hydrogen Bonding Regulates Microsecond Conformational Transitions. *J. Chem. Theory Comput.* **2015**, *11* (3), 1330–1336. https://doi.org/10.1021/ct501156t.

(46) Jha, A.; Ishii, K.; Udgaonkar, J. B.; Tahara, T.; Krishnamoorthy, G. Exploration of the Correlation between Solvation Dynamics and Internal Dynamics of a Protein. *Biochemistry* **2011**, *50* (3), 397–408. https://doi.org/10.1021/bi101440c.

(47) Sherman, E.; Itkin, A.; Kuttner, Y. Y.; Rhoades, E.; Amir, D.; Haas, E.; Haran, G. Using Fluorescence Correlation Spectroscopy to Study Conformational Changes in Denatured Proteins. *Biophys J* **2008**, *94* (12), 4819–4827. https://doi.org/10.1529/biophysj.107.120220.

(48) Basak, S.; Chattopadhyay, K. Studies of Protein Folding and Dynamics Using Single Molecule Fluorescence Spectroscopy. *Phys. Chem. Chem. Phys.* **2014**, *16* (23), 11139–11149. https://doi.org/10.1039/c3cp55219e.

(49) Chattopadhyay, K.; Saffarian, S.; Elson, E. L.; Frieden, C. Measuring Unfolding of Proteins in the Presence of Denaturant Using Fluorescence Correlation Spectroscopy. *Biophys J* **2005**, *88* (2), 1413–1422. https://doi.org/10.1529/biophysj.104.053199.

(50) Das, N.; Khan, T.; Subba, N.; Sen, P. Correlating Bromelain's Activity with Its Structure and Active-Site Dynamics and the Medium's Physical Properties in a Hydrated Deep Eutectic Solvent. *Phys. Chem. Chem. Phys* **2021**, *23* (15), 9337–9346. https://doi.org/10.1039/d1cp00046b.

(51) Chattopadhyay, K.; Saffarian, S.; Elson, E. L.; Frieden, C. Measurement of Microsecond Dynamic Motion in the Intestinal Fatty Acid Binding Protein by Using Fluorescence Correlation Spectroscopy. *Proc. Natl. Acad. Sci. U. S. A.* **2002**, *99* (22), 14171–14176. https://doi.org/10.1073/pnas.172524899.

(52) Nandy, A.; Chakraborty, S.; Nandi, S.; Bhattacharyya, K.; Mukherjee, S. Structure, Activity, and Dynamics of Human Serum Albumin in a Crowded Pluronic F127 Hydrogel. *J. Phys. Chem. B* **2019**, *123* (16), 3397–3408. https://doi.org/10.1021/acs.jpcb.9b00219.

(53) Sasmal, D. K.; Mondal, T.; Sen Mojumdar, S.; Choudhury, A.; Banerjee, R.; Bhattacharyya, K. An FCS Study of Unfolding and Refolding of CPM-Labeled Human Serum Albumin: Role of Ionic Liquid. *J. Phys. Chem. B* **2011**, *115* (44), 13075–13083. https://doi.org/10.1021/jp207829y.

(54) Krichevsky, O.; Bonnet, G. Fluorescence Correlation Spectroscopy: The Technique and Its Applications. *Rep. Prog. Phys.* **2002**, *65* (2), 251–297. https://doi.org/10.1088/0034-4885/65/2/203.

(55) McMahon, B. H.; Frauenfelder, H.; Fenimore, P. W. The Role of Continuous and Discrete Water Structures in Protein Function. *Eur. Phys. J. Spec. Top* **2014**, *223* (5), 915–926. https://doi.org/10.1140/epjst/e2014-02125-y.

(56) Fenimore, P. W.; Frauenfelder, H.; McMahon, B. H.; Young, R. D. Bulk-Solvent and Hydration-Shell Fluctuations, Similar to α- and β-Fluctuations in Glasses, Control Protein Motions and Functions. *Proc. Natl. Acad. Sci. U. S. A.* **2004**, *101* (40), 14408–14413. https://doi.org/10.1073/pnas.0405573101.

This page left blank intentionally

Chapter 6

Dropping the Guard: How Denaturants Undermine Osmolyte-Mediated Protection

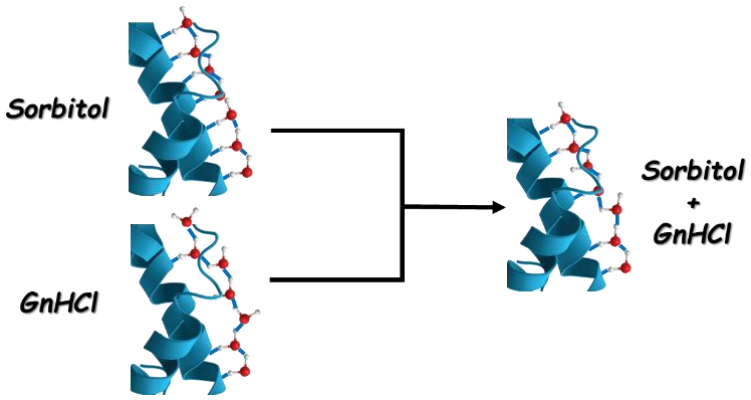

Kuldeep Singh Negi, Subhajit Rana, Tanmoy Khan and Pratik Sen

Manuscript under preparation

Abstract

Deciphering how stabilizing osmolytes and destabilizing agents modulate protein stability is essential for understanding protein folding and function under cellular stress. In this study, we explore the mechanism by which a chemical denaturant counteracts the stabilizing effect of an osmolyte on the protease papain. Building on our proposed Associated Water Stabilization Mechanism (AWSM), we demonstrate that sorbitol enhances protein thermal stability by strengthening water–water and water–protein surface interactions, which in turn promote cohesive bonding among core amino acid residues. Conversely, guanidinium hydrochloride (GnHCl) disrupts these hydration networks and weakens residue-residue interactions, leading to destabilization. When both osmolyte (sorbitol) and denaturant (GnHCl) are present together, GnHCl diminishes the efficacy of sorbitol by reducing its ability to enhance the local water structure, thereby attenuating the strengthening of the protein's interior and thereby counteract the stabilizing effect of sorbitol on thermal stability of papain. Our findings indicate that the counteracting influence of GnHCl on sorbitol-induced stabilization can be understood within the AWSM framework. Apart from a weak direct interaction between sorbitol and GnHCl, their opposing impacts on hydration dynamics also contribute to the counteraction effect. This study highlights AWSM as a promising conceptual tool for understanding protein-osmolyte interactions and offers molecular-level insight into how chemical environments govern protein stability.

6.1. Introduction

Proteins are fundamental to virtually every biological process, acting as enzymes, structural components, signalling molecules, and more. The ability of a protein to perform its function depends critically on the integrity of its three-dimensional structure, which is maintained through a delicate balance of non-covalent interactions such as hydrogen bonding, hydrophobic interactions, and electrostatic forces [1,2]. However, this native conformation is only marginally stable and can be easily perturbed by changes in environmental conditions such as temperature, pH, ionic strength, or the presence of chemical agents [3,4].

To combat these destabilizing influences, many organisms accumulate small organic molecules known as osmolytes. These compounds, which include sugars, polyols, amino acids, and methylamines, are known to stabilize protein structure [4]. Despite several proposed theories, the mechanism of protein–osmolyte interactions remains vague and needs deeper exploration due to its significance [3]. Timasheff and group suggested that proteins stabilize when solute concentration is lower at the protein surface than in the bulk, a concept based on surface tension [5–11]. Bolen and coworkers supported this with experimental evidence, showing that stabilizing osmolytes repel the protein surface known as the preferential interaction theory [12–14]. However, direct surface tension measurements at the protein-solvent interface are technically challenging [15]. Another view, the water structure modulation hypothesis, proposes that water actively enhances protein stability by strengthening its hydrogen-bond network in the presence of osmolyte solutions [15]. Hishida et al. found protein stability correlates with enhanced water structure near osmolytes [16–18]. The water structure modulation hypothesis is opposed in literature while describing the destabilizing effect of denaturants on protein though water structure weakening effect [19–24]. Recently a hypothesis named Associated Water Stabilization Mechanism (AWSM) has been put forward by our group to explain the protein-osmolyte interactions, where the thermal stabilization of protein in osmolyte is shown to be an outcome of the strengthened interior (retarded conformational dynamics) of the

protein caused by the osmolyte strengthened water-residue and water-water bonding (retarded associated water dynamics) at the protein surface [25–30]. This theory has advantage over others in explaining the protein-osmolyte interactions that are protein specific in nature which are otherwise not possible to understand by traditional theories [27].

The biological relevance of studying the counteraction between osmolytes and denaturants lies in understanding how cells maintain protein homeostasis under stress. In vivo, proteins are often exposed to competing influences of stabilizing osmolytes and destabilizing agents such as urea or GnHCl particularly under pathological or extreme environmental conditions [31]. Deciphering the interplay between these opposing forces can shed light on protein folding diseases, cellular stress responses, and the development of therapeutic formulations. Sorbitol, a sugar alcohol, is one such osmolyte that is widely recognized for its ability to enhance protein thermal stability and biological significance [3]. Conversely, denaturants such as guanidinium hydrochloride (GnHCl) exert the opposite effect and known to counteract the stabilizing effect of osmolytes [32]. In this study, we aim to dissect the counteracting effects of sorbitol and GnHCl on protein thermal stability, using model proteins and spectroscopic techniques. We focus specifically on how changes in hydration-layer dynamics and intra-protein interactions, following the AWSM hypothesis, contribute in counteraction of the stabilizing effect of osmolyte on protein by denaturant. By systematically varying the concentrations of sorbitol and GnHCl, we seek to understand the molecular basis of this antagonistic interaction and its implications for protein stability in complex biological environments. This study might help in understanding the protein-osmolyte interaction in depth.

6.2 Results and Discussion

Proteins are dynamic and highly sensitive to environmental changes such as temperature, pressure, pH, and salinity [3]. These perturbations can alter protein

conformation by shifting the equilibrium between folded (native) and unfolded (denatured) states, a process known as denaturation or melting. Heat typically drives this equilibrium toward the unfolded state [20,33–35]. In this study, thermal denaturation is monitored using fluorescence spectroscopy, leveraging the solvatochromic response of intrinsic fluorescent residues like tryptophan [36,37]. As these tryptophan residues are spread all over the protein as is shown in figure 1(a) providing information over the whole denaturation of the protein. The protein interior is composed of less polar residues, making it relatively hydrophobic, while the surrounding aqueous environment is hydrophilic [36]. Upon unfolding, buried tryptophan residues gets exposed to polar water molecules. As temperature increases, unfolding occurs, leading to a red shift in the emission spectrum (excited at 295 nm) due to the positive solvatochromic response of tryptophan [27,36]. and is illustrated by the shift in the emission maximum in figure 1(d). The melting plot of papain in buffer shown in figure 1(d) is normalized (shown by violet dots) by employing the equation 6.2.1 as shown in figure 1(e).

$$f_D = \frac{\lambda_i - \lambda_N}{\lambda_D - \lambda_N} \tag{6.2.1}$$

where λ_i, represents the emission maximum corresponding to any temperature i, λ_N represents the emission maximum representative of the native state and λ_D represents the emission maximum representative of the denatured state of the protein under thermal study. The melting plot of a protein in a solvent system is used to describe its stability. The temperature at which the native and the denatured conformations are equally populated (described by $f_D = 0.5$), the protein system is said to be half denatured and is qualitatively called the melting temperature (denaturation temperature, T_m) of the protein as shown by the red dot in figure 1(e). The normalized melting plot is then fitted using equation 6.2.2 to quantify the melting temperature of the buffer and is represented by the x_half [27].

$$y = a + b/(1 + \exp\,(x\_half - x))/d)) \quad (6.2.2)$$

where "a" represents the value of lower asymptote which is taken as 0 and signifies native state $(i.e.,\ f_N = 0)$, "b" represents the distance from 'a' to the upper asymptote which is taken as 1 and signifies the denatured state $(i.e.,\ f_D = 1)$, "x_half" represents the inflection point and signifies the melting temperature (T_m) and "d" represents the distance from x_half of the zone of compliance. The melting temperature of papain is found ~ 355 K which matches well with the previous literature [27]. Here in this study to probe the mechanism of counteraction of the stabilizing effect of osmolyte by denaturant we have employed sorbitol as model stabilizer and GnHCl as model destabilizer or denaturant as shown in figure 1(b) and 1(c) respectively. To measure the thermal stability of papain in the presence of sorbitol, GnHCl and in the 1:1 molar ratio of the two, the same procedure has been followed and melting plots are given in Figure 2. As expected with the addition of 1M sorbitol the melting temperature of the papain increases and reaches a value of ~ 359 K. The increased value of T_m in 1M of sorbitol relative to buffer signifies the stabilizing effect of sorbitol on the thermal stability of papain. The addition of 1M of GnHCl destabilizes the protein as is evident by the T_m of ~350 K which is less than that in buffer only system. If GnHCl counteracts the stabilizing effect of sorbitol on papain, the mixture of sorbitol and GnHCl is expected to have melting temperature in between that of GnHCl only and sorbitol only system. The experimental value of T_m in 1:1 molar solution of GnHCl and sorbitol is measured ~353 K and has seemed to lie in between the GnHCl (1M) only and sorbitol (1M) only system. This clearly shows that the extra stability that has been provided by the sorbitol $(T_m = 359\ K)$ to papain $(T_m = 355\ K)$ has been counteracted by the presence of GnHCl $(T_m = 353\ K)$. The order of thermal stability is as follows

$$T_m(GnHCl(1M)) < T_m(Sorbitol(1M) + GnHCl(1M)) < T_m(Buffer) < T_m(Sorbitol\ (1M))$$

This observation justifies the counteraction of stabilizing effect of sorbitol by GnHCl.

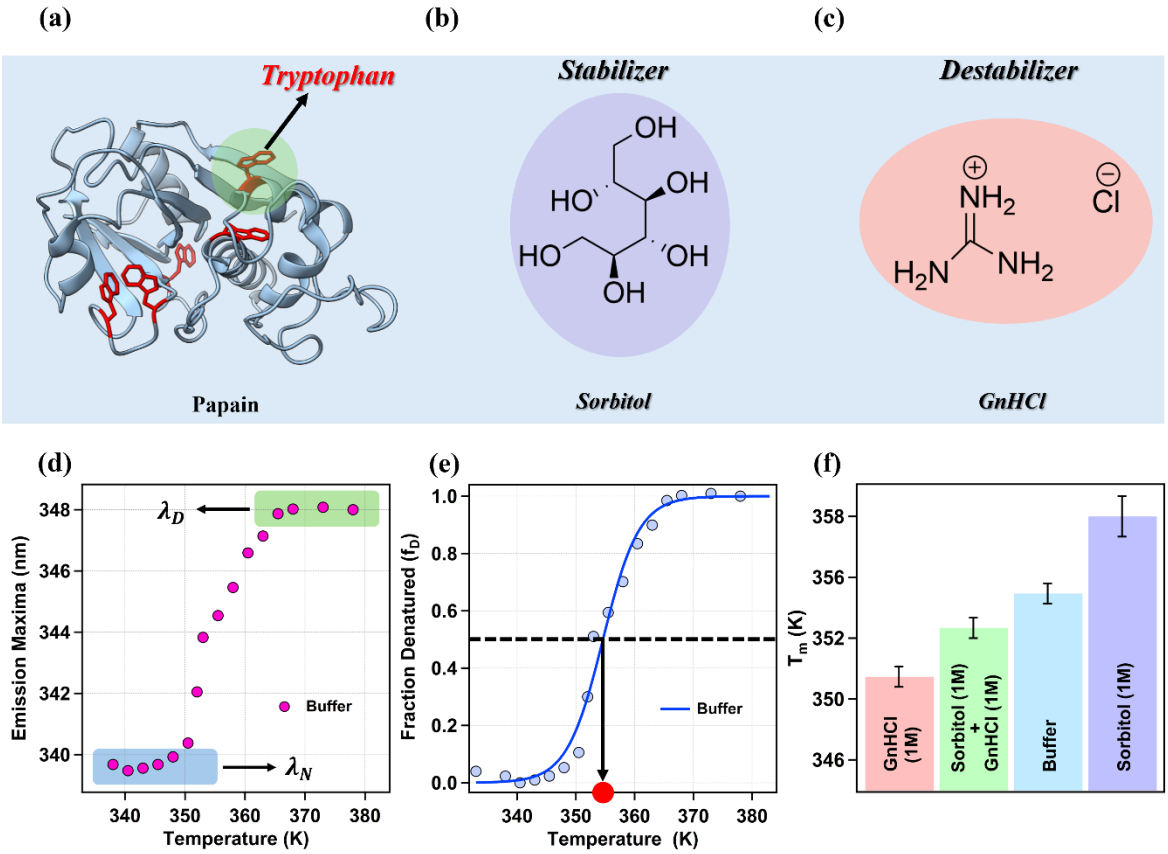

Figure 1: Representation of the (a) distribution of tryptophan residues in papain (b) sorbitol as stabilizer (c) GnHCl as destabilizer. Variation in the (d) emission maximum of papain (excited at 295nm) in buffer with temperature where, $\lambda_N = 339\ nm$ and $\lambda_D = 348\ nm$ are the signature wavelength for the native and the denatured state of papain in buffer respectively. (e) Normalized plot representing the fraction of denatured papain at corresponding temperature fitted with a sigmoidal function represented by equation 6.2.2 to determine the melting temperature (T_m). (f) variation of the melting temperature of papain in the presence and absence of sorbitol (1M), GnHCl (1M) and the 1:1 molar mixture of two.

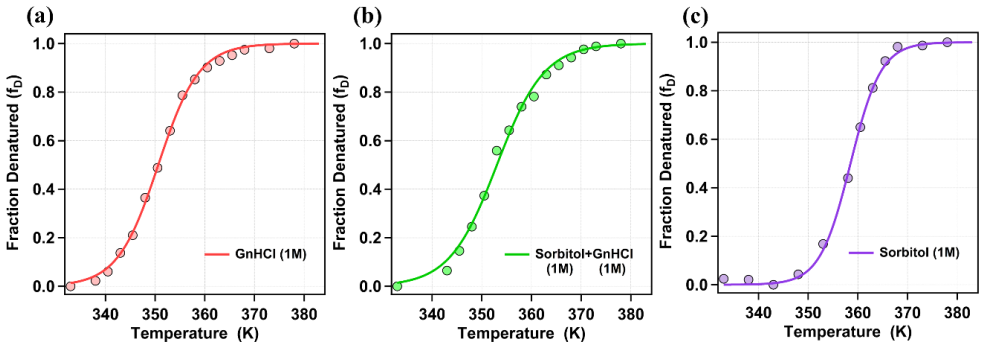

Figure 2: Melting plots of papain in aqueous solution of (a) GnHCl (1M), (b) Sorbitol (1M)+GnHCl (1M) and (c) Sorbitol (1M).

The reduction in the stabilizing power of the osmolyte in the presence of denaturant is believed to translate through the direct interaction of the denaturant with the osmolyte molecules but the strength of the interaction among the two is considered not enough to translate this phenomenon of counteraction effectively [31]. Recently a mechanism has been proposed by our group to understand the stabilizing effect of osmolyte on the thermal stability of the protein and is known as Associated Water Stabilization Mechanism (AWSM) [25–30,37]. This theory states that the osmolyte stabilizes the protein by strengthening the interior of the protein which is indirectly translated by the osmolyte induced strengthening of the bonding among the water-water and water-amino acid residues of the protein and denaturants does the opposite [27]. To understand the mechanism of counteraction we have employed the approach proposed by the AWSM hypothesis. Application of this theory needs to probe the bonding between the water-water molecules and water-amino acid residues in the hydration layer of the protein, and among the residues within the protein. We have gathered information on bonding between the water-water molecules and water-amino acid residues by performing the solvation study to probe the associated water dynamics and performed the conformational dynamics study to probe the interior of the protein providing information on the bonding among the amino acid residues.

The solvation study is performed on the fluorescently labelled CPM tag papain where the CPM dye is cite specifically tagged to Cys-25 of papain as shown in figure

3(a). During excitation using laser pulse ($\lambda_{ex} = 375nm$) the attached fluorophore to the proteins, CPM gets excited. Upon excitation, the dipole moment of CPM increases in the excited state. Since excitation is instantaneous, solvent molecules initially retain their ground-state arrangement, creating a thermodynamically unstable environment. To stabilize the system, the solvent dipoles reorient around the new dipole of the excited dye, this process is known as solvent relaxation [38,39]. By employing the solvation methodology, we got the emission spectrum of the fluorophore corresponding to different energy states observed at the respective times during the relaxation process known as Time resolved Emission Spectra (TRES) and after normalization are shown in figure 3(b). The emission maxima of representative emission spectra are plotted against the corresponding time as depicted in figure 3(c) and is normalized to generate the solvent response function (S(t)) by employing equation 6.2.3 as shown in figure 3(d) by violet dots.

$$S(t) = \frac{\bar{\nu}(t) - \bar{\nu}(\infty)}{\bar{\nu}(0) - \bar{\nu}(\infty)} \quad (6.2.3)$$

S(t) is fitted using the biexponential equation as shown in figure 3(d) shown by violet line. The same procedure has been carried out with other systems and the solvent response function along with fitting for other osmolyte systems are provided in Figure 4.

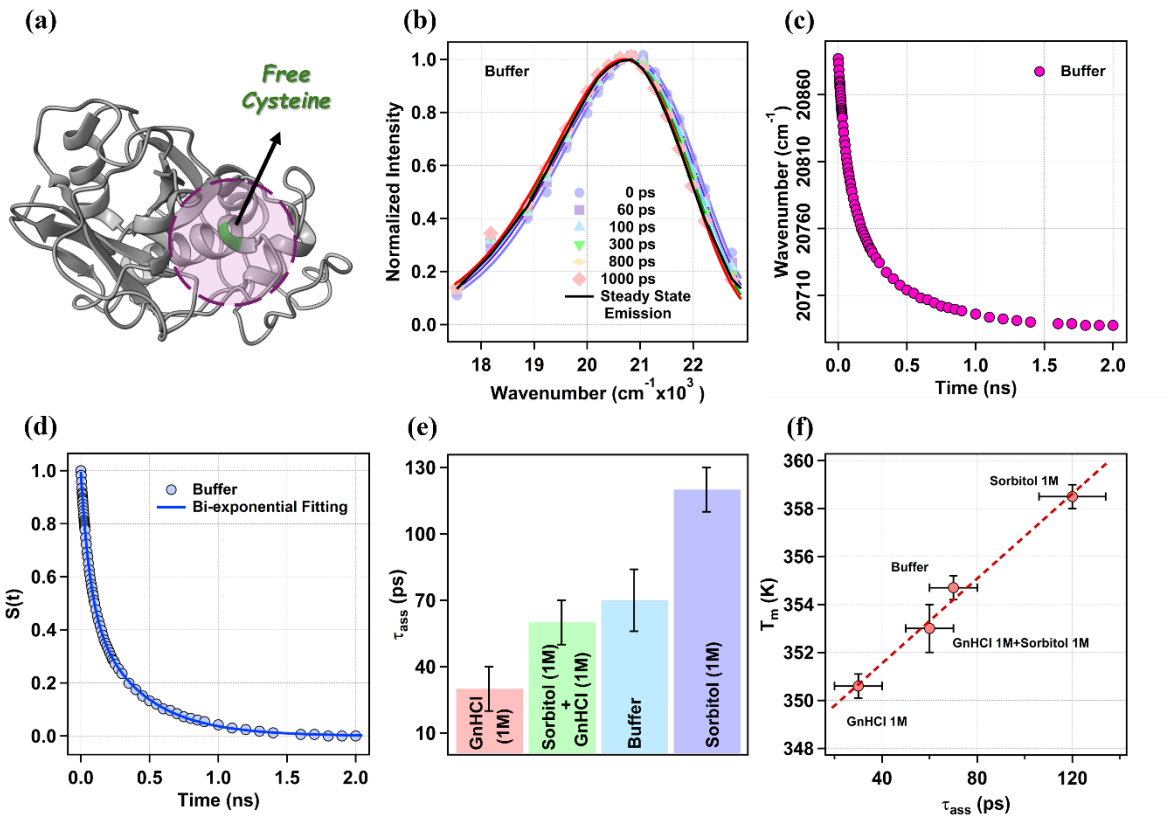

Figure 2: (a) Schematic representation of the free cysteine (green) in papain to which the CPM dye is attached. (b) The normalized time resolved emission spectra (TRES) for papain in buffer. The relaxation of the excited state represented by the (c) variation of the corresponding wavenumber maximum of the representative emission spectra with time and is normalized using the equation 6.2.3 to get the (d) solvent correlation function S(t) along with the fitting line obtained by employing the biexponential function. (e) Variation in the associated water dynamics (τ_{ass}) of CPM tag papain in the presence and absence of sorbitol (1M), GnHCl (1M) and the 1:1 molar mixture of two. (f) Correlation depicting the modulation in the melting temperature (T_m) with the associated water dynamics (τ_{ass}). Experiments were performed at 298 K.

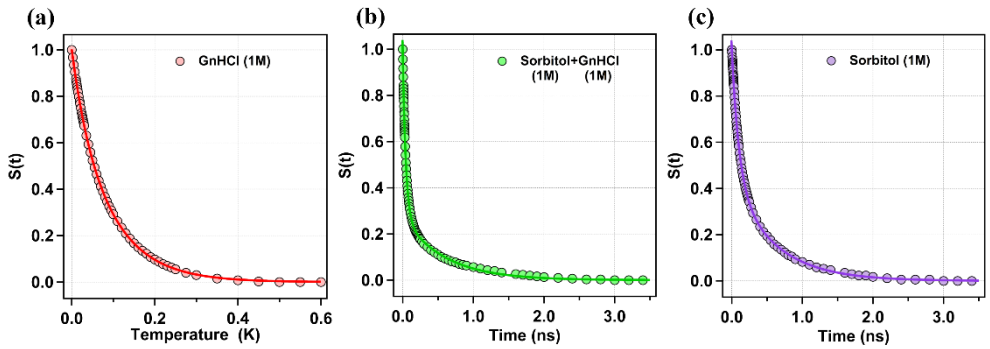

Figure 4: Solvent response function of papain in aqueous solution of (a) GnHCl (1M), (b) Sorbitol (1M)+GnHCl (1M) and (c) Sorbitol (1M). Experiments were performed at 298 K.

Proteins generally show a broad spectrum of solvation events in the picosecond (ps) to nanosecond (ns) range, where the event with time scale of ~1ps comes from the water motions in the bulk [40,41]. The relaxation in the time range ~ 5ps is from the frustrated motions of the water molecules in the protein hydration layer [42–46]. The dynamics in the range ~ 20ps – 200ps originates from the concerted motions of the protein side chains and the water molecules attached to these side chains on the protein surface [45,47–52]. These motions are known to be initiated by the overall network movement of water molecules in the hydration layer [27]. To distinguish this slow motion originating from the water network from the faster motions of the frustrated water molecules in the hydration layer, the dynamics linked with these motions are entitled as associated water dynamics. The dynamics >200ps comes from the various protein motions [53]. As stated earlier, we aim to probe the associated water layer, focusing on motions involving both water and protein. Given the characteristic motions of proteins, this aligns with the dynamics of associated water, typically occurring on the 20–200 ps timescale and the instrument used here i.e., TCSPC (with an IRF ~75ps and detection capability of dynamics as fast as ~30ps with sharp precision) is suitable for observing dynamics in this range provided the protein shows the associated water dynamics (τ_{ass}) in the range ≥30ps. For papain, the value of τ_{ass} is observed experimentally around 70ps (figure 3(e)) in buffer only system which matches well with our previous publication. We have experimentally found out that the value of τ_{ass} increases to ~ 120ps with 1M sorbitol solution and decreases to 30ps in the presence of 1M GnHCl as shown in figure 3(e). This clearly shows the retardation in associated water dynamics in the presence of 1M sorbitol and acceleration in the presence of 1M GnHCl. When the CPM tag papain is added to a mixed solution of 1M sorbitol and 1M GnHCl the value of τ_{ass} becomes 50ps which lies in between that of pure 1M GnHCl($\tau_{ass} = 30ps$) and 1M sorbitol

($\tau_{ass} = 120ps$) as depicted in figure 3(e). It appears to be very close to that of papain in buffer ($\tau_{ass} = 70ps$). The retardation in the associated water dynamics follows the order

$$\tau_{ass}(GnHCl(1M)) < \tau_{ass}(Sorbitol(1M) + GnHCl(1M)) < \tau_{ass}(Buffer) < \tau_{ass}(Sorbitol\ (1M))$$

This clearly shows the counteraction of the retardation in the associated water dynamics of papain induced by the 1M sorbitol ($\tau_{ass} \sim 120ps$) because of the presence of 1M GnHCl ($\tau_{ass} \sim 50ps$).

As per the theory, the solute system in the presence of which the associated water dynamics of the protein gets retarded relative to buffer, the protein under observation will be get thermally stabilized and vice-versa. If the theory is capable to explain the counteraction of stabilizing effect of sorbitol by GnHCl, the solvent system where the associated water dynamics of the papain gets retarded relative to buffer only system as is the case with 1M sorbitol the thermal stability of the papain is expected to get enhanced and where the associated water dynamics of the papain gets accelerated relative to buffer as is the case with 1M GnHCl, the thermal stability of the protein is expected to be get reduced. As the associated water dynamics in the mixture of 1M sorbitol and 1M GnHCl accelerates relative to buffer only system the thermal stability of the protein is expected to be less than that of buffer. To understand how the associated water dynamics (τ_{ass}) of papain correlate with the thermal stability (T_m) of the papain in different solvent systems employed here we have plotted τ_{ass} against T_m as shown in figure 3(f). We have observed that with 1M sorbitol, the papain gets thermally stabilized and with 1M GnHCl the papain gets thermally destabilized. The papain gets thermally destabilized in the mixture of 1M sorbitol and 1M GnHCl relative to buffer. All the observation through the correlation

plot goes parallel with the expectation as per the hypothesis. It could be concluded here that the sorbitol enhances the associated water structure around the protein as is confirmed by the increased value of τ_{ass} and thus the protein gets thermal stabilization but as the incorporation of GnHCl weakens the water structure as evidence by the reduced value of τ_{ass} and the protein gets thermally destabilized. As sorbitol and GnHCl are having opposite effect on the water structure, the counteraction of the thermal stabilization of papain in the presence of sorbitol by GnHCl could be understood in terms of reduction is the water enhancement capability of sorbitol by the presence of GnHCl which has water structure weakening property.

The correlation plot in figure 2(f) just provides a relation between the associated water dynamics and the thermal stability but doesn't provide molecular insights to understand the phenomenon in depth and left us with a thought of how the modulation in associated water dynamics helps the denaturant molecules to counteract the stabilizing effect of stabilizer. Since hydration-layer water molecules are in direct interaction with the protein surface, changes in their dynamics or arrangement can influence intramolecular bonding among amino acid residues within the protein. This changed energetics among the residues might bring about the change in the overall thermodynamics of the protein and thus might also alter the thermal stability of the protein which might help in understanding the counteraction mechanism in detail [53,54]. In our recent study, we provide mechanistic insight into this phenomenon by establishing a strong link between associated water modulation and conformational fluctuation dynamics in the presence of osmolytes [27]. To understand how changes in associated water dynamics translate into altered thermal stabilization, the protein interior must be examined. However, with hydrodynamic radii typically in the Ångström range, direct observation of subtle changes in the interior of the protein is challenging. Therefore, the interior must be probed indirectly. For this we have employed fluorescence correlation spectroscopy (FCS) as a tool where an observation volume in femtolitre dimension is formed using the

laser source ($\lambda_{ex} = 532\ nm$) and the fluctuations in the emission intensity of the fluorophore with time is measured in two different detectors which are then correlated by giving the time lag to produce a cross-correlation function [55–57] ($G(\tau)\ vs\ time$). A detailed discussion on the instrumentation can be found in our recent literature [27]. The dynamics of any event that induces the changes in the intensity of the fluorophore can be probed here, provided the dynamics must not be slower than the diffusion dynamics of the fluorophore in the observation volume and should not be faster than the detection limit of the overall FCS setup [35]. Here we have employed TMR tag papain, where the TMR dye is attached to Cys-25 of papain, for the FCS study as shown in figure 5(a) [27]. The TMR is surrounded by five tryptophan residues positioned at distinct locations from the free cysteine residue (CYS 25) of papain to which the TMR dye is attached. The fluorescence intensity of tagged TMR is expected to be quenched by the interaction of the π cloud of the tryptophan residues which is evident in other studies as well and as the interaction depends on the distance of the quencher from the fluorophore, the quenching is expected to be dominated with the nearest tryptophan residue (TRP 177) [35,57]. The quenching will be influenced by other relatively distant tryptophan residues as all are within the proximity of the attached TMR dye owing to the small size of the papain $\left(R_h = \sim 18\ \text{Å}\right)$. Free (untagged) TMR dye shows a triplet state dynamics in the microsecond time scale. On being attached covalently to the free cysteine of the papain, the inherent microsecond triplet state dynamics of the TMR dye is expected to be observed in the case of TMR tagged papain as well with a slight modulation in the absolute value [56,58]. Based on the discussion, TMR-tagged papain is expected to exhibit three types of dynamics: diffusion, conformational changes due to quenching by nearby tryptophan residues, and the intrinsic triplet-state dynamics of the TMR dye [27].

The cross-correlation function for papain in buffer only system is shown in figure 5(b) which is then fitted by various equations. From the residuals of fitting the model with one diffusion and 2 exponential term is observed to be the most suitable as this

model reasonably accounts for the existence of three different dynamics in the system [27,58]. The normalized cross correlation plot with fitting by employing equation 6.2.4 is shown in figure 5(c).

$$G(\tau) = \frac{1}{N}\left(1+\frac{\tau}{\tau_D}\right)^{-1}\left(1+\frac{\tau}{\omega^2\tau_D}\right)^{-\frac{1}{2}}\left(1+K\,exp\left(-\frac{\tau}{\tau_R}\right)\right)\left(1+\frac{p}{1-p}\,exp\left(-\frac{\tau}{\tau_T}\right)\right) \quad (6.2.4)$$

Fitting gives three different events with time constants ~ $5\mu s$, ~ $41\mu s$ and ~ $120\mu s$. As the event associated with the diffusion of TMR papain through the observation volume is supposed to be the slowest one and thus the dynamics with time constant ~ $120\mu s$ is ascribed to diffusion. Of the two faster events, the ~41 μs component arises from conformational dynamics, as confirmed in our previous work by its invariance with change in observation volume. The ~5 μs event originates from the triplet-state dynamics of the TMR dye, also validated previously by the observed increase in triplet population with increasing laser power [27].

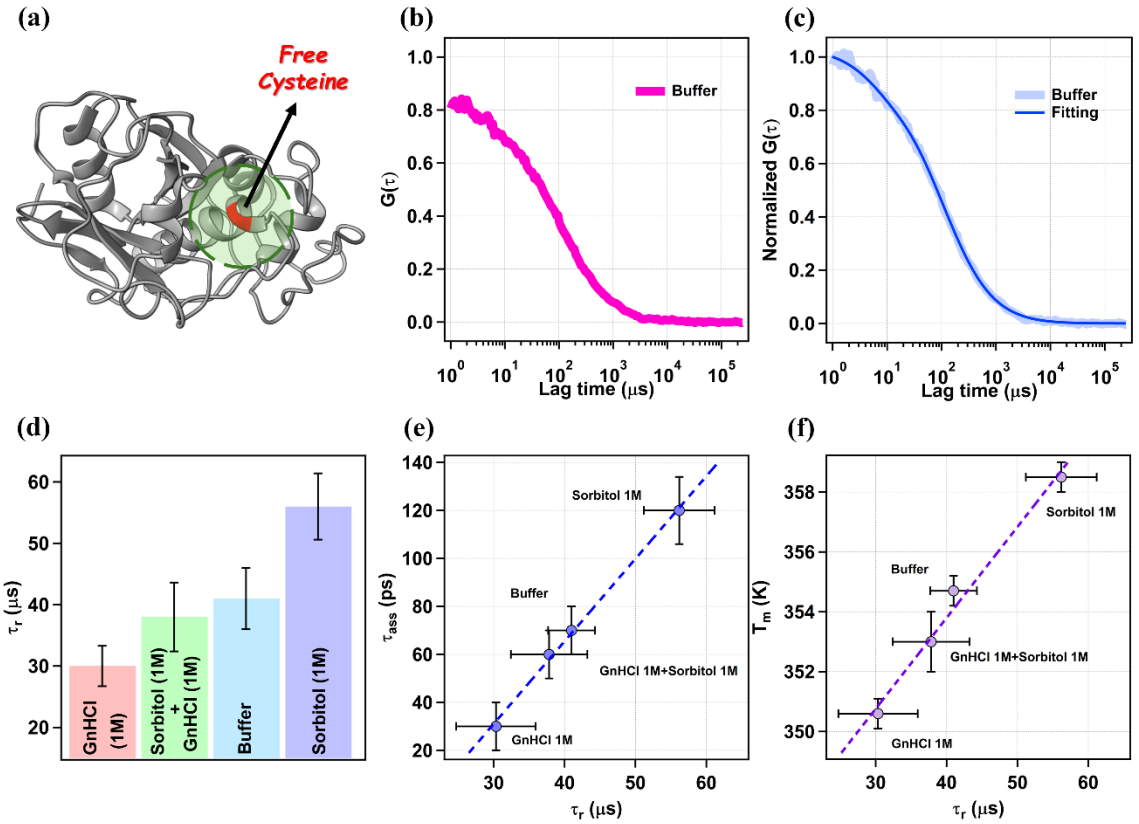

Figure 3: (a) Schematic representation of the free cysteine (green) in papain to which the TMR dye is attached. (b) Cross-correlation function for papain in buffer and (c) normalized cross-correlation function for TMR tag papain in buffer with the fitting line by employing equation 6.2.4. (d) Variation in the conformational dynamics (τ_r) of TMR tag papain in buffer (light blue), 1M GnHCl (light red) and 1M Sorbitol (light violet) and 1M sorbitol+1M GnHCl (light green). Correlation of the conformational dynamics (τ_r) with (e) associated water dynamics (τ_{ass}) and (f) thermal stability (T_m) of papain. Experiments were performed at 298 K.

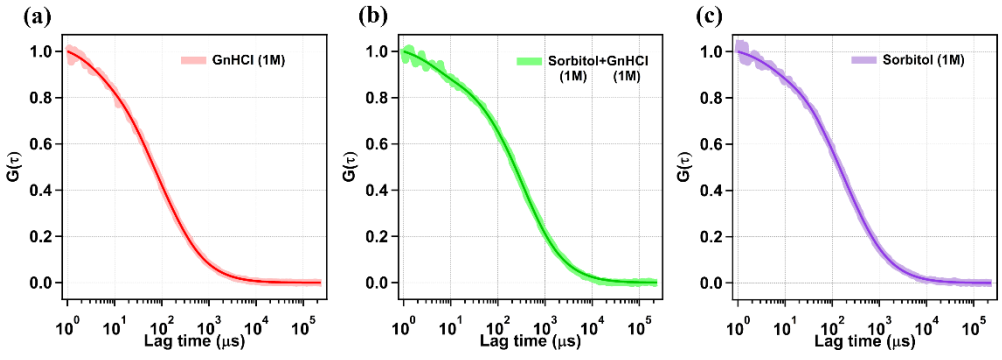

Figure 4: Cross-correlation plots along with fitting for papain in aqueous solution of (a) GnHCl (1M), (b) Sorbitol (1M)+GnHCl (1M) and (c) Sorbitol (1M). Experiments were performed at 298 K.

The time constant associated with the conformational dynamics (τ_R) of papain is observed ~ $41\mu s$ which matches closely with our previous study [30]. The value of τ_R increases to ~ $56\mu s$ and decreases to ~ $30\mu s$ with 1M sorbitol and 1M GnHCl as shown in figure 5(d). With the mixture containing 1M sorbitol along with 1M GnHCl the value of τ_R is experimentally observed ~ $38\mu s$ which is close to that observed in case of buffer only system. The normalized correlation plots for papain with other osmolyte systems are shown in Figure 6. The addition of 1M sorbitol ($\tau_R \sim 56\mu s$) retards whereas the presence of 1M GnHCl ($\tau_R \sim 30\mu s$) accelerates the conformational dynamics if compared to buffer ($\tau_R \sim 41\mu s$) only system. The addition of 1M GnHCl to 1M sorbitol ($\tau_R \sim 38\mu s$) also retards the conformational dynamics relative to 1M sorbitol ($\tau_R \sim 56\mu s$). This clearly shows the counteraction of the retardation in the conformational dynamics of papain induced by the 1M sorbitol ($\tau_R \sim 56\mu s$) by the 1M GnHCl ($\tau_R \sim 38\mu s$).

The retardation in the conformational dynamics of the protein could be because of the two mere reasons. First being the increase in the modulation in the associated water dynamics and second being the bulk viscosity of the solution brought out by the addition of osmolyte. This notion has also been supported by the findings of the work done by one of the pioneers in the field of protein science i.e., Hans Frauenfelder, who showed that the large scale motions of the proteins are controlled by the viscosity of the solvent and the small scale motions are dictated by the modulation in the properties of the water molecules in the direct contact of the protein surface for which we have used the terminology, associated water [59–62]. Both the factors might impact the conformational dynamics of the protein in the microsecond regime whereas it has recently been observed in our recent publication that the modulation in the associated water dynamics has a pronounced effect on conformational dynamics in microsecond regime over the viscosity [27]. To seek for the molecular insight over how the osmolyte induced modulation in associated water impacts the interior of the protein we have plotted τ_{ass} against τ_R in figure 5(e). The correlation between the τ_{ass} and τ_R in figure 5(e) describes somewhat straight-line

relation which imply that the solute system where there is a retardation in the associated water dynamics it is followed by the retardation in the conformational dynamics. The presence of 1M GnHCl in 1M sorbitol ($\tau_R \sim 38\mu s, \tau_{ass} \sim 50ps$) counteracts the retardation in the associated water dynamics relative to the 1M sorbitol solution ($\tau_R \sim 56\mu s, \tau_{ass} \sim 120ps$) and the same counteraction phenomenon has also been observed with the conformational dynamics of the papain. The observed link between associated water dynamics and conformational dynamics may be due to the direct contact between hydration-layer water molecules and surface residues of the protein. These surface residues are connected to the core residues through physical bonds, such as hydrogen bonds. Therefore, any change in water-water or water-residue interactions at the surface captured through associated water dynamics might influence the internal bonding within the protein, reflected as conformational dynamics. as is depicted in figure 5(e). The connected nature of the two dynamics suggests that the bond-strengthening effect of sorbitol on water–water and water–residue interactions is counteracted by the bond-weakening effect of GnHCl. This interplay appears to extend to the protein interior, where sorbitol enhances internal residue bonding, while GnHCl reverses this effect. As a result, thermal stability increases in the presence of sorbitol alone but decreases when GnHCl is added, as shown in Figure 5(f).

6.3 Conclusion

Sorbitol strengthens water–water and water–residue interactions, which in turn enhances bonding between residues in the protein core, leading to increased thermal stability. In contrast, GnHCl follows the same pathway but has the opposite effect—it weakens these interactions, reducing the protein's internal stability. When these two are present together the stabilizing capacity of sorbitol towards papain gets decreased by the presence of destabilizing character of GnHCl. It has been observed that the counteraction effect of GnHCl over the stabilizing effect of sorbitol could

be understood within the same framework of AWSM. The addition of GnHCl in sorbitol solution reduces the efficacy of the sorbitol molecules to enhance the water structure around the protein surface as both impart their individual effect which are opposite because of which the enhancement in the bonding among the water-water and water-residues are less which enhances the bonding among the amino acid residues to a lesser extent. Ultimately resulting in less stabilization compared to the observed thermal stability of papain in only sorbitol system. Along with this effect, the direct interaction between sorbitol and GnHCl might also be acting to counteract the stabilizing effect of sorbitol by GnHCl but might not be the major one as the interaction among the two is observed to be feeble. The AWSM hypothesis seems to be promising in addressing the molecular level understanding of the protein-osmolyte interactions and might foster research in the field of protein science and inspire others to explore and understand the field of protein more.

6.4 References

(1) Yadav, R.; Sengupta, B.; Sen, P. Conformational Fluctuation Dynamics of Domain i of Human Serum Albumin in the Course of Chemically and Thermally Induced Unfolding Using Fluorescence Correlation Spectroscopy. *J. Phys. Chem. B* **2014**, *118* (20), 5428–5438. https://doi.org/10.1021/jp502762t.

(2) Janin, J.; Bahadur, R. P.; Chakrabarti, P. Protein-Protein Interaction and Quaternary Structure. *Quarterly Reviews of Biophysics*. May 2008, pp 133–180. https://doi.org/10.1017/S0033583508004708.

(3) Wang, W. Protein Aggregation and Its Inhibition in Biopharmaceutics. *International Journal of Pharmaceutics*. January 31, 2005, pp 1–30. https://doi.org/10.1016/j.ijpharm.2004.11.014.

(4) Yancey, P. H. Organic Osmolytes as Compatible, Metabolic and Counteracting Cytoprotectants in High Osmolarity and Other Stresses. *J. Exp. Biol.* August 2005, pp 2819–2830. https://doi.org/10.1242/jeb.01730.

(5) Timasheff, S. N. Water as Ligand: Preferential Binding and Exclusion of Denaturants in Protein Unfolding. *Biochemistry* **1992**, *31* (41), 9857–9864.

(6) Timasheff, S. N. *THE CONTROL OF PROTEIN STABILITY AND ASSOCIATION BY WEAK INTERACTIONS WITH WATER: How Do Solvents Affect These Processes?*; 2025. www.annualreviews.org.

(7) Arakawa, T.; Timasheff, S. N. The Stabilization of Proteins by Osmolytes. *Biophys. J* **1985**, *47* (3), 411–414. https://doi.org/10.1016/S0006-3495(85)83932-1.

(8) Lee, J. C.; Timasheff, S. N. The Stabilization of Proteins by Sucrose. *J. Biol. Chem.* **1981**, *256* (14), 7193–7201. https://doi.org/10.1016/s0021-9258(19)68947-7.

(9) Noelken, M. E.; Timasheff, S. N. Preferential Solvation of Bovine Serum Albumin in Aqueous Guanidine Hydrochloride. *J Biol Chem* **1967**, *242* (21), 5080–5085. https://doi.org/10.1016/s0021-9258(18)99478-0.

(10) Lin' And, T.-Y.; Timasheff, S. N. *On the Role of Surface Tension in the Stabilization of Globular Proteins*; Cambridge University Press, 1996; Vol. 5.

(11) Lin, T.; Timasheff, S. N. Why Do Some Organisms Use a Urea-Methylamine Mixture as Osmolyte? Thermodynamic Compensation of Urea and Trimethylamine N-Oxide Interactions with Protein. *Biochemistry* **1994**, *33* (42), 12695–12701.

(12) Bolen, D. W. The Peptide Backbone Plays a Dominant Role in Protein Stabilization by Naturally Occurring Osmolytes. *Biochemistry* **1995**, *34* (39), 12884–12891.

(13) Rg Rö, J.; Pettitt, B. M.; Bolen, D. W. Protein Folding, Stability, and Solvation Structure in Osmolyte Solutions. *Biophys J* **2005**, *89* (5), 2988–2997. https://doi.org/10.1529/biophsyj.105.067330.

(14) Street, T. O.; Wayne Bolen, D.; Rose, G. D.; Jenkins, T. C. A Molecular Mechanism for Osmolyte-Induced Protein Stability. *Proc. Natl. Acad. Sci. U. S. A.* **2006**, *103*, 13997–14002.

(15) Kumar, V.; Chari, R.; Sharma, V. K.; Kalonia, D. S. Modulation of the Thermodynamic Stability of Proteins by Polyols: Significance of Polyol Hydrophobicity and Impact on the Chemical Potential of Water. *Int J Pharm* **2011**, *413* (1–2), 19–28. https://doi.org/10.1016/j.ijpharm.2011.04.011.

(16) Hishida, M.; Anjum, R.; Anada, T.; Murakami, D.; Tanaka, M. Effect of Osmolytes on Water Mobility Correlates with Their Stabilizing Effect on Proteins. *Journal of Physical Chemistry B* **2022**, *126* (13), 2466–2475. https://doi.org/10.1021/acs.jpcb.1c10634.

(17) Hishida, M.; Kaneko, A.; Yamamura, Y.; Saito, K. Contrasting Changes in Strongly and Weakly Bound Hydration Water of a Protein upon Denaturation. *J Phys Chem B* **2023**, *127* (28), 6296–6305. https://doi.org/10.1021/acs.jpcb.3c02970.

(18) Higuchi, Y.; Saleh, M. A.; Anada, T.; Tanaka, M.; Hishida, M. Rotational Dynamics of Water near Osmolytes by Molecular Dynamics Simulations. *Journal of Physical Chemistry B* **2024**, *128* (20), 5008–5017. https://doi.org/10.1021/acs.jpcb.3c08470.

(19) Funkner, S.; Havenith, M.; Schwaab, G. Urea, a Structure Breaker? Answers from THz Absorption Spectroscopy. *J. Phys. Chem. B* **2012**, *116* (45), 13374–13380. https://doi.org/10.1021/jp308699w.

(20) Shukla, N.; Narayan Bhatt, A.; Aliverti, A.; Zanetti, G.; Bhakuni, V. Guanidinium Chloride-and Urea-Induced Unfolding of FprA, a Mycobacterium NADPH-Ferredoxin Reductase Stabilization of an Apo-Protein by GdmCl. *FEBS J* **2005**, *272* (9), 2216–2224. https://doi.org/10.1111/j.1742-4658.2005.04645.x.

(21) Bhuyan, A. K. Protein Stabilization by Urea and Guanidine Hydrochloride. *Biochemistry* **2002**, *41* (45), 13386–13394. https://doi.org/10.1021/bi020371n.

(22) Rezus, Y. L. A.; Bakker, H. J. Effect of Urea on the Structural Dynamics of Water. *Proc. Natl. Acad. Sci* **2006**, *103* (49), 18417–18420.

(23) Soper, A. K.; Castner, E. W.; Luzar, A. Impact of Urea on Water Structure: A Clue to Its Properties as a Denaturant? *Biophys. Chem.* **2003**, *105*, 649–666. https://doi.org/10.1016/S0301-4622Ž03.00095-4.

(24) Sathish, H. A.; Kumar, R.; Prakash, V. Effect of Urea at Lower Concentration on the Structure of Papain-Formation of a Stable Molten Globule and Its Characterization. *Indian J. Biochem. Biophys* **2002**, *39* (3), 155–162.

(25) Das, N.; Tarif, E.; Dutta, A.; Sen, P. Associated Water Dynamics Might Be a Key Factor Affecting Protein Stability in the Crowded Milieu. *J. Phys. Chem. B* **2023**, *127* (14), 3151–3163. https://doi.org/10.1021/acs.jpcb.2c09043.

(26) Khan, T.; Halder, B.; Das, N.; Sen, P. Role of Associated Water Dynamics on Protein Stability and Activity in Crowded Milieu. *J. Phys. Chem. B* **2024**, *128* (36), 8672–8686. https://doi.org/10.1021/acs.jpcb.4c04337.

(27) Negi, K. S.; Das, N.; Khan, T.; Sen, P. Osmolyte Induced Protein Stabilization: Modulation of Associated Water Dynamics Might Be a Key Factor. *Phys. Chem. Chem. Phys* **2023**, *25* (47), 32602–32612. https://doi.org/10.1039/d3cp03357k.

(28) Khan, T.; Das, N.; Negi, K. S.; Bhowmik, S.; Sen, P. Understanding the Intricacy of Protein in Hydrated Deep Eutectic Solvent: Solvation Dynamics, Conformational Fluctuation Dynamics, and Stability. *Int. J. Biol. Macromol.* **2023**, *253* (P5), 127100. https://doi.org/10.1016/j.ijbiomac.2023.127100.

(29) Khan, T.; Das, N.; Bhowmik, S.; Negi, K. S.; Sen, P. Critical Role of Water beyond the Media to Maintain Protein Stability and Activity in Hydrated Deep Eutectic Solvent. *J. Phys. Chem. B* **2024**, *129*, 162–175. https://doi.org/10.1021/acs.jpcb.4c07039.

(30) Negi, K. S.; Rana, S.; Khan, T.; Mondal, D.; Sen, P. Interplay of Protein Fluctuation and Associated Water Dynamics in Osmolyte-Induced Stabilization. *Biophys J* **2025**, *124* (12), 2082–2091. https://doi.org/10.1016/j.bpj.2025.05.006.

(31) Malik, R.; Chandra, A. Counteracting Effects of Trimethylamine N-Oxide against Urea in Aqueous Solutions: Insights from Theoretical Two-Dimensional Infrared Spectroscopy. *Journal of Physical Chemistry B* **2023**, *127* (33), 7372–7383. https://doi.org/10.1021/acs.jpcb.3c03864.

(32) Judy, E.; Kishore, N. Quantitative Calorimetric Evidences into Counteraction Mechanism of Denaturing Effect of Guanidine Hydrochloride by Citrulline and Betaine. *J Mol Liq* **2021**, *323*. https://doi.org/10.1016/j.molliq.2020.114953.

(33) Fersht, A. R.; Daggett, V. *Protein Folding and Unfolding at Atomic Resolution*; 2002; Vol. 108.

(34) Tejaswi Naidu, K.; Prakash Prabhu, N. Protein-Surfactant Interaction: Sodium Dodecyl Sulfate-Induced Unfolding of Ribonuclease A. *J. Phys. Chem. B* **2011**, *115* (49), 14760–14767. https://doi.org/10.1021/jp2062496.

(35) Chattopadhyay, K.; Saffarian, S.; Elson, E. L.; Frieden, C. Measuring Unfolding of Proteins in the Presence of Denaturant Using Fluorescence Correlation Spectroscopy. *Biophys J* **2005**, *88* (2), 1413–1422. https://doi.org/10.1529/biophysj.104.053199.

(36) Moon, C. P.; Fleming, K. G. Using Tryptophan Fluorescence to Measure the Stability of Membrane Proteins Folded in Liposomes. In *Methods in Enzymology*; Academic Press Inc., 2011; Vol. 492, pp 189–211. https://doi.org/10.1016/B978-0-12-381268-1.00018-5.

(37) Mohan, V.; Sengupta, B.; Das, N.; Banerjee, I.; Sen, P. Domain-Specific Stabilization of Structural and Dynamic Responses of Human Serum Albumin by Sucrose. *Protein Pept Lett* **2019**, *26* (4), 287–300. https://doi.org/10.2174/0929866526666190122115702.

(38) Horng, M. L.; Gardecki, J. A.; Papazyan, A.; Maroncelli, M. Subpicosecond Measurements of Polar Solvation Dynamics: Coumarin 153 Revisited. *J. Phys. Chem* **1995**, *99* (48), 17311–17337. https://doi.org/10.1021/j100048a004.

(39) Maroncelli, M.; Fleming, G. R. Picosecond Solvation Dynamics of Coumarin 153: The Importance of Molecular Aspects of Solvation. *J Chem Phys* **1987**, *86* (11), 6221–6239. https://doi.org/10.1063/1.452460.

(40) Nandi, N.; Bagchi, B. Dielectric Relaxation of Biological Water. *J Phys Chem B* **1997**, *101* (50), 10954–10961.

(41) Peon, J.; Pal, K.; Zewail, A. H. Hydration at the Surface of the Protein Monellin: Dynamics with Femtosecond Resolution. *Proc. Natl. Acad. Sci* **2002**, *99* (17), 10964–10969.

(42) Bhattacharyya, S. M.; Wang, Z. G.; Zewail, A. H. Dynamics of Water near a Protein Surface. *J. Phys. Chem. B* **2003**, *107* (47), 13218–13228. https://doi.org/10.1021/jp030943t.

(43) Kamal, J. K. A.; Zhao, L.; Zewail, A. H. Ultrafast Hydration Dynamics in Protein Unfolding: Human Serum Albumin. *Proc. Natl. Acad. Sci* **2004**, *101* (37), 13411–13416.

(44) Mukherjee, S.; Mondal, S.; Bagchi, B. Distinguishing Dynamical Features of Water inside Protein Hydration Layer: Distribution Reveals What Is Hidden behind the Average. *J. Chem. Phys* **2017**, *147* (2), 024901. https://doi.org/10.1063/1.4990693.

(45) Mondal, S.; Mukherjee, S.; Bagchi, B. On the Origin of Diverse Time Scales in the Protein Hydration Layer Solvation Dynamics: A Molecular Dynamics Simulation Study. *J. Chem. Phys* **2017**, *147*, 154901.

(46) Bagchi, B. *Water in Biological and Chemical Processes: From Structure and Dynamics to Function*; Cambridge University Press, 2013. https://doi.org/10.1017/CBO9781139583947.

(47) Qin, Y.; Jia, M.; Yang, J.; Wang, D.; Wang, L.; Xu, J.; Zhong, D. Molecular Origin of Ultrafast Water-Protein Coupled Interactions. *Journal of Physical Chemistry Letters* **2016**, *7* (20), 4171–4177. https://doi.org/10.1021/acs.jpclett.6b01954.

(48) Qin, Y.; Wang, L.; Zhong, D. Dynamics and Mechanism of Ultrafast Water-Protein Interactions. *Proc Natl Acad Sci U S A* **2016**, *113* (30), 8424–8429. https://doi.org/10.1073/pnas.1602916113.

(49) Guha, S.; Sahu, K.; Roy, D.; Mondal, S. K.; Roy, S.; Bhattacharyya, K. Slow Solvation Dynamics at the Active Site of an Enzyme: Implications for Catalysis. *Biochemistry* **2005**, *44* (25), 8940–8947. https://doi.org/10.1021/bi0473915.

(50) Sen, P.; Roy, D.; Sahu, K.; Kumar Mondal, S.; Bhattacharyya, K. Hydration Dynamics of a Protein in the Presence of Urea and Sodium Dodecyl Sulfate. *Chem Phys Lett* **2004**, *395* (1–3), 58–63. https://doi.org/10.1016/j.cplett.2004.07.052.

(51) Dutta, P.; Sen, P.; Halder, A.; Mukherjee, S.; Sen, S.; Bhattacharyya, K. Solvation Dynamics in a Protein-Surfactant Complex. *Chem Phys Lett* **2003**, *377* (1–2), 229–235. https://doi.org/10.1016/S0009-2614(03)01143-6.

(52) Sen, P.; Mukherjee, S.; Dutta, P.; Halder, A.; Mandal, D.; Banerjee, R.; Roy, S.; Bhattacharyya, K. Solvation Dynamics in the Molten Globule State of a Protein. *J. Phys. Chem. B* **2003**, *107* (51), 14563–14568. https://doi.org/10.1021/jp036277d.

(53) Buchenberg, S.; Schaudinnus, N.; Stock, G. Hierarchical Biomolecular Dynamics: Picosecond Hydrogen Bonding Regulates Microsecond Conformational Transitions. *J. Chem. Theory Comput.* **2015**, *11* (3), 1330–1336. https://doi.org/10.1021/ct501156t.

(54) Jha, A.; Ishii, K.; Udgaonkar, J. B.; Tahara, T.; Krishnamoorthy, G. Exploration of the Correlation between Solvation Dynamics and Internal Dynamics of a Protein. *Biochemistry* **2011**, *50* (3), 397–408. https://doi.org/10.1021/bi101440c.

(55) Sherman, E.; Itkin, A.; Kuttner, Y. Y.; Rhoades, E.; Amir, D.; Haas, E.; Haran, G. Using Fluorescence Correlation Spectroscopy to Study Conformational Changes in Denatured Proteins. *Biophys J* **2008**, *94* (12), 4819–4827. https://doi.org/10.1529/biophysj.107.120220.

(56) Basak, S.; Chattopadhyay, K. Studies of Protein Folding and Dynamics Using Single Molecule Fluorescence Spectroscopy. *Phys. Chem. Chem. Phys.* **2014**, *16* (23), 11139–11149. https://doi.org/10.1039/c3cp55219e.

(57) Chattopadhyay, K.; Saffarian, S.; Elson, E. L.; Frieden, C. Measurement of Microsecond Dynamic Motion in the Intestinal Fatty Acid Binding Protein by Using Fluorescence Correlation Spectroscopy. *Proc. Natl. Acad. Sci. U. S. A.* **2002**, *99* (22), 14171–14176. https://doi.org/10.1073/pnas.172524899.

(58) Krichevsky, O.; Bonnet, G. Fluorescence Correlation Spectroscopy: The Technique and Its Applications. *Rep. Prog. Phys.* **2002**, *65* (2), 251–297. https://doi.org/10.1088/0034-4885/65/2/203.

(59) Frauenfelder, H.; Chen, G.; Berendzen, J.; Fenimore, P. W.; Jansson, H.; McMahon, B. H.; Stroe, I. R.; Swenson, J.; Young, R. D. A Unified Model of Protein Dynamics. *Proc. Natl. Acad. Sci. U. S. A.* **2009**, *106* (13), 5129–5134. https://doi.org/10.1073/pnas.0900336106.

(60) Fenimore, P. W.; Frauenfelder, H.; McMahon, B. H.; Young, R. D. Bulk-Solvent and Hydration-Shell Fluctuations, Similar to α- and β-Fluctuations in Glasses, Control Protein Motions and Functions. *Proc. Natl. Acad. Sci. U. S. A.* **2004**, *101* (40), 14408–14413. https://doi.org/10.1073/pnas.0405573101.

(61) McMahon, B. H.; Frauenfelder, H.; Fenimore, P. W. The Role of Continuous and Discrete Water Structures in Protein Function. *Eur. Phys. J. Spec. Top* **2014**, *223* (5), 915–926. https://doi.org/10.1140/epjst/e2014-02125-y.

(62) Frauenfelder, H.; Fenimore, P. W.; McMahon, B. H. Hydration, Slaving and Protein Function. *Biophys. Chem.* **2002**, *98* (1–2), 35–48. https://doi.org/10.1016/S0301-4622(02)00083-2.

This page left blank intentionally

Chapter 7

Summary and Future Outlooks

7.1. Summary of Chapter 3

This chapter investigates the impact of protein–osmolyte interactions on the hydration layer dynamics and thermal stability of two model proteins: papain and bromelain. The authors propose and validate a model termed the Associated Water Stabilization Mechanism (AWSM), which posits that osmolytes modulate protein stability primarily by altering the dynamics of the associated water layer, a layer that is distinct from bulk water. Using lifetime and steady-state fluorescence measurements, the study quantifies the associated water dynamics (hydration/solvation dynamics) and thermal stability of the proteins in the presence of osmolyte respectively.

Key findings:

- Osmolyte significantly retards the dynamics of the associated water layer around papain more than around bromelain.
- Osmolyte thermally stabilizes the papain.
- Osmolyte significantly retards the dynamics of the associated water layer around papain
- This retardation correlates with enhanced thermal stability for papain.
- Destabilizing osmolytes follows the opposite trend.
- Stabilization of papain and destabilization of bromelain at 0.5 M concentration of sucrose could be understood following the correlation or hypothesis.
- Destabilization at 0.5 M and stabilization at 2 M sucrose of bromelain could also be understood following the hypothesis.
- The modulation of the associated water layer was shown to be more predictive of protein stability than direct interaction metrics.

Overall, the study provides experimental evidence for the protein-specific nature of osmolyte stabilization and suggests that associated water dynamics offer a more universal parameter for interpreting such effects.

Limitations:

While the study is rigorous and methodologically sound, several limitations are evident:

- Protein Scope: The findings are limited to two cysteine proteases (papain and bromelain). The generalizability of the AWSM model to other protein classes (e.g., membrane proteins, multimeric complexes) is not established.
- Indirect Observation of Water Dynamics: The conclusions regarding water dynamics are inferred from spectroscopic proxies rather than direct observations, such as those from terahertz spectroscopy, neutron scattering, or ultrafast IR.
- No Molecular Simulation: While AWSM is conceptually sound, molecular dynamics simulations could provide atomic-level insights into osmolyte-induced hydration effects and validate the proposed mechanisms more deeply.

Future Direction:

To strengthen and expand the current findings, several future directions are recommended:

- Broaden Protein Selection: Test the AWSM hypothesis on proteins with different topologies, charge distributions, and functions, including membrane proteins.
- Use Direct Probes of Water Dynamics: Combine FCS with techniques like ultrafast IR spectroscopy, THz absorption spectroscopy, or 2D IR to observe hydration layer dynamics more directly.
- Perform Molecular Dynamics Simulations: Computational modelling would allow visualization of osmolyte distribution, water network reorganization, and local flexibility changes, lending mechanistic depth to AWSM.
- Investigate Thermodynamic Parameters: Explore free energy landscapes, entropy–enthalpy compensation, and solvation energy contributions in greater detail to quantify stabilization mechanisms.

- Translate to Industrial Formulations: Apply findings to real-world protein formulations, such as therapeutic antibodies or enzymes, to assess how hydration dynamics influence long-term storage and efficacy.

7.2. Summary of Chapter 4

This chapter explores the modulations in the interior of the papain under the influence of osmolyte, by employing Fluorescence Correlation Spectroscopy (FCS). Here the modulations in the interior of the protein correlates well with the modulations in the associated water dynamics of the protein influence by the presence of osmolyte.

Key findings:

- Osmolyte enhances the thermal stability of papain by reducing internal flexibility and retarding water dynamics.
- GnHCl induces destabilization by enhancing internal fluctuations and disrupting hydration structure.

These observations are interpreted through the Associated Water Stabilization Mechanism (AWSM), emphasizing the role of interfacial water in mediating protein stability through the modulation of the interior of the protein.

Limitations

- No Structural Validation: Conformational fluctuations are inferred from fluorescence data. High-resolution techniques (e.g., NMR, SAXS, or crystallography) could validate conformational ensembles more rigorously.
- Absence of Molecular Simulations: Computational insights could support and extend AWSM by showing molecular-level interactions between solutes, water, and protein surfaces.

- Physiological Relevance Not Explored: Although the solute concentrations used mimic stress conditions, their correlation with physiological relevance or in vivo protection is not discussed.

Future Direction

- Apply AWSM to Other Protein Classes: Test whether the model applies to disordered proteins, membrane proteins.
- Combine with High-Resolution Techniques: Integrate spectroscopy with SAXS, NMR, FTIR, or cryo-EM to capture both global and local conformational shifts in the presence of mixed solutes.
- Thermodynamic Quantification: Derive ΔG, ΔH, ΔS, and preferential interaction coefficients using isothermal titration calorimetry (ITC) or vapor pressure osmometry to quantify stabilization and destabilization mechanisms.
- Leverage Molecular Dynamics Simulations: Simulate the impact of sorbitol and GnHCl on water structuring and protein hydration to directly validate the AWSM model and predict response under mixed conditions.
- Translate to Applied Systems: Use findings to optimize biopharmaceutical formulations, especially where proteins need to be stabilized during storage or exposed to chaotropic agents.
- Explore Time-Resolved Water Dynamics: Employ ultrafast IR or 2D IR spectroscopy to directly capture water mobility near protein surfaces and validate the kinetic model of hydration modulation.

7.3. Summary of Chapter 5

This chapter investigates the different stabilization of papain and bromelain by the same concentration of sorbitol in the view of the proposed hypothesis i.e., Associated Water Stabilization Mechanism. Fluorescence spectroscopy, lifetime

measurement and FCS studies were performed to perform the thermal, solvation and conformational studies of the two proteins.

Key Findings:

- Sorbitol stabilizes the papain better than that of bromelain.
- Direct implementation of AWSM doesn't explain the observation.
- Higher extent of stabilization of papain over bromelain could be understood better in terms greater extent of retardation in associated water dynamics and conformational dynamics.

Limitations

Despite a strong experimental narrative, several limitations exist:

- Inferences on hydration dynamics are indirect. There is no direct structural data (e.g., 2D-IR, neutron scattering, or dielectric relaxation) to visualize ion-induced changes in water networks.
- No energetic parameters such as ΔG, ΔS, or preferential interaction coefficients were calculated to quantitatively validate stabilization claims.
- Bromelain and papain share structural and functional similarities. Extrapolation to other proteins with different surface charges or topologies remains uncertain.
- Simulations could have helped verify the AWSM model under varying ionic strengths and clarified water structure near the protein surface.

Future Direction

Several important directions emerge for future investigation:

- Employ ultrafast infrared spectroscopy, THz dielectric measurements, or neutron scattering to observe water restructuring at protein interfaces in the presence of salts.

- Perform molecular dynamics (MD) simulations to visualize ion distribution, water structuring, and dynamic fluctuations in the hydration layer.
- Use ITC, vapor pressure osmometry, or preferential interaction coefficient calculations to obtain detailed thermodynamic profiles of salt-induced stabilization.
- Explore how controlled salt concentrations can be tuned to stabilize enzymes, therapeutic proteins, or vaccine formulations during long-term storage.

8.4. Summary of Chapter 6

This chapter addresses the combined effects of stabilizing (sorbitol) and destabilizing (GnHCl) solutes on the protein papain, under thermal stress conditions. The study is revolves around the Associated Water Stabilization Mechanism (AWSM) framework, proposing that proteins modulate their internal flexibility and hydration shell dynamics in response to solute environments. Thus, counteraction of stabilizing effect of sorbitol by GnHCl is an outcome of it. Fluorescence spectroscopy, lifetime measurement and FCS studies were performed to perform the thermal, solvation and conformational studies of the two proteins.

Key Findings:

- In presence of both sorbitol and GnHCl, papain shows a distinct intermediate thermal denaturation profile, different from its behaviour with either solute alone.
- Papain maintains a lower conformational flexibility compared to GnHCl alone, yet higher than in sorbitol-only conditions relative to 1:1 molar mixture of two. Same is the observation with the flexibility in associated water dynamics
- This behavior is interpreted as the result of counteracting molecular actions:

- Sorbitol slows down water and stabilizes intramolecular bonding in protein.
- GnHCl disrupts water structure and weakens intramolecular bonding in protein.

Limitations

While the findings are insightful and novel, several limitations are noted:

- Single Protein System: The study is focused only on papain, limiting generalization to other proteins with different folding topologies or surface properties.
- Limited Structural Characterization: Direct structural characterization (e.g., NMR, CD, SAXS) is absent, which would validate the existence and nature of these intermediates.
- Lack of Thermodynamic Dissection: The work does not separate enthalpic and entropic contributions to stabilization or destabilization under different solvent conditions.
- No Molecular Simulations: Computational modelling would help reveal the molecular basis in depth.
- Biological Relevance Not Established: While intermediate states are proposed to resemble misfolded forms, no cellular or pathological correlation is made.

Future Direction

To further validate and expand on these findings, the following future directions are recommended:

- Expand to Additional Proteins: Test whether intermediate states arise in other globular proteins, membrane proteins under similar ternary solute conditions.

- Use High-Resolution Structural Techniques: Apply SAXS, circular dichroism, or multidimensional NMR to characterize structural changes directly.
- Employ Molecular Dynamics Simulations: Simulate the effect of sorbitol and GnHCl on the hydration layer, internal flexibility, and energy landscape of proteins to validate AWSM predictions.
- Quantification of Thermodynamic Parameters: Use of DSC, ITC, or model fitting of denaturation curves to estimate changes in ΔG, ΔH, and ΔS associated with intermediate states.
- Explore Cellular and Pathological Relevance: Investigate whether similar intermediate states arise in vivo under osmotic stress or during misfolding diseases like ALS or Alzheimer's.

This page left blank intentionally

List of Publications

5. Interplay of Protein Fluctuation and Associated Water Dynamics in Osmolyte-induced Stabilization.
Kuldeep Singh Negi, Subhajit Rana, Tanmoy Khan, Dipankar Mondal, Pratik Sen*
Biophys. J., **2025**, *124*, 1-10.

4. Critical Role of Water beyond the Media to Maintain Protein Stability and Activity in Hydrated Deep Eutectic Solvent.
Tanmoy Khan, Nilimesh Das, Suman Bhowmik, **Kuldeep Singh Negi**, Pratik Sen*
J. Phys. Chem. B, **2025***, 129,* 162–175.

3. Understanding the Intricacy of Protein in Hydrated Deep Eutectic Solvent: Solvation dynamics, Conformational Fluctuation Dynamics, and Stability.
Tanmoy Khan, Nilimesh Das, **Kuldeep Singh Negi**, Suman Bhowmik, Pratik Sen*ss
Int. J. Biol. Macromol., ***2023****, 253,* 127100.

2. Osmolytes Induced Protein Stabilization: Modulation of Associated Water Dynamics Might be a Key Factor.
Kuldeep Singh Negi, Nilimesh Das, Tanmoy Khan, Pratik Sen*
Phys. Chem. Chem. Phys., **2023**, *25*, 32602-32612.

1. Does Microsecond Active-Site Dynamics Primarily control Proteolytic Activity of Bromelain? Clues from Single Molecular Level Study with a Denaturant, a Stabilizer and a Macromolecular Crowder.
Nilimesh Das*, Sandeep Yadav, **Kuldeep Singh Negi**, Pratik Sen*
BBA Adv., **2022**, *2*, 100041.

This page left blank intentionally

PCCP

PAPER

View Article Online
View Journal | View Issue

Cite this: *Phys. Chem. Chem. Phys.*, 2023, **25**, 32602

Osmolyte induced protein stabilization: modulation of associated water dynamics might be a key factor†

Kuldeep Singh Negi, Nilimesh Das, Tanmoy Khan and Pratik Sen *

Received 15th July 2023,
Accepted 13th November 2023

DOI: 10.1039/d3cp03357k

rsc.li/pccp

The mechanism of protein stabilization by osmolytes remains one of the most important and long-standing puzzles. The traditional explanation of osmolyte-induced stability through the preferential exclusion of osmolytes from the protein surface has been seriously challenged by the observations like the concentration-dependent reversal of osmolyte-induced stabilization/destabilization. The more modern explanation of protein stabilization/destabilization by osmolytes considers an indirect effect due to osmolyte-induced distortion of the water structure. It provides a general mechanism, but there are numerous examples of protein-specific effects, *i.e.*, a particular osmolyte might stabilize one protein, but destabilize the other, that could not be rationalized through such an explanation. Herein, we hypothesized that osmolyte-induced modulation of associated water might be a critical factor in controlling protein stability in such a medium. Taking different osmolytes and papain as a protein, we proved that our proposal could explain protein stability in osmolyte media. Stabilizing osmolytes rigidify associated water structures around the protein, whereas destabilizing osmolytes make them flexible. The strong correlation between the stability and the associated water dynamics, and the fact that such dynamics are very much protein specific, established the importance of considering the modulation of associated water structures in explaining the osmolyte-induced stabilization/destabilization of proteins. More interestingly, we took another protein, bromelain, for which a traditionally stabilizing osmolyte, sucrose, acts as a stabilizer at higher concentrations but as a destabilizer at lower concentrations. Our proposal successfully explains such observations, which is probably impossible by any known mechanisms. We believe this report will trigger much research in this area.

1. Introduction

1.1. Osmolytes are essential for keeping proteins active and stable in living cells

Proteins are responsible for countless phenomena occurring throughout the lifespan of a living system. The native structure of a protein can be perturbed under stressed conditions created through changes in its environment, such as the presence of additives, pressure, salinity, temperature, *etc.* The protein under perturbed conditions may lose its quaternary, tertiary and secondary structures. Alternatively, it may assume an intermediate conformation or aggregate into accumulating β-amyloid fibrils, which have been observed to exhibit toxicity towards cells.[1] Nevertheless, Nature is well-equipped with many defense mechanisms to combat the deleterious effect of these perturbations, and osmolytes play an important role in this process. The osmolytes are small natural organic molecules, which are accumulated in the cells while in stress to protect proteins and enzymes.[2] Osmolytes are usually stabilizing and crudely can be of four types: sugars, polyols, amino acids, and methyl amines (and their derivatives). Surprisingly, there are some osmolytes (like urea) that generally destabilize a protein.[3] One of the long-standing and most debated topics of biophysics is how these osmolytes stabilize/destabilize a protein,[4] though the molecular-level understanding is far from complete. In this report, we attempted to provide a unique mechanistic view of the osmolyte-induced stabilization/destabilization of proteins.

Department of Chemistry, Indian Institute of Technology Kanpur, Kanpur-208016, Uttar Pradesh, India. E-mail: psen@iitk.ac.in; Fax: +91-512-259-6806; Tel: +91-512-259-6312

† Electronic supplementary information (ESI) available: Tagging of the fluorescent dye to papain and bromelain, thermal denaturation study of papain in buffer and osmolyte solutions, thermal denaturation study of bromelain in buffer and sucrose solutions, solvation dynamics study of papain in buffer and other osmolyte solutions, solvation dynamics study of bromelain in buffer and sucrose solutions, emission spectra of CPM-tagged papain and bromelain in buffer and osmolyte solutions, CD spectra of CPM-tagged papain and bromelain in buffer and osmolyte solutions, fluorescence intensity autocorrelation function of TMR tagged papain and bromelain in buffer and osmolyte solutions, fluorescence up-conversion study of CPM-tagged papain in buffer, and variation of the size and structure of bromelain in buffer and osmolyte solutions are provided. See DOI: https://doi.org/10.1039/d3cp03357k

This page left blank intentionally

Biophysical Journal
Article

Biophysical Society

Interplay of protein fluctuation and associated water dynamics in osmolyte-induced stabilization

Kuldeep Singh Negi,[1] Subhajit Rana,[1] Tanmoy Khan,[1] Dipankar Mondal,[1] and Pratik Sen[1,*]
[1]Department of Chemistry, Indian Institute of Technology Kanpur, Kanpur, UP 208016, India

SUMMARY The mechanism behind osmolyte-induced protein stabilization remains elusive despite extensive research. Among various hypotheses, the associated water-modulation hypothesis has proved to be the most effective in explaining osmolyte-induced stabilization effects. Earlier, we demonstrated that osmolytes that slow down associated water dynamics enhance protein thermal stability, whereas those that accelerate it promote destabilization. However, the molecular basis of this correlation remains unclear. Using fluorescence correlation spectroscopy, we observe that osmolyte-induced changes in the associated water dynamics directly affect the internal flexibility of the protein, which is assessed through conformational fluctuation dynamics, serving as a tool to measure the protein's internal flexibility. The osmolytes that induce retardation in the associated water dynamics make the interior of the protein less flexible, as reflected by the slowed conformational fluctuation dynamics of the protein, leading to enhanced thermal stabilization. The destabilizers induce effects that are exactly opposite to stabilizers. These findings provide new insights into the interplay of associated water dynamics, protein flexibility, and stability, contributing to a deeper understanding of osmolyte-induced protein stabilization.

SIGNIFICANCE Our findings show that osmolyte-induced protein stabilization is connected to the interplay of associated water dynamics and the conformational fluctuation dynamics of the protein, without altering its overall structure. This novel insight provides a deeper understanding of the molecular mechanisms underlying protein stabilization. Our research contributes to the growing knowledge of osmolyte-protein interactions and lays the groundwork for future studies on the role of associated water dynamics in biology.

INTRODUCTION

Proteins are indispensable for the proper functioning of living organisms. They are composed of amino acid residues that fold into a specific three-dimensional (3D) structure, referred to as the native state. The native conformation is critical for the biological activity of proteins. Even a marginal alteration in the environment, such as a change in the temperature, pressure, pH, and salt concentration, can change the native state conformation and may modify protein's functional efficacy (1,2). Osmolytes, a class of small organic molecules including sugars, polyols, and amino acids, play a critical role in preserving protein structural integrity under diverse environmental conditions (1–3). These molecules are broadly categorized based on their effects on protein stability: stabilizing osmolytes, such as sucrose and trimethylamine N-oxide, enhance the structural robustness of proteins, whereas destabilizing osmolytes (known as denaturants), e.g., urea and guanidine hydrochloride (GnHCl), promote protein unfolding (4,5). Due to their ability to modulate protein stability, osmolytes have significant applications in the pharmaceutical industry, where they are employed to prolong the shelf life of biopharmaceutical products, thereby ensuring their stability and efficacy over extended periods (6,7).

Over the past few decades, extensive research has focused on understanding osmolyte-protein interactions due to their significance in both fundamental science and applications (7–13). Although substantial progress has been made (Scheme 1), a concise understanding of these interactions remains elusive. Timasheff's group first proposed a model based on the phenomenon of surface tension, specifically the excess surface free energy of water molecules at the protein-water interface (10,14,15). This model differentiates between stabilizing osmolytes (such as sucrose) and destabilizing osmolytes (such as urea) by introducing a parameter known as preferential interaction

Submitted February 13, 2025, and accepted for publication May 8, 2025.
*Correspondence: psen@iitk.ac.in
Editor: Scott Showalter.
https://doi.org/10.1016/j.bpj.2025.05.006